AXON PATHOLOGY IN MOUSE MODELS OF HUNTINGTON'S DISEASE

Martina Marangoni, MSc.

Thesis submitted to the University of Nottingham

For the degree of Doctor of Philosophy

MAY 2014

Declaration

This dissertation is the result of my own work and includes nothing which is the outcome of work done in collaboration except where specifically stated in the text. The work presented here is not substantially the same as any I have submitted for a degree or diploma or other qualification at any other University.

Abstract

AXON PATHOLOGY IN MOUSE MODELS OF HUNTINGTON'S DISEASE

Martina Marangoni

Axon or synapse dysfunction parallels or precedes symptom onset in many neurodegenerative disorders. In some of these conditions, not only do axon and synapse loss determine the course of pathology, but protection of those neuronal compartments is mandatory to alleviate the disease. Whether this is also the case in Huntington's disease (HD), a devastating neurodegenerative disorder characterised by progressive deterioration of both physical and mental abilities and inevitable early death, remains unclear. Present therapeutic strategies do not address protection of axons and synapses, which may help explain why there is no effective treatment currently in use. Moreover, an accurate characterisation of the development of axon pathology relative to neuronal loss and to the deposition of mutant-Huntingtin (mHTT) aggregates, neuropathological hallmark of HD, is lacking.

In the present thesis I have carried out a detailed study aiming to investigate axon degeneration in the R6/2 transgenic (Tg) and the HdhQ140 knock-in (KI) mice, two HD models, and to assess whether this occurs early in and contributes to the course of pathology. I tested the hypothesis that axon degeneration precedes or at least parallels degeneration of other neuronal compartments in these mice. To characterise axon pathology and its spatio-temporal relationship to aggregate formation, neuronal loss and symptom onset, I crossed R6/2 and HdhQ140 mice with YFP-H transgenic mice that express the yellow fluorescent protein (YFP) in a subset of neurons. Neuronal pathways labelled by YFP in this model include some reported to be affected in HD. In these mice individual fluorescent neurons can be tracked over long distance and axons can be traced back to their cell bodies.

Using a powerful axon imaging method that was developed and successfully applied to study Alzheimer's disease, I was able to place axon degeneration accurately in the sequence of pathological events and develop methods to quantify it as readout for future therapeutic studies from our group and elsewhere.

I found that the morphology of axons was strikingly abnormal in some brain areas in HdhQ140 homozygous mice ($Hdh^{Q140/Q140}$) where large axonal swellings were

detected at 6 months and at 12 months of age in *stria terminalis* and striatum. In these mice, the number of axonal swellings increased age-dependently and was significantly higher than that found in wild-type littermates. However, I did not detect degeneration in cell bodies, dendrites or synapses suggesting that axon pathology is the main feature of the disease in this model.

To better characterise the KI model, I also performed a battery of behavioural tests to assess motor and cognitive impairment during disease progression. I used tests of locomotor activity, motor coordination and balance and sensorimotor gating to measure motor function and tests of spatial working memory and anxiety-like behaviour to assess cognitive and behavioural symptoms, respectively. A longitudinal study from 1 to 12 months was carried out to detect pathological changes from early stage and relate them to swelling formation. In all tests, I found a strong reduction in locomotor activity in HdhQ140 mice compared to the controls although balance and coordination seemed not to be impaired as rotarod performance was unaltered. Alterations were also detected in prepulse inhibition, suggesting sensorimotor defects occur in these mice, while no abnormal cognitive or psychiatric behaviour was detected in the time-frame of the study. Behavioural symptoms, as well as abnormal morphological changes found in axons, worsened with time and major impairments were found at the latest time-point, 12 months of age.

Finally, I asked whether alterations in the NAD biosynthetic pathway could underline the signs of axon pathology detected in HdhQ140 homozygous mice, as it has recently emerged that this pathway regulates axon survival and axon and synapse degeneration in many neurodegenerative disorders. To this purpose, I looked at possible alterations in the level of nucleotides (NMN, NAD) and in the activity of key enzymes in this pathway (NMNAT, NAMPT). I also tested the hypothesis that mHTT interacts with NMNAT enzymes and with the Wallerian degeneration slow protein (WLD^s), an NMNAT fusion protein, and interferes/impairs their normal function. As WLD^s delays axon degeneration in acute and neurodegeneration models, future works may address beneficial role of WLD^s in HD/*Wld*^{S} crossed mice. Despite no detected alterations in nucleotide levels or enzymatic activity in the KI mice compared to the controls, colocalisation was found between mHTT and WLD^s and between mHTT and NMNAT2, an important axon survival factor, suggesting a possible interaction between these proteins which could play a role in HD neurodegeneration.

Acknowledgments

I would like to thank all those people who made this thesis possible and these years of PhD an unforgettable experience.

First I would like to express my sincere gratitude to my supervisor Dr Laura Conforti for her continuous support and guidance. Her knowledge and enthusiasm helped me in all the times of research and writing of this thesis.

My thank goes also to all my fellow lab mates, the" Italian and international gang", for their precious support and true friendship shown at work and outside the lab. I thank Jamie Webster for precious technical assistance, Jaskaren Kholi for help with Western blotting and Tim Self for support with confocal imaging. I would like to thank Dr Marie Christine Pardon and Dr Rebecca Trueman for their advice and guidance on planning the behavioural testing. Special thanks go to the present and former collaborators in Cambridge, Dr Michael Coleman and Dr Robert Adalbert for the interesting scientific discussions and support; and Miss Lucie Janeckova and Miss Jane Patrick for their technical help. I am thankful to Prof Frederic Saudou and Dr Diana Zala for the kind gift of the pARIS-htt constructs. Finally I thank Dr Giuseppe Orsomando and Valerio Mori from the University of Ancona, for their technical training and scientific support in the biochemical studies of NAD metabolism.

I remember with affection Dr Terry Parker, a great person and a superb scientist who has followed my work and given me precious technical and scientific advice since the first year of my PhD.

My deepest gratitude is for my family and in particular my mother, who has always encouraged me and supported me with her love.

Publications

Marangoni M, Adalbert R, Janeckova L, Patrick J, Kohli J, Coleman MP and Conforti L. 2014. Age-related axonal swellings precede other neuropathological hallmarks in a knock-in mouse model of Huntington's disease. Neurobiol Aging, 35, 2382-93. (Appendix).

List of abbreviations

3-HK	3-hydroxykynurenine
ADPR	ADP-ribose
BAC	bacterial artificial chromosome
BDNF	brain derived neurotrophic factor
cADPR	cyclic ADP-ribose
CAG	cytosine adenine guanine
EPM	elevated plus maze
FAT	fast axonal transport
HAP1	huntingtin-associated protein-1
HD	Huntington's disease
Hdh	mouse huntington's disease gene homolog
HEK	human embryonic kidney
HIP1	huntingtin-interacting protein 1
HIP14	huntingtin-interacting protein 14
HTT	huntingtin protein
IT15	interesting transcript 15
KI	knock-in
KMO	kynurenine 3-monooxygenase
mHTT	mutant huntingtin protein
MSSNs	medium sized spiny neurons
NA	nicotinic acid
NAD	nicotinamide adenine dinucleotide
NAMPT	nicotinamide phosphoribosyltransferase
NGF	nerve growth factor
NIIs	neuronal intranuclear inclusions
NMDA	N-methyl-D-aspartate receptor
NMN	nicotinamide mononucleotide
NMNAT	nicotinamide mononucleotide adenylyltransferase
NOR	novel object recognition
pARIS	adaptable, RNAi insensitive & synthetic plasmid
PARP	poly (ADP-ribose) polymerase
PC12	rat pheocromocytoma cells

PFA	paraformaldehyde
polyQ	poly glutamine
PPI	prepulse inhibition
PSD95	post synaptic density 95
QA	quinolinic acid
REST	repressor element-1 transcription factor
SA	spontaneous alternation
SCG	superior cervical ganglia
SH3	Src homology 3
SIRT	sirtuins
SOD	superoxide dismutase
Tg	transgenic
UBE4B	ubiquitination factor E4B
VCP	valosin containing protein
WD	Wallerian Degeneration
Wld^{S}	Wallerian degeneration slow gene
WLD^{s}	Wallerian degeneration slow protein
YAC	yeast artificial chromosome
YFP	yellow fluorescent protein
YFP-H	YFP expressing mice line H

List of Figures

Page

List of Tables

Table of contents

Page

Above all, don’t fear difficult moments.

The best comes from them

Rita Levi-Montalcini

CHAPTER 1

Introduction

1.1 Huntington's disease

Huntington's disease (HD) is a progressive, autosomal dominant neurodegenerative disease caused by a cytosine adenine guanine (CAG) triplet expansion in the coding region of the *IT15* (*interesting transcript 15*) gene which results in an abnormal poly-glutamine (polyQ) stretch in the Huntingtin protein (HTT). It is also known as Huntington's chorea from the Greek word *chorea* (dance) as HD patients writhe, twist, and turn in a constant, uncontrollable dance-like motion. It is characterised by a triad of symptoms including motor dysfunction, cognitive impairment and psychiatric abnormalities which dramatically affect the social and economic life of the patients and their families as it interrupts a person's ability to live an independent life. Symptoms typically appear in middle age, although they can appear earlier (juvenile HD) or later, and progress to inevitable death within 15-20 years from onset (Bates, 2001). HD occurs in various geographic and ethnic populations worldwide with prevalence estimated at 5-10/100,000 in Caucasian population and the diagnosis is based on a neurological evaluation with the manifestation of motor symptoms together with a positive genetic test for the *HD* CAG expansion or a confirmed family history of HD. Fewer than 5% of individuals at risk for the disease choose to actually pursue predictive genetic testing which is not without consequences (Laccone et al., 1999); psychological distress and suicide cases increase following a positive result (Almqvist et al., 1999, Almqvist et al., 2003).

The first accurate description of the disease was made in 1872, by a 22 year old American physician working in New York, George Huntington, in a paper called *On Chorea: "And now I wish to draw your attention more particularly to a form of the disease which exists, so far as I know, almost exclusively on the east end of Long Island. It is peculiar in itself and seems to obey certain fixed laws"* (Fig. 1). It took over a century though to clarify the genetic nature of HD. In 1983, the HD locus was mapped on chromosome 4p16.3 using RFLP (restriction fragment length polymorphism) genetic markers (Gusella et al., 1983) and only 10 years later, scientists from all over the world joined together into *The Huntington Disease Collaborative Research Group* and reported the discovery of the gene responsible for HD and its associated mutation (HDCRG, 1993).

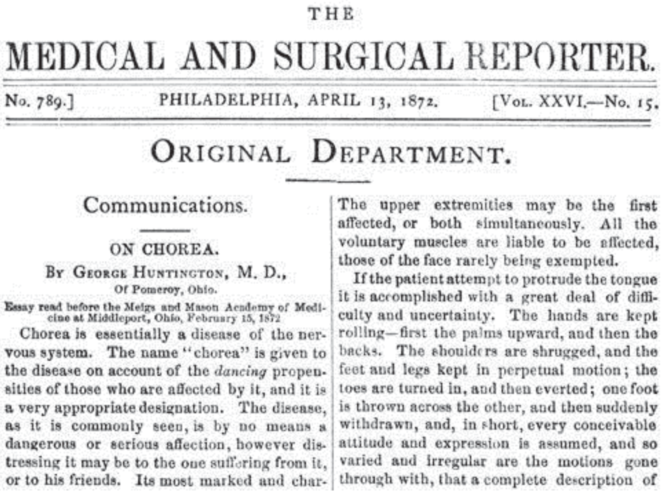

THE

MEDICAL AND SURGICAL REPORTER.

No. 789.] PHILADELPHIA, APRIL 13, 1872. [Vol. XXVI.—No. 15.

ORIGINAL DEPARTMENT.

Communications.

ON CHOREA.

By George Huntington, M. D.,
Of Pomeroy, Ohio.

Essay read before the Meigs and Mason Academy of Medicine at Middleport, Ohio, February 15, 1872

Chorea is essentially a disease of the nervous system. The name "chorea" is given to the disease on account of the *dancing* propensities of those who are affected by it, and it is a very appropriate designation. The disease, as it is commonly seen, is by no means a dangerous or serious affection, however distressing it may be to the one suffering from it, or to his friends. Its most marked and char-

The upper extremities may be the first affected, or both simultaneously. All the voluntary muscles are liable to be affected, those of the face rarely being exempted.

If the patient attempt to protrude the tongue it is accomplished with a great deal of difficulty and uncertainty. The hands are kept rolling—first the palms upward, and then the backs. The shoulders are shrugged, and the feet and legs kept in perpetual motion; the toes are turned in, and then everted; one foot is thrown across the other, and then suddenly withdrawn, and, in short, every conceivable attitude and expression is assumed, and so varied and irregular are the motions gone through with, that a complete description of

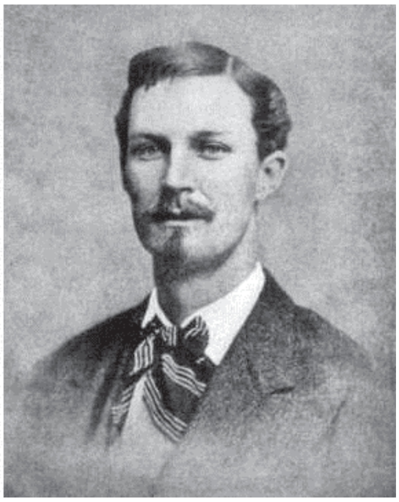

Fig. 1

George Huntington and his original paper on Chorea.

1.2 Genetics and neuropathology

HD is one of at least nine inherited neurodegenerative diseases caused by an expanded CAG triplet encoding an abnormal polyQ expansion in disease proteins. Spinocerebellar ataxias (SCA) 1, 2, 3, 6, 7 and 17, spinobulbar muscular atrophy (SBMA or Kenedy's disease) and dentatorubralpallidoluysian atrophy (DRPLA) are among the others. Despite different function and cellular localization, all polyQ expanded proteins share the common tendency to aggregate and form inclusion bodies whose role is still not fully understood.

The normal *IT15* gene contains from 9 to 35 CAG repeats, while in HD affected individuals the number rises above 40 and up to 100. Subjects with CAG repeat number ranging between 36 and 39 show incomplete penetrance and may or may not develop the signs and symptoms of the disease. An inverse relationship exists between CAG length and age of onset: patients with a large number of repeats tend to develop symptoms at an earlier age and juvenile HD, which appears in childhood or adolescence, is normally associated to repeat length of 60 or greater (Brinkman et al., 1997, Duyao et al., 1993). Moreover, while repeats in the normal range are stably inherited, abnormal repeats are unstable and can increase in length due to meiotic instability during development, resulting in earlier onset disease in later generations. This phenomenon is known as "genetic anticipation" (Ranen et al., 1995). Meiotic

instability may occur in both maternal and paternal transmission but the risk of expansion is enhanced during spermatogenesis. It has been suggested that expansion of the repeat tract can occur during mitotic divisions in the germ-line due to replication slippage, a commonly observed replication error which occurs at the repetitive sequences when the new strand mispairs with the template strand. The larger number of mitotic divisions in male spermatogenesis compared to the ones in oogenesis could explain the higher risk of anticipation when the disease gene is inherited from the father (Pearson, 2003).

Pathological changes in HD are brain specific. On external post-mortem examination 80% of HD human brains show atrophy of frontal lobes (Halliday et al., 1998) (Fig. 2) and macroscopic analysis reveals extended atrophy of the striatum although cortex, substantia nigra, hippocampus, cerebellum, hypothalamus, and thalamus are also severely compromised (Spargo et al., 1993, Macdonald et al., 1997, Kremer et al., 1991, Heinsen et al., 1999).

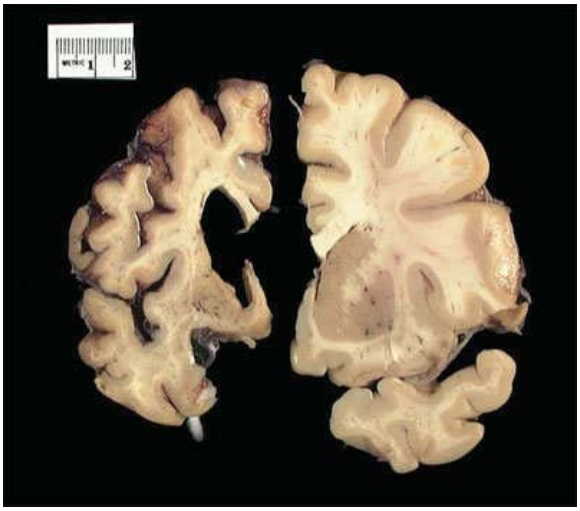

Fig. 2

Atrophy of HD brain. Normal brain (right) and Huntington's disease patient brain (left). From Harvard Brain Tissue resource centre.

In 1985, Jean Paul Vonsattel introduced the first grading system to describe the severity of HD degeneration in post-mortem brain specimens, according to the degree of macroscopic and microscopic neuropathological striatal variations. 5 grades (0-4)

were described in ascending order of severity: grade-0 brain is a brain apparently indistinguishable from the normal one, with no discernible neurological abnormalities; grade-1 to 4 brains show progressively more severe atrophy, neuronal loss and astrogliosis in the striatum (Vonsattel et al., 1985). Later studies described in more detail the differential degeneration of striatal neurons (Ferrante et al., 1985, Ferrante et al., 1987, Ferrante et al., 1986) and revealed that within the striatal neuronal subpopulations, projection neurons rather than interneurons are most affected (Albin et al., 1990b, Ferrante et al., 1987, DiFiglia, 1990) and among these, those termed medium sized spiny neurons (MSSNs). MSSNs are γ-aminobutyric acid (GABA) neurons that represent about 90% of all neurons in the striatum and are divided in D1 MSSNs, which express substance P, dynorphin and D1 dopaminergic receptors; and D2 MSSNs which express enkephalin and D2 dopaminergic receptors. Both types take part in the basal ganglia neuronal circuits formed by the striatal projections to the globus pallidus (GP) and substantia nigra (STN) that in turn project to the ventrolateral nucleus of the thalamus, ultimately controlling the activity of cortical areas important for motor function (Albin et al., 1989) (Fig. 3). In particular, D1 neurons are part of the direct pathway which receives excitatory inputs (E) from the cortex and makes inhibitory connections (I) with the globus pallidus pars interna (GPi) and STN. These make inhibitory connections with the thalamus which sends excitatory connections back to the cortex, stimulating its activity (+):

$$\text{Cortex} \xrightarrow{E} \text{Striatum} \xrightarrow{I} \text{GPi} \xrightarrow{I} \text{Thalamus} \xrightarrow{E} \overset{(+)}{\text{Cortex}}$$

D2 neurons are instead part of the indirect pathway. This sends inhibitory projections to the globus pallidus pars externa (GPe) which makes inhibitory connections with the subthalamic nucleus which in turn sends excitatory connections to the GPi and this ultimately results in inhibition of the cortex (-):

$$\text{Cortex} \xrightarrow{E} \text{Striatum} \xrightarrow{I} \text{GPe} \xrightarrow{I} \text{Subthalamic nucleus} \xrightarrow{E} \text{GPi} \xrightarrow{I} \text{Thalamus} \xrightarrow{E} \overset{(-)}{\text{Cortex}}$$

In HD, neurons of the indirect pathway are affected first and without the normal inhibitory influence on the thalamus that is provided by the indirect pathway, thalamic

neurons can fire inappropriately, causing the motor cortex to execute motor programs with no control resulting in increased movement, *chorea* (Reiner et al., 1988; Albin et al., 1992). At later stage of the disease, both subpopulations are affected and this results in a rigid bradykinetic state (Albin et al., 1989).

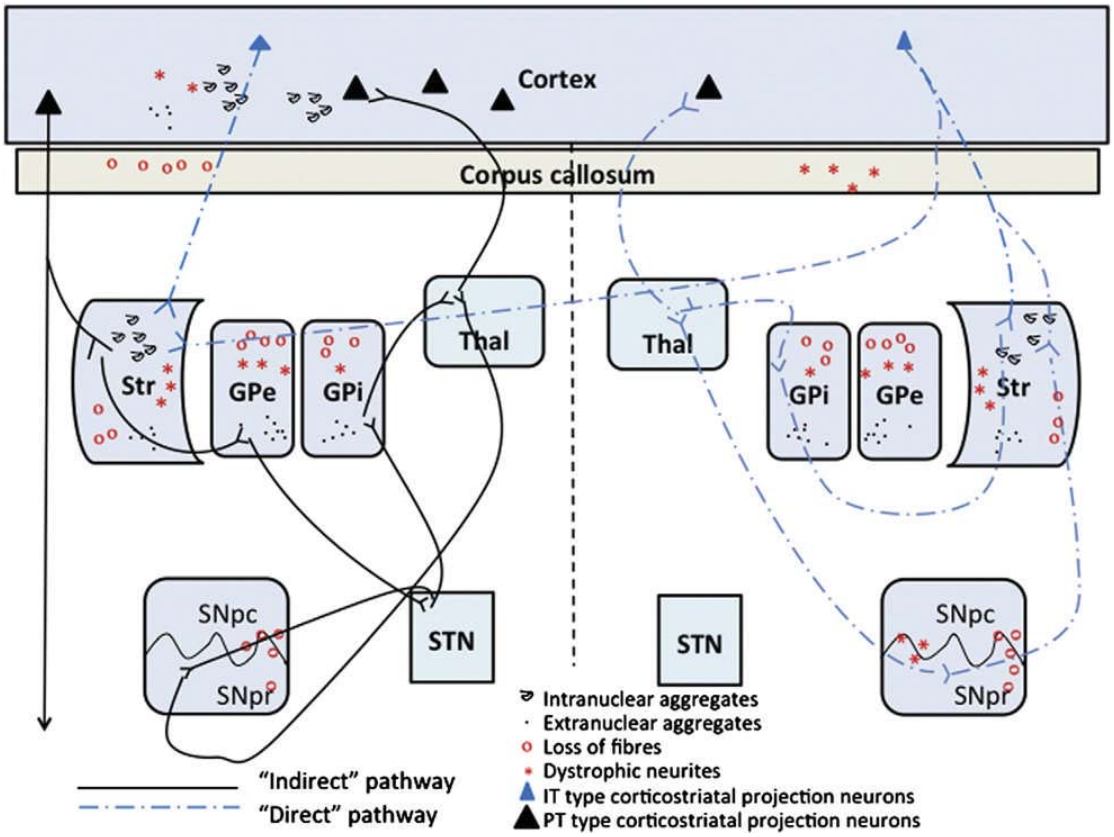

Fig. 3

Schematic representation of the cortical inputs to striatal neurons and the major projections of striatal MSSN. From (Li and Conforti, 2013). *The direct and indirect loops of the basal ganglia are represented on different parts of the brain, for clarity. The location of intranuclear and extranuclear mHTT aggregates, of dystrophic neurites and of fibre loss is also represented. Str =corpus striatum, Thal=thalamus, STN=subthalamic nucleus, GPi=globus pallidus (internal segment), GPe=globus pallidus (external segment), SNpc =substantia nigra (pars compacta), SNpr = substantia nigra (pars reticulata).*

Microscopically, HD brains present nuclear (NIIs) and cytoplasmic (neuropil) inclusions of mutant Huntingtin (mHTT) as the mutated protein is more prone to be cleaved and form aggregates than normal HTT, and this is a specific hallmark of the disease. Whether the nuclear inclusions are toxic is still controversial. Inclusion

formation can be linked to disease progression but so far no correlation with neuronal degeneration has been fully documented (Gutekunst et al., 1999, Slow et al., 2005). On the other hand, it has been proposed that nuclear aggregates may form as an attempt of the cell to degrade or inactivate the toxic soluble mHTT (Saudou et al., 1998, Arrasate et al., 2004).

1.3 Models of Huntington's disease

Modelling HD in non-human organisms is fundamental to understand the mechanisms underlying pathology, to identify therapeutic targets and to validate the efficacy and safety of potential drugs in preclinical trials. Before the discovery of the gene responsible for HD, the disease was induced in animals by injection of neurotoxins such as kainic acid (KA) and other glutamate agonists or mitochondrial toxins such as malonate and 3-nitropropionic acid (3-NPA). These toxins were injected directly into the striatum and were able to induce selective degeneration of striatal neurons (McGeer and McGeer, 1976, Beal et al., 1986, Beal et al., 1991) and in some cases behavioural changes similar to HD. However, they could not reproduce the pathophysiological mechanisms induced by the mutant gene and for this reason could be of limited use in developing and testing treatments for the disease. Moreover, the acute nature of these lesions was sharply contrasting the slow progression of HD which in patients takes decades to manifest. Soon after the discovery of the *IT15* gene and its mutation in HD, several genetic animal models became available, allowing a more precise reproduction of the human pathology. Models included invertebrates such as *Caenorhabditis elegans* and *Drosophila melanogaster*, and small and large mammals such as mice, rats and monkeys. Models differed in the expression of either truncated or full-length HTT; in the length of the CAG repeat inserted; in the expression of the mutant gene which could be a transgene or a knock-in into the endogenous *Hdh* locus; and in the use of cDNA or genomic DNA containing all the introns and regulatory sequences which influence the level of expression of the gene.

Invertebrate models

Although phylogenetically very distant from mammals, simpler organisms such as worms and flies have been demonstrated to be useful models to study the genetics and

the mechanisms of cellular processes. The main advantage of these models is that they have rapid generation time and reproduce the pathological phenotypes in a very short period of time. Successful transgenic nematode and fly models have been generated expressing truncated N-terminal fragments of human mHTT in targeted neurons (Parker et al., 2001, Gunawardena et al., 2003, Marsh and Thompson, 2006). *C. elegans* does not contain a HTT homologue or other polyQ proteins however it expresses homologues of HTT-interactors and these can interact with the inserted *HTT* transgene. Thus, this model can represent a useful tool to study protein-protein interactions. Several transgenic worms expressing a HTT fragment with 57 to 171 aminoacids in sensory neurons were generated and showed age-dependent increase defects in sensory neurons and axonal abnormalities preceding cell loss (Faber et al., 1999, Parker et al., 2001, Li and Le, 2013).

In *Drosophila*, expression of full-length or N-terminal fragments of 65 to 548 aminoacids of the human HTT was driven by a UAS/GAL4 system in the photoreceptor neurons of the eye. In the fly, integrity of photoreceptor cells of the eye and motor function are used as a readout to identify genetic modifiers of neurotoxicity. Similarly to humans, fly models exhibit a polyQ length dependency, late onset neuronal degeneration, and motor abnormalities (Jackson et al., 1998, Krench and Littleton, 2013).

Rodent models

Rodents are the most commonly used animals to model HD and they recapitulate many aspects of the human disease. Mouse models are the most exploited and among them, the following sub-categories are found (Table 1):

- *Truncated HTT Transgenic models:* these models were generated by insertion of N-terminal fragments of the human *HTT* gene into the mouse genome. The first transgenic (Tg) mouse line, termed R6, was generated by introducing in the mouse genome a fragment of 1.9 Kb including the promoter and exon1 of *IT15* gene carrying an expanded CAG repeat. Several lines (R6/1, R6/2, R6/5 and R6/0) differing in the CAG repeat length, ranging from 115 to 150, were characterised (Mangiarini et al., 1996). Among these, R6/2 mice (145 CAG) represent one of the most commonly used model for the study of HD since several of the characteristics specific of the pathology are modelled in these

mice. Brain atrophy has been detected as early as 5 weeks, weight loss by 8 weeks, mHTT inclusions by 3.5 weeks (Davies et al., 1997) and first signs of behavioural deficits from 5-6 weeks of age (Carter et al., 1999). Another N-terminal transgenic mouse is the N171-82Q line which expresses a 171 amino acid mHTT N-terminal fragment with 82 glutamines under the regulation of the mouse prion protein promoter vector (Schilling et al., 1999). In general, Tg N-terminal fragment mice exhibit a rapid onset of symptoms including motor, cognitive and behavioural deficits. They also exhibit neuropathological changes and shortened life-span and for this reason they are a popular choice for therapeutic trials. In these mice however, the exogenous HTT fragment inserts randomly, in multiple copies, in the mouse genome and can interact with the activity of other genes not related to HD. Also, the transgene expression above physiological concentrations and driven by artificial promoters may lead to a phenotype that does not correctly mimic the disease. Moreover, striatal neuronal loss widely reported in HD patients is minimal in these mice and appears evident only at a very late stage of the disease, after the appearance of behavioural symptoms (Mangiarini et al., 1996, Davies et al., 1997, Turmaine et al., 2000);

- *Full-Length HTT Transgenic models:* these models were created using yeast artificial chromosome (YAC) and bacterial artificial chromosome (BAC) technology. They provide better insights into the events and factors determining the selective cell vulnerability typical of HD, since the expanded polyQ stretch is expressed in the context of the entire HTT protein. YAC-72 mice were created in 1999 by cloning the entire HD gene with 72 CAG repeats in the Yeast Artificial Chromosome (YAC), under the control of the endogenous promoter (Hodgson et al., 1999). These mice showed typical HD behavioural phenotype and significant neuronal loss but mHTT aggregates were rarely detected and, despite levels of mHTT expression were higher than in R6/2 mice, motor symptoms appeared late and with slow progression;

- *Knock-In models:* they are considered the most genetically accurate model for HD. These mice carry the mutation in the appropriate genomic and protein context and at a physiological concentration. They were generated by gene targeting of the endogenous mouse homolog of human *IT15* gene (*Hdh*) on

chromosome 5 of the mouse genome with insertion of either a chimeric *IT15*–*Hdh* exon1 containing an expanded CAG repeat or an expanded CAG repeat into the endogenous mouse gene. Initial results were disappointing as the first knock-in (KI) mice generated, with 70-80 CAG repeats (HdhQ70-80), had normal life-span and did not show the classical HD motor deficits (Shelbourne et al., 1999) but further studies on mice with larger repeats revealed subtle behavioural abnormalities at an early age (Menalled et al., 2000). Even in those mice tough, behavioural deficits are not as pronounced as the ones seen in transgenic mice and they usually take longer to develop. Mice with 94 and 140 CAG repeats (Hdh94-140) show abnormal behaviour characterised by hyperactivity at around 2 months of age followed by hypoactivity at 4 months (Menalled and Chesselet, 2002). In HdhQ140 mice, diffuse nuclear staining and micro-aggregates of mHTT are detected in the striatum at around 6 months of age, a relatively early phase of the disease (Wheeler et al., 2000, Lin et al., 2001), while nuclear inclusions are detected only around 10–18 months; no cell death is reported in these mouse models although the striatal volume is decreased (Hickey et al., 2008) (Fig. 5).

Hdh gene knock-out in mice revealed the important role of normal HTT in embryonic development as the complete inactivation of the gene was embryonically lethal by embryonic day 8.5 (Duyao et al., 1995, Nasir et al., 1995, Zeitlin et al., 1995, White et al., 1997) while conditional knock-out of HTT in brain and testes resulted in neuronal dysfunctions (Dragatsis et al., 2000).

Large animal models

Large animal models offer some distinct advantages over rodent models, including a larger brain, more easily used for imaging and intracerebral therapy, longer lifespan, and a more human-like neuro-architecture. Primates in particular, are genetically more similar to humans, have similar lifespan, metabolism, and physiology and for these reasons probably better models for monitoring disease progression and the effectiveness of experimental drugs. On the other hand, they are more expensive, take longer time to develop pathology and raise more ethical concerns than non-primate models.

The use of primates as model of HD was very limited before 2008 and disease was replicated by acute lesions of basal ganglia by quinolinic acid (QA) or 3-nitroproprionic acid (3-NPA) (Brouillet et al., 1999). These early models manifested chorea similar to human HD but had the limitations of the neurotoxin model previously discussed. In 2008, the first transgenic non-human primate HD model was generated by injecting rhesus monkey eggs with lentiviral vectors expressing exon 1 of the human *HTT* gene with 84 CAG repeats and the GFP protein under the control of the human poly-ubiquitin promoter, and then fertilized and introduced into surrogate mothers. The transgenic monkeys exhibited similar features to human HD, including extended nuclear and neuropil mHTT aggregate inclusions and motor defects such as chorea and dystonia, although the rapid progression of the disease made them survive for no longer than 6 months (Yang et al., 2008). Other large HD models included a transgenic sheep and a transgenic miniature pig. The pig model like the monkey expressed only a fragment of human *HTT* including the CAG repeat expansion while the sheep was obtained by microinjecting the full-length human *HTT* cDNA with the expanded triplet under the control of the human *HTT* promoter (Jacobsen et al., 2010, Yang et al., 2010).

Cellular models

Several cellular systems are also available, with constitutive or inducible expression of wild-type or mHTT. They represent a good system to study some of the molecular mechanisms underlying the disease. Non neuronal cells such as the human embryonic kidney (HEK) 293 cells, transiently transfected with wild-type and mHTT, have been used as a model to study the effect of the polyQ extension on aggregate formation and localisation (Martindale et al., 1998). Also primary neurons have been used to investigate the role of normal HTT and the mechanisms of polyQ toxicity (Saudou et al., 1998, Moulder et al., 1999); and embryonic stem cells from knock-out mice (Metzler et al., 1999, Metzler et al., 2000). Several neuronal-like cellular systems with stable expression of HTT have been developed. Among these, the pheochromocytoma 12 cells (PC12) are widely utilised and their properties are well known (Greene and Tischler, 1976). PC12 cells differentiate into neuronal-like cells in the presence of neuronal growth factor (NGF). Engineered PC12 systems expressing the N-terminal portion of mHTT show intranuclear polyQ aggregate formation, cellular defects and altered gene expression. They also present abnormal morphology and neurite

development, and they are more susceptible to apoptotic stimulation (Li et al., 1999b, Wyttenbach et al., 2001). Human HD cell models based on induced pluripotent stem (iPS)-cell technology have been recently generated (Park et al., 2008) and characterised (Zhang et al., 2010, HDiPSCConsortium, 2012). They represent a novel method to generate pluripotent stem cells bypassing the ethical issues related to the use of human embryonic stem (ES) cells (Hanley et al., 2010) and also provide a valid HD cellular model to be used for drug screening and understanding the molecular mechanisms leading to pathology.

LINE	CAG EXPANSION AND GENETIC EXPRESSION	AGE OF ONSET AND BEHAVIORAL PHENOTYPE	NEUROPATHOLOGY	SURVIVAL
N171-82Q (chimeric fragment transgenic) C57BL/6JxC3H/HeJ	N-terminal fragment expressing first 171 AA of human HTT, 82 repeats, mouse PrP promoter.	Progressive weight loss by 4–6 weeks before death as well as tremor and hypokinesis, and clasping. Progressive accelerated rotarod deficit by 12 weeks.	NIIs <50% in the cortex, hippocampus, amygdala, less in the striatum. Astrocytic reactive gliosis and neuropil aggregates (GFAP, EM48), 16 weeks. Neuronal loss and neurodegeneration in the cortex and striatum, 20 weeks .	20-24 weeks.
R6/2 (chimeric fragment transgenic) CBAxC57BL/6 mix background strain	Human exon 1 N-terminal fragment: ~150 CAGs. HD promoter.	Progressive weight loss , 8 weeks. Accelerated rotarod deficit, 5 weeks. Clasping, 6 weeks. Increase in limb movement, 10 weeks . Decrease in grip strength, 11 weeks. Circling behavior, 12 weeks. Cognitive deficits: water Morris maze (3.5 weeks), T-maze (5 weeks), two choice swim tank (6.5 weeks), visual discriminate learning (7–8 weeks).	Decreased brain weight, 4 weeks. 44% decrease in brain volume, 41% decrease in striatal volume. Htt aggregates by postnatal day 1 in cortical layers II, V, VI, neostriatum and hippocampus. 25% reduction in striatal neuron number, 60% decrease in striatal neuron area and increase in reactive astrogliosis, 12 weeks. NIIs and neuropil aggregates, 12 weeks. Decrease in dopamine D1 and D2 receptors in striatum.	12-15 weeks.
Full length HD Cdna (chimeric full length transgenic) FVB/N background strain	CMV promoter: 89 CAGs.	Clasping, 8 weeks. Hyperactive, unilateral rotation, excessive grooming, 20 weeks. Decrease in exploratory and locomotor activity, 24 weeks .	PolyQ aggregates, 12 weeks. NIIs in cerebellum, cortex, hippocampus, thalamus, and <1% in striatum. Astrocytic reactive gliosis (GFAP). ~20% fewer striatal MSNs in homozygous (H&E and TUNEL staining).	Normal lifespan.
YAC 128 (chimeric full length transgenic) FVB/N background strain	Full length HD/mouse exon 1: 120 CAGs , HD promoter.	Hyperkinetic, 12 weeks and hypokinetic, 48 weeks (open field). Accelerated rotarod deficit, 24 weeks. Progressive cognitive deficits, 8 weeks (accelerated rotarod), 32 weeks (water Morris maze, open field habituation, and T-maze).	10.4–15% reduction in striatal and 7–8.6% in cortical volumes, 48 weeks. 9.1% reduction in striatal and 8.3% in cortical neuron number, 48 weeks. Striatal htt nuclear immunoreactivity (EM48), 12 weeks , >cortex, hippocampus, and cerebellum but no NIIs detected, 48 weeks. EM 48 positive inclusions detected in striatal cells, 72 weeks. Increase in NMDA receptor binding (dentate gyrus, inner cortex, and whole brain), increase in AMPA (cerebellum and whole brain), mGluR I (whole brain) and mGluR II receptor binding (dentate gyrus and whole brain). No change in striatal dopamine, GABA-A/B or adenosine receptor binding at 48 weeks.	Normal lifespan.
BACHD (chimeric full length transgenic) FVB/NJ mix background	Full length human huntingtin: 97 CAGs. HD promoter.	Weight gain of 20–30% compared to WT between 8 weeks and 24 weeks. Maintained weight gain between 24 weeks and 48 weeks. Subtle but significant motor impairment initially at 8 weeks (accelerated rotarod) and progressed by 24 weeks.	Gross atrophy (48 weeks). 20% decrease in whole brainweight compared to WT. 32% decrease in cortical and 28% decrease in striatal volume , 48 weeks. No significant striatal neuron loss, 48 weeks (NeuN staining, stereology). mhtt inclusions predominantly found in neuropil and few in cortex and striatum, 48 and 72 weeks (hematoxylin and EM48).	Normal lifespan.
Hdh/Q72-80 (knock-in) 129/Svx C57BL/6 mix background strain or 129/Svx FVB/N mix background strain	Hdh promoter: 72–80 CAGs.	Increased male aggression and a lesser extent in females, 12 weeks. No observed weight loss compared to WT, 72 weeks. Rotarod (non-accelerated) deficit beginning at 16 weeks (C57BL/6 N6 generation).	No neuron loss or reactive gliosis. No NIIs detected. No loss in enkephalin or calbindin immunoreactivity, 72 weeks. Neuropil aggregates, 28–96 weeks. Striatal nuclear htt aggregates, 96 weeks . Decrease in dopamine D2 receptor binding and increase in GABA/benzodiazepine receptor binding in the striatum and cortex, 68–72 weeks.	Normal lifespan.
HdhQ111 (knock-in) 129/CD1 mix background strain	Chimeric human/mouse exon1: 109 CAGs. Hdh promoter.	Gait impairment 96 weeks (painted-feet). No accelerated rotarod deficits.	Diffuse striatal nuclear-reactivity, 6 weeks (EM48). NIIs, 48 weeks. Striatal neuropil aggregates, 68 weeks. Neurodegeneration and reactive gliosis, 96 weeks (toluidine blue GFAP).	Normal lifespan.
HdhQ140 (knock-in) 129Sv/C57BL6 mix background strain	Chimeric human/mouse exon1: 140 CAGs. Hdh promoter.	No obvious abnormal behavior up to 48 weeks. No abnormal weight loss. Decrease in locomotor activity, 8–24 weeks (open field). Hyperactivity, 4 weeks and hypoactivity, 12 weeks. Gait abnormalities, 48 weeks (painted-feet).	Striatal htt nuclear staining at 8 weeks and more widespread by 24 weeks. Nuclear and neuropil aggregates prominent at 16 weeks in the striatum, nucleus accumbens, olfactory tubercle (EM48), as well as nuclear staining in cortical layers II/III, and V, hippocampus, and regions of the olfactory system.	Normal lifespan.
Hdh(CAG)150 (knock-in) 129/ Ola and C57BL/J6 mix background strain	Murine Hdh: 150 CAGs. Hdh promoter.	Motor abnormalities: Accelerated rotarod, Balance beam, painted-feet, 70–100 weeks. Resting tremor and ataxic, 100 weeks.	Striatal nuclear htt immunoreactivity, 28 weeks. Striatal NIIs, 37 weeks. Reactive astrocytic gliosis, 56 weeks. Robust striatal NIIs and striatal neuron receptor loss, 70–100 weeks. Loss of striatal perikarya and volume, 100 weeks. Decrease in striatal dopamine D1 and D2 receptors and dopamine transporters (DAT).	Normal lifespan.

Table 1

Genetic mouse models of HD. From (Heng et al., 2008).

1.4 Huntingtin protein structure and potential function

Huntingtin is a large protein of around 3150 amino acids (350 kDa), highly conserved among vertebrates (Baxendale et al., 1995, Tartari et al., 2008) and with no sequence homology with any other protein. It is expressed ubiquitously with highest levels in neurons of the central nervous system (Vonsattel and DiFiglia, 1998, DiFiglia et al., 1995), particularly in cortical pyramidal neurons in layers III and V that project to the striatum (Fusco et al., 1999). Inside the cell, it localises in different compartments such as nucleus (Kegel et al., 2002), cell body, neurites and synapses and associates with a number of organelles including Golgi (Strehlow et al., 2007), endoplasmic reticulum, mitochondria (Panov et al., 2002) and vesicles (DiFiglia et al., 1995). Its ubiquitous distribution and subcellular localisation make it difficult to understand the function, which at present is still not fully clarified.

HTT is a multi-domain protein (Fig. 4) with a polymorphic glutamine/proline (Q/P)-rich domain at the N terminus. The polyQ tract starts at amino acid 18 and it is immediately followed by two proline-rich domains (polyP) containing 11 and 10 prolines. Numerous proteins with Q/P-rich domains are involved in transcriptional regulation (Gerber et al., 1994), suggesting a similar function for this domain in HTT. Downstream of the polyQ domain there are HEAT (Huntingtin, Elongator factor3, PR65/A regulatory subunit of PP2A, and Tor1) repeats which are sequences of ~40 amino acids organised in 3 main clusters. The function of HEAT repeats is still unclear, although they seem to play a role in protein-protein interaction and are found in a variety of proteins involved in intracellular transport and chromosomal segregation (Andrade and Bork, 1995, Takano and Gusella, 2002), suggesting a similar function in HTT.

Other regions of interest in the HTT sequence are an export signal (NES) at the C-terminus and a nuclear localisation signal (NLS) at the N-terminus, that suggest that HTT might have a role in transporting molecules from the nucleus to the cytoplasm. In support of this, it has been shown that the 17 amino acids preceding the polyQ region interacts with the nuclear pore protein TPR (translocated promoter region) and allows HTT to shuttle to and from the nucleus (Cornett et al., 2005); and alterations in this amino acid sequence increases HTT nuclear accumulation of (Xia et al., 2003).

HTT contains also consensus cleavage sites for proteolytic enzymes such as caspase-3 and 7 at amino acids 513 and 552, caspase-6 at amino acid 586, caspase-2 at amino acid 552 (Hermel et al., 2004, Wellington et al., 2002, Wellington et al., 2000) and calpain (Gafni and Ellerby, 2002). Both wild-type and mHTT are cleaved by caspases into fragments but the mutant form is more susceptible to the cut and its fragments are more likely to aggregate into the inclusions found in cytoplasm and nucleus (Lunkes et al., 2002). The importance of cleavage in wild-type HTT is still unclear however, some lines of evidence show that modifications in the activity of caspase and calpain reduce the proteolysis and the toxic effect of the mutant protein, ultimately delaying disease progression (Wellington et al., 2002, Gafni and Ellerby, 2002, Ona et al., 1999, Graham et al., 2006).

HTT N-terminal region is subjected to post-translational modifications (Wang et al., 2010). Ubiquitination occurs at lysines (K) 6, 9, and 15 at the N-terminus and directs HTT to the proteasome for degradation (Kalchman et al., 1996). In the presence of mHTT the ubiquitin/proteasome system is impaired and causes accumulation of HTT fragments and inclusion formation. The same lysines can be also sumoylated and this modification reduces HTT accumulation and promotes repression of nuclear transcription (Steffan et al., 2004). Phosphorylation occurs at serine 421 by the protein kinase B (PKB or Akt) and at serine 434, 1181 and 1201 by the cyclin-dependent kinase 5 (CDK5) (Anne et al., 2007). Phosphorylation by Akt has been shown to be neuroprotective by reducing the pro-apoptotic activity of mHTT (Humbert et al., 2002), while phosphorylation by CDK5 reduces the cleavage of HTT by caspases at residue 513, diminishing aggregate formation and toxicity (Luo et al., 2005). Palmitoylation is carried out by the HTT partner Huntingtin-Interacting Protein 14 (HIP14), a palmitoyl acyl transferase (PAT) that binds to HTT and palmitoylates it at cysteine 241. This is important for vesicle trafficking and function and evidence showed that it is crucial for its normal trafficking to the Golgi (Yanai et al., 2006). In the presence of mutant HTT, reduced interaction between HTT and HIP14 and consequently reduced palmitoylation, increases aggregation and toxicity (Yanai et al., 2006, Singaraja et al., 2002).

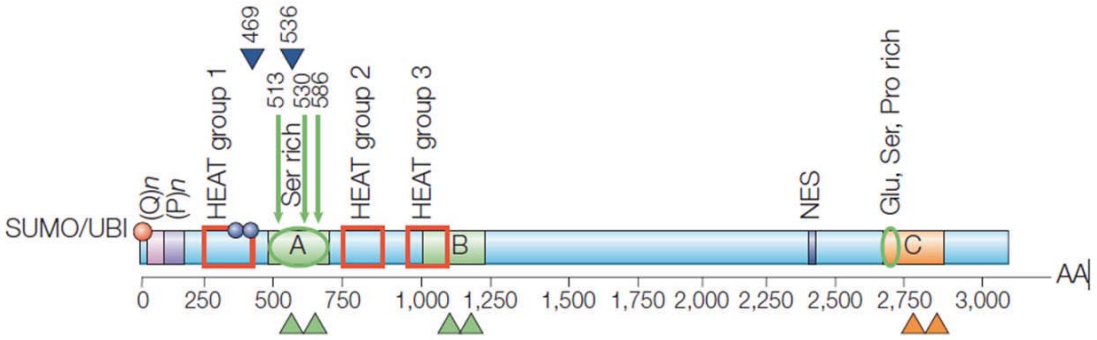

Fig. 4

Schematic representation of the AA sequence of Huntingtin protein. From (Cattaneo et al., 2005). *(Q)n = polyglutamine tract; (P)n = polyproline tract; red squares = three main clusters of HEAT repeats; arrows = caspase cleavage sites and their amino acid positions; blue arrowheads = calpain cleavage sites and their amino acid position. NES = nuclear export signal; red and blue circles = post-translational modifications: ubiquitination (UBI) and/or sumoylation (SUMO) (red), and phosphorylation at serine 421 and serine 434 (blue). The glutamic acid (Glu)-, serine (Ser)- and proline (Pro)-rich regions are indicated (serine-rich regions encircled in green).*

Given the large size and the complexity of its structure, it is not surprising that wild-type HTT interacts with a great variety of partners, in this way influencing a number of biological functions; and that these are lost or aberrantly carried out by mutant HTT in disease.

1.5 Mechanisms of pathogenesis: loss of function vs gain of function

Given the large number of functions, HTT is a very important protein and its loss or reduced activity alters fundamental biological processes. In HD, it is now accepted that it is the combination of *loss of function* of HTT and toxic *gain of function* of mHTT to trigger neuropathology (Zuccato et al., 2010).

Normal Huntingtin function

Several studies have tried to identify the exact function of HTT linked to HD symptomatology. Despite a specific role has not been found, these studies have demonstrated the importance of wild-type HTT both in development and in adulthood in mammals (Cattaneo et al., 2005):

- *Role in embryogenesis:* HTT is important for embryonic development. Its complete inactivation in knock-out mice (Hdh-/-) is lethal before gastrulation and formation of the nervous system (Duyao et al., 1995, Nasir et al., 1995, Zeitlin et al., 1995) while conditional knock-out in forebrain and testes results in progressive degenerative neuronal phenotype and sterility, suggesting that the protein is required for neuronal function and survival in the brain (Dragatsis et al., 2000). Expression of mHTT in knock-out mice rescued from embryonic lethality (Leavitt et al., 2001, Van Raamsdonk et al., 2005a) and humans homozygous for HTT mutation develop normally (Wexler et al., 1987), suggesting that mHTT can compensate for the absence of normal HTT during development. After gastrulation in mice, reduction in HTT level below 50% causes defects in the epiblast, structure that gives rise to the neural tube, and malformations in cortex and striatum (White et al., 1997), indicating that HTT participates in the formation of the CNS. Moreover, HTT plays a role in neuronal survival; experiments on chimeras created by injection of Hdh-/- embryonic stem cells into the blastocyst showed cell degeneration specific to the striatum, cortex and thalamus, supporting the idea that in these areas HTT synthesis is required for neuronal development and differentiation (Reiner et al., 2003);

- *Anti-apoptotic role: In vitro* experiments on conditionally immortalized striatum-derived cells demonstrated that overexpression of wild-type HTT is neuroprotective in cells exposed to various apoptotic stimuli (Rigamonti et al., 2000, Rigamonti et al., 2001); *in vivo*, mice with null mutations of HTT in neurons showed apoptotic cells in the hippocampus, cortex, and striatum which led to neurological abnormalities and progressive degeneration (Dragatsis et al., 2000). The mechanisms of HTT protection from apoptotic cell death have been partially elucidated. Wild-type HTT directly inhibits the proteolitic action of caspases such as caspase 3 and 9 or inhibits the formation of the pro-apoptotic complex constituted by the huntingtin interacting protein 1 (HIP1) and its interacting partner HIP-1 protein interactor (HIPPI), which controls the activation of caspase 8 (Rigamonti et al., 2000, Rigamonti et al., 2001). Moreover, HTT is a substrate for the kinase Akt which is involved in activating survival pathways and blocks cell death (Rangone et al., 2004,

Humbert et al., 2002), thus HTT might act as a survival factor in the phosphoinositide 3-kinase (IP3K)/Akt signaling pathway and contribute to stimulate the expression of survival genes such as Bcl-xL or brain derived neurotrophic factor (BDNF) and repress pro-apoptotic genes such as BAX or Bcl-2 (Harjes and Wanker, 2003);

- *Role in controlling BDNF production:* HTT stimulates cortical production of brain derived neurotrophic factor (BDNF), a neurotrophin important for survival of striatal neurons. *In vitro* and *in vivo* studies showed that wild-type HTT, and not the mutated form, stimulates cortical BDNF production by regulating its gene transcription (Zuccato et al., 2001). In particular, HTT enhances transcription from BDNF promoter II which contains the silencing sequence repressor element-1 (RE1) recognised by the repressor element-1 transcription factor (REST), a transcriptional repressor of BDNF transcription. HTT binds to REST and sequesters it in the cytoplasm thus inhibiting its translocation into the nucleus and its activity (Zuccato et al., 2003). The binding of HTT to REST occurs indirectly through the formation of a complex with HAP1 and REST-interacting LIM domain protein (RILP), a protein that directly binds REST and promotes its nuclear translocation (Shimojo, 2008);

- *Role in axonal transport:* HTT is associated with vesicles (DiFiglia et al., 1995, Block-Galarza et al., 1997) and enhances both anterograde and retrograde transport of vesicles containing neurotransmitters, neurotrophic factors such as BDNF and organelles, through binding to the microtubules. In support of this role, studies in *Drosophila* showed that reduction of HTT disrupts axonal transport and causes degeneration in the eye (Gunawardena et al., 2003). In primary cortical neurons, wild-type HTT was shown to stimulate BDNF vesicular trafficking and this effect was attenuated by reducing its levels by RNAi (Gauthier et al., 2004). Other *in vitro* and i*n vivo* studies also implicated HTT in fast axonal transport (FAT) of mitochondria in mammals: in primary striatal neurons taken from mice expressing only one copy of the wild-type allele or knock-down expressing <50% of normal HTT, mitochondria were progressively immobilized (Trushina et al., 2004). HTT associates with microtubules by direct binding with dynein intermediate chain (Caviston et al., 2007) and indirect binding with huntingtin-associated protein-

1 (HAP1) which in turn interacts with the p150(Glued) subunit of dynactin and kinesin (Engelender et al., 1997, Li et al., 1998, Gauthier et al., 2004, McGuire et al., 2006);

- *Role in synaptic activity:* HTT interacts with cytoskeletal and synaptic vesicles proteins essential for exo- and endocytosis at the synaptic terminals controlling synaptic activity in neurons (Smith et al., 2005). Direct binding of HTT with the Src homology 3 (SH3) domains of the postsynaptic density protein 95 (PSD-95) controls its binding to N-methyl-D-aspartate (NMDA) and kainate glutamate receptors and ultimately glutamate release; overexpression of HTT has been reported to attenuate neuronal toxicity induced by NMDA receptors and mHTT (Sun et al., 2001).

All the above mentioned roles reveal the importance and beneficial effects of wild-type HTT in the mature brain and several lines of evidence showed its loss in HD contributes to neuropathology. Both in humans and mouse models, a more severe phenotype was found in homozygotes for the HD mutations compared with heterozygotes with the same CAG expansion (Reddy et al., 1998, Squitieri et al., 2003). In YAC128 mice lacking expression of wild-type HTT (YAC128-/-) but expressing the same amount of mHTT as normal YAC128 mice (YAC128+/+), performance in the rotarod test of motor coordination was disrupted and testicular atrophy and degeneration were markedly worsened (Van Raamsdonk et al., 2005a). Moreover, an *in vivo* study on YAC transgenic mice showed direct evidence of a role of wild-type HTT in decreasing HTT cellular toxicity. In these mice, increased apoptosis in male testes in the presence of mHTT and absence of the wild-type form was rescued by increasing endogenous HTT levels (Leavitt et al., 2001). All these data suggested that elimination of wild-type HTT expression results in the exacerbation of behavioural deficits and survival although the absence of more severe striatal abnormalities indicated that the striatal phenotype is dependent primarily on mHTT toxicity.

The role of mutant Huntingtin in neurodegeneration

The exact mechanism of neurotoxicity induced by mHTT has not been yet clarified however, a number of biological processes have been demonstrated to be influenced

by the mutant protein and several theories have been proposed to explain its toxic role (Zuccato et al., 2010) (Fig. 5):

- *Transcriptional dysregulation:* microarray studies revealed alterations of gene expression in cellular and mouse models of HD at an early stage of HD, before symptom onset, suggesting that transcriptional dysregulation is an important causative factor in the disease. Altered mRNAs were those associated with transcriptional processes, neurotransmitter receptors, synaptic transmission, cytoskeletal and structural proteins, intracellular signaling, and calcium homeostasis, all affected in HD (Sipione et al., 2002, Luthi-Carter et al., 2000, Luthi-Carter et al., 2002, Chan et al., 2002). Both HTT and mHTT directly bind to several transcriptional regulators such as specificity protein 1 (Sp1), TATA-box-binding protein-associated factor II, 130kDa(TAFII130), cAMP-response–element binding protein (CREB) and repressor element 1-silencing transcription factor/neuron-restrictive silencing factor (REST/NRSF) (Buckley et al., 2010) thus regulating expression of a number of genes. Aberrant protein–protein interaction of mHTT with the transcriptional machinery either by direct interaction with genomic DNA or by modification of chromatin such as histone modification, is accounted for the dysregulation. Indeed, mHTT aberrantly binds to specific transcription factor proteins forming an inactive transcriptional complex that functions essentially as a repressor or forms complexes with co-repressor proteins and therefore aberrantly de-represses transcription of normally silent genes (Cha, 2000). Moreover, mHTT sequesters transcription factors through aberrant interactions, depleting the levels of required factors within the cell (Cha, 2007, Kumar et al., 2014). For instance, mHTT abnormal binding to REST leads to the translocation of the latter into the nucleus where it acts by inhibiting BDNF transcription and production (Zuccato et al., 2003, Shimojo, 2008);

- *Excitotoxicity:* alterations in the glutamatergic neurotransmission have been found in HD brains. In the cortex of HD patients, over-activation of glutamate receptors is triggered by an increased release of glutamate from cortical afferents and by a reduced uptake by glial cells where mHTT is also expressed. Loss of striatal glutamate N-Methyl-D-aspartate (NMDA) receptor binding sites is also observed in early symptomatic HD patients and even in pre-

symptomatic stages as well as changes in their subunit composition which alters the function (Albin et al., 1990b, DiFiglia, 1990, Dure et al., 1991, London et al., 1981, Young et al., 1988). Moreover, hypersensitivity of NMDAR on striatal projection neurons leading to impaired synaptic plasticity (Fan and Raymond, 2007), linked to altered intracellular Ca^{2+} homeostasis and mitochondrial dysfunction as downstream consequences, is believed to contribute to neuropathology (DiFiglia, 1990, Beal et al., 1986, Coyle and Schwarcz, 1976). mHTT aberrant interaction with the post synaptic density 95 (PSD95), a scaffolding protein at the excitatory postsynaptic density, results in the sensitization of NMDA receptors and promotes neuronal apoptosis induced by glutamate (Sun et al., 2001); mHTT also induces phosphorylation of NMDAR subunits and contributes to over-activation of NMDAR (Song et al., 2003). Finally, mHTT alters NMDAR trafficking destabilizing the complex HTT-HIP1 responsible for NMDAR endocytosis (Metzler et al., 2007). Moreover, mHTT binds the C-terminus of the inositol 1,4,5-triphosphate receptor 1 (InsP3R1) on the endoplasmic reticulum and makes the receptors more sensitive to IP3, leading to increased calcium release from InsP3R1 (Tang et al., 2003). Recent studies demonstrated that the consequences of NMDAR activity are determined by the subcellular location of the receptor: synaptic NMDAR transmission drives neuroprotective gene transcription (Kohr, 2006), whereas extrasynaptic NMDAR activation promotes cell death. Extrasynaptic receptors are increased in HD mouse striatum and this is believed to contribute to neuropathology, as pharmacological block of extrasynaptic NMDARs with the selective antagonist memantine reversed motor learning deficits observed in mice (Milnerwood et al., 2010, Zhou et al., 2013);

- *Aggregate toxicity:* mHTT is more likely to be cleaved by caspases than wild-type HTT. The cleavage of mHTT releases N-terminal toxic fragments that easily aggregate and accumulate in the nucleus leading to activation of other proteolytic enzymes responsible for cell death (Davies et al., 1997, DiFiglia et al., 1997, Kim et al., 2001, Lunkes et al., 2002, Wellington et al., 2002). The toxicity of nuclear aggregates is based on the evidence that inclusion formation in cultured cells leads to cell death (Hackam et al., 1998, Ho et al., 2001).

Studies report that mHTT aggregates accumulate in the nucleus and sequester transcriptional regulators of important neuron survival genes (Cha, 2007, Nucifora et al., 2003). In contrast, some studies support the idea of a non-pathogenic role of these aggregates which would be an attempt to reduce the soluble more toxic fraction of the mutated protein (Kuemmerle et al., 1999, Saudou et al., 1998). In addition to nuclear inclusions, the presence of mHTT aggregates is found in neuronal processes and axonal terminals where they are correlated with disease progression and axonal degeneration in HD mice (Li et al., 1999a, Li et al., 2001). Extranuclear or neuropil aggregates are reported to impair axonal transport, synaptic vesicle recycling and receptor endocytosis by aberrantly interacting with proteins involved in these processes or physically impairing axonal transport (Gunawardena et al., 2003, Li et al., 2001, Li and Conforti, 2013);

- *Autophagy:* in the presence of mHTT aggregates, the inhibitor of the mammalian Target Of Rapamycin (mTOR), an activator of autophagy, is sequestered into the aggregates and clearance of the aggregates is enhanced (Ravikumar et al., 2004). This suggests a positive role of mHTT aggregates. A recent study showed that HTT and HAP1 are regulators of autophagosome transport in neurons and that in the presence of mHTT, abnormal transport leads to inefficient autophagosome maturation and results in defective clearance of both mHTT aggregates contributing to neurodegeneration and cell death in HD (Wong and Holzbaur, 2014);

- *Mitochondrial dysfunction:* mHTT perturbs mitochondrial function by altering transcription of nuclear-encoded mitochondrial proteins or by direct interaction with the organelle and modulation of its metabolic activity and trafficking. Abnormal interaction between mHTT and the transcriptional regulator p53 results in p53 increased levels in the nucleus and increased transcriptional activity, leading to the upregulation of pro-apoptotic targets as well as mitochondrial membrane depolarization (Bae et al., 2005); mHTT also represses the transcription of genes involved in mitochondria biogenesis and respiration (Cui et al., 2006). Altered mitocondrial morphology and dynamics are also reported in HD (Costa and Scorrano, 2012). Abnormal interaction between mHTT and molecular motors or physical blockade exerted by mHTT

inclusions along the axons causes reduction in mitochondrial motility (Orr et al., 2008, Trushina et al., 2004, Reddy and Shirendeb, 2012); mHTT elicits an imbalance in mitochondrial fission and fusion that initiates neurodegeneration (Reddy and Shirendeb, 2012, Labbadia and Morimoto, 2013, Guo et al., 2013).

Given the multiple roles of HTT and mHTT in controlling biological processes, therapeutic intervention needs to focus on multiple targets in order to alleviate disease.

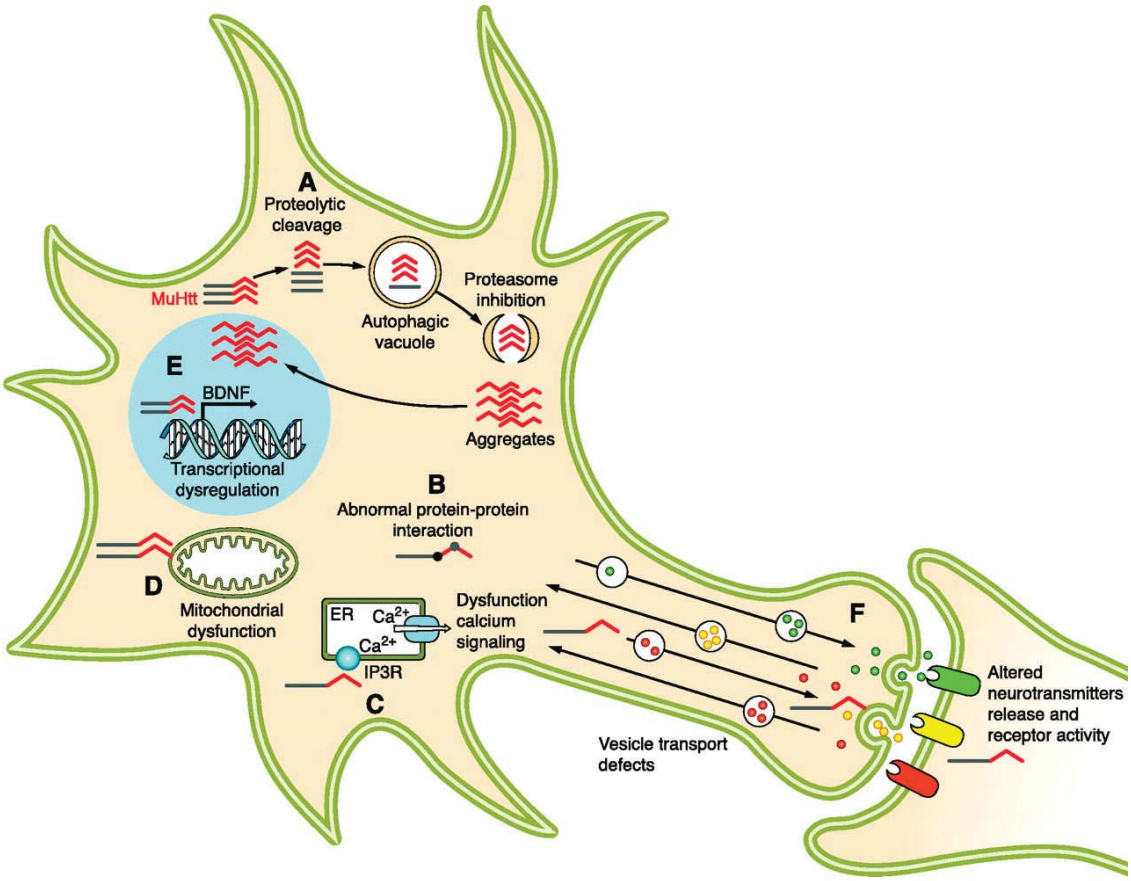

Fig. 5

General scheme of the proposed pathologic pathways involved in HD. From (Zuccato et al., 2010). *(A) mHTT causes a conformational change of the protein that leads to partial unfolding or abnormal folding of the protein, which can be corrected by molecular chaperones. Full-length mHTT is cleaved by proteases in the cytoplasm. In an attempt to eliminate the toxic HTT, fragments are ubiquitinated and targeted to the proteasome for degradation. However, the proteasome becomes less efficient in HD. Induction of the proteasome activity as well as of autophagy protects against the toxic insults of mHTT proteins by enhancing its clearance. B: NH2-terminal fragments containing the polyQ strech accumulate in the cell cytoplasm and interact with several proteins causing impairment of calcium*

signaling and homeostasis (C) and mitochondrial dysfunction (D). E: NH2-terminal mutant huntingtin fragments translocate to the nucleus where they impair gene transcription or form intranuclear inclusions. F: the mutation in huntingtin alters vesicular transport and recycling. muHtt, mutant huntingtin.

1.6 Current therapies and targets for therapeutic intervention

Currently no effective therapies for preventing or delaying the onset of HD are available. Therapies are symptomatic and include the use of antichoreic drugs to control the involuntary movements and the use of psychotropic medications to address depression, obsessive compulsive symptoms, or psychosis. Medications often have side effects and do not repair damage or stop the disease from progressing. Speech therapy and physical therapy are useful in addressing the swallowing and walking difficulties that many HD patients experience (Bilney et al., 2003).

Genetic animal models provide an opportunity to test potential treatments to translate to human patients, and therapies successful in mice represent good candidates for clinical trials. So far, therapeutic strategies in animal models of HD have been focusing on the following targets:

- Reducing aggregate formation through pharmacological targeting of toxic conformational changes of mHTT. A polyphenol (epigallocatechin gallate (EGCG)) was found to decrease toxic forms of mHTT (Ehrnhoefer et al., 2008) while an aggregation inhibitor (a sulfobenzoic acid derivative termed C2-8) showed a beneficial effect on behavioural phenotypes and striatal neuronal volume in the R6/2 mouse model of HD although it had no effect on survival (Chopra et al., 2007). Intracellular antibodies developed against an epitope of human HTT specifically bind to mHTT and reduce its toxicity in cellular and animal models (Colby et al., 2004, Khoshnan et al., 2002, Wang et al., 2010, Wolfgang et al., 2005);

- Enhancing clearance of aggregates through autophagy. Treatment with rapamycin or its analog CCI-779, inhibitors of mTOR, stimulated mHTT clearance in cells (Ravikumar et al., 2004, Ravikumar et al., 2002) and improved phenotype in fly and mouse models of HD (Ravikumar et al., 2004);

- Reducing proteolitic cleavage of HTT. Studies in transgenic YAC mice expressing mutant HTT with alterations at the position 586, cleavage site for caspase 6, showed reduced pathological effects (Graham et al., 2006). Inhibition of caspases 1 and 3 has been proved to be beneficial in mouse models of HD (Chen et al., 2000, Ona et al., 1999) and in patients, treatment with the caspase inhibitor minocycline resulted in slight improvements in both neuropsychological performance and motor function (Bonelli et al., 2003, Thomas et al., 2004);

- Targeting abnormal gene expression due to transcription dysregulation. Administration of inhibitors of histone deacetylases (HDACs), enzymes which cause transcriptional repression, were found to ameliorate the HD phenotype in mouse and invertebrate models (Steffan et al., 2001, Hockly et al., 2003, Pallos et al., 2008, Bates et al., 2006), and are now ready to be used in clinical trials phase I;

- Targeting excitotoxicity blocking the excessive release of glutamate or its action at the postsynaptic receptors. Glutamate receptor blockers have been used on HD patients with disappointing results: a clinical trial of lamotrigine, a glutamate antagonist, showed no significant effect on slowing disease progression despite a reduction in chorea (Kremer et al., 1999); other glutamate antagonist under trial such as riluzole (Landwehrmeyer et al., 2007) and remacemide (Huntington Study, 2001) had same negative results. Studies in HD mice revealed that therapeutic treatments aimed at blocking NMDA receptors should be designed to target extrasynaptic receptors. In YAC mice, treatment with low but not high dosages of memantine ameliorated adverse neuropathological and behavioural effects (Okamoto et al., 2009). Indeed, memantine at low dosages, more selectively targets the extrasynaptic receptors (Hardingham and Bading, 2010). A pilot study on human patients showed promising results of the use of memantine (Ondo et al., 2007);

- Targeting reduced mitochondrial activity and energy impairment. Treatments aimed at amelioration of the cellular energy deficit and improvement of mitochondrial function in HD through the use of metabolic antioxidants (creatine, α-lipoic acid, N-acetyl-carnitine and coenzyme Q10), which are

involved in cellular energy production and act as cofactors of several metabolic enzymes, could be beneficial (Moreira et al., 2010). In transgenic mice, treatment with Q10 was found to promote survival, attenuate striatal lesions and reduce weight loss and motor deficits (Matthews et al., 1998) and in patients, two major phase III trials (2CARE and CREST-E) are testing coenzyme Q10 and creatine, respectively. Treatments with inhibitors of the enzyme kynurenine 3-monooxygenase (KMO), key enzyme of the kynurenine pathway which is disrupted in HD, also ameliorates behavioural and neuropathological deficits in HD models (Thevandavakkam et al., 2010);

- Reducing the amount of pathogenic protein by genetic manipulation such as conditional knock-out or siRNA, aiming at decreasing mHTT production (Yamamoto et al., 2000, DiFiglia et al., 2007, Boudreau et al., 2009) or by enhancing clearance through autophagy and lysosome system (Renna et al., 2010) or molecular chaperones (Perrin et al., 2007, Vacher et al., 2005). Yamamoto and collaborators showed for the first time that blockade of expression of mHTT in a conditional transgenic mouse model of HD at symptomatic stage, leads to the disappearance of inclusions and to the amelioration of the behavioural phenotype (Yamamoto et al., 2000). In a more recent study performing selective reduction of mHTT expression in cortex, striatum or both brain areas, in a conditional transgenic HD mouse model, demonstrates distinct but interacting roles of cortical and striatal mHTT in HD pathogenesis and suggests that optimal HD therapeutics may require targeting mHTT in both cortical and striatal neurons (Wang et al., 2014). Another approach based on allele-specific silencing of mHTT targeting single nucleotide polymorphisms (SNP), proved to be successful in a BACH mouse model of HD and in HD human stem cells resulted in functional recovery of the vesicular transport of BDNF along microtubules (Drouet et al., 2014). In patients, gene therapy using siRNA and shRNA to silence CAG repeats have also shown promising results (Brett et al., 2014);

- Reducing loss of BDNF, crucial for striatal neuronal survival. *In vitro*, administration of BDNF to cultured mammalian neurons or to primary neurons expressing mHTT was found protective against the toxicity induced by the mutant protein (Saudou et al., 1998, Zala et al., 2005). Other *in vivo* studies in

R6/1 and R6/2 mice treated intrathecally via a mini-pump confirmed the neuroprotective effect of BDNF delivery (Canals et al., 2004, Giampa et al., 2013). Limitations to this approach include the difficulty to determine the actual amount of BDNF reaching the affected neurons as BDNF is quite unstable and only a small quantity crosses the blood brain barrier; and clinical trials based on subcutaneous or intrathecal administration had little success (Zuccato and Cattaneo, 2007). More recently, other methods of administration such as *in vivo* and *ex vivo* gene transfer aimed at stimulating the synthesis of endogenous BDNF, or the use of BDNF mimetic drugs have been investigated (Nagahara and Tuszynski, 2011).

- Targeting cell loss through striatal and stem cell transplantation. Preclinical studies on mouse excitotoxic HD models showed that foetal striatal grafts transplanted into the lesioned area can survive and improve motor and cognitive impairment (Dunnett et al., 1998, van Dellen et al., 2001) suggesting that grafts restore functional circuits with the cortex (Dunnett, 1995). Clinical trials on HD patients using human striatal foetal tissue from spontaneously aborted foetuses were carried out with contrasting results. A successful transplant where increases in motor and cognitive function were seen 2 years after implant of intrastriatal grafts was described by Bachoud-Levi and colleagues (Bachoud-Levi et al., 2000) but 6 years after graft implant the same group reported that the initial beneficial effects were largely lost (Bachoud-Levi et al., 2006). Transplant of embryonic stem cells (Aubry et al., 2008) or induced pluripotent stem cells extracted from adult somatic cells into rodents showed that these did form clusters of medium spiny neurons but they also induced the formation of tumours (Roy et al., 2006). Further studies are needed to improve the quality and quantity of the neurons obtained and to establish whether this approach could be one day safely and effectively transferred to human patients.

1.7 Axon degeneration in neurodegenerative diseases

The axon is the most extensive part of a neuron accounting for up to 99.8% of the total volume of the cell. In adult humans it can stretch up to 1 m in length in motoneurons

and collateral branches can further increase the total volume. Such a long structure is required to connect functionally distant regions and deliver electric impulses, newly synthesized molecules and other axonally-transported molecules and organelles from the cell body to the axon terminal, but at the same time represents a vulnerable structure that can be affected in many pathological conditions (Perlson et al., 2010). Not surprisingly, several types of insults such as mechanical lesions, chemical toxins, metabolic or neurodegenerative disorders can affect the axon and trigger a similar degenerative process.

The first to describe the process of degeneration of an axon was Augustus Waller in 1850. After lesioning of the glossopharyngeal and the hypoglossal nerves of a frog, Waller observed that the distal stump of nerves from the site of injury, which were separated from their cell bodies, became disorganized by 5-6 days after the cut and by 12-15 days all structures were completely degenerated (Stoll et al., 2002). This process was named after him "Wallerian degeneration (WD)" and became an important experimental tool to study the mechanisms underlying these events in both peripheral and central nervous system. In mammals, WD normally occurs over a time course of around 24-48 h following mechanical (transection, crush and blunt trauma), chemical (acrylamide), or metabolic (ischemia) injury (Neukomm and Freeman, 2014). Early morphological changes during WD are focal swelling and beading of the axons (Waller, 1850) followed by disintegration and degeneration of the axoplasma and axolemma which is completed within 24-48 h (George et al., 1995). Subsequently, breakdown of myelin sheath occurs, macrophage infiltration and Schwann cell proliferation (LeBlanc and Poduslo, 1990) to clear axonal remains and to promote regenerative attempts at the proximal stump (Fig. 6). Cytoskeleton breakdown is mediated by extracellular calcium influx and involves activation of axonal proteases (Schlaepfer and Bunge, 1973, George et al., 1995). During this process, molecular changes such as upregulation of neurotrophins, cytokines and neural cell-adhesion molecules produced by Schwann cells occur in the degenerating distal stump of the nerve (Stoll and Muller, 1999, Kury et al., 2001).

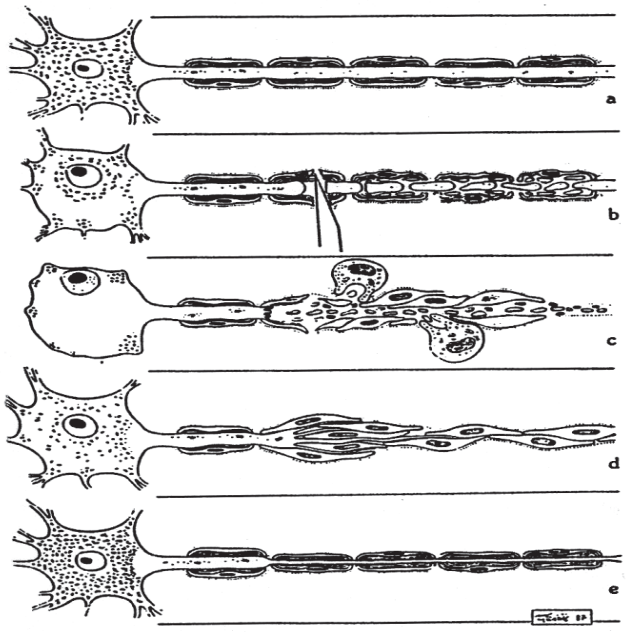

Fig. 6

Schematic representation of Wallerian degeneration. From Weiqian Mi PhD dissertation, 2003*. (a) Intact axon with its surrounding myelin sheath, (b) fragmentation of axon and myelin following cut, (c) phagocytosis of axon and myelin fragments by macrophages, (d) Schwann cells guide regeneration of nerve, (e) Regenerated fibers.*

WD shares morphological features with axonal pathology in some disease states such as toxic or genetic neuropaties, inflammation and neurodegenerative disorders such as Alzheimer's disease (AD), Parkinson's disease (PD), multiple sclerosis (MS) or amyotrophic lateral sclerosis (ALS), which for this reason is known as "Wallerian like" degeneration (Coleman and Freeman, 2010). Increasing evidence suggests that axonal degeneration occurs early in neurodegenerative diseases often determining the course of pathology (Conforti et al., 2007a). For example, in MS, magnetic resonance (MR) studies have detected early loss of axons, suggesting that axon pathology may precede degeneration of other neuronal compartments (Narayanan et al., 1997, van Waesberghe et al., 1999). In AD, live imaging using transgenic or virally-encoded fluorescent proteins revealed highly dystrophic axons close to amyloid plaques and dendrites losing spines before breaking (Tsai et al., 2004, Spires et al., 2005); and *in vitro* and *in vivo* imaging of fluorescent neurons in AD mice crossed with yellow fluorescent protein mice (YFP-H) revealed dystrophic axons close to the amyloid plaques in the absence of cell-body death (Adalbert et al., 2009, Crowe and Ellis-

Davies, 2013). In addition, immunohistochemistry studies for β-amyloid precursor protein (β-APP) showed that β-APP accumulates in damaged axons in areas of acute inflammation and demyelination (Sherriff et al., 1994, Ferguson et al., 1997). In ALS considerable axonal loss is found both in human and in animal models. Studies on transgenic mice expressing mutant Cu/Zn superoxide dismutase (SOD1) showed that axon degeneration parallels symptom onset (Fischer et al., 2004, Pun et al., 2006). Mutant α-synuclein transgenic mouse models of PD also show early synapse loss and Lewy with axonal swellings (Martin et al., 2006). Although the axonal damage in each of these disorders may be the result of a variety of different triggers, the similarity in pathology suggests the existence of an underlying common mechanism in axon degeneration. The study of the molecular mechanisms underlying WD is therefore useful to elucidate pathology in these diseases and the axon could be a promising target for therapeutic intervention (Conforti et al., 2014).

Axon degeneration in HD

Much is still unknown about axon degeneration in HD. Morphological alterations in dendritic arbors and spines of MSSNs, as well as in axons, have been reported in early studies on post-mortem material from HD patients using Golgi impregnation (Graveland et al., 1985) and immunostaining with calbindin D28K (Ferrante et al., 1991) and with SMI32 and SMI31 (Nihei and Kowall, 1992). More recently, the use of *in vivo* neuroimaging has revealed reduction of fractional anisotropy, measure of white matter integrity, in presymptomatic HD subjects indicating early white matter disorganization (Reading et al., 2005, Weaver et al., 2009); and several studies have related white matter abnormalities in early patients to deficits in behaviour (Dumas et al., 2012, Beglinger et al., 2005). In animal models, behavioural abnormalities resemble those seen in HD patients and often appear at a stage of the disease where no overt signs of neuropathology are present, suggesting that neurological dysfunction more than cell loss is responsible for the behavioural phenotype (Crook and Housman, 2011). Morphological and functional dendritic abnormalities have been reported in several HD mice (Guidetti et al., 2001, Laforet et al., 2001, Milnerwood et al., 2010, Lerner et al., 2012) as well as alterations in synaptic activity (Cepeda et al., 2003, Milnerwood et al., 2006, Cummings et al., 2007) and abnormalities in the expression and release of neurotransmitter receptors (Cha et al., 1999, Klapstein et al., 2001, Li et al., 2003, Andre et al., 2006) and synaptic vesicle proteins at early stage (Smith et al.,

2005). Impaired axonal trafficking of synaptic vesicles and mitochondria, by increased stalling of transported vesicles, was detected at early stage in *C. elegans* and *Drosophila* models of HD (Gunawardena et al., 2003, Parker et al., 2001, Sinadinos et al., 2009) as well as in mammalian neurons (Trushina et al., 2004, Chang et al., 2006). Abnormalities have also been detected in axons of transgenic HD mice but whether these precede or parallel symptom onset and cell body degeneration remains unclear (Li et al., 2001). Thus, further investigations are needed to assess whether axon degeneration occurs before death of other neuronal compartments and can be a target for future therapeutic strategies.

1.8 Axon degeneration as a therapeutic target

Historically research on neurodegenerative diseases has focused on the cell body as it was commonly believed that axon degeneration occurred as a secondary event following cell body death. For long time, axon degeneration has been considered a passive breakdown of the axon due to lack of cell body-derived trophic factors (Lubinska, 1977, Lubinska, 1982) or activation of Ca^{2+}-dependent proteases (Schlaepfer and Hasler, 1979) and not surprisingly therapeutic approaches aiming at protecting the cell body compartment only had not been successful in long-term trials.

The discovery of the spontaneous mutant mouse *Wld*^{S} (Wallerian degeneration slow) (Perry et al., 1990) drastically changed this assumption and highlighted that axon degeneration is an active self-destructing process involving a determined molecular cascade which is different and independent from apoptosis (Raff et al., 2002, Whitmore et al., 2003, Deckwerth and Johnson, 1994). In the *Wld*^{S} mouse, axon degeneration after acute injury is delayed by 10-fold and a stable synaptic activity is recorded for more than 2 weeks after separation from the cell body (Lunn et al., 1989). The spontaneous mutation responsible for this phenotype has been identified as an 85 kb tandem triplication mapping to mouse chromosome 4 (Coleman et al., 1998). This unusual rearrangement brings two endogenous genes together forming a chimeric gene that encodes an in-frame fusion protein that is absent in wild-type mice (Coleman et al., 1998, Conforti et al., 2000). The protein contains the amino (N)-terminal 70 amino acids (N70) fragment of the ubiquitination factor E4B (UBE4B), the complete sequence of the enzyme nicotinamide adenylyltransferase 1 (NMNAT1) and a linking portion of 18 AA originally belonging to the 5' untranslated region of

the *Nmnat1* gene (Conforti et al., 2000) (Fig. 7). NMNAT is the central enzyme of NAD synthesis and it catalyses the reaction NMN + ATP => NAD + PPi, the last step in all NAD biosynthetic pathways. NMNAT1 is one of the three mammalian NMNAT isoforms (1, 2 and 3) which have different subcellular localization. NMNAT1 is a nuclear protein while NMNAT2 and 3 are mainly associated with Golgi and mitochondria, respectively (Berger et al., 2005). N70 contains, in its N-terminal 16 amino acids (N16) region, a binding site for the valosin containing protein (VCP), a ubiquitous cytoplasmic AAA-ATPase with several roles including one in the ubiquitin proteasome system (UPS) (Laser et al., 2006). The direct binding of WLD^s to VCP is responsible for the distribution of WLD^s in nuclear foci (Wilbrey et al., 2008). It has been demonstrated that both N70 and NMNAT1 are required for the protecting phenotype *in vivo* (Conforti et al., 2009, Conforti et al., 2007b).

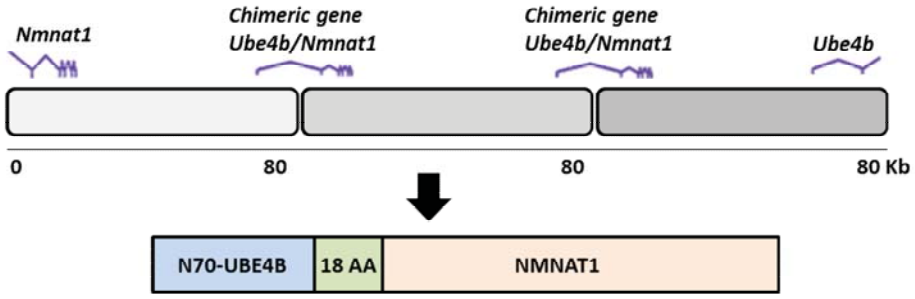

Fig. 7

Schematic representation of Wld^S gene. *An 85Kb tandem triplication results in a chimeric gene that encodes for a chimeric protein, a fusion of the N-terminal seventy amino acids of the ubiquitination factor E4b (UBE4B), the full sequence of the enzyme nicotinamide mononucleotide adenylyltransferase 1(NMNAT1) and a linking portion of 18 AA originally belonging to the 5' untranslated region of the Nmnat1 gene.*

Introducing the Wld^S gene in the genome of different species replicates the protecting phenotype. For example, it was found to protect physically injured axons in transgenic rats (Adalbert et al., 2005), injured olfactory receptor neurons (ORN) in Drosophila (Hoopfer et al., 2006, MacDonald et al., 2006) and axotomised trigeminal neurons in zebrafish (Martin et al., 2010), suggesting a similar conserved mechanism trough evolution. Importantly, Wld^S neuroprotective efficacy extends to a variety of disease models suggesting that similar mechanisms regulate axon degeneration in both acute

injuries and chronic diseases. For example it was found to extend life span and alleviate symptoms in the progressive motor neuronopathy (*pmn*) mouse model of motoneuron disease (Ferri et al., 2003), in Parkinson's disease mouse models (Sajadi et al., 2004, Hasbani and O'Malley, 2006), in a rat glaucoma model (Beirowski et al., 2008) and in a gracile axonal dystrophy mouse model (Mi et al., 2005). However, *Wld*^{S} failed to protect in some model of neurodegenerative diseases including a mutant SOD1 mouse model of ALS (Vande Velde et al., 2004, Fischer et al., 2005), in mouse models of spinal muscular atrophy (SMA) (Kariya et al., 2009) and in prion infected mice (Gultner et al., 2009), suggesting that there are distinct pathways to axon degeneration that can be distinguished by their sensitivity to *Wld*^{S} (Conforti et al., 2014).

The molecular mechanisms of *Wld*^{S}-mediated protection are still not fully understood but progresses have been made in understanding since its first discovery (Coleman and Freeman, 2010, Wang et al., 2012, Conforti et al., 2014). WLD^s is predominantly nuclear (Mack et al., 2001) but recent studies reported a cytoplasmic and potentially axonal site of action (Beirowski et al., 2009, Sasaki et al., 2009a, Yahata et al., 2009, Babetto et al., 2010, Cohen et al., 2012). The binding of VCP protein to the N16 region of N70 allows the relocation of nuclear NMNAT1 to the axon where it acts to confer the protective phenotype. In ΔN16*Wld*^{S} transgenic mice, lacking the N16 region, no protection was detected (Conforti et al., 2009, Avery et al., 2009). Thus, for axon protection, both NMNAT enzyme activity and its localization in the axon are necessary to confer protection (Conforti et al., 2009, Babetto et al., 2010). An interesting model to explain WLDS^s axonal protection has been recently proposed (Gilley and Coleman, 2010). According to this study endogenous NMNAT2, which is the most labile NMNAT isoform with a half-life of less than an hour, is an essential survival factor for maintenance of healthy axons. Its depletion by transection of mouse superior cervical ganglia (SCG) neurites or by specific RNAi in the absence of acute cut is sufficient to induce spontaneous axon degeneration. In normal conditions, NMNAT2 is continuously transported along the axons (Milde et al., 2013c, Gilley and Coleman, 2010) but after injury, NMNAT2 present in the distal stump of the axon is rapidly depleted before signs of degeneration. When in the injured axon is present WLD^s, capable of enzymatic NAD synthesis by its NMNAT1 activity and much more stable compared to NMNAT2, this substitutes for loss of endogenous NMNAT2

maintaining its activity for a prolonged period (Gilley and Coleman, 2010, Gilley et al., 2013) (Fig. 8). *Wld*^{S} mice, rats and *Drosophila* crossed with disease models are a unique experimental tool to explore axon degeneration, investigate novel biochemical pathways and determine how axon degeneration contributes to neurodegenerative pathology and symptoms, ultimately leading the way to new therapeutic approaches.

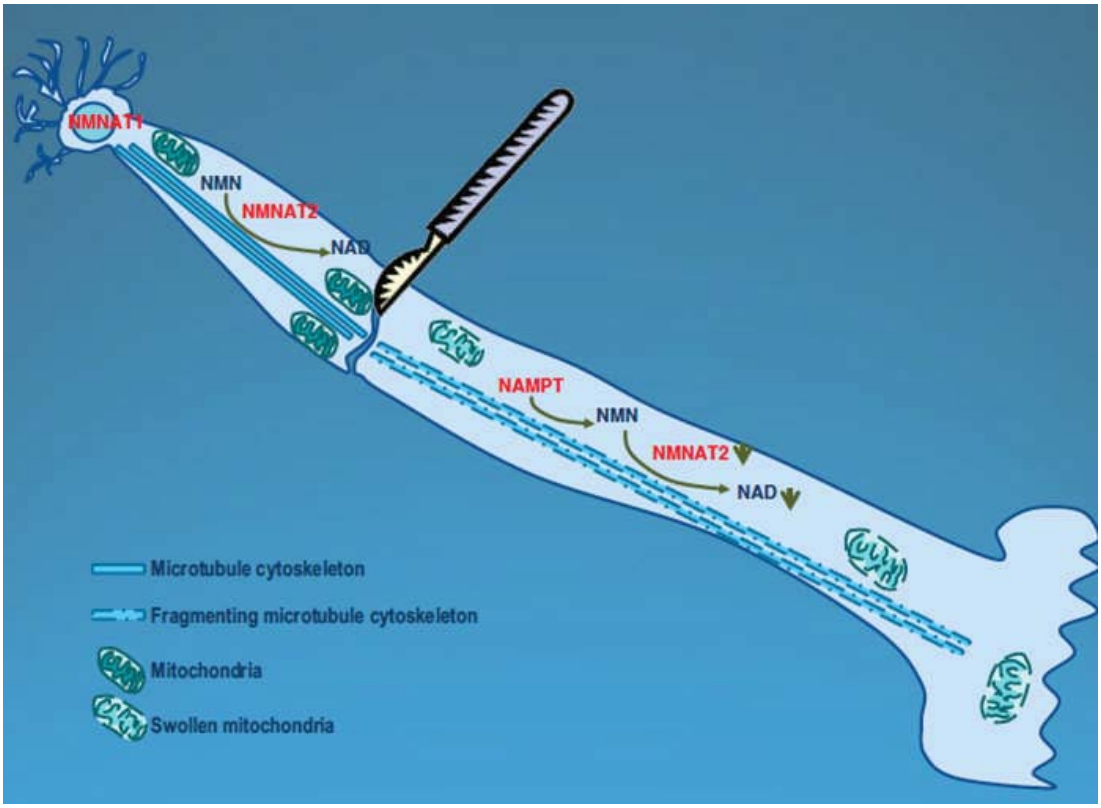

Fig. 8

A molecular model of Wld^{S}-mediated axon protection. From (Di Stefano and Conforti, 2013). *NAD metabolism controls axon degeneration. In neurons, NMNAT2 is transported along the axon, and its catalytic activity maintains axon viability. However, in degenerating axons after an injury, NMNAT2 is rapidly degraded, leading to a decrease in NAD levels and other not yet elucidated events which may lead to degeneration, which may not be the critical event promoting axon degeneration (see text). The neuronal compartments are not shown to scale.*

1.9 Aims and Objectives

The present thesis intends to expand our understanding of the role of axon degeneration in HD mouse models; to characterise its development and to address whether this precedes the death of other neuronal compartments and therefore can represent an early target for therapeutic intervention. Indeed, while axon pathology has been reported previously in patients and animal models, an accurate characterisation of its spatio-temporal development in relation to neuronal loss and to the deposition of mHTT aggregates is lacking.

Thus, the present thesis aims to:

1. Clarify the involvement of axon degeneration in HD.

   To this aim:

- Using as models R6/2 transgenic and HdhQ140 knock-in mice crossed with YFP-H mice, I studied axon and cell body morphology at various time-points by imaging of fluorescent neurons. The YFP-H mouse, which expresses the marker protein YFP in a subset of neurons affected in HD, allows visualising neurons and axons over hundreds of microns and has recently been used successfully to dissect neuronal pathology in neurodegeneration models. Using this powerful tool in HD mouse models, I tested the hypothesis that axon fragmentation or swelling, signs of axon degeneration, precede or at least parallel the onset of synapse loss and dysfunction and neuronal loss;

- I investigated how axon degeneration relates to mHTT aggregate formation through immunofluorescent labelling and imaging. This part of my study addresses a long lasting and topical question in the HD field of whether or not mHTT nuclear and extranuclear aggregates have a toxic role;

- I performed a longitudinal behavioural characterisation of the HdhQ140 mouse behaviour, using a battery of motor and cognitive trials, testing the hypothesis that axon pathology develops in parallel to symptom onset and progression. Indeed, although severe motor symptoms have been generally associated with neuronal loss mainly in the striatum and cortex, more subtle axonal defects could account for behavioural changes and cognitive abnormalities observed in the early phase of the disease.

2. Study potential changes in NAD metabolism as a possible mechanism leading to axonal dysfunction in HD.

   To this aim:

- I checked for alteration in the activity of key enzymes in the NAD biosynthesis (NMNAT and NAMPT), in their expression levels and in the levels of the substrates and products of these enzymes, the nucleotides NAD and NMN, testing the hypothesis that pathology in these mice correlates with alterations in the NAD biosynthetic pathway, recently linked to axon survival and axon and synapse degeneration in many neurodegenerative disorders;

- I looked at possible interactions between wild-type and mHTT and NMNATs enzymes, including the WLD^{s} protein, in a cellular model of HD by transfection and imaging techniques, testing the hypothesis that mHTT can interfere/impair the normal function of this enzyme by direct interaction, contributing to neuropathology.

CHAPTER 2

Material & Methods

Note: *Some sections are reported in a manuscript produced as a result of this work, Marangoni et al., 2014. Age-related axonal swellings precede other neuropathological hallmarks in a knock-in mouse model of Huntington's disease, Neurobiol Aging,* 35, 2382-93.

2.1 Mouse origins and breeding

Hemizygous R6/2 and homozygous HdhQ140 ($Hdh^{Q140/Q140}$) males (Mangiarini et al., 1996, Menalled et al., 2003) were bred to female Thy1.2-YFP-H homozygotes on a C57BL/6 background (Feng et al., 2000) to produce R6/2/YFP-H and heterozygous HdhQ140/YFP-H ($Hdh^{Q140/+}$/YFP-H) in the F1 generation. The latter were then intercrossed to produce mice homozygous for the Q140 mutation and hemizygous for YFP ($Hdh^{Q140/Q140}$/YFP-H). 4 and 12 week old R6/2/YFP-H mice and YFP-H littermate controls were used whereas HdhQ140/YFP-H and YFP-H littermates were used at 4 and 12 months for heterozygous and at 6 and 12 months for homozygous mice. All mice were obtained from The Jackson's laboratories (USA) and kept at the Babraham Institute in Cambridge and at the University of Nottingham. All breeding and procedures were performed as authorised under the Animals (Scientific Procedures) Act 1986, under project licences 80/2254, 40/3576 and 40/3482.

2.2 Genotyping

Tail tips or ear biopsies of 10-day old mice were collected under isoflurane anaesthesia. DNA was extracted from biopsies and genotyping was performed by PCR using the following forward (for) and reverse (rev) primers according to The Jackson's Lab Protocols (http://www.jax.org/):

R6/2

for: 5'- CCGCTCAGGTTCTGCTTTTA-3'
rev1: 5'-TGGAAGGACTTGAGGGACTC-3'
rev2: 5'-GGCTGAGGAAGCTGAGGAG-3'

HdhQ140

for1: 5'-CATTCATTGCCTTGCTGCTAAG-3'

rev1: 5’-CTGAAACGACTTGAGCGACTC-3’

for2: 5’-GATCGGCCATTGAACAAGATG-3’

rev2: 5’-AGAGCAGCCGATTGTCTGTTG-3’

For YFP genotyping, primers used were as follows:

for: 5’-CGAACTCCAGCAGGACCATGTGA-3’

rev: 5’-CTTCTTCAAGGACGACGGCAACT-3’

R6/2 and HdhQ140 DNA samples were sent to Laragen Inc. (USA) for CAG repeat sizing.

2.3 Methods for chapter 3

2.3.1 Histology and Immunohistochemistry

Tissue processing

R6/2/YFP-H and HdhQ140/YFP-H mice, together with the corresponding YFP-H littermate controls, were perfused transcardially with 4% phosphate-buffered paraformaldehyde (PFA) and brains dissected and processed as previously described (Adalbert et al., 2009). Brains were post-fixed by overnight immersion in the same fixative and then cryoprotected in 30% sucrose at 4°C for at least 48 h before processing. On the day of sectioning, brains were split into two halves and from each half free-floating 50 µm sagittal and 20 µm coronal brain sections, respectively, were obtained using a Leica CM1850 cryostat.

H&E staining

For evaluation of gross brain morphology, 20 µm coronal sections were mounted onto Superfrost slides (BDH), air dried and stained with Haematoxylin and Eosin (H&E) (Lillie, 1965).

Hoechst staining

For morphological analysis of YFP expressing (YFP+) neurons, 50 µm sagittal sections were incubated for 10 min with nuclear staining Hoechst 33258 (Invitrogen, 1:500) in PBS with 1% Triton, washed 3 times in PBS and then mounted onto

Superfrost slides in Vectashield mounting medium (Vector Laboratories) (Adalbert et al., 2009) .

Nissl staining

To stain neuronal cell bodies, 20 µm coronal sections were incubated with NeuroTrace fluorescent Nissl stain in PBS (Invitrogen-Molecular Probes, 1:300) for 20 min and then washed in PBS for 2 h at room temperature before being mounted onto slides in Vectashield containing DAPI.

Immunohistochemistry

For immunohistochemistry, 20 µm coronal sections were incubated in PBS with 1% Triton for 10 min, washed 3 times in PBS and then blocked for 1 h at room temperature with 3% BSA in PBS, before overnight incubation at 4°C with mouse anti-human Huntingtin (Chemicon clone EM48, 1:100). Goat anti-mouse Alexa Fluor 568 (Invitrogen, 1:200) was used as secondary antibody (Adalbert et al., 2009). After incubation in secondary antibody, sections were washed 3 times in PBS and then mounted onto Superfrost slides in Vectashield mounting medium containing DAPI (Vector Laboratories).

2.3.2 DiI staining

A separate set of WT/YFP-H mouse fixed brains were used to mark corticostriatal projection neurons with 1,1′-dioctadecyl-3,3,3′,3′-tetramethylindocarbocyanine perchlorate (DiI) fluorescent neurotracer (Sigma), a lipophilic membrane stain (Godement et al., 1987). Crystals of DiI were inserted into perfused brains and were kept for at least 2 weeks in 4% PFA, at 37°C to speed up the uptake process which is slower in fixed tissues (Holmqvist et al., 1992). In some brains, DiI crystals were inserted into the cortex while in some others into the striatum. Crystal insertion was carried out using the tip of a fine gauge needle and under a dissection microscope to guide it. After 2 weeks, 50 µm sagittal brain slices were obtained using a Vibratome (Leica vt1000s) and mounted onto Superfrost slides.

2.3.3 Golgi staining

A separate set of HdhQ140/YFP-H mouse brains were used to visualise striatal neurons with Golgi staining. For this technique, brains were perfused with PBS and

4% PFA. After fixation they were immediately immersed in the impregnation solution (solutions A + B in equal parts) from FD Rapid GolgiStain Kit (FD Neuro Technologies, USA) (Gao et al., 2011, Milatovic et al., 2010) for about two weeks, according to manufacturer's instructions. After this time, brains were transferred to another solution (solution C) from the kit and kept in the dark at 4°C for 24 h for up to 1 week. Later, brains were rapidly frozen by immersion in iso-pentane pre-cooled (-70°C) in dry ice and sliced with a cryostat to obtain 50 µm sagittal sections. Brain slices were mounted onto gelatine-coated microscope slides and stained according to manufacturer's instructions.

2.3.4 Western blot

Western blot was carried out as previously described (Conforti et al., 2007b). Fresh frozen striata and cortices from R6/2, HdhQ140 and wild-type littermate mice were homogenised in RIPA lysis buffer containing protease inhibitors (Complete mini, Roche), protein samples loaded on a 10% SDS polyacrylamide gel and then transferred to nitrocellulose membrane using a semi-dry blotting apparatus (BioRad). Membranes were then blocked for 1h in 5% BSA in PBS plus 0.2% Tween-20 (PBST), incubated overnight with primary antibody in 5% BSA in PBST at 4°C and subsequently washed in PBST and incubated for 1h at RT with HPRT-linked secondary antibody in 2% BSA in PBST. Finally membranes were washed, treated with ECL (Enhanced Chemiluminescence detection kit; GE Healthcare) and exposed to film for an appropriate time. The following primary antibodies were used: mouse anti-synaptophysin (Dako clone Y38, 1:10000) and mouse anti-PSD-95 (Abcam, 1:2000). As loading control, mouse anti-β-tubulinIII was used (Sigma, 1:5000).

2.3.5 Imaging and quantitative analysis

Fluorescently labelled section

Z-stack images were acquired by confocal microscopy (Zeiss LSM 710 Laser Scanning Microscope) at 1 Airy Unit (AU) with the following excitation/emission filters: DAPI/Hoechst 405nm/420–480nm, YFP 488nm/505–550nm, AlexaFluor 568 and NeuroTrace 561nm/575–615nm. All quantitative analyses on confocal images were performed manually using ImageJ software, on maximum projection images resulting from the superimposition of the single z-stacks. In particular:

- For morphological characterisation of YFP+ neurons and axons, confocal images were acquired with a 20X air-objective (Plan-Apochromat 20X/0.8) and axonal swellings quantified in 3 images per section, corresponding to cortex, striatum dorsal and striatum ventral, in 3 sections per animal (n = 3-6, see Fig. 3 B). A cut-off of approximately 5 μm was used for swelling quantification and the analysis was carried out independently by two different persons, at least one of whom blinded to the mouse genotype (Bridge et al., 2009);

- For visualisation and colocalisation analysis of mHTT aggregates, confocal images were acquired using a 63X oil-immersion objective (Plan-Apochromat 63X/1.40). Colocalisation studies were performed using Volocity 6.1 software which allows 3D reconstruction of maximum projection images;

- For analysis of nuclear size of Hoechst stained 50 μm sagittal sections in cortex and amygdala, a 40X oil-immersion objective (Plan-Apochromat 40X/1.3) was used and quantification was performed in three different brain sections per animal (n = 4-6). In the amygdala, a 0.035 mm^2 box was randomly placed within the imaged section and size of Hoechst stained nuclei of YFP+ cell bodies was measured within it (Adalbert et al., 2009);

- Nissl stained sections were imaged at 40X and the number of Nissl positive neurons was quantified in three different striatal fields per section, in three sections per animal (n = 4-6, see Fig. 2 A);

- DiI stained slices were imaged at 63X and reconstruction images of superimposing YFP+ and DiI+ neurons used to show colocalisation between the two colours.

H&E stained sections

Sections were imaged by low power (Plan-NEOFLUOAR 1.25X/0,035) light microscopy (Zeiss Axioplan) and the area of the lateral ventricle was measured using Volocity 6.1 software. Sections representative of 4 different antero-posterior brain areas were matched between control and HD mice and used for the analysis (n = 4).

Golgi stained sections

Sections were imaged under bright field microscopy (DMIRB, Leica), using a 63X oil-immersion objective and with z-stack acquisition (n = 2).

Western blots

WB bands were analysed using imageJ gel analysis software. For each band, the relative density was measured and then the adjusted density value, referred to the β-tubulin III loading control for each sample, was calculated (n = 7-8).

2.3.6 Statistical analysis

Data are presented as mean ± SEM. Student's t-test or One-way ANOVA followed by Bonferroni post hoc test for multiple comparison was performed for statistical analysis: group comparison was considered statistically significant when p-value was < 0.05. Analysis and graphs were obtained using Prism GraphPad 5.0 software.

2.4 Methods for chapter 4

2.4.1 Behavioural assays

In order to evaluate a range of motor and cognitive behavioral functions in the KI homozygous model, mice were subjected to a battery of behavioral tests that were adapted from previous validated studies (Rising et al., 2011). 14 $Hdh^{Q140/Q140}$ mice (7 males and 7 females) and 12 WT controls (6 males and 6 females) were used for the study. A longitudinal study was carried out and mice were tested at age 1, 3, 6, 9 and 12 months. For each time-point, mice performed in the following tests over a period of two weeks (Fig. 9):

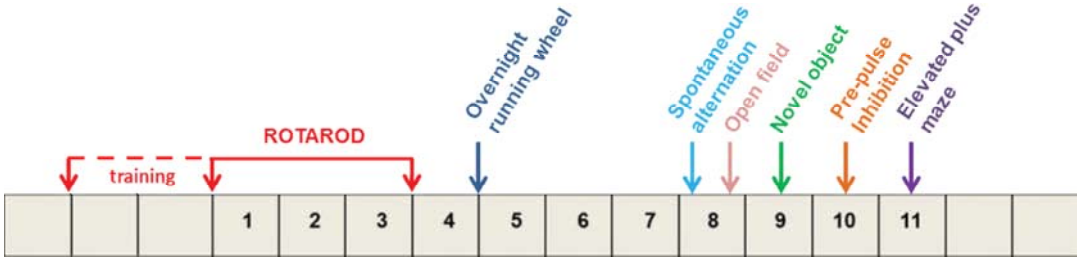

Fig. 9

Schematic representation of the behavioural assessment. *Behavioural tests were performed over a period of two weeks at each time-point. Rotarod, overnight running wheel and open field tests are measure of locomotor activity, pre-pulse inhibition of sensorymotor gating, spontaneous alternation*

and novel object recognition tests of cognitive function and open field and elevated plus maze tests of anxiety-related behaviour.

Rotarod: mice were placed on a rotating rod of a Rotarod apparatus (Letica Scientific Instruments), facing the direction of movement. The latency to fall was recorded over

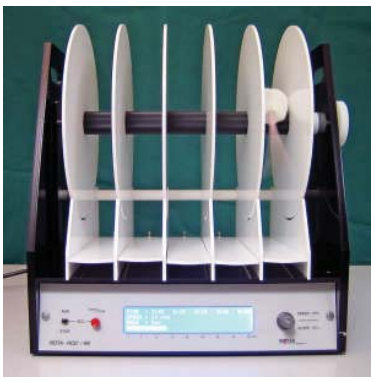

a period of 10 min during which speed was set to increase from 5 to 35 RPM, as a measure of motor coordination with natural fear of falling response. The test was carried out over 3 consecutive days (day 1-3), with an extra 2-day training phase preceding it, at 1 month only. For each day, three trials were performed with a 1 to 2 h inter-trial time and each trial was repeated twice with a 5 minute interval. Motor skill learning, related to cognitive impairment, was also evaluated in the 3 trials per day over the 3 days of testing;

Overnight running wheel: between day 4 and 5 mice were placed in single cages fitted

with a running wheel connected to a sensor recording the number of rotations and the average speed per hour completed by the mouse as measure of the locomotor activity during nocturnal hours in which rodents are more active. All mice tested were singly housed at 6 pm on day 4. Data were collected at 9:30 am on the following day and mice placed back in the homecage. Food and water were provided at all times.

Spontaneous alternation task: a Y-shaped maze comprised of three transparent

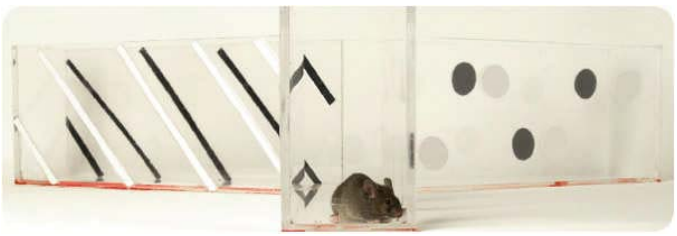

Plexiglas® arms at a 120° angle from each other was used for this test. The start point was located in the centre of the maze and the animal was allowed to freely explore the three arms over 5 min. Alternation rate of arm choice and total number of arm entries were measured as parameter of spatial working memory and locomotor activity, respectively. This test was conducted on day 8 before the open-field test;

Open-field: on day 8, following the spontaneous alternation task, mice were placed in

the open-field arena (30 cm x 35 cm x 30 cm) and allowed to move freely for 30 min. Their behavior was recorded using Ethovision Software (Noldus, Wageningen, Netherlands). The total distance moved and the percentage of time spent in the centre of the arena was considered as index of locomotor activity and anxiety-related behaviour, respectively;

Novel object recognition task (NO): on day 9, mice were placed in the same arena used for the open-field test in which two objects were placed. The task consisted of

three trials of 6 min each separated by a 10 min interval between the first and second trial and a 20 min one between the second and the third in which mice were placed back into the home cage. In the first trial (Habituation) two objects (object 1 and 2) of the same shape were placed into the arena and the animal was allowed to freely explore them over 6 min. In the second trial (Location) the object 2 was moved to a different location in the arena while in third trial (Discrimination) the object 2 was replaced by an object of different shape. The total distance moved and the time spent exploring the objects were recorded using Ethovision Software. Data from location and recognition trials were used as a measure of spatial and recognition memory respectively, based on the spontaneous tendency of normal rodents to spend more time exploring a novel object (object 2) rather than a familiar one (object 1);

Prepulse inhibition (PPI): on day 10, mice were placed into a Plexiglas cylinder inside a chamber (SR-LAB San Diego Instruments, USA), equipped with fan and light, that prevents external noise or vibrations from interfering with the experiment. A speaker was producing acoustic stimuli and mouse movements were detected and recorded as measure of sensory gating. The test session was adapted from Brody et al., 2004 (Brody et al., 2004) and consisted of 72 trials of different trial types: 40 ms-long 120 dB stimuli (pulse alone trial); 20 ms-long of either 68, 72, 80 or 90 dB stimuli preceding the 120 dB (prepulse + pulse trial) and 65 dB background white noise (no

stimulus trial). Trial types were presented in an irregular, counter-balanced order with around 15 sec inter-trial time and proceeded by 5 min acclimation period during which the background noise was presented alone. Startle magnitude was calculated as the average response to the pulse alone trials and % of PPI was calculated as follows:

[1−(startle response to prepulse+pulse)÷(startle response to pulse alone)]×100

Elevated plus maze (EPM): on the last day of testing, animals were placed in a plus-shaped apparatus with two open and two enclosed arms constructed from white

opaque acrylic, each with an open roof and elevated around 80 cm from the floor. Mice were placed at the junction of the four arms of the maze and allowed to explore freely over 5 min. Their behaviour was recorded with Ethovision. The preference for being in open arms over closed arms (expressed as either as a percentage of entries and/or a percentage of time spent in the open arms) was calculated as measure of anxiety-like behaviour. This test relies upon rodents' tendency toward dark, enclosed spaces and an unconditioned fear of heights/open spaces.

Mice were weighed monthly and on day 1 during testing phase.

2.4.2 Statistical analysis

Data are presented as mean±SEM. Two- or Three-way ANOVA was used for statistical analysis: group comparison was considered statistically significant when p-value was < 0.05. Weight was considered as a covariate in tests, such as rotarod, running wheel and PPI, where it was shown to affect performance. Analysis was performed using InVivoStat software.

2.5 Methods for chapter 5

2.5.1 Determination of NMN and NAD levels and NMNAT enzyme activity

This analysis was carried out during my visit to the Università Politecnica delle Marche in Ancona (Italy), in collaboration with Dr. Giuseppe Orsomando.

Nucleotide levels in $Hdh^{Q140/Q140}$ and corresponding wild-type littermates were determined accordingly to previously described methods (Formentini et al., 2009, Graeff and Lee, 2002). Frozen cortices (n = 6-8) and striata (n = 4-6), previously dissected from 6 and 12 month old $Hdh^{Q140/Q140}$ and fresh frozen in liquid nitrogen, were weighed and grinded with a pestle on liquid nitrogen. Samples were then collected in a tube, acidified by addition of $HClO_4$, sonicated and then neutralized by addition of K_2CO_3 and kept at -80°C till use. On the day of use, samples were defrosted, centrifuged and in each extract NMN and NAD levels were determined as follows: NMN was measured upon derivatisation with acetophenone and spectrofluorometric HPLC analysis (Formentini et al., 2009): each sample was incubated with acetophenone (C_8H_8O) and potassium hydroxide (KOH) for 15 min at 4°C, then formic acid (HCOOH) was added and the solution incubated at 100°C for 5 min and finally centrifuged. Derivatization allowed NMN to be converted into a highly fluorescent compound (Fig. 10). A duplicate sample containing NMN spike of a known amount was analysed in parallel. Pure NMN standard (Sigma) was dissolved in water and solution analysed by HPLC with fluorimetric detection.

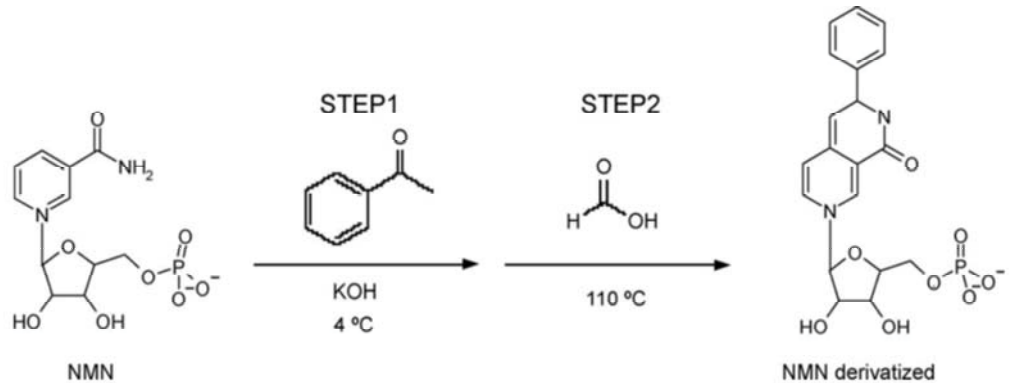

Fig. 10

Derivatisation of NMN. *NMN is converted into a fluorescent compound upon reaction with acetophenone and formic acid.*

NAD content was instead measured by a fluorescence cyclic assay (Graeff and Lee, 2002) carried out onto a 96-well plate reader (Bio-Tek). Each well was loaded with appropriate volumes of the sample homogenates (5, 10 and 20 µl, plus or minus NAD spikes at known amounts) diluted to 150 µl with water, further added with 100 µl of fresh cycling reagent containing 96% ethanol, 0.3 M TFNa pH8, 1 mg/ml alcohol dehydrogenase/1.5 mg/ml BSA_gelfit, 0.1 mM resazurin in 0.1M TFK pH8, diaphorase, 1 mM FMN. The increase in the resorufin fluorescence was measured using the fluorescence plate reader.

Total NMNAT enzymatic activity was measured as previously described (Balducci et al., 1995, Conforti et al., 2011). Grinded cortical and striatal samples (n = 2) were homogenised in a buffer containing protease inhibitors and sonicated. For each sample, a reaction mix containing 50 mM HEPES/KOH pH 7.5, 1 mM ATP, 20 mM NaF (Sodium fluoride), 25 mM $MgCl_2$, 1 mM DTT (DL Dithiotreitol), BSA 0.6 mg/ml and appropriate aliquot of the brain homogenate was prepared. 1 mM NMN was added at the end to start the reaction and incubated at 37°C. 4 sets of reactions were prepared and stopped at time 0, 3, 6 and 9 min, respectively, by addition of ice-cold $HClO_4$. Samples were then neutralised and run on HPLC for determination of the product (NAD).

2.5.2 Western blot

Fresh frozen striata and cortices from 6 and 12 month old $Hdh^{Q140/Q140}$ and wild-type littermate mice were collected and processed as described for samples in chapter 2.3.2. Mouse anti-NAMPT (Enzo Life Sciences, 1:2000) (Laiguillon et al., 2014) and anti-mouse HRP-conjugated (GE Healthcare, 1:2000) were used as primary and secondary antibodies respectively. Membranes were incubated overnight at 4°C with anti-NAMPT diluted in 5% Milk in PBST. Anti-β-Actin (Abcam, 1:3000) in 5% BSA in PBST was used as loading control. WB bands were analysed as in 2.3.5 and data normalised to β-Actin levels.

2.5.3 Cell culture

PC12 and HEK293 cells

For WLD^s studies, an inducible line of rat pheochromocytoma (PC12) cells expressing a GFP-tagged exon1 fragment of the human HD gene containing a 21 (PC12 Q21) and

72 (PC12 Q72) CAG repeat driven by a doxycycline-dependent Tet-ON promoter (Wyttenbach et al., 2000, Gossen et al., 1995) was used. Cells were cultured on collagen-coated flasks (collagen from rat-tail, Sigma) in high glucose Dulbecco's Modified Eagle's medium (DMEM, Sigma D6546) supplemented with 5% fetal bovine serum (FBS tetracycline free, PAA), 10% heat inactivated horse serum (GIBCO), 2 mM L-glutamine and 100 µg/ml penicillin/streptomycin (Invitrogen), 100 µg/ml G418 (PAA) and 70 µg/ml Hygromycin B (Invitrogen). For transfection cells were seeded onto treated ibidi µ-dishes (Thistle Scientific) coated with collagen from rat tail (Sigma) and allowed to reach 60-80% of confluence. On the same day of transfection, cells were treated with differentiating medium containing DMEM supplemented with 2% B27, 1:1000 gentamycin and 100 ng/ml 7S NGF and treated with 1 µg/ml doxycycline to induce aggregate formation.

For cotransfection and colocalisation studies between full-length human wild-type and mutant Huntingtin and NMNATs proteins, wild-type PC12 and Human embryonic kidney (HEK) 293 cells were used. Wild-type PC12 cells were cultured on collagen coated flasks as for the Tet-ON PC12 in the same medium without G418 and Hygromycin B. HEK293 cells were cultured in high-glucose DMEM supplemented with 10% FBS, 110 mg/L sodium pyruvate, 2mM glutamine, and 1X penicillin/streptomycin (10,000 u/mL).

Primary cultures

For studies of colocalisation and live axonal transport, superior cervical ganglia (SCG) explants were dissected from 2 day old C57/BL6 mouse pups and dissociated as previously described (Buckmaster et al., 1995). Dissected SCG ganglia were incubated in 0.025% trypsin (Sigma) in PBS (without CaCl2 and MgCl2) for 30 min followed by 0.2% collagenase type II (Gibco) in PBS for 30 min. Ganglia were then gently triturated using a pipette and then plated onto ibidi µ-dishes pretreated with 20 µg/ml Laminin (Invitrogen) in DMEM, and cultured in DMEM (Sigma D6546) medium supplemented with 10% FBS, 2 mM L-glutamine, 100 µg/ml Penicillin/Streptomycin, and 100 ng/ml 7S NGF (Invitrogen) and 4 µM aphidicolin (Calbiochem) to reduce the number of dividing cells. Medium was changed every 2-3 days.

2.5.4 Plasmids

To study the effect of WLD^s on Tet-ON PC12 expressing wild-type or mHTT, cells were transfected with *Wld*^{S} in DsRed vector. To study colocalisation between mHTT aggregates and WLD^s or NMNAT1 in Tet-ON PC12, cells were transfected with *Wld*^{S}-mCherry in pCDNA3 vector or NMNAT1-DsRed in pDsRed2-N1 vector. HEK 293 cells were instead cotransfected with a synthetic vector termed pARIS-htt (Adaptable, RNAi Insensitive&Synthetic) encoding the full-length wild-type (pARIS-httQ23) or mutant (pARIS-httQ100) human HTT fused to mCherry, kindly donated by Prof. Frederic Saudou in Paris (Pardo et al., 2010); and NMNAT2-EGFP in pEGFP-N1 vector to study colocalisation. Shorter vector encoding only the N-terminal part of wild-type (pARIS htt 1-586-Q23 in pENTRY vector) and mutan Huntingtin (pARIS htt 1-586-Q100 in pCDNA vector) were also used (kind gift of Dr. Diana Zala and Prof. Frederic Saudou). Primary neurons were contransfected with these shorter versions of pARIS-htt vector and NMNAT2-EGFP to study colocalisation and transport along the axons.

2.5.5 Transfection

Lipofectamine

Transfection of Tet-ON and wild-type PC12 cells was performed using Lipofectamine 2000 (Invitrogen) in Opti-MEM (GIBCO), using plasmids purified by EndoFree Plasmid Maxi-kit (Qiagen). For transfection in 35 mm ibidi µ-dishes, 0.8 µg DNA and 2 µl of Lipofectamine 2000 were used, according to the manufacturer's instructions.

Microinjection

Dissociated SCGs were transfected by microinjection as previously described (Gilley and Coleman, 2010). 3-4 days after plating, when neurites were sufficiently extended, cells were microinjected using a Zeiss Axiovert S100 microscope with an Eppendorf FemtoJet transjector and 5171 micromanipulator system and Eppendorf Femtotips. Plasmids were diluted in 0.5×PBS to the desired concentration and passed through a Spin-X filter (Costar). The mix was injected directly into the nuclei of SCG neurons in dissociated cultures. All constructs were used at a concentration of 100 ng/µl while DsRed was used at 20 ng/µl to avoid cytotoxicity (Zhou et al., 2011).

2.5.7 Imaging and quantitative analysis

For colocalisation studies and quantitative analysis cells were fixed in 4% PFA, nuclei stained with Hoechst dye (as for 2.3.1) and confocal images acquired as for 2.3.3. Hoechst stained healthy nuclei were counted manually with imageJ software.

For live axonal transport studies on dissociated SCGs, time-lapse imaging was conducted using a Total Internal Reflection Fluorescence (TIRF) microscope (Axio ObserverZ1, Zeiss) with a 100X oil-immersion objective (Alpha Plan-Apochromat 100X/1.46) and single image frames were acquired every second for 3 minutes. Neurons were imaged within 24 h after microinjection. Videos were then analysed using Difference tracker ImageJ plugin (Andrews et al., 2010) to measure the average number of moving particles and their average speed.

2.5.8 Statistical analysis

Data are presented as mean ± SEM. Student's t-test or One-way ANOVA followed by Bonferroni post hoc test for multiple comparisons were performed for statistical analysis: group comparison was considered statistically significant when p-value was < 0.05. Analysis and graphs were obtained using Prism GraphPad 5.0 software.

CHAPTER 3

Characterisation of axon pathology in R6/2 and HdhQ140 mice

3.1 Introduction

3.1.1 Choice of the model

The present study focuses on two mouse models of HD: R6/2 transgenic and HdhQ140 knock-in.

R6/2 mice were the first to be analysed. The choice of this particular model was driven by the fact that R6/2 (Mangiarini et al., 1996) is the best characterised mouse model and the most widely used in preclinical trials. These mice were the first to be made available in the literature and to be rapidly placed into a commercial breeding facility becoming accessible to scientists. Moreover, their rapid disease progression including behavioural changes, brain pathology and premature death, make them suitable for preclinical drug testing. Extensive atrophy of the striatum, cortex and other brain areas was shown in these mice with histopathological techniques (Stack et al., 2005) and MRI imaging (Sawiak et al., 2009) accompanied by little or no neuronal loss (Li and Li, 2004). Thinner dendrites and reduced dendritic spines were also described (Klapstein et al., 2001) as well as synapse dysfunction and loss in the striatum at early stages of the disease, which may be the structural correlates to the development of cognitive dysfunction in the asymptomatic phase (Murphy et al., 2000, Cepeda et al., 2003). And in axon terminals, where mHTT aggregates are present, reduction in normal level of synaptic vesicles was shown by electron microscopy (EM), suggesting abnormal association between aggregates and vesicles which could be responsible for synaptic impairment (Li et al., 2003).

While several pathological aspects of the disease are modelled in R6/2, the relevance to the human pathology is still to be fully clarified. First, Tg mice are genetically not representative of the disease as it appears in humans. HD patients have only one normal copy of the *HTT* gene and one mutated copy while Tg mice usually contain multiple copies of the mutant *HTT* gene. Moreover, the random insertion of the human *HTT* gene in the mouse genome may interfere with the normal function of other genes not related to HD. Furthermore, the expression of *HTT* in these mice is driven by an artificial promoter, whose spatial and temporal control of expression is different from that of the endogenous mouse *Hdh* promoter. In addition to the different genetics, the extremely short lifespan of these mice, which die prematurely around 15 weeks, represents a limitation to the study of an age-related disease which in humans appears

late and takes decades to progress. Not surprisingly, successful therapeutic trials on R6/2 often failed to succeed in clinical trials on patients. For instance, treatment with the glutamate antagonists riluzole and remacemide, and with the metabolic antoxidant coenzyme Q10 successfully ameliorated the disease phenotype in R6/2 mice (Schilling et al., 2001, Ferrante et al., 2002, Schiefer et al., 2002) but were not beneficial for patients (Huntington Study, 2001, Landwehrmeyer et al., 2007).

KI mice are a genetically more precise model of HD. Here, *mHTT* is inserted in the appropriate genomic context, which is in the endogenous mouse *Hdh* locus and under the endogenous promoter. Although these mice show milder phenotype and slower disease progression compared to the transgenic, pathological changes have also been described. In particular in HdhQ140 mice (Menalled et al., 2003), object of this study, several neuronal abnormalities are reported making them a good candidate model to study axon pathology in HD. Reduction in striatal volume is documented, together with dendritic complexity and spine density alterations in Golgi stained striatal neurons (Lerner et al., 2012) accompanied by limited neuronal loss (Hickey et al., 2008). Alterations in striatal synaptic activity is also reported (Cummings et al., 2007) as well as degenerative processes at the level of the axon (Li et al., 2001). In axon terminals, an EM study detected at an early stage of the disease the presence of degenerated organelles including mitochondria in the proximity of mHTT aggregates suggesting that aggregates block the transport of organelles or vesicles along the axon (Li et al., 2001).

3.1.2 YFP-H mice: a tool to dissect neuropathology in models of disease

For the study of axon pathology in R6/2 and HdhQ140 mice, both models were crossed to YFP-H mice which express the YFP protein in restricted subsets of neurons thus allowing longitudinal imaging of neuronal structures including axons.

YFP-H mice were first generated in 2000 by Feng and collaborators (Feng et al., 2000), together with other transgenic mouse lines constitutively expressing different fluorescent proteins (XFPs, X = red, yellow, green or cyan) in subsets of neurons under the control of the modified neuron-specific promoter Thy-1.2. All XFPs

labelled neurons in their entirety, including axons, nerve terminals, dendrites, and dendritic spines (Fig 11).

The generation of XFP mice helped the study of neurodegeneration and brought advantages over previously available techniques of visualization of neurons and their compartments. Most of the above mentioned studies describing neuritic pathology in R6/2 and HdhQ140 mice utilise techniques such as immunohistochemistry and electron microscopy which limit the analysis to restricted areas of individual neuronal compartments, or use selective stainings such as Golgi staining which are unpredictable, require fixed tissue and if neurons have already degenerated, stain only contiguous segments. To understand the progression of a disease and to optimize effective treatments to prevent or block neuronal death, it is very important to identify the neuronal compartment where degeneration first occurs (axon, dendrites, synapses, or cell body) and how it progresses with time. Thus, imaging neurons in their full length is important to investigate their structure and correlate it to pathology and genetic approaches, based on the expression of fluorescent proteins restricted to few neurons, represent a useful tool to do so.

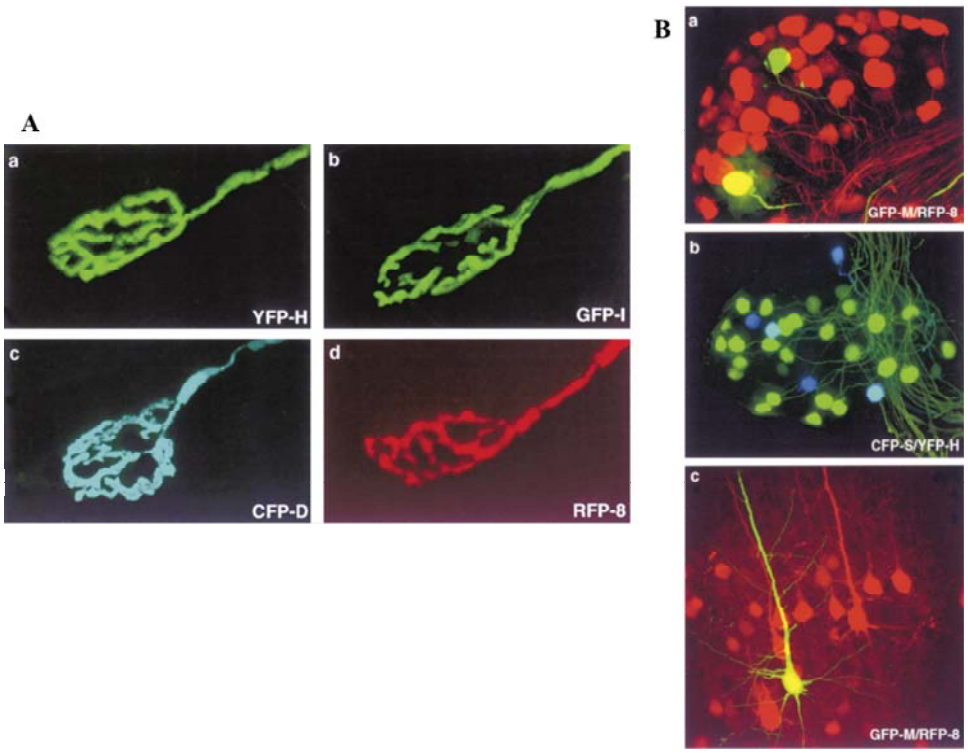

Fig. 11

XFP staining in transgenic mice. From (Feng et al., 2000). *(A) Four distinct XFPs as Vital Stains in Transgenic Mice. Neuromuscular junctions from thy1-YFP line H (a), thy1-GFP line H (b), thy1-CFP*

line D (c), and thy1-RFP line 8 (d) transgenic mice. (B) Multiple Neuronal Subsets in thy1-XFP Double Transgenic mice. (*a) Dorsal root ganglion from a GFP/RFP double transgenic (thy1)-GFP line M and thy1-RFP line 8); (b) Dorsal root ganglion from a CFP/YFP double transgenic (thy1- distinct patterns of expression. Together, these features CFP line S and thy1-YFP line H). Many neurons are YFP positive, and subsets are also YFP or YFP/CFP positive; (c) Section from the cortex of the mouse shown in (a).*

The Thy1.2 cassette was previously modified from the gene of the Thy1 glycoprotein, expressed in a variety of tissues and cell types including thymus, nervous system, and connective tissue fibroblasts, by partial deletions of genomic regions required for the expression in non-neural cells but not in neurons (Vidal et al., 1990, Caroni, 1997) (Fig. 12). Transgene expression begins at P6–10 and some variations in the number of fluorescently labelled neurons exist between different XFP transgenic mouse lines.

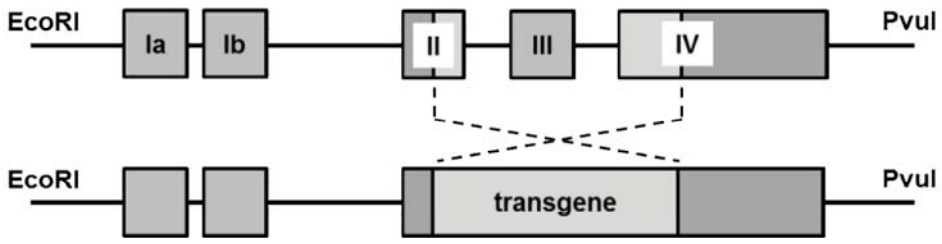

Fig. 12

Schematic representation of the Thy-1.2 expression cassette. Modified from (Caroni, 1997). *The mouse Thy1 glycoprotein gene (top) is deleted to develop the modified Thy1.2 cassette, for expression of transgenes in a random subset of neurons. Part of exons II, the whole exon III and part of exon IV, together with the introns in between, are deleted and substituted with an XhoI site, for cloning purposes. The deleted regions contain portions essential for the expression of the Thy glycoprotein in the thymus. EcoRI site and PvuI site are at the extremities of the cassette. The deletions disrupt the expression of the Thy1 glycoprotein.*

A comprehensive mapping of the specific neurons labelled in adult and postnatal YFP-H mice has been provided (Porrero et al., 2010) (Fig. 13). The YFP transgene is selectively expressed in projection neurons and limited to a few neuronal subpopulations among them. Most of YFP+ neurons are located in the cortex,

hippocampus and amygdala but smaller, additional projection neurons are also present in some brainstem nuclei (Porrero et al., 2010).

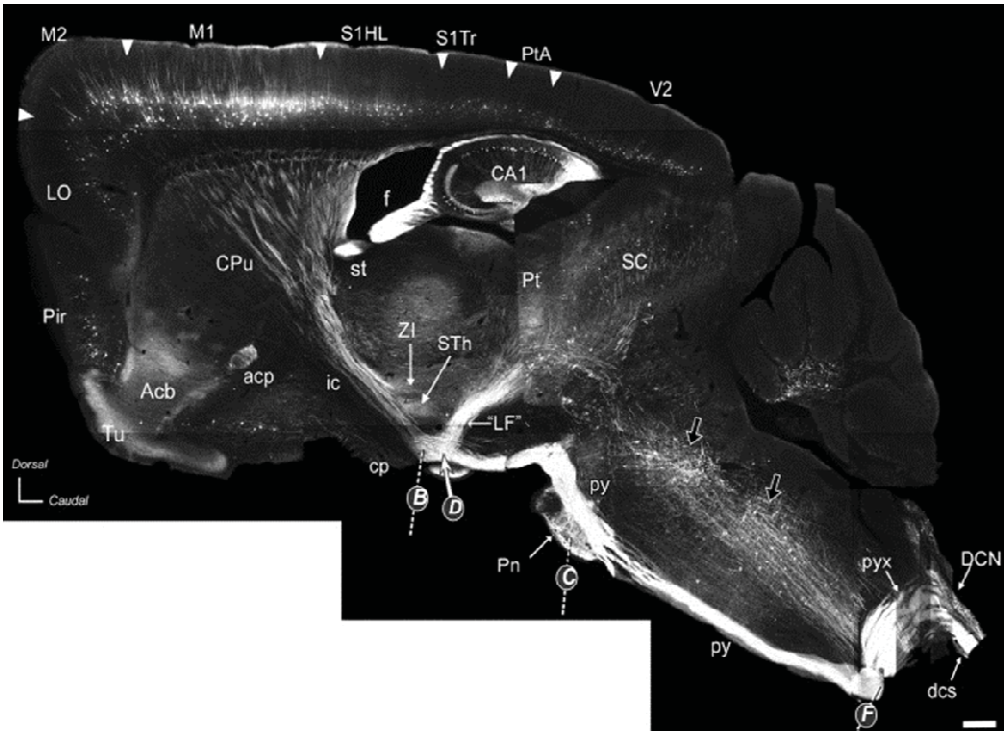

Fig. 13

Fluorescent neurons in YFP-H mouse brain sagittal section. From (Porrero et al., 2010). *Photomontage made from serial sagittal section images shows a panoramic view of corticofugal cell somata in the cerebral hemisphere as well as the path followed by their axons through the internal capsule (ic), cerebral peduncle (cp), pyramidal tract (py) and pyramidal decussation (pyx) towards the dorsal corticospinal tract of the spinal cord (dcs). A fiber bundle emerging perpendicularly from the CP towards the pretectum (Pt), deep superior collicular layers (SC) and mesencephalic tegmentum is labeled "LF" ("lenticular fasciculus") following Valverde (1998). Additional terminal fields are distinguishable in the zona incerta (ZI), subthalamic nucleus (STh), and pontine nuclei (Pn). In addition to corticofugal cells, a subpopulation of eYFP+ reticular formation neurons and their axons (black arrows) are also visible in the photomontage. Labeling in hippocampus (CA), nucleus accumbens (Acb), olfactory turbercle (Tu) and stria terminalis (st) reflects additional eYFP+ expression in other pathways.*

The YFP-H line has been extensively characterized and successfully used to assess neurodegeneration both in CNS and PNS. Crossing of these mice with *Wld*^{S} transgenic mice have been successfully used to follow, *in vivo*, the rate of Wallerian degeneration over a distance of up to 2–3 cm in peripheral nerves (Beirowski et al., 2004) and in the CNS, to study axonal and dendritic damage induced by ischemic

damage (Zhang et al., 2005, Enright et al., 2007). Crossing with a mouse model of AD, the PDAPP mouse, allowed imaging of neuritic swellings in the presence of β-amyloid (Brendza et al., 2003); and crossing with a 3xTg-AD model showed loss of dendritic spines of individual dendrites (Bittner et al., 2010). In another AD model, the TgCRND8 mouse, YFP-H expression allowed visualization of severe proximal axonal dystrophy in the vicinity of amyloid plaques (Adalbert et al., 2009) (Fig.14). This last study is particularly relevant to the present thesis as I conducted a similar analysis to detect axon pathology in HD mouse models. Adalbert and collaborators, viewing axonal, somatic and dendritic compartments of individual cortical neurons simultaneously through longitudinal imaging, showed that cell bodies and dendrites remain normal up to 1 year after appearance of axonal dystrophy (Fig. 14 B), raising the prospect of a therapeutic window for functional rescue of individual neurons after their axons become highly dystrophic (Adalbert et al., 2009).

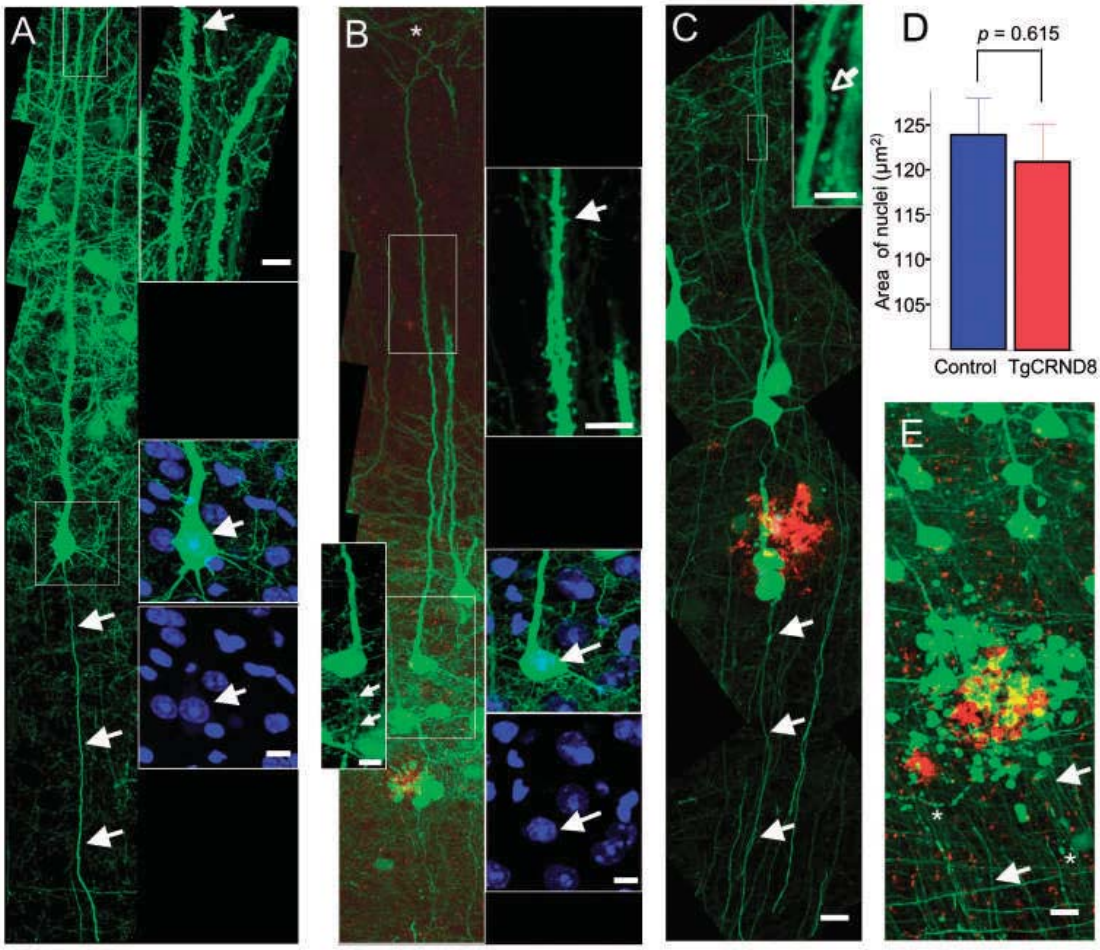

Fig. 14

Axonal dystrophy in TgCRND8/YFP-H mice leaves other parts of the same neuron morphologically unaltered. From (Adalbert et al., 2009). (*A) Cortical neuron from a control YFP-H mouse; (B) cortical neuron from a 5-month-old TgCRND8/YFP-H mouse with severe proximal axonal dystrophy but normal cell body and nuclear size (arrow, bottom) and abundant dendritic spines on apical dendrite (arrow, top); (C) another neuron with severe, proximal axonal dystrophy from a 5-month-old TgCRND8/YFP-H mouse also retains axon continuity and basal dendrites. (D) Quantification of cross sectional nuclear area reveals no significant difference between TgCRND8/YFP-H neurons with severe axonal dystrophy within 250 mm of the cell body and control YFP-H neurons. (E) Axonal dystrophy at a plaque in a 14-month-old TgCRND8 mouse. The majority of axons emerging from the dystrophic region are continuous and unswollen (arrows), cell bodies retain normal morphology and nuclear size and location. Green = YFP; Red = Ab deposits; Blue (where present) = Hoechst 33258 dye. Scale bar: A, B, C and E: 20mm (insets, 10 mm).*

3.1.3 Hypothesis and aim of the chapter

Based on the evidence discussed above, here I tested the hypothesis that axon pathology in HD mice occurs as an early degenerative process that precedes death of other neuronal compartments. To this purpose, this work aims to characterise axon

pathology, as previously described in models of different neurodegenerative diseases, by detecting morphological abnormalities along YFP positive axons of HD/YFP-H mice. By means of fluorescence imaging and immuno- and dye-staining I looked at axon integrity as well as at the status of the cell body and correlated them to the formation of neuropil and nuclear mHTT aggregates.

3.2 Results

Some sections are reported in a manuscript produced as a result of this work, Marangoni et al., 2014. Age-related axonal swellings precede other neuropathological hallmarks in a knock-in mouse model of Huntington's disease, Neurobiol Aging, 35, 2382-93.

3.2.1 R6/2 and $Hdh^{Q140/Q140}$ mouse brains show an age-dependent enlargement of the lateral ventricle but no striatal neuronal loss

To assess neuropathology in our HD mice I first looked at gross alterations in brain morphology in H&E stained sections. I compared matching sagittal sections (20 μm) representative of four different antero-posterior brain levels. In YFP-H control mice, the area of the lateral ventricle in sections representative of all four levels increased during aging, becoming significantly larger at 12 months of age compared to 3 and 6 months. Instead, there was no difference between 3 and 6 month of age (Fig. 15 and Table 2). Consistent with previous studies describing brain atrophy in R6/2 (Sawiak et al., 2009, Aggarwal et al., 2012) and $Hdh^{Q140/Q140}$ mice (Lerner et al., 2012), our results showed a significant enlargement of the lateral ventricle in 3 month old R6/2 and 6 and 12 month old $Hdh^{Q140/Q140}$ mice compared to control littermates (Fig. 15 and Table 2).

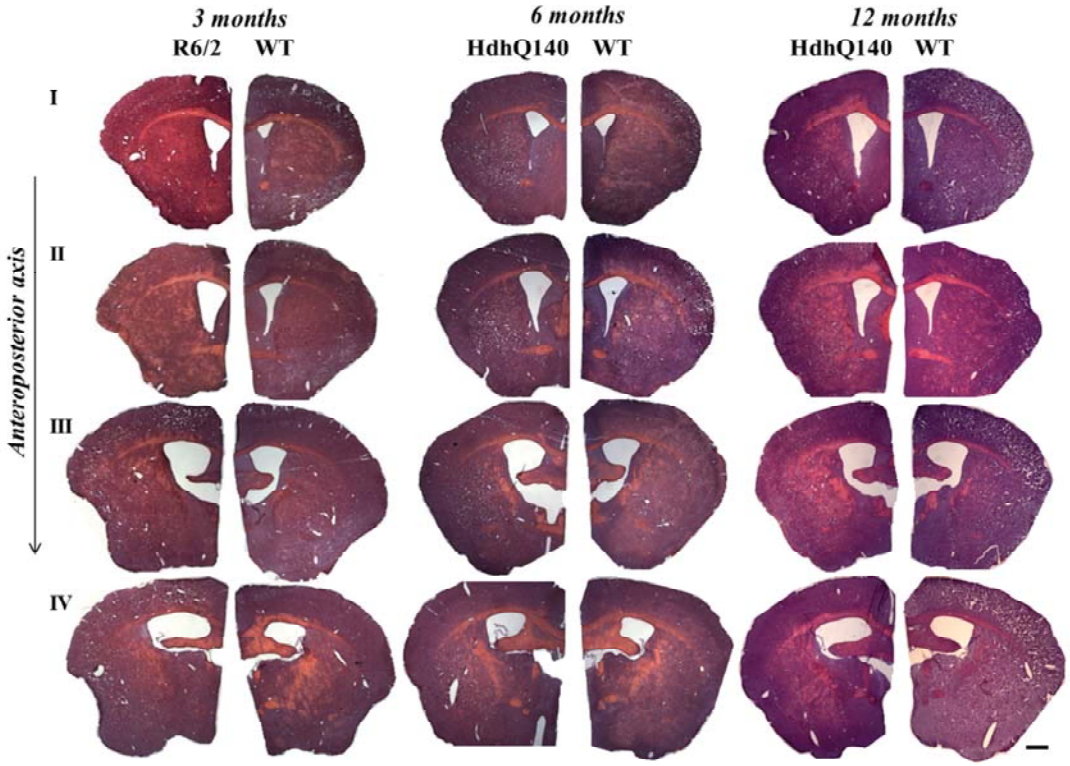

Fig. 15

HD mice show enlargement of the lateral ventricle. *H&E stained coronal brain sections (20 µm) of 3 month old R6/2/YFP-H and 6 and 12 month old* $Hdh^{Q140/Q140}$*/YFP-H mice and corresponding YFP-H control littermates. Sections from four different antero-posterior brain levels were matched between HD and control mice and imaged (1.25X) for analysis of gross brain morphology (see Methods). The area of the lateral ventricle was then measured for each section as described in the Methods. Representative sections from each genotype, brain level and age are shown. Scale bar, 330 µm.*

AGE (months)	BRAIN REGION (anteroposterior axis)	WT (μm^2, mean±SEM)	R6/2 (μm^2, mean±SEM)	$Hdh^{Q140/Q140}$ (μm^2, mean±SEM)
3	I	293072 ± 27844, n=13	** 579573 ± 81474, n=13	
	II	526545 ± 20375, n=9	** 760064 ± 59105, n=9	
	III	978491 ± 79757, n=6	* 1.367e+006 ± 99906, n=6	
	IV	756578 ± 35586, n=11	** 1.050e+006 ± 73208, n=11	
6	I	235160 ± 29300, n=10		** 401635 ± 22087, n=10
	II	482997 + 62436, n=9		** 853790 + 71517, n=9
	III	1.018e+006 ± 42237, n=9		*** 1.549e+006 ± 61988, n=9
	IV	657449 ± 49223, n=8		* 1.007e+006 ± 108675, n=8
12	I	^^, ∫∫∫ 373382 ± 46166, n=11		489113 ± 64883, n=11
	II	^^^, ∫∫∫ 839953 + 57302, n=11		851451 + 62147, n=11
	III	^^^, ∫∫ 1.282e+006 ± 31097, n=9		* 1.412e+006 ± 37081, n=9
	IV	^^, ∫∫∫ 743956 + 73181, n=11		* 1.034e+006 + 91635, n=11

Table 2

Quantification of the area of the lateral ventricle shows significant enlargement in HD mice. *Lateral ventricle areas (μm^2) were measured using Volocity 6.1 software in coronal brain sections of four different brain levels (I-IV) of 3 month old R6/2 and 6 and 12 month old $Hdh^{Q140/Q140}$ and corresponding control littermates. A significant increase was found in all the four brain areas considered in R6/2 and $Hdh^{Q140/Q140}$ compared to control mice, at all time-points (n = 3, mean±SEM, unpaired Student's t-test, *, P<0.05, **, P<0.01, ***P<0.001). A significant enlargement was also found within control mice at 12 months compared to 3 months (n = 3, mean±SEM, one-way ANOVA followed by Bonferroni post hoc test, ^^, P<0.01, ^^^, P<0.001) and to 6 months (n = 3, mean±SEM, one-way ANOVA followed by Bonferroni post hoc test, ∫∫,P<0.01, ∫∫∫, P<0.001).*

To investigate whether this was due to neurodegeneration, I determined the number of neurons in coronal sections (20 µm) of R6/2 and HdhQ140 mouse brain striatum stained with Nissl dye (Fig. 16). Although with differences to the human phenotype, the striatum of HD mouse models remains the brain area where the majority of neuropathological hallmarks, such as deposition of mHTT aggregates, has been described (Davies et al., 1997, Hickey et al., 2008) and where any potential neurodegeneration is most likely to be detected. I counted the number of Nissl stained neurons in striatal sections of 12 week old R6/2 (Fig. 16 B), 12 month old $Hdh^{Q140/+}$

(Fig. 16 C) and 6 and 12 month old $Hdh^{Q140/Q140}$ (Fig. 16 D) mice and found no significant reduction compared to their control littermates. These results are consistent with previous evidence that HD mouse models show little or no neuronal loss at least until very late time-points (Davies et al., 1997, Hickey et al., 2008) and suggest that more subtle changes preceding cell death might account for brain atrophy. Altered dendritic morphology such as reduced branching and spine density described in both HD patients and mouse models (Nithianantharajah and Hannan, 2013) could explain the brain atrophy found in these mice.

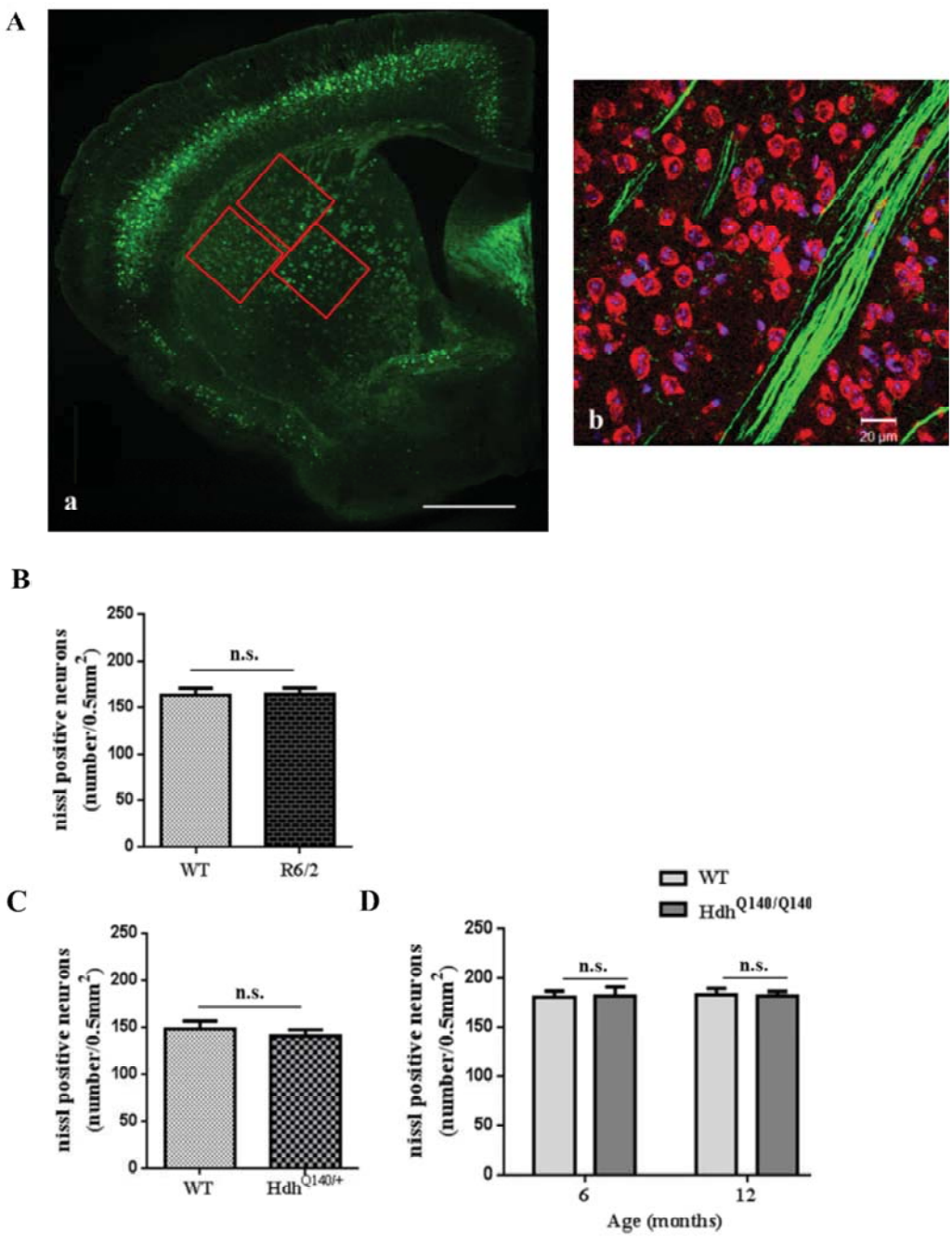

Fig. 16

The number of striatal neurons in HD mice is unaltered compared to controls. *(A) The number of Nissl positive neurons was evaluated in coronal brain sections (20 µm) of HD/YFP-H mice and corresponding YFP-H control littermates. (a) Representative fluorescent image (2.5X) of a coronal brain section showing the 3 striatal fields (red boxes) acquired per each section for quantification of neuronal number (see Methods). Scale bar, 100 µm. (b) Representative confocal image (40X) of a Nissl stained section corresponding to one of the fields quantified. Scale bar, 20µm. Green: YFP, red: Nissl, blue: DAPI. (B-D) Quantitative analysis shows no significant cell loss in 3 month old R6/2/YFP-H (B), 12 month old* $Hdh^{Q140/+}$*YFP-H (C) and 6 and 12 month old* $Hdh^{Q140/Q140}$*/YFP-H (D) compared to the relative controls (n = 3-6, mean±SEM, unpaired Student's t-test and one-way ANOVA followed by Bonferroni post hoc test).*

3.2.2 Axon swelling is an early feature of $Hdh^{Q140/Q140}$ mice

I then analysed the morphology of corticostriatal neurons and axons of R6/2 and HdhQ140 mice crossed with YFP-H mice. Because of the restricted expression of the fluorescent protein, the YFP-H mouse line allows longitudinal tracing of individual neurons running from the cortical layer V towards the striatum passing through the corpus callosum and therefore enables visualisation of all structures of these neurons, from dendrites to cell bodies to the long projection axons (Adalbert et al., 2009).

I first analysed brain sections of 4 and 12 week old R6/2/YFP-H mice corresponding to early and late stages of the disease in this mouse model (Mangiarini et al., 1996). At both time-points, the majority of fluorescent axons of R6/2/YFP-H mice looked morphologically normal and did not show signs of degeneration such as swellings or spheroids, typical features of the central nervous system (CNS) axonal dysfunction during normal aging and in many disorders (Ferguson et al., 1997, Galvin et al., 1999, Tsai et al., 2004, Bridge et al., 2009) (Fig. 17 A). I found a limited number of swellings in both R6/2 and control mice with a non-significant trend to an increase in the R6/2 mice (Fig. 17 B-C). Moreover, no significant reduction in nuclear size of YFP+ cortical neurons stained with Hoechst was detected in these mice suggesting that the health status of the cell bodies was good (Adalbert et al., 2009) (Fig. 17 D-E).

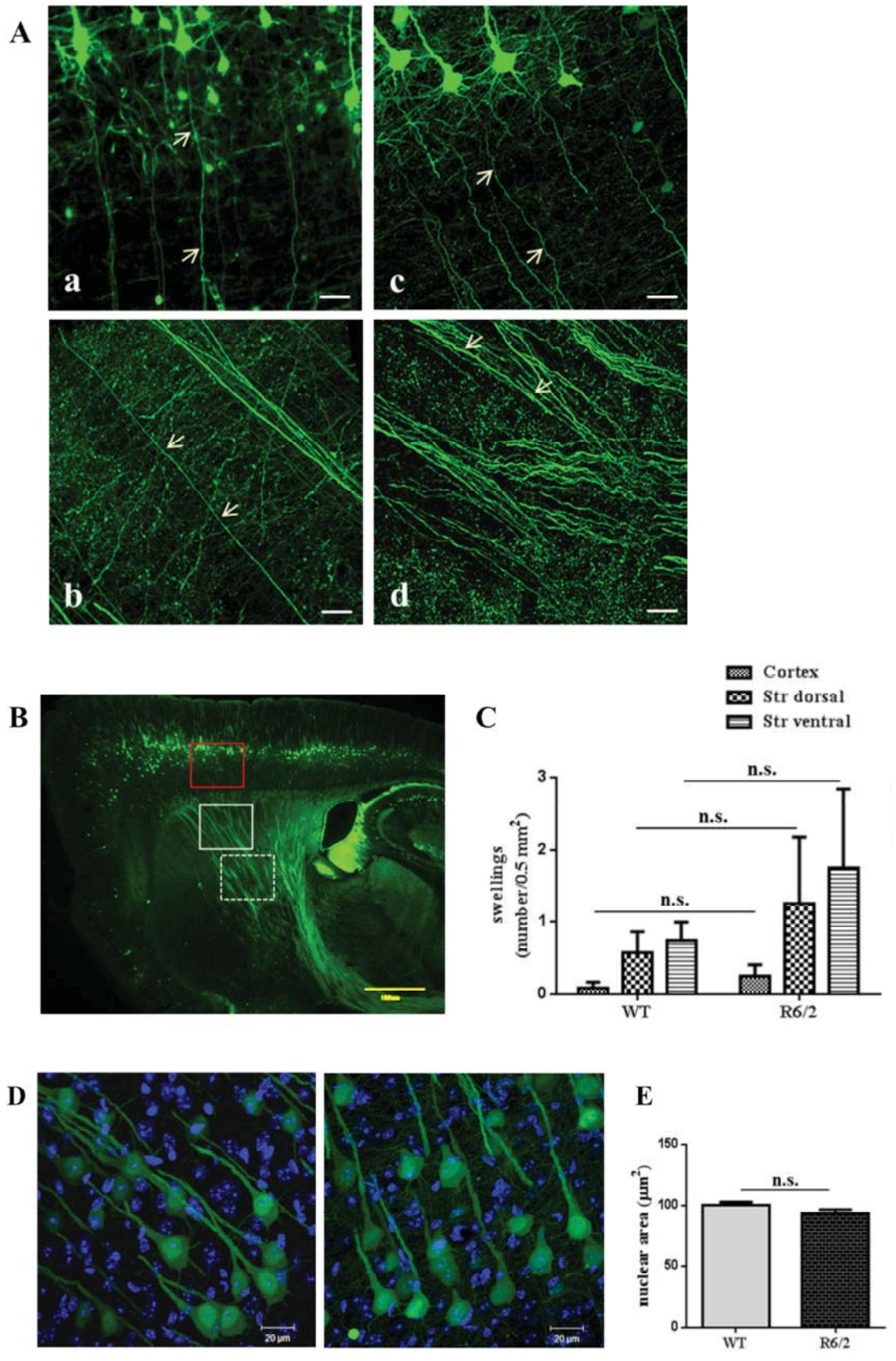

Fig. 17

R6/2 mice have normal cell bodies and no obvious axon abnormality. *Sagittal brain sections (50 µm) of R6/2/YFP-H mice and corresponding YFP-H control littermates were imaged with confocal*

microscopy (20X) for analysis of axon morphology. (A) 4 week (a-b) and 12 week (c-d) old mice show morphologically intact YFP+ neurons and projections both in cortex (a-c) and striatum (b-d). Arrows indicate continuous axonal tracts in cortex and striatum. Scale bar, 50 µm. (B-C) Quantification of the occasional swellings in cortex (red box), dorsal (white continuous box) and ventral (white dashed box) striatum shows a tendency to an increase in R6/2/YFP-H mice compared to controls albeit with no significant difference (n = 4, mean±SEM, one-way ANOVA followed by Bonferroni post hoc test). Scale bar, 100 µm. (D) Confocal images (40X) of YFP+ cortical neurons of YFP-H (a) and R6/2/YFP-H (b) mice in sagittal brain sections stained with Hoechst show no gross morphological changes in cell body morphology and (E) quantification of their nuclear size reveals no difference between the two genotypes (n = 4, mean±SEM, unpaired Student's t-test). Green: YFP, blue: Hoechst. Scale bar, 20 µm.

In order to have an additional confirmation that the YFP+ axons labelled in the striatum of the YFP-H mouse belong to either intratelencephalic (IT) or pyramidal tract (PT)-type terminals of cortical layer 5 neurons, I performed DiI staining of a WT/YFP-H mouse brain. A single DiI crystal was placed either into the cortex (Fig. 18 A), for diffusion from the cell body towards axon terminals in the striatum, or in the striatum (Fig. 18 B) for diffusion back to the cortex. Confocal imaging of brain sections were acquired two weeks after crystal placement and showed extensive colocalisation of DiI and YFP fluorescence in the fibres projecting from the cortex supporting the idea that the majority of YFP+ neurons were part of corticostriatal projection neurons. YFP/DiI co-labelled axons, part of IT and PT projections, are described to send excitatory inputs to striatal D1 or D2 neurons, respectively (Reiner et al., 2010, Li and Conforti, 2013).

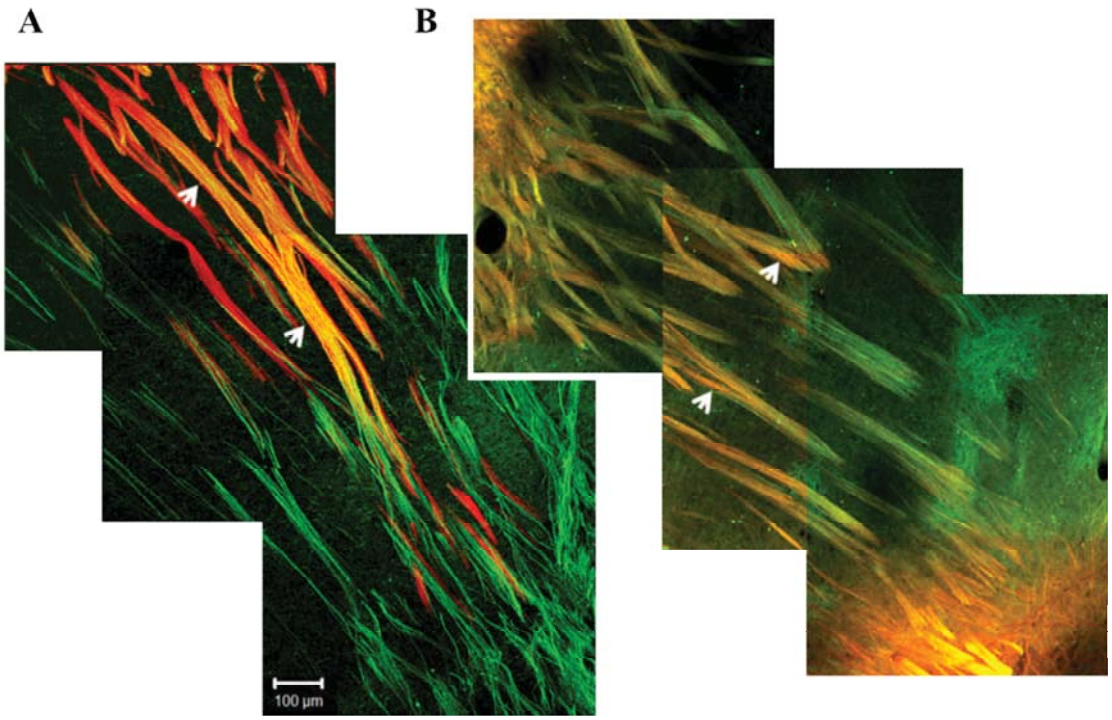

Fig. 18

YFP positive fibers in YFP-H mice are part of the corticostriatal pathway. *Photomontage made from serial confocal images (20X) of sagittal brain sections (50 µm) of WT/YFP-H transgenic mice two weeks after a single DiI crystal was placed in cortex (A) and striatum (B). Both images show colocalisation (arrows) between YFP positive fibers and DiI labeled fibers. Green=YFP; red=DiI, scale bar, 100 µm.*

Next, I analysed brain sections of 4 and 12 month old $Hdh^{Q140/+}$ mice corresponding to early and advanced stage in this model which carries the mutation in the appropriate genomic and protein context and at a heterozygous, physiological concentration. At 4 months I could not find any abnormalities in the KI model compared to control mice (not shown). However, interestingly I found an increase in the number of axonal swellings of $Hdh^{Q140/+/}$YFP-H mice compared to YFP-H wild-type mice at 12 months (Fig. 19 A) albeit this increase did not reach a statistically significant value (Fig. 19 D).

Therefore, to test whether increasing mutant *Hdh* gene dosage accentuates the axonal morphological abnormalities I detected in the heterozygous HdhQ140 mice, I analysed $Hdh^{Q140/Q140}$ mice at 6 and 12 months of age. Importantly, homozygotes retain the advantages of normal gene expression pattern, physiological expression

level, and normal RNA splicing despite differing from human patients in having two mutant copies of the gene. At 6 months the number of swellings in corticostriatal axons was not significantly different from that of the controls and generally lower than that found in 12 month old heterozygotes (Fig. 19 B-D). However, I observed a striking, highly significant increase in the number of axonal swellings in 12 month old $Hdh^{Q140/Q140}$/YFP-H compared to that in YFP-H wild-type controls (Fig. 19 C-D). Morphological alterations appeared to be limited to the axonal compartment as the nuclear size of the YFP+ neurons remained unaltered (Fig. 19 E-F) as well as their gross dendritic morphology (Fig. 19 G-H).

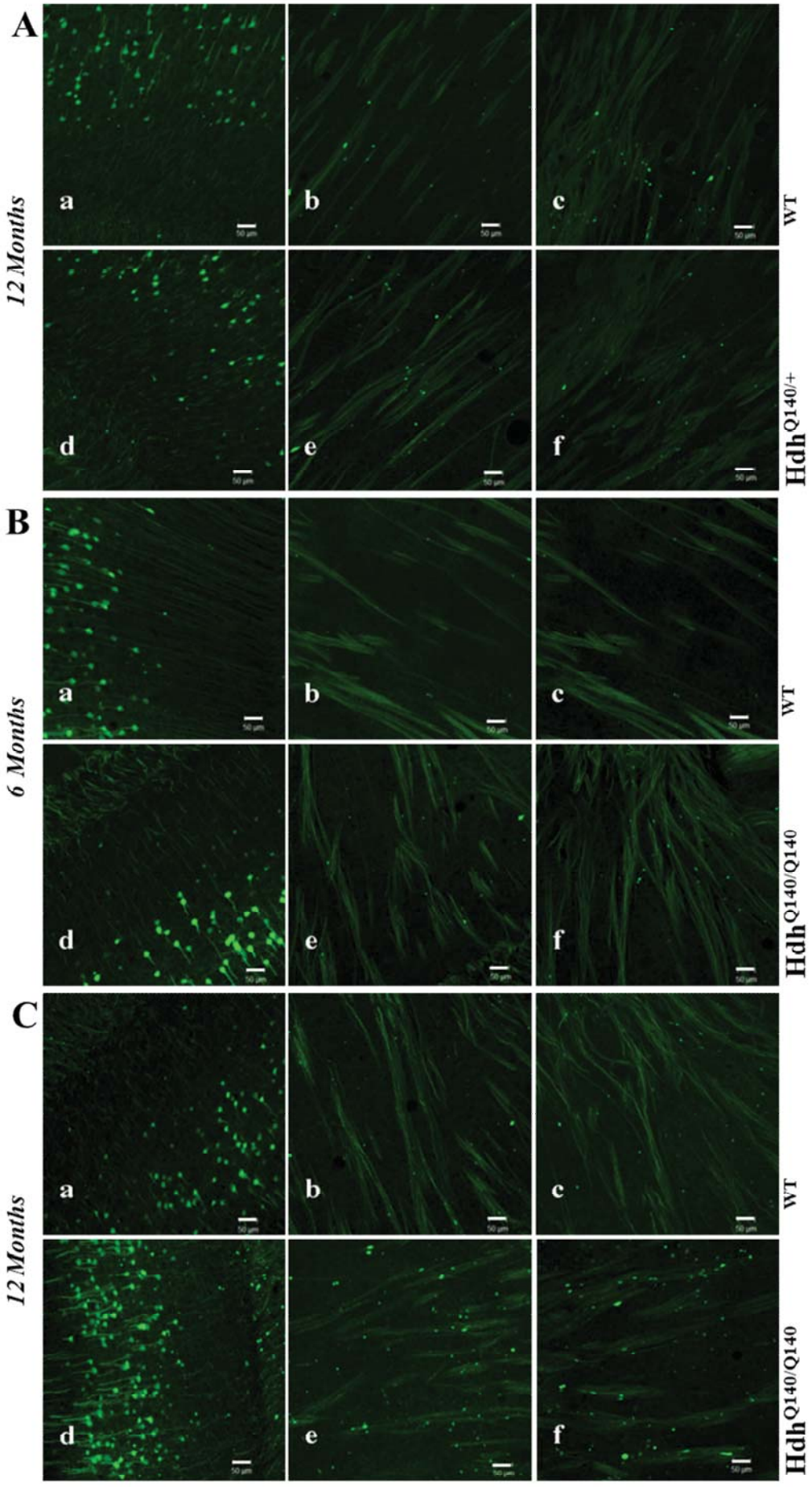
A
12 Months
a
b
c
WT
d
e
f
Hdh Q140/+
B
6 Months
a
b
c
WT
d
e
f
Hdh Q140/Q140
C
12 Months
a
b
c
WT
d
e
f
Hdh Q140/Q140

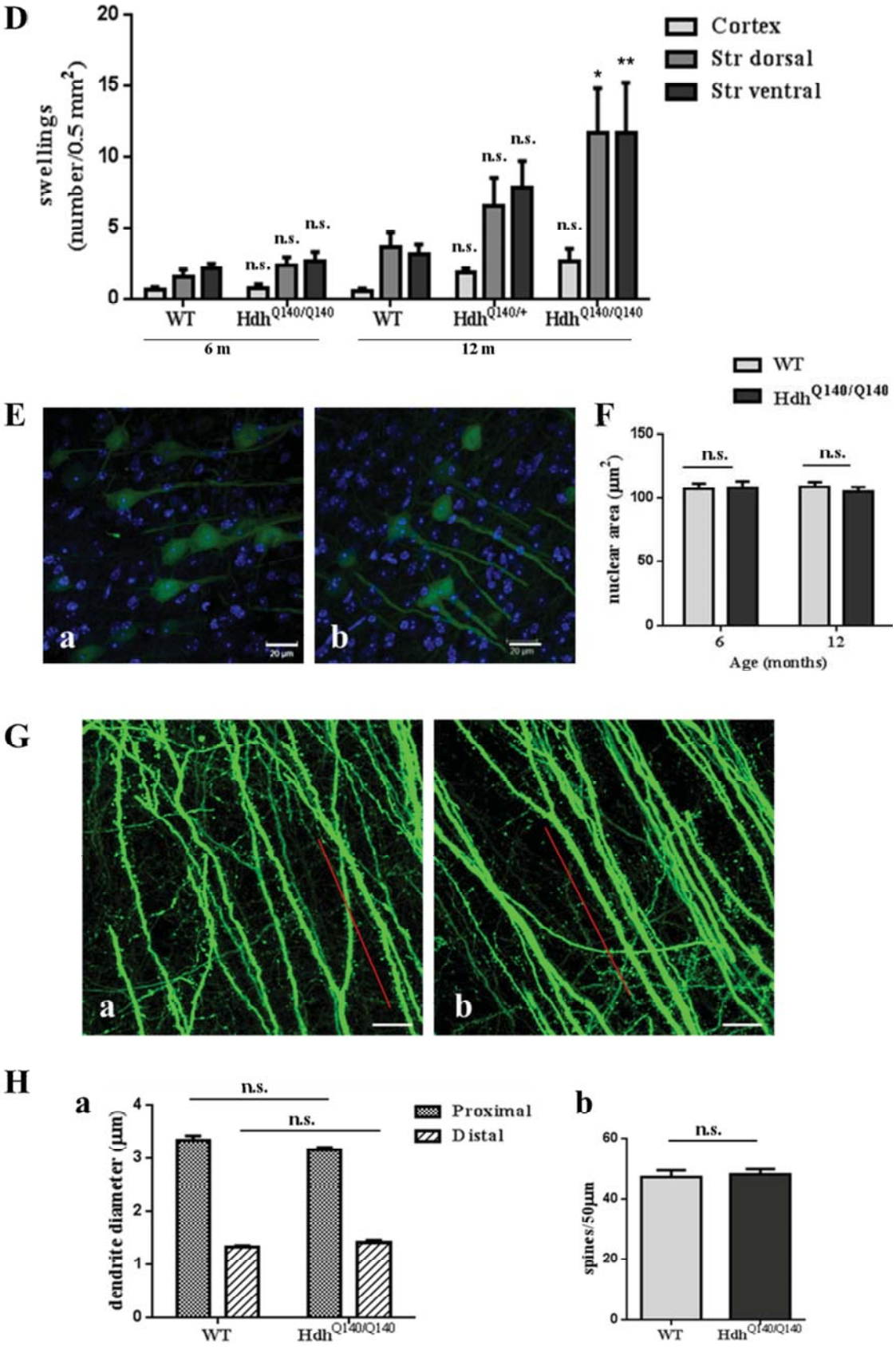
D
swellings (number/0.5 mm²)
Cortex
Str dorsal
Str ventral
n.s.
*
**
WT
Hdh Q140/Q140
Hdh Q140/+
6 m
12 m
E
a
b
20 µm
F
WT
Hdh Q140/Q140
nuclear area (µm²)
Age (months)
G
a
b
H
a
dendrite diameter (µm)
Proximal
Distal
b
spines/50µm

Fig. 19

Axonal swellings are detected in Hdh$^{Q140/Q140}$ mice before changes in cell bodies and dendrites.

*Confocal images (20X) of sagittal brain sections (50 µm) from (A) 12 month old WT/YFP-H (a-b-c) and Hdh$^{Q140/+}$/YFP-H (d-e-f) mice, from (B) 6 month old WT/YFP-H (a-b-c) and Hdh$^{Q140/Q140}$/YFP-H (d-e-f) mice and (C) 12 month old WT/YFP-H (a-b-c) and Hdh$^{Q140/Q140/}$YFP-H (d-e-f) mice, show increased axonal swellings in the KI model compared to the controls. Scale bar, 50 µm. (D) Quantification of the number of swellings in cortex and striatum dorsal and ventral reveals a significant increase in the striatum of Hdh$^{Q140/Q140}$ mice compared to controls at 12 months of age. No difference could be detected in Hdh$^{Q140/Q140}$ at 6 months, while in Hdh$^{Q140/+}$ mice at 12 months we could detect a trend to an increase although it was not statistically significant (n = 3-6, mean±SEM, one-way ANOVA followed by Bonferroni post hoc test, *, P<0.05, **, P<0.01, compared to the corresponding WT). (E) Confocal images (40X) of YFP+ neurons with nuclei stained with Hoechst in the cortex of (a) 12 month old Hdh$^{Q140/Q140}$ and (b) control YFP-H mice show no gross morphological changes. Scale bar, 20 µm. (F) Quantification of their nuclear areas did not show gross difference between the genotypes. (G) Dendrite morphology appears normal in 12 month old Hdh$^{Q140/Q140}$ (a) compared to YFP-H control mice (b). (H) Quantification of (a) dendrite diameter and (b) spine density over 50 µm (red bar in (G) a, b) shows no significant difference in Hdh$^{Q140/Q140}$ mice compared to YFP-H (n = 4, mean±SEM, Student's t-test). Scale bar, 20 µm. Green: YFP, blue: Hoechst.*

A big increase in axonal swellings in Hdh$^{Q140/Q140}$/YFP-H mice was detected in axons running through the *stria terminalis*, a limbic forebrain structure located in the proximity of the striatum and the lateral ventricle. Neurons whose axons form this structure are also YFP+ in the HD/YFP-H mice (Porrero et al., 2010) (Fig. 20 A). Upon quantification, the number of axonal swellings in this area in Hdh$^{Q140/Q140}$ mice resulted to be significantly increased compared to the control mice already at 6 months and was even greater at 12 months (Fig. 20 B). The morphology of YFP+ cell bodies located in the amygdala, an area that contains the cell bodies of the axons running in *stria terminalis* (Fig. 20 C), appeared generally normal and their nuclear size was not altered in HdhQ140 compared to wild-type mice (Fig. 20 D); only occasionally I could detect some dysmorphic cell bodies in a few of the mice, irrespective of the genotype (data not shown).

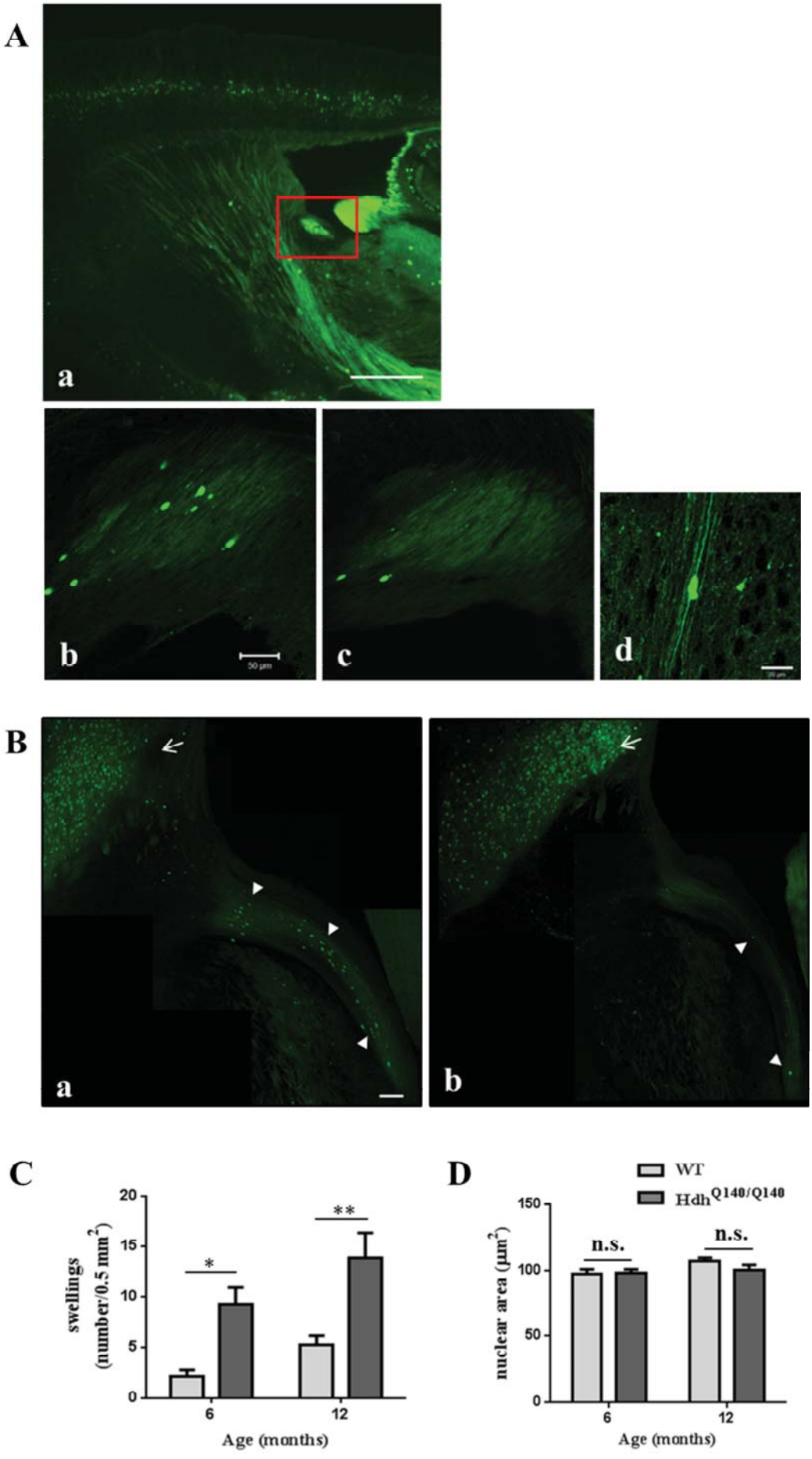
A
a
b
c
d
B
a
b
C
swellings (number/0.5 mm²)
20
15
10
5
0
*
**
6
12
Age (months)
D
WT
Hdh^Q140/Q140
nuclear area (µm²)
150
100
50
0
n.s.
n.s.
6
12
Age (months)

Fig. 20

Increased number of axonal swellings is detected in stria terminalis of HdH$^{Q140/Q140}$ mice. *(A) Sagittal brain sections (50 μm) of Hdh$^{Q140/Q140}$/YFP-H and WT/YFP-H mice. (a) Representative fluorescent image (2.5X) of a sagittal brain section; the red box indicates the brain area of stria terminalis where a great number of axonal swellings was found. Scale bar, 100 μm. 20X images of stria terminalis of (b) 6 month old Hdh$^{Q140/Q140}$ and (c) control mice show increased swellings in the KI model compared to WT. Scale bar, 50 μm. (d) Higher magnification image reveals that axon continuity is maintained at both sides (white arrows) of the swelling. Scale bar, 20 μm. (C) Quantitative analysis of swellings in stria terminalis of Hdh$^{Q140/Q140}$ at 6 and 12 months of age shows significant increase compared to control mice. (B) Confocal reconstruction images of sagittal sections show a big number of axonal swellings in 12 month old Hdh$^{Q140/Q140}$ mice (a) compared to control littermates (b) in axons running in the stria terminalis (white arrowheads). Their corresponding cell bodies are located in the amygdala (white arrows). Scale bar, 100 μm. (D) Quantification of the Hoechst stained nuclear area of YFP+ cell bodies in the amygdala reveals no significant difference between the genotypes (n = 4-5, mean±SEM; one-way ANOVA, *, P<0.05, **, P<0.01).*

Taken together, these results suggest that axon dystrophy precedes cell body and dendrite abnormalities in the HdhQ140 HD model. In addition, they suggest that the corticostriatal pathway may not be the first site of degeneration which can instead originate in other brain areas. On the other hand, a different sequence of neuropathological events characterises the R6/2 model in which significant axonal degeneration could not be detected.

In addition, in Hdh$^{Q140/Q140}$ mouse brains at 6 months, I performed Golgi staining to look at alterations in MSSNs, which are reported to be affected first in HD. Using this technique; I aimed to see whether morphological alterations were present in these neurons which are not YFP labelled in the YFP-H model. No gross morphological changes were found in KI mice compared to the ones of control mice as similar cell bodies and abundant dendritic spines were observed in both genotypes (Fig. 21).

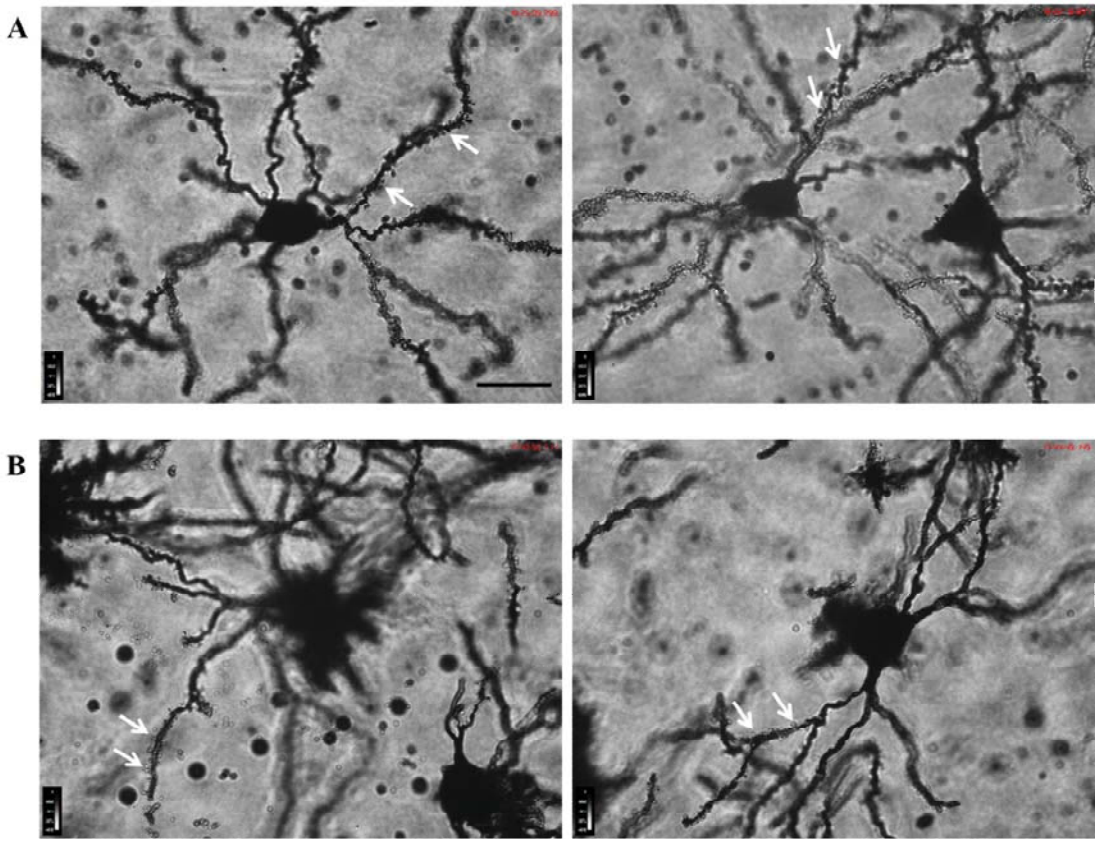

Fig. 21

Golgi staining shows normal morphology of MSSNs in Hdh$^{Q140/Q140}$ mice. *Bright field images (63X) of Golgi stained sagittal brain sections (50 µm) of 6 month old WT (A) and Hdh$^{Q140/Q140}$ mice (B) show no gross alteration in dendritic spines (arrows) and cell body of striatal neurons in HD mice compared to controls (n = 2). Scale bar, 20 µm.*

3.2.3 mHTT inclusions do not correlate with axon pathology

Next, I asked whether axon abnormalities correlate with the deposition of mHTT aggregates in HD mouse models. As aggregates are mostly believed to have a toxic function, a possibility was that degenerating axons were those containing inclusions. Thus I wanted to test whether this was the case in my HD/YFP+ mouse models.

First, I analysed by confocal microscopy brain sections of R6/2 mice at 4 weeks of age stained with EM48, an antibody widely used to detect human mHTT in mouse models (Gutekunst et al., 1999). I confirmed the presence of widespread small NIIs and neuropil aggregates in cortex and striatum at this time-point, in addition to nuclear diffused fluorescence (Fig. 22 A a-b-e). At 12 weeks, NIIs appeared as one single larger inclusion per nucleus (Fig. 22 A c-d-f). These findings are in agreement with an

earlier study which described the age-dependent deposition of NIIs in the cortex and the striatum of R6/2 mice (Davies et al., 1997). 3D reconstruction of confocal images confirmed colocalisation between mHTT aggregates and some YFP+ neurons in our models (Fig. 23 A, suppl. video 1A); however I was unable to detect any colocalisation between the small neuropil aggregates and the YFP+ axons with this imaging approach (Fig. 23 B, suppl. video 1B). Thus, neurons of R6/2 mice develop big mHTT intranuclear aggregates and yet maintain normal axon morphology.

In agreement with previous characterisations (Menalled et al., 2003), the deposition of mHTT aggregates follows a slower time course in HdhQ140 mice. In the striatum of $Hdh^{Q140/+}$ mice at 4 months of age only small NIIs were detected, whereas no immunostaining was visible in the cortex (Fig. 21 B a-b-g). At this time-point, in contrast to the earlier description from Menalled and collaborators (Menalled et al., 2003), I could not clearly detect neuropil inclusions in striatum and cortex. At 12 months, striatal NIIs increased in size but still no immunoreactivity could be detected in the cortex (Fig. 22 B c-d-h).

In $Hdh^{Q140/Q140}$ mice at 6 months, large NIIs were detected in the striatum, while no immunoreactivity was present in the cortex, similar to heterozygotes at 12 months (Fig. 22 C a-b-i). In addition to the large NIIs in the striatum, small extranuclear aggregates appeared in the cortex of $Hdh^{Q140/Q140}$ mice at 12 months (Fig. 22 C c-d-l). Neither in the amygdala nor in the *stria terminalis*, could mHTT immunoreactivity be detected in homozygous KI mice (data not shown).

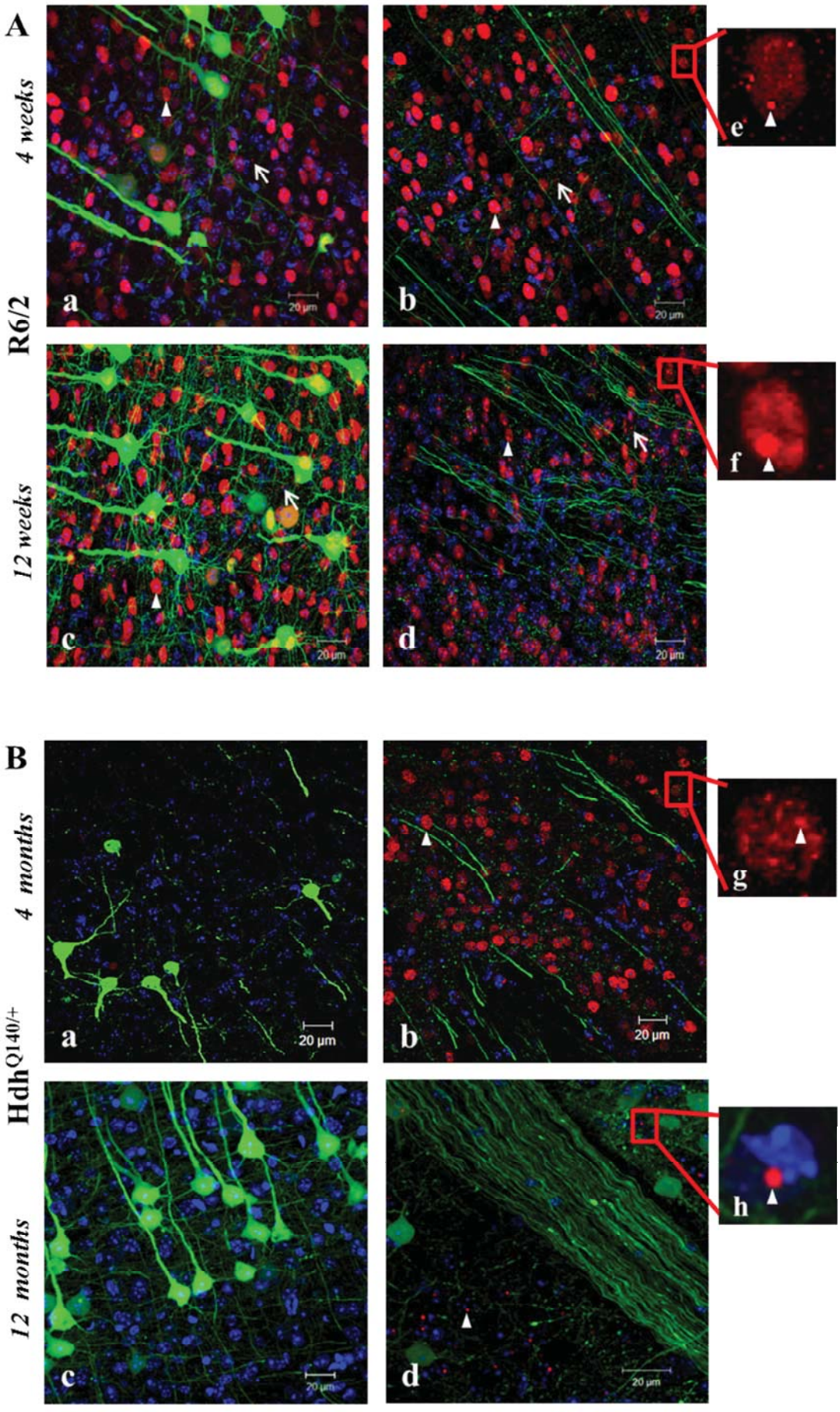
A
4 weeks
R6/2
12 weeks
a
b
c
d
e
f
20 µm
B
4 months
Hdh Q140/+
12 months
a
b
c
d
g
h
20 µm

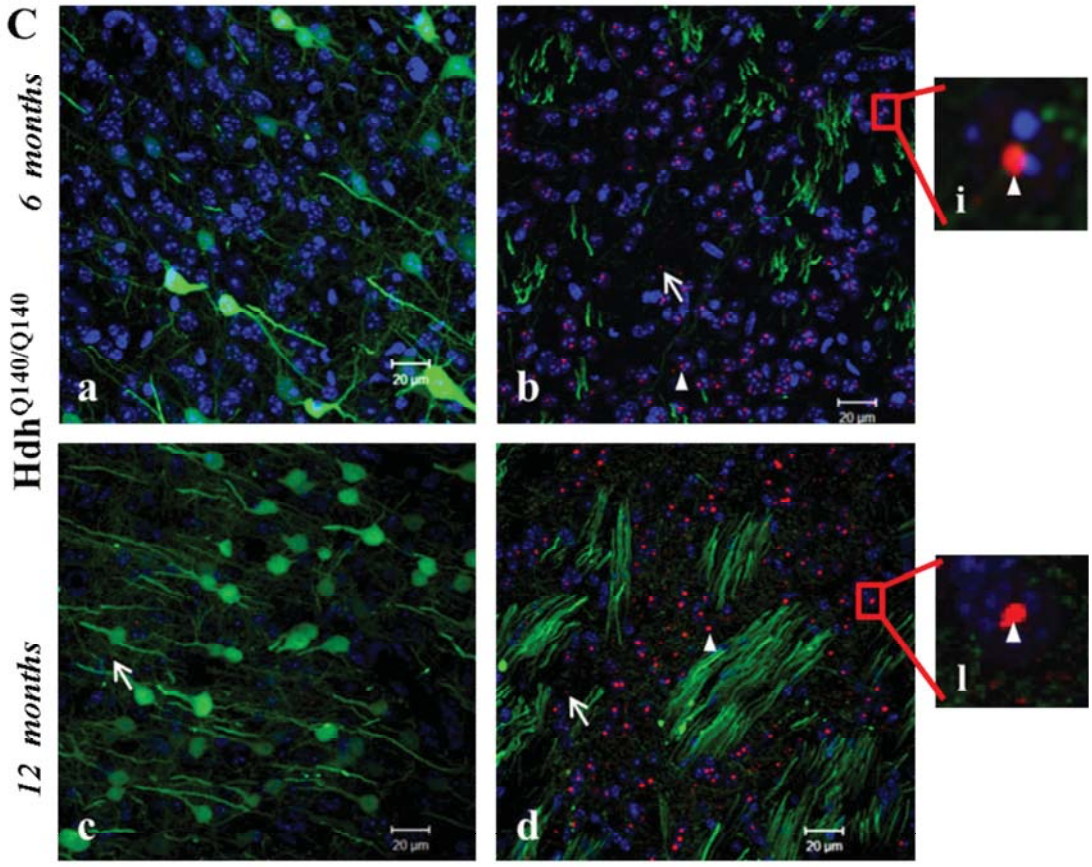

Fig. 22

Spatio-temporal characterisation of mHTT aggregate formation in HD models. *Coronal sections (20 µm) of R6/2/YFP-H and HdhQ140/YFP-H mice. Sections were immunostained with anti-HTT antibody (EM48) and imaged under high resolution (63X) confocal microscopy to characterise mHTT inclusions. (A) 4 week old R6/2 mice show small intranuclear (arrowhead) and extranuclear (arrow) mHTT aggregates both in (a) cortex and (b) striatum. 12 week old R6/2/YFP-H mice show small intranuclear (arrowhead) and large exanuclear (arrow) mHTT aggregates both in (c) cortex and (d) striatum. Strong diffused nuclear staining is also visible. (B) 4 month old* $Hdh^{Q140/+/}$*YFP-H mice show small intranuclear (arrowhead) mHTT aggregates in the (b) striatum while no immunostaining is detected in (a) the cortex. 12 month old* $Hdh^{Q140/+/}$*YFP-H mice show a large intranuclear aggregate (arrowhead) in the (d) striatum and no aggregates in (c) the cortex. (C)* $Hdh^{Q140/Q140}$*/YFP-H mice at 6 months of age show large intranuclear aggregates (arrowhead) in (b) the striatum and no staining in (a) the cortex. In 12 month old* $Hdh^{Q140/Q140}$*/YFP-H mice small extranuclear aggregates appear in the cortex (c, arrow) in addition to the large NIIs detectable in striatum (d, l). (e, f, g, h, i, l) enlarged images from the corresponding boxed areas show mHTT aggregates in the nucleus (arrowheads). Scale bar, 20 µm. Green: YFP, red: mHTT, blue: DAPI.*

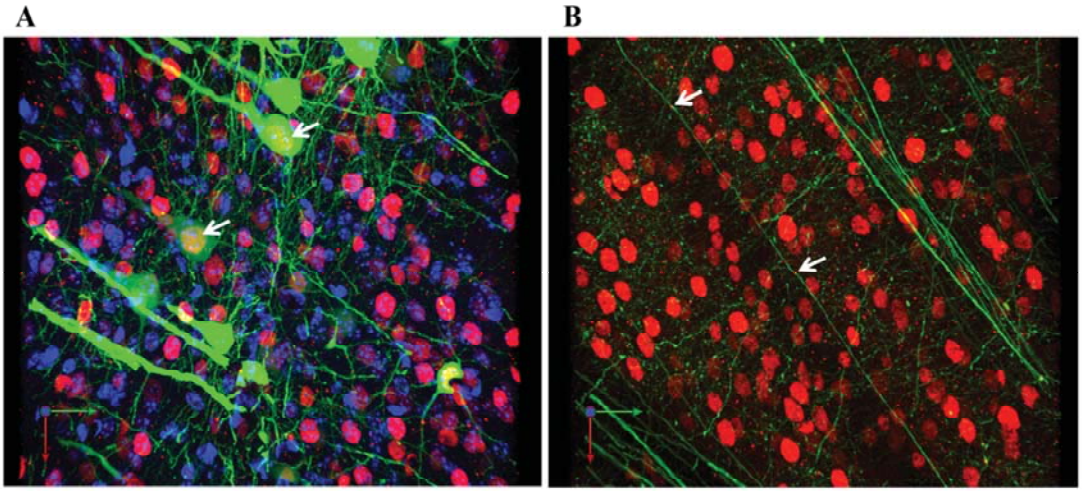

Fig. 23

Neuropil mHTT inclusions do not colocalise with YFP+ axons in R6/2 mice. *(A) YFP+ neurons of R6/2 mice accumulate mHTT nuclear aggregates. Confocal images (63X) of coronal sections (20 µm) of 3 month old R6/2/YFP-H mice immunostained with anti-HTT antibody (EM48). In the cortex, mHTT aggregates colocalise with the nucleus of YFP+ neurons (arrow) and this is confirmed by 3D reconstruction (Suppl. video 1A). (B) Neuropil mHTT aggregates do not colocalise with YFP+ axons in R6/2 mice. In the striatum, colocalisation between mHTT neuropil aggregates and YFP+ axons is not confirmed by 3D reconstruction (Suppl. video 1B). Scale bar: 20 µm. Green: YFP, red: mHTT, blue: DAPI.*

While these data confirm the subtle and progressive onset of mHTT deposition in our mouse models, they argue against a correlation between mHTT aggregates and the formation of axonal swellings. However, the presence and detrimental role of soluble mHTT in the abnormal axons cannot be excluded (Arrasate et al., 2004).

3.2.4 Synaptic abnormalities in HD mouse models

Synaptic transmission is altered in HD and abnormalities have been described at early time-points in HD models (Smith et al., 2005). To investigate potential synaptic defects in our R6/2 and HdHQ140 mice and evaluate their temporal pattern of onset in relation to the axonal abnormalities, I looked at the expression levels of the pre- and post- synaptic marker proteins synaptophysin and PSD-95 by Western blotting.

In R6/2 mice at 12 weeks of age, a late time-point in this mouse model but when axons still look intact (Fig. 24), the levels of both these synaptic markers appeared

significantly reduced in the striatum, while no significant difference was found in the cortex (Fig. 24 A-B).

Alterations in the level of neither synaptophysin nor PSD-95 were detected in cortex and striatum of $Hdh^{Q140/Q140}$ mice both at 6 and 12 months of age (Fig. 24 C-D). The same result was found at 12 months in the hypothalamus, one of the main areas where the axons running in *stria terminalis* project their synapses (Fig. 24 E).

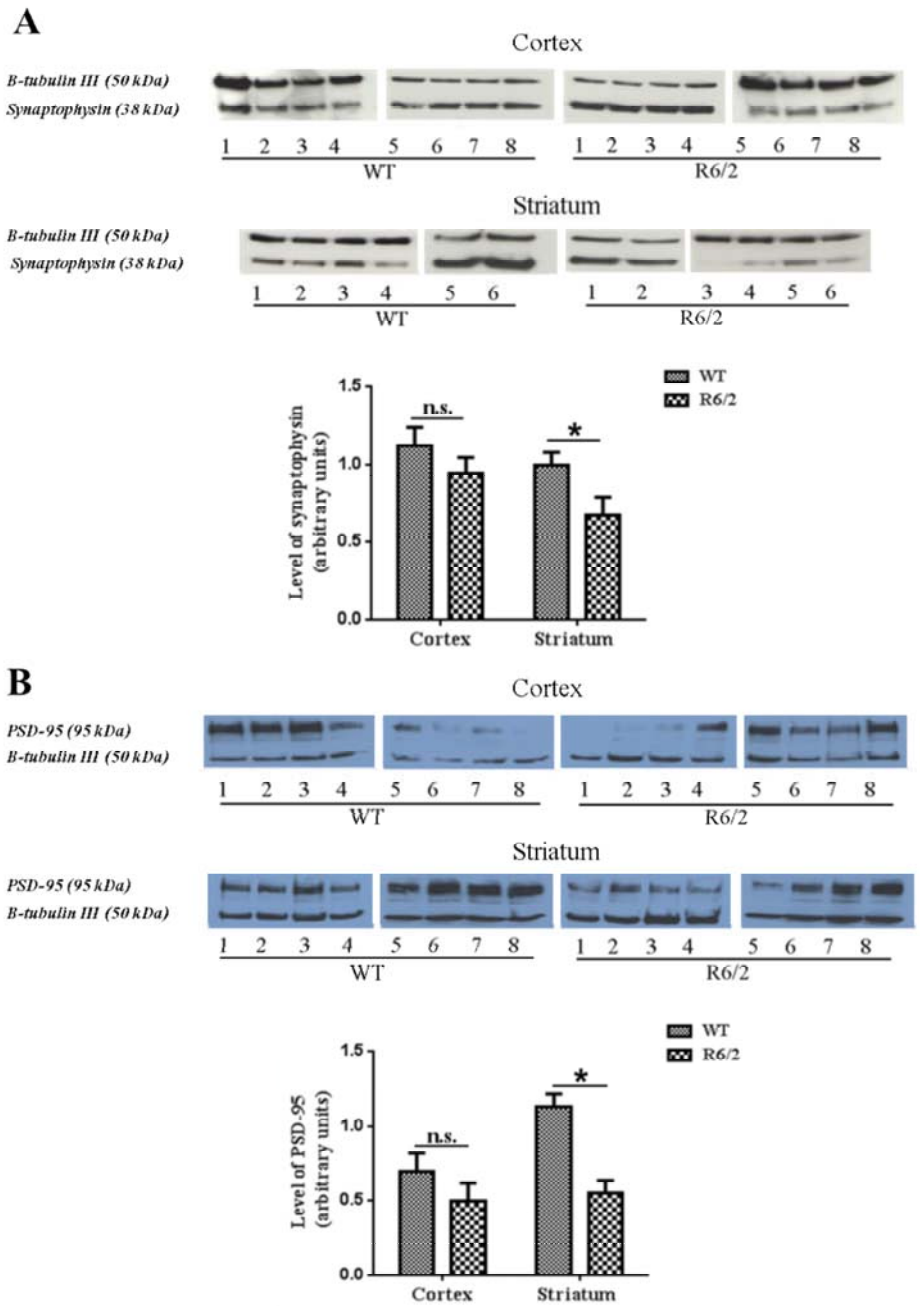

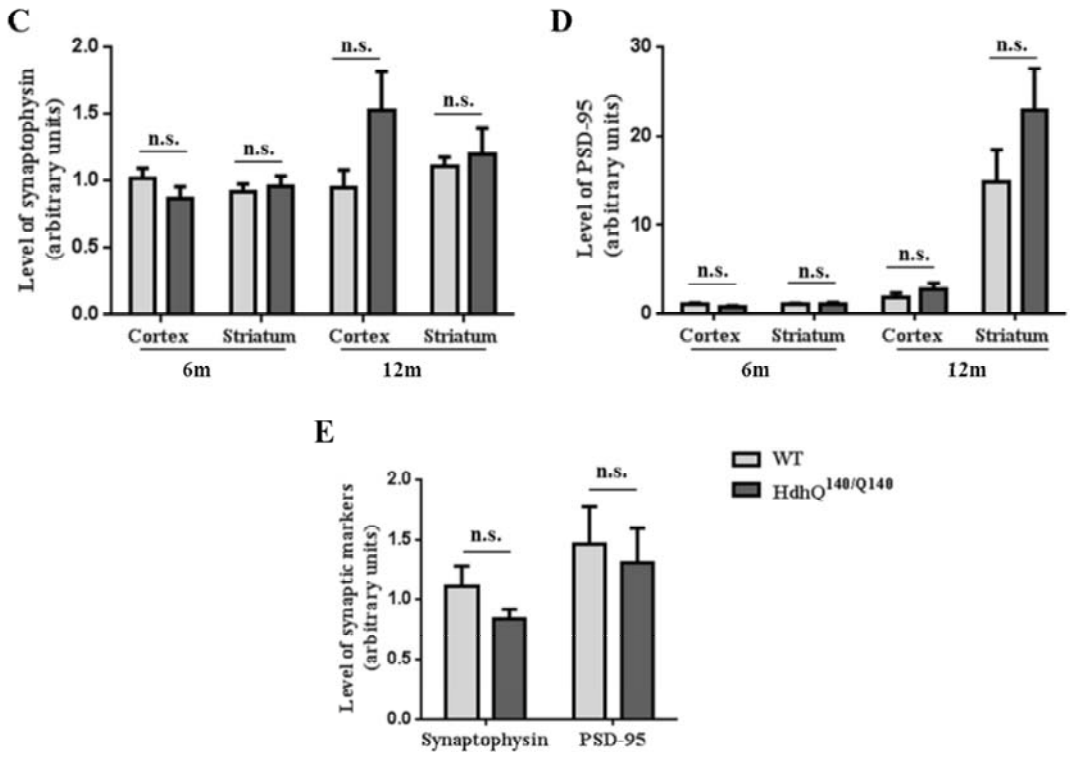

Fig. 24

Levels of synaptic markers in HD mouse brains. *Western Blots of mouse brain homogenates probed with antibodies against the presynaptic marker protein synaptophysin and PSD-95. β-tubulin III was used as a loading control in all blots (KDa 50). Blots for (A) synaptophysin (KDa 38) and (B) PSD-95 (KDa 95) of cortical and striatal homogenates of 12 weeks old R6/2 and WT mice and corresponding quantification (right) show no significant reduction of both markers in the cortex of 3 month old R6/2 compared to WT mice. In striatum, the level of synaptophysin (A) and PSD-95 (B) are significantly reduced compared to WT mice (n = 8, mean±SEM, unpaired Student's t-test, *, P<0.05). In* $Hdh^{Q140/Q140}$ *mice at 6 and 12 months of age we found no significant difference in the levels of (C) synaptophysin and (D) PSD-95 (n = 7-8, mean±SEM, one-way ANOVA followed by Bonferroni post hoc test). (E) The levels of synaptic markers in the hypothalamus of 12 months old* $Hdh^{Q140/Q140}$ *mice do not differ from those of control littermates (n = 7-8, mean±SEM, one-way ANOVA followed by Bonferroni post hoc test).*

Taken together, these results suggest synaptic dysfunction is a prominent feature of disease in R6/2 transgenic mice and this precedes degeneration of other neuronal compartments. However, in HdhQ140 KI mice, the level of synaptic markers are not altered at a time when axonal abnormalities are evident, suggesting that the sequence of neuropathological events can vary depending on the genetic model and that axonal abnormalities are the first signs of pathology in this mouse.

3.3 Discussion

These data show that in HdhQ140 homozygous mice, axon pathology precedes death of other neuronal compartments. In $Hdh^{Q140/Q140}$/YFP-H mice at 6 months of age, a striking increase in the number of axonal swellings compared to wild-type mice is found and this precedes signs of degeneration in cell bodies, dendrites and synapses. Data also demonstrate that increase in swellings is detected first in the *stria terminalis*, a brain area which is part of the limbic system and plays a role in fear and anxiety-related behaviour. In support of these results, recent studies have reported the involvement of the limbic system in early behavioural symptoms in HD patients (Petersen and Gabery, 2012) and mice (Van Raamsdonk et al., 2005b). Furthermore, a recent study describes early onset anxiety-related behaviour in HdhQ140 mice (Hickey et al., 2008), which is consistent with the findings that degenerative processes in axons are on-going in this area. At the later time-point of 12 months, significant axon pathology extends also to the corticostriatal axons of $Hdh^{Q140/Q140}$ mice. These findings highlight the importance of studying on multiple brain areas also in human patients in order to detect early axon degeneration in HD.

Axonal swellings are morphologically similar to those seen during normal aging but appear earlier and their number is significantly higher. Importantly, morphological abnormalities in HdhQ140 axons seem to be independent from mHTT inclusion formation since no aggregate could be detected in YFP+ neurons in the cortex and in the amygdala, two areas where the cell bodies of corticostriatal axons and of *stria terminalis* axons are located. However, other factors such as the presence of the toxic undetectable fraction of mHTT could play a critical role in this process.

HdhQ140 mice represent a more accurate model to investigate axon degeneration during HD progression. KI mice are genetically more similar to human HD patients than transgenic mice; they have normal life-span and milder phenotype resembling the presymptomatic stage of the disease in human patients. And here I show that the sequence of pathological events more closely resembles findings in human patients (Li and Conforti, 2013). Possibly, the combination of full-length mHTT expression at a physiological level, rather than just mutant N-terminal fragments expressed at high levels as in transgenic models like the R6/2 mouse, and the slower progression of the disease which allows normal aging in these mice in parallel with disease onset, explain the appearance of morphological signs of axon pathology. Moreover, these

results suggest that a certain level of mHTT is required to induce axonal pathology as only homozygous HdhQ140 mice, and not heterozygotes, exhibit a significantly higher number of swellings compared to control mice at 1 year of age. In $Hdh^{Q140/+/}$YFP-H mice at 12 months, the increase in number of axonal swellings may be in part related to normal aging and potentially to YFP accumulation in aging animals rather than to HD pathology, as an increase with ageing was observed both in KI mice and in control littermates with no statistically significant difference between the genotypes. This is consistent with previous observations suggesting that long term expression of the YFP transgene itself increases age-related swellings in some axons (Bridge et al., 2009). In heterozygotes, possibly the number of swellings would increase and become significantly higher than that in control mice at time-points later than 12 months.

Results in R6/2 mice confirm previous observations of synaptic abnormalities in the striatum of these mice (Klapstein et al., 2001, Cepeda et al., 2003) and these are found to occur before cell body or axonal death. These abnormalities could result either by synaptic degeneration or by synaptic remodeling (Torres-Peraza et al., 2008). Conversely, axonal swellings and spheroid formation is not a prominent feature in these mice, nor is striatal neuronal death. These findings point out the limitations of the transgenic model which partially recapitulate the human pathology. The aggressive phenotype with early death around 12-15 weeks of age makes the R6/2 mice particularly convenient for preclinical testing and therapy screening but less suitable for the investigation of the early mechanisms of an age-related disease that in human patients has late onset and slow progression. Considerations should be made on the role of mHTT aggregates in R6/2. Here, immunostaining with an anti-mHTT antibody reveals the presence of both intranuclear and neuropil mHTT aggregates but only the first is found to colocalise with YFP+ neurons. However a colocalisation and a toxic effect of neuropil aggregates on axons of non YFP+ neurons cannot be excluded.

Finally, this study reveals how the YFP-H mouse is a powerful tool to detect morphological changes when crossed with neurodegenerative disease models and to assess axon pathology both in CNS and peripheral nerves. In a similar study on a mouse model of Alzheimer's disease (Adalbert et al., 2009), axonal swellings in the absence of any morphological sign of cell body dysfunction is also observed. The

similarities between this and the present study suggest analogies in the sequence of events leading to degeneration in these two different disease models. However, due to the limited expression of the fluorescent protein to subsets of neurons, in both HD models, we cannot exclude that axon degeneration occurs in non YFP+ neurons. Striatal D2 neurons, which are affected very early in HD progression, are not fluorescently labelled in the YFP-H mouse line (Reiner et al., 1988, Albin et al., 1992) and we cannot rule out degeneration occurring in these neurons. Indeed, Golgi staining revealed no gross alteration in dendritic spines of individual neurons but technical problems and the unpredictability of the technique itself made it difficult to draw a final conclusion on these neurons.

In summary, axon pathology was found in the HdhQ140 mouse as a primary event which may initiate in brain areas other than those considered most susceptible to mHTT toxicity, while corticostriatal axons are affected at a later stage. Results also underline important differences in the site where the first abnormalities are observed depending on the HD mouse model under study. Understanding the mechanism at the basis of axon pathology is likely to be crucial to alleviate symptom onset and delay progression in HD.

CHAPTER 4

Longitudinal behavioural assessment of HdhQ140 homozygous mice

4.1 Introduction

4.1.1 Behavioural profile of HD

As mentioned in the first introductory chapter, HD patients suffer from a triad of symptoms which include motor, cognitive and behavioural abnormalities. These reflect the pathological changes affecting a number of brain areas including the striatum, which suffers the greatest damage, the cortex and subcortical regions such as the substantia nigra (SN), globus pallidus (GP), subthalamic nucleus (STN), amygdala, thalamus and hypothalamus, all affected at varying degrees and all tightly inter-connected by neural circuits.

The uncontrollable movements (chorea) that characterize HD and originally gave the name to the disease are now accepted to be only one part of the behavioural profile. Initially basal ganglia, which striatum is one of the main components, were thought to be purely a motor structure but later observations that striatal damage was leading to cognitive and emotional dysfunction as well as motor symptoms, suggested a more complex system of connections, ultimately controlling a variety of functions (Divac et al., 1967). The pioneer work of Alexander and collaborators led to the concept of the "functional loop" which proposed the existence of 5 structurally and functionally distinct circuits (motor, oculomotor, dorsolateral, ventral/orbital and anterior cingulate) connecting cortex, basal ganglia and thalamus (Fig. 25), 3 of which connect to non-motor areas of the frontal lobes, involved in planning, working memory, rule-based learning attention and other functions (Alexander et al., 1990, Alexander et al., 1986).

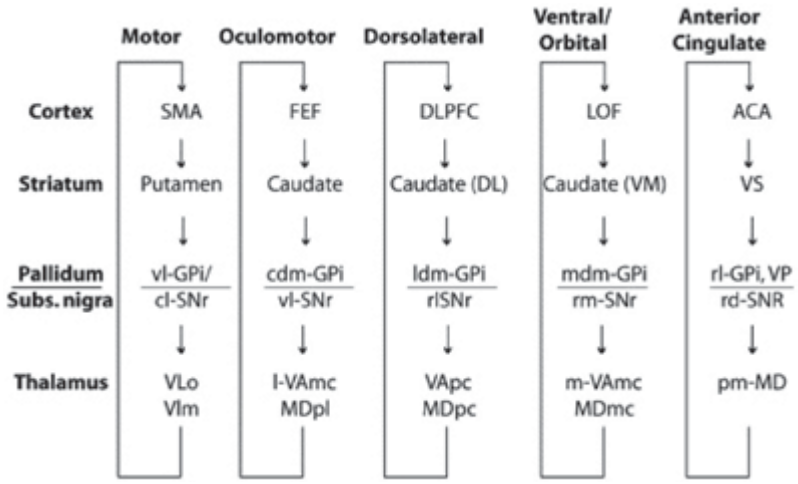

Fig. 25

Parallel organization of functionally segregated circuits linking basal ganglia and cortex. From (Grahn et al., 2009). *The dorsal and ventral striatum are differentially connected to discrete prefrontal cortical regions in segregated corticostriatal circuits. The putamen plays a critical role within the so-called 'motor circuit' while the caudate forms part of the oculomotor, dorsolateral and ventral/orbital circuits. SMA= supplementary motor area, vl-GPi = ventrolateral globus pallidus (internal segment), cl-SNr = caudolateral substantia nigra pars reticulata, VLo = ventrolateral nucleus of thalamus pars oralis, Vlm = ventrolateral nucleus of thalamus pars medialis, FEF = frontal eye fields, cdm-GPi = caudodorsomedial globus pallidus (internal segment), vl-SNr = ventrolateral substantia nigra pars reticulata, l-VAmc= lateral ventral anterior nucleus of thalamus pars magnocellularis,MDpl = parvocellular subnucleus ofmediodorsal nucleus of the thalamus, DLPFC = dorsolateral prefrontal cortex, Caudate (DL) = dorsolateral caudate, Caudate (VM) = ventromedial caudate, mdm-GPi = dorsomedial globus pallidus (internal segment), rm-SNr = rostromedial substantia nigra pars reticulata, m-VAmc=medial ventral anterior nucleus of thalamus pars magnocellularis, MDmc=magnocellular subnucleus of mediodorsal nucleus of the thalamus, ACA= anterior cingulate area, VS = ventral striatum, rl-GPi = rostrolateral globus pallidus (internal segment), VP = ventral posterior nucleus of the thalamus, rd-SNr = rostrodorsal substantia nigra pars reticulata, pm-MD= posteromedial mediodorsal nucleus of the thalamus.*

Cognitive and behavioral symptoms in HD can appear up to 15 years prior to the time of motor diagnosis, in the preclinical phase (Paulsen, 2011, Brooks and Dunnett, 2013) and have strong impact on patients quality of life. Early disturbances include personality and psychiatric symptoms, such as lack of concentration, changes of mood, aggressive behaviour, depression, apathy and anxiety (Paulsen et al., 2001, Dewhurst et al., 1970, Caine and Shoulson, 1983); and mild cognitive impairment

such as deficits in learning (Knopman and Nissen, 1991, Lawrence et al., 1998), in working memory and in executive memory (Paulsen, 2011, Lawrence and AD, 1998, Lawrence et al., 1996). These early symptoms reflect pathological changes both at striatal and cortical level and dysfunctions of neural circuits. In particular, defects in executive functions such as in the ability to solve complex problems like learning new information, planning ahead, regulating actions according to the environmental stimuli, are associated with alterations in the *dorsolateral circuit*; irritability, emotional instability, and lack of empathy are instead associated with damage to the *ventral/orbital circuit*. Damage to the *anterior cingulate circuit* that projects to the ventral striatum, which also receives limbic input from the hippocampus, amygdala, and entorhinal cortex, is instead associated with decreased motivation such as akinetic mutism, apathy, indifference to pain, thirst or hunger and lack of spontaneous movements, verbalization and response to commands (Tekin and Cummings, 2002).

Early symptoms include also alterations in sexual behaviour, in the wake-sleep cycle and symptoms not directly associated to brain changes such as progressive weight loss, skeletal-muscle wasting and testicular atrophy (Politis et al., 2008, van der Burg et al., 2009). Recent studies have highlighted the important contribution of hypothalamic dysfunction and changes in the limbic system in the early non-motor features of the disease (Petersen and Gabery, 2012). Indeed, the limbic system regulates emotion, sleep, circadian rhythm, temperature and body weight, all functions disrupted in HD. As pathology progresses, personality changes become more accentuate and cognitive impairments worsen leading to dementia often accompanied by psychotic symptoms.

In line with the observations of an early contribution of limbic system dysfunction to symptoms in HD patients, are results from chapter 3. The early pathological changes found in axons of *stria terminalis* in $Hdh^{Q140/Q140}$ mice indicated possible alterations in the limbic system and hinted further investigation of the behavioural phenotype in these mice.

Motor symptoms occur later in the disease progression and develop over a period of 10-15 years. Typically, the earliest motor signs are eye movement abnormalities (Avanzini et al., 1979), followed by the progressive appearance of orofacial dyskinesias, involving the head, neck, trunk and arms, before becoming chorea

(Brouillet et al., 1999). Dysarthria, speech difficulties, is present at early stages and becomes more pronounced with disease progression and dysphagia, difficulties in swallowing, develops in advanced stages and may lead to choking. Hyperkinesia, linked to the choreic involuntary movements, is the main feature of HD but together with this, impairment in voluntary movements such as bradykinesia (Thompson et al., 1988), the slow execution of movement, akinesia (Albin et al., 1990a), the inability to initiate movement and hypokinesia (van Vugt et al., 1996), the reduction of movement, have also been reported to coexist in patients. These manifestations reflect the pathological changes in the normal function of the motor circuits of the basal ganglia (see chapter 1.2). In particular, the preferential loss of striatal neurons projecting to the external segment of the Globus Pallidus (GPe) (indirect pathway) results in chorea and at a more advanced stage, the additional loss of striatal neurons projecting to the internal segment of the Globus Pallidus (GPi) (direct pathway) results in a rigid-akinesia. Alterations in sensorimotor gating of the startle reflex, measured by prepulse inhibition (PPI), are also well documented in HD patients (Swerdlow et al., 1995, Swerdlow et al., 2001). These are regulated by circuitry within the limbic system and frontal cortex, basal ganglia, and pons which seem to be affected in HD.

At a late stage, severe dementia and progressive motor dysfunction make patients unable to walk, talk, eat and ultimately to care for themselves. As the disease progresses, abnormal involuntary movements and dementia occur (Anderson and Marder, 2001, Rosenblatt, 2007, Politis et al., 2008) (Fig. 26).

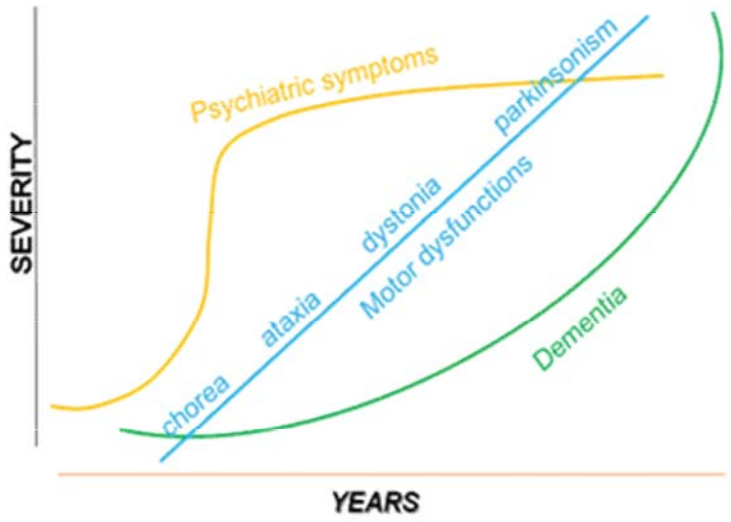

Fig. 26

Schematic representation of HD symptoms and progression with time.

4.1.2 Behavior of HD mouse models and its assessment

The characteristic late onset of HD pathology makes any attempt to reproduce the human phenotype within the life span of a mouse particularly challenging. Despite the limitations, genetic mouse models are the most common HD models used in behavioural studies since motor, cognitive and psychiatric symptoms, resembling those seen in patients, are observed in these animals (see Table 1) and a number of standardized batteries of tests are now available to assess them. A certain grade of variability exists depending on the type of tests used and also on the characteristics of the genetic model (CAG repeat number, expression of fragment or full length HTT and type of insertion of the mutant gene) as well as the specific background strain (Pouladi et al., 2013). In general, mHTT fragment transgenic models exhibit early onset and robust behavioral phenotype associated with significant weight loss and premature death. Although these mice display many of the behavioral and neuropathological features observed in HD patients, they do not mimic the genetic disease-initiating mechanism of HD, moreover, the rapid disease progression and the broad extra-striatal profile of the pathology make detailed analysis of behavior more difficult (Hickey and Chesselet, 2003). By contrast, knock-in mice which are the most precise genetic model of HD, show slower, more progressive impairment, allowing a detailed analysis of behavioural changes (Menalled et al., 2002, Kirkwood et al., 2001).

Motor function is found altered in HD mice. This can be assessed in mice by tests of general locomotor activity such as open-field and running wheel; coordination and balance such as rotarod, balance beams, swimming, climbing and grip strength; and sensorimotor gating such as prepulse inhibition (Brooks and Dunnett, 2009). N-terminal transgenic models generally display an early onset of severe motor symptoms: R6/2 mice, the most extensively studied and best characterized, show resting tremor, chorea-like movements, stereotypic involuntary grooming movements, and dystonia of the limbs (Mangiarini et al., 1996, Stack et al., 2005) which is also found in patients (Myers et al., 1988, Pratley et al., 2000). Alterations are also observed in grip strength measurements and in rotarod test starting as early as 40 days of age (Luesse et al., 2001). Full-length transgenic models such as YAC mice display more delayed motor symptoms compared to fragment models: in YAC72 mice a significant impairment in rotarod test is detected not earlier than 16 months (Seo et al., 2008) and in YAC128 mice around 6–7 months of age (Slow et al., 2003, Van Raamsdonk et al., 2005b). Knock-in mice often do not display the overt motor symptoms seen in transgenic models: in HdhQ92, HdhQ111 mice rotarod and gait deficits are not described until 2 years of age (Trueman et al., 2009, Menalled et al., 2009, Heng et al., 2007) and in HdhQ140 early mild gait abnormalities are seen at 1 year (Menalled et al., 2003) and subtle rotarod impairment at 4 months (Hickey et al., 2008). Abnormal sensorimotor gating is also found in HD mice as in human patients. Reduced PPI is found in R6/2 transgenic mice and this appear as early in disease progression (Carter et al., 1999).

Cognitive deficits which resemble those in patients are also found in HD mice and often, as in patients, precede the appearance of overt motor symptoms. Tests such as Morris water maze, T maze and Y maze (swimming or elevated) as well as operant chambers, can assess learning and memory dysfunctions in mice. Transgenic fragment mice such as the R6/2 mice show early cognitive defects by 3.5 weeks of age (Lione et al., 1999) while in full-length models such as YAC128 mice impairments appear later at around 8 months (Van Raamsdonk et al., 2005b). Among the knock-in HD mouse models, HdhQ92 mice show deficits around 10 months while HdhQ150 displayed no learning abnormalities (Heng et al., 2007).

Finally, psychiatric disturbances such as depression and anxiety are also modelled in HD mice and measured by a number of tests such as forced swim test (FST), tail

suspension test (TST), open-field test, elevated plus maze (EPM), and others (Tarantino and Bucan, 2000). Depression-like behaviour is found in female R6/1, in female HdhQ111 and in YAC128 mice (Pang et al., 2009, Orvoen et al., 2012, Pouladi et al., 2009). Increase in anxiety-like behaviour is reported in R6/2 transgenic mice (Menalled et al., 2009); in YAC128 mice (Menalled et al., 2009) and in HdhQ140 mice (Hickey et al., 2008).

In addition to motor, cognitive, and behavioural symptoms, HD mice display also some of the additional symptoms found in patients such as sleep abnormalities (Fisher et al., 2013, Kantor et al., 2013); circadian disturbances (Kudo et al., 2011, Davies et al., 1997) and changes in body weight (Menalled et al., 2009, Phan et al., 2009).

4.2 Hypothesis and aim of the chapter

This chapter aims to detect the onset and progression of potential behavioural abnormalities in HdhQ140 homozygous mice and correlate them to the neuropathological changes observed in these mice and described in chapter 3. I hypothesized that the increased formation of axonal swellings from 6 months of age in brain areas such as the limbic system particularly relevant for behavior parallels onset and progression of behavioural symptoms. To this aim, mice were subjected to a battery of tests specific to assess behavioural dysfunctions linked to alterations in cortex, striatum or limbic system; in a longitudinal follow-up in order to improve detection of early changes in these mice. Tests of sensorimotor function included rotarod, running wheel, open-field and prepulse inhibition; while tests of cognitive and behavioural included spontaneous alternation, novel object recognition, elevated plus maze and open-field.

4.3 Results

4.3.1 Locomotor activity is decreased in $Hdh^{Q140/Q140}$ mice but motor balance and coordination remain normal

First I used the rotarod test accelerated paradigm (see methods) to assess motor coordination and balance, and motor learning in HdhQ140 homozygous mice. Rotarod is one of the most commonly used assay to measure motor function in rodents

(Dunham and Miya, 1957). In addition, overnight running wheel test was used to measure voluntary locomotor activity during dark phase when mice are most active (93% of total activity is in dark phase) (Hickey et al., 2008, Hickey et al., 2005, Van Raamsdonk et al., 2007); and open-field test to assess general locomotor activity in light phase (Christmas and Maxwell, 1970) (see methods). Mice were tested at 1, 3, 6, 9 and 12 months of age.

Performance in rotarod test was not impaired in HdhQ140 mice compared to C57BL/6 control mice and both genotypes showed an age-dependent worsening of the performance (Fig. 27). Motor function at day 3 showed no overall genotype effect, suggesting no alterations in coordination and balance in the KI mice (Fig. 27 A). A significant effect of genotype was found on motor learning only at 1 month of age when the latency to fall during the three days of testing (learning curve) was significantly reduced in HdhQ140 mice compared to control mice (Fig. 27 B). At all other time-points a non-significant trend to increase was found in the KI mice (Fig. 27 C, D, E, F) compared to control mice, suggesting motor learning function is not impaired in this mice up to 12 months of age. A significant effect of gender was found only at 3 months (Fig. 27 C).

A Rotarod test, day3

	Num. df	Den. df	F-value	p-value
weight (g)	1	84	80.96	< 0.001
gender	1	22	0.22	0.645
genotype	1	22	1.31	0.265
age (months)	4	84	6.12	< 0.001
gender:genotype	1	22	0.02	0.877
gender:age (months)	4	84	1.56	0.192
genotype:age (months)	4	84	13.94	< 0.001
gender:genotype:age (months)	4	84	1.35	0.260

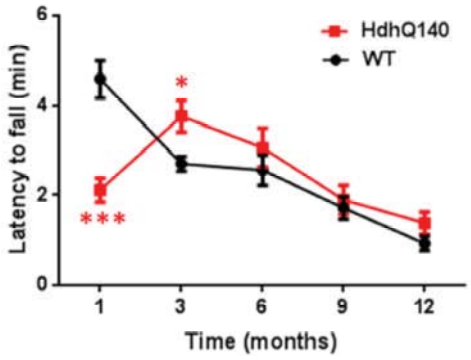

B Rotarod test, learning curve 1 month

	Num. df	Den. df	F-value	p-value
weight (g)	1	21	3.66	0.069
gender	1	21	1.35	0.258
genotype	1	21	19.91	< 0.001
trial	8	176	18.40	< 0.001
gender:genotype	1	21	7.11	0.014
gender:trial	8	176	0.33	0.954
genotype:trial	8	176	6.08	< 0.001
gender:genotype:trial	8	176	1.47	0.171

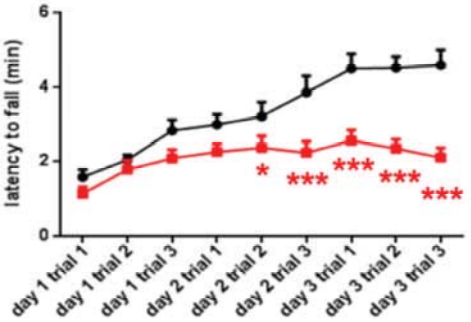

C Rotarod test, learning curve 3 months

	Num. df	Den. df	F-value	p-value
weight (g)	1	21	10.38	0.004
gender	1	21	5.71	0.026
genotype	1	21	0.02	0.899
trial	8	176	13.21	< 0.001
gender:genotype	1	21	0.01	0.916
gender:trial	8	176	1.04	0.410
genotype:trial	8	176	3.46	< 0.001
gender:genotype:trial	8	176	2.30	0.023

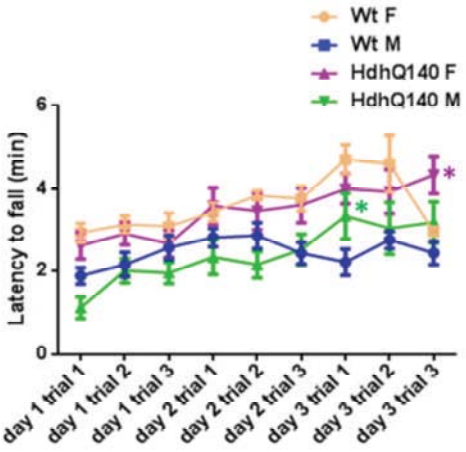

D Rotarod test, learning curve 6 months

	Num. df	Den. df	F-value	p-value
weight (g)	1	20	0.83	0.374
gender	1	20	0.21	0.655
genotype	1	20	0.13	0.720
trial	8	168	5.77	< 0.001
gender:genotype	1	20	1.96	0.177
gender:trial	8	168	3.87	< 0.001
genotype:trial	8	168	3.13	0.003
gender:genotype:trial	8	168	0.94	0.488

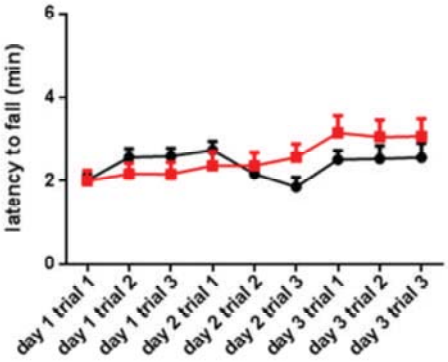

E Rotarod test, learning curve 9 months

	Num. df	Den. df	F-value	p-value
weight (g)	1	20	4.03	0.058
gender	1	20	0.03	0.864
genotype	1	20	0.03	0.874
trial	8	168	1.58	0.133
gender:genotype	1	20	0.59	0.453
gender:trial	8	168	0.33	0.954
genotype:trial	8	168	3.22	0.002
gender:genotype:trial	8	168	1.34	0.226

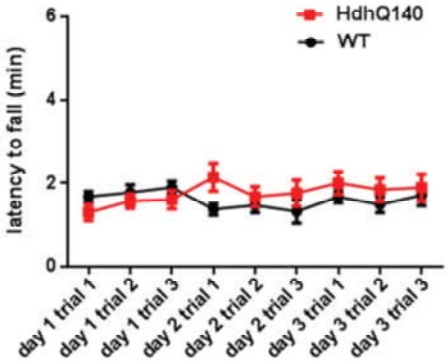

F Rotarod test, learning curve 12 months

	Num. df	Den. df	F-value	p-value
weight (g)	1	20	5.92	0.024
gender	1	20	0.02	0.884
genotype	1	20	0.14	0.711
trial	8	168	1.75	0.091
gender:genotype	1	20	0.31	0.586
gender:trial	8	168	1.62	0.123
genotype:trial	8	168	3.83	< 0.001
gender:genotype:trial	8	168	2.07	0.041

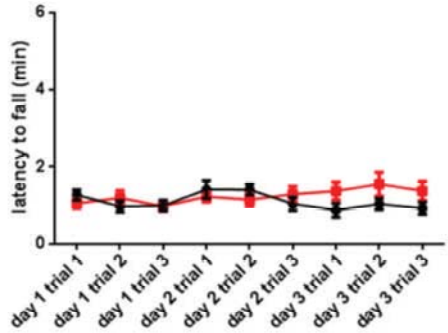

Fig. 27

Rotarod performance is not impaired in Hdh$^{Q140/Q140}$ mice. *Latency to fall (min) was measured in three trials per day over three days of testing. Graphs report the latency to fall at day 3 only with time (A) and the learning curves at 1 (B), 3 (C), 6 (D), 9 (E) and 12 (F) months. The effect of gender/genotype/age interactions is reported in the tables for each time-point. (A) Motor function has no overall genotype effect although at 1 month of age KI perform significantly worse, with no gender effect. Learning curves reveal a genotype effect at 1 month of age (B) when KI mice perform significantly worse than WT mice at day 2 and 3 (n = 12-14, mean±SEM, two-way ANOVA with Tuckey post-hoc test, compared to wild-type, *, P<0.05, ***, P<0.001); while at 3 (C), 6 (D), 9 (E) and 12 months of age (F) no difference is found between genotypes. Only at 3 months of age (C) a significant effect of sex is found (n = 6-7, mean±SEM, 3-way ANOVA with Bonferroni post-hoc test, compared to wild-type, *, P<0.05) while at all other time-points data are pulled together (two-way ANOVA). Body weight was used as covariate in all statistical analyses.*

Voluntary wheel running performance showed instead significant difference between HdhQ140 and relative control mice from 9 months of age with a general trend to decrease from 3 months. The distance run (km) was significantly reduced in the KI mouse model compared to WT mice (Fig. 28 A), with a significant effect of gender

(Fig. 28 A-b), but the speed of run (km/h) was not altered at all the time-points tested (Fig. 28 B).

A **Running wheel, total distance run**

	Num. df	Den. df	F-value	p-value
weight (g)	1	84	0.02	0.878
gender	1	22	16.76	< 0.001
genotype	1	22	4.57	0.044
age (months)	4	84	2.38	0.058
gender:genotype	1	22	0.02	0.897
gender:age (months)	4	84	0.58	0.676
genotype:age (months)	4	84	1.21	0.311
gender:genotype:age (months)	4	84	0.16	0.959

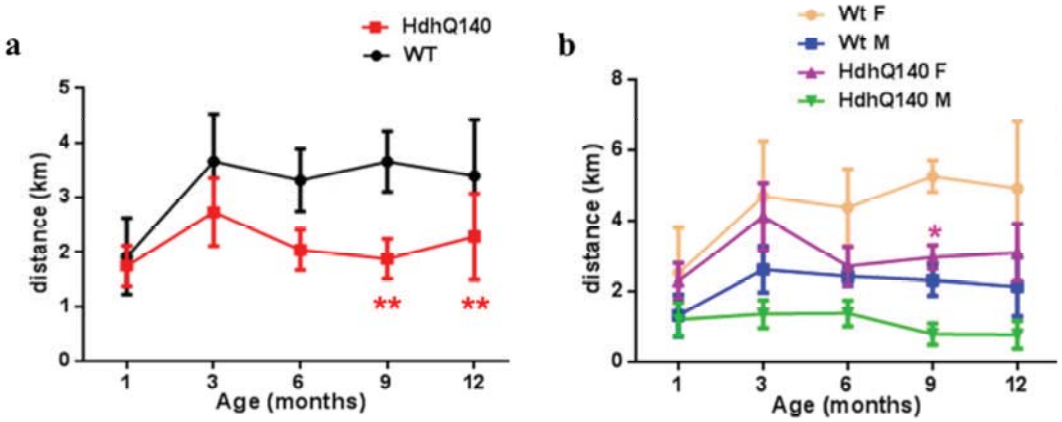

B **Running wheel, average speed**

	Num. df	Den. df	F-value	p-value
weight (g)	1	84	0.00	0.975
gender	1	22	7.31	0.013
genotype	1	22	0.14	0.709
age (months)	4	84	0.89	0.471
gender:genotype	1	22	0.48	0.494
gender:age (months)	4	84	0.40	0.809
genotype:age (months)	4	84	1.06	0.383
gender:genotype:age (months)	4	84	0.11	0.977

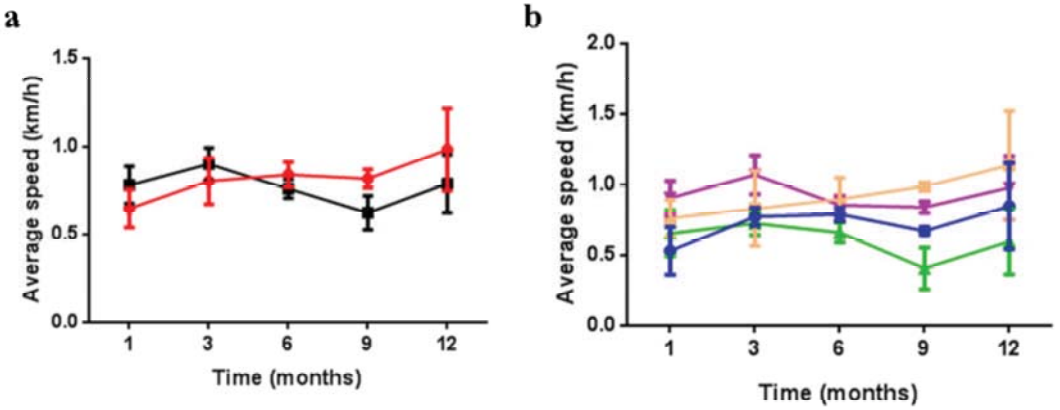

Fig. 28

Running wheel test performance is impaired in Hdh$^{Q140/Q140}$ mice. *Mice were singly housed during dark phase and the distance and the average speed run on a wheel were automatically recorded. The effect of gender/genotype/age interactions is reported in the tables. A significant genotype effect is found in the distance run (Km) (A) as KI mice run less than WT mice with a significant difference at 9 and 12 months of age (A-a) (n = 12-14, mean±SEM, two-way ANOVA followed by Bonferroni post-hoc test, compared to wild-type, **, P<0.01). A gender effect is also found and HdhQ140 females perform significantly worse than WT females at 9 months (A-b) (n = 6-7, mean±SEM, 3-way ANOVA with bonferroni post-hoc test, compared to wild-type, *, P<0.5). Average speed (B) is instead unaltered at all time-points and no effect of genotype is detected (B a). Body weight was used as a covariate in all statistical analyses.*

Weight was considered as a covariate in statistical analysis of rotarod and running wheel data as it is believed to affect performance. Strain differences in rotarod performance had been previously correlated with variations in body weight (McFadyen et al., 2003). Mice were weighed monthly and at the beginning of each experimental time-point and a significant loss was found at 12 months of age in HdhQ140 mice compared to controls (Fig. 29 a), with a significant gender effect (Fig. 29 b).

Weight

	Num. df	Den. df	F-value	p-value
gender	1	22	85.47	< 0.001
genotype	1	22	4.97	0.036
age (months)	4	85	646.93	< 0.001
gender:genotype	1	22	0.38	0.546
gender:age (months)	4	85	28.09	< 0.001
genotype:age (months)	4	85	8.10	< 0.001
gender:genotype:age (months)	4	85	3.70	0.008

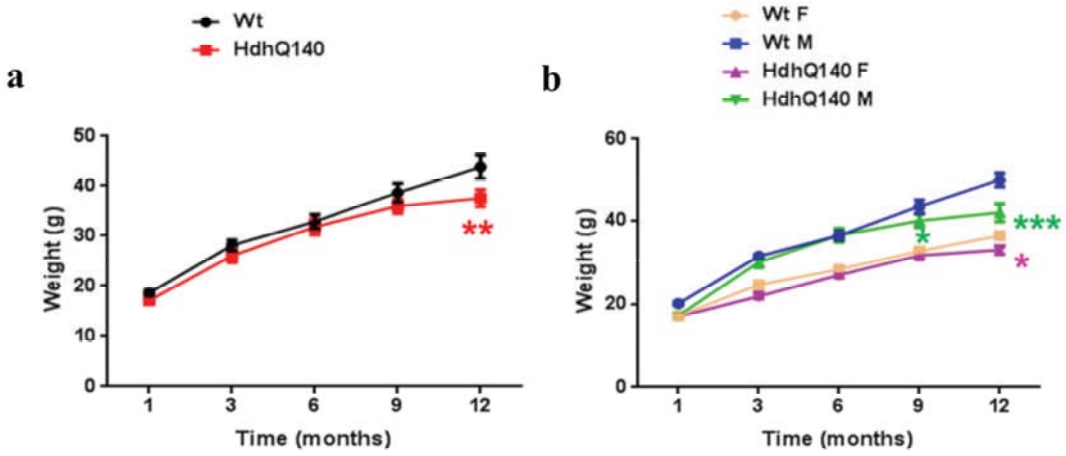

Fig. 29

Weight loss is significantly higher in Hdh$^{Q140/Q140}$ compared to WT mice. *Significant weight loss is recorded in HdhQ140 mice at 12 months of age (a) (n = 12-14, mean±SEM, two way ANOVA followed by Bonferroni post-hoc test, compared to wild-type, **, P<0.01, mean±SEM) with a significant gender effect as both KI females and males weigh significantly less than the corresponding WT (b) (n = 6-7, mean±SEM, 3-way ANOVA with Bonferroni post-hoc test, compared to wild-type *, P<0.05, ***, P<0.001). The effect of gender/genotype/age interactions is reported in the tables.*

Open-field test confirmed reduced locomotor activity in HdhQ140 mice and this was detected already at 3 months of age and later (Fig. 30 A-a), with a significant gender effect (Fig. 30 A-b). Thus, defects in motor activity develop early in these mice, prior to any detectable sign of pathology and deposition of mHTT aggregates in corticostriatal neurons (see Fig. 22 C).

Open field, total distance moved in the arena

	Num. df	Den. df	F-value	p-value
gender	1	22	6.15	0.021
genotype	1	22	44.86	< 0.001
age (months)	4	85	48.55	< 0.001
gender:genotype	1	22	7.98	0.010
gender:age (months)	4	85	2.67	0.038
genotype:age (months)	4	85	7.71	< 0.001
gender:genotype:age (months)	4	85	1.24	0.298

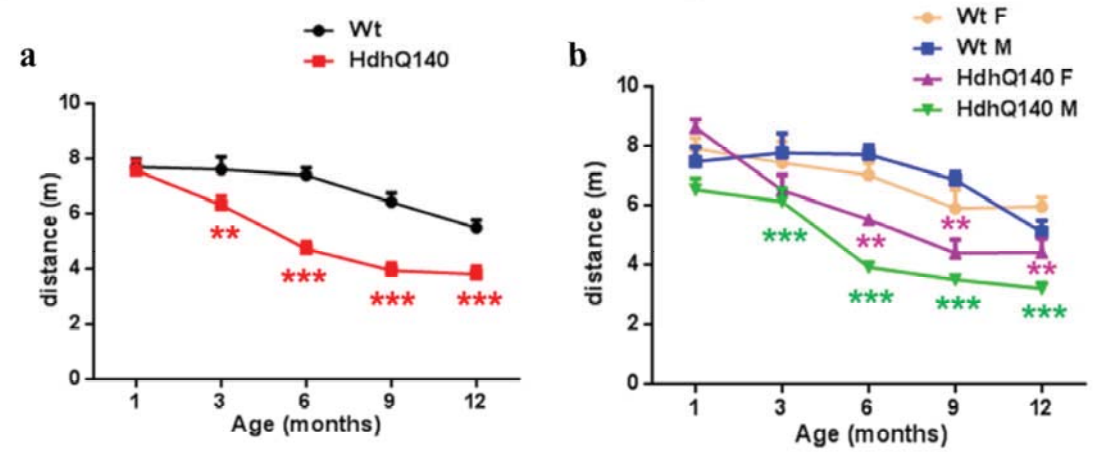

Fig. 30

Locomotor activity is reduced in Hdh$^{Q140/Q140}$ mice on open-field test. *Mice were allowed to move freely in an open-field arena for 30 min and the total distance moved was measured. The effect of gender/genotype/age interactions is reported in the tables. A significant effect of genotype, gender and age was found (table). Significant reduction in general locomotor activity is recorded early by 3 months of age (a) (n = 12-14, mean±SEM, two-way ANOVA followed by Bonferroni post-hoc test, compared to wild-type **, P<0.01, ***, P<0.001) with difference found both in the KI males and females compared to the corresponding controls (b) (n = 6-7, mean±SEM, 3-way ANOVA with Bonferroni post-hoc test, compared to wild-type **, P<0.01, ***, P<0.001). Body weight was used as covariate in all statistical analyses.*

4.3.2 The prepulse inhibition of startle test shows sensory-gating deficits in Hdh$^{Q140/Q140}$ mice

To assess sensorimotor processes in HdhQ140 mice, I tested animals in the prepulse inhibition of startle test (PPI) (see methods), measure of sensorimotor gating (Davis, 1980) which is reported to be impaired in several psychiatric disorders and also in HD patients and mouse models, where disruption of corticostriatal circuits and limbic system occur (Swerdlow et al., 1995, Geyer et al., 2002).

Data showed altered peak startle response and latency in HdhQ140 mice compared to WT controls (Fig. 31). At 3 and 12 months of age startle response was significantly lower (Fig. 31 A-a) and startle latency was significantly higher (Fig. 31 B-a) in the HD mice compared to control mice, with a significant gender effect (Fig. 31 A-b, B-b). PPI results (Fig. 32) showed a significant impairment in HdhQ140 mice compared to WT controls at 12 months of age (Fig. 32 E), while at all other time-points, an overall non-significant difference was detected (Fig. 32 A-B-C-D), although HdhQ140 males performed worse than WT males at 3 and 9 months of age (Fig. 32 B-b, D-b). These results suggest the presence of abnormal sensorimotor gating in this HD mouse model which reaches its peak at 12 months of age although some changes are observed already by 3 months.

A **Startle Response**

	Num. df	Den. df	F-value	p-value
weight (g)	1	84	0.81	0.369
gender	1	22	33.37	< 0.001
genotype	1	22	30.71	< 0.001
age (months)	4	84	9.74	< 0.001
gender:genotype	1	22	15.90	< 0.001
gender:age (months)	4	84	1.95	0.110
genotype:age (months)	4	84	8.40	< 0.001
gender:genotype:age (months)	4	84	1.34	0.261

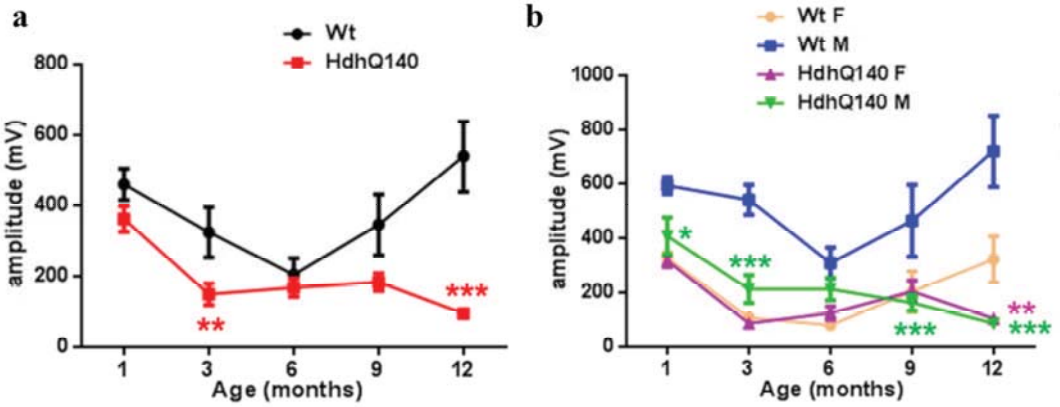

B **Startle Latency**

	Num. df	Den. df	F-value	p-value
weight (g)	1	84	8.92	0.004
gender	1	22	5.49	0.029
genotype	1	22	15.66	< 0.001
age (months)	4	84	41.21	< 0.001
gender:genotype	1	22	1.80	0.194
gender:age (months)	4	84	1.83	0.130
genotype:age (months)	4	84	4.54	0.002
gender:genotype:age (months)	4	84	1.34	0.261

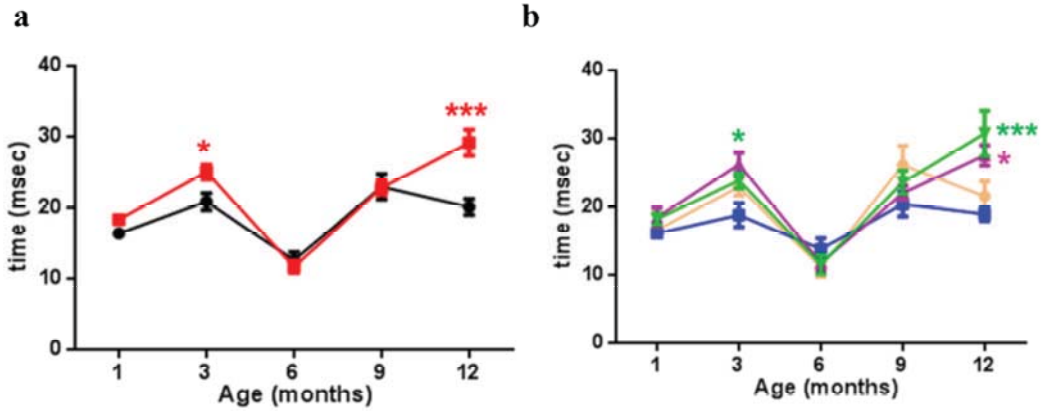

Fig. 31

Acoustic startle response and latency are altered in Hdh$^{Q140/Q140}$ mice. *(A-a) Measure of startle magnitude in response to the 120 dB acoustic peak reveals HD mice have tendency to startle less compared to the WT and the difference reaches statistical significance at 3 and 12 months of age (n = 12-14, mean±SEM, two-way ANOVA followed by Bonferroni post-hoc test, compared to wild-type, **, P<0.01, ***, P<0.001). (A-b) A significant gender effect is also found and HdhQ140 males perform significantly worse than WT males at almost all time-points, while HdhQ140 females are worse only at 12 months of age (n = 6-7, mean±SEM, 3-way ANOVA with Bonferroni post-hoc test, compared to wild-type, *, P<0.05, ***, P<0.001). (B-a) Average latency to peak startle is increased in HD mice compared to the WT and this is also significant at 3 and 12 months. (B-b) analysis as a function of sex shows significant increase in latency in HD males versus WT males at 3 and 12 months and of HD females at 12 months only. Body weight was used as covariate in all statistical analyses. The effect of gender/genotype/age interactions is reported in the tables.*

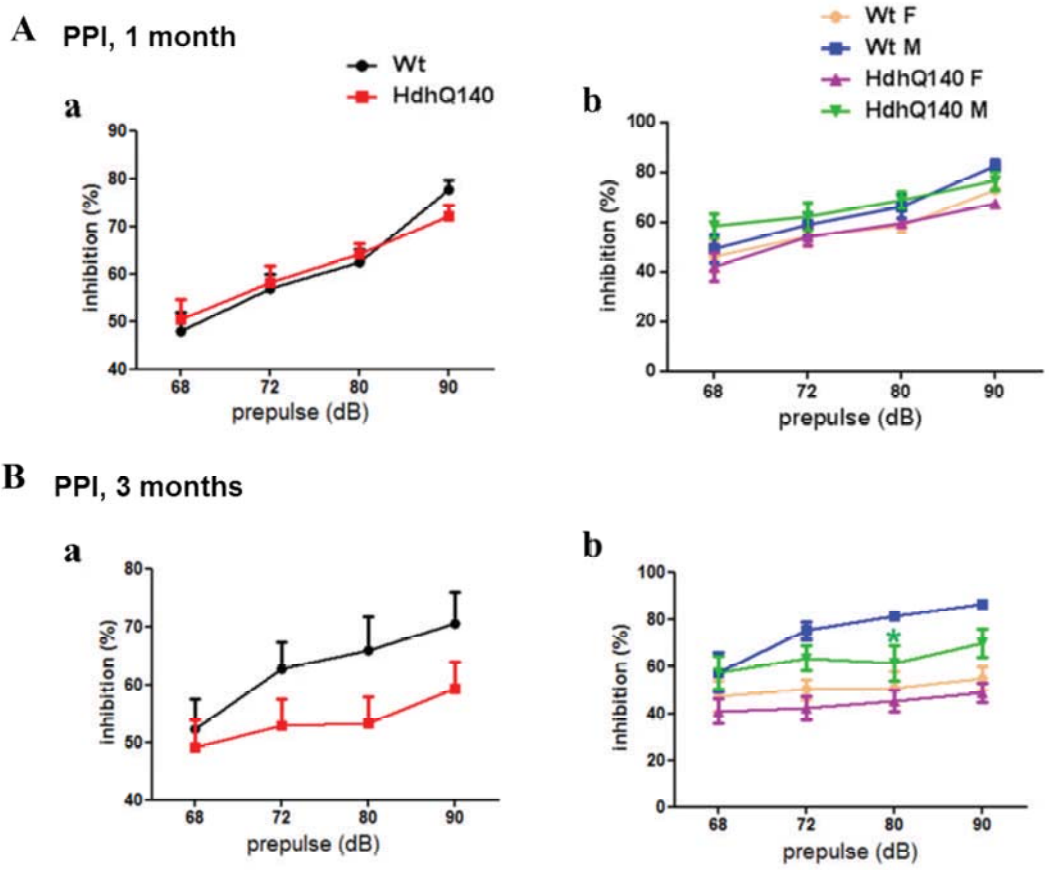

C PPI, 6 months

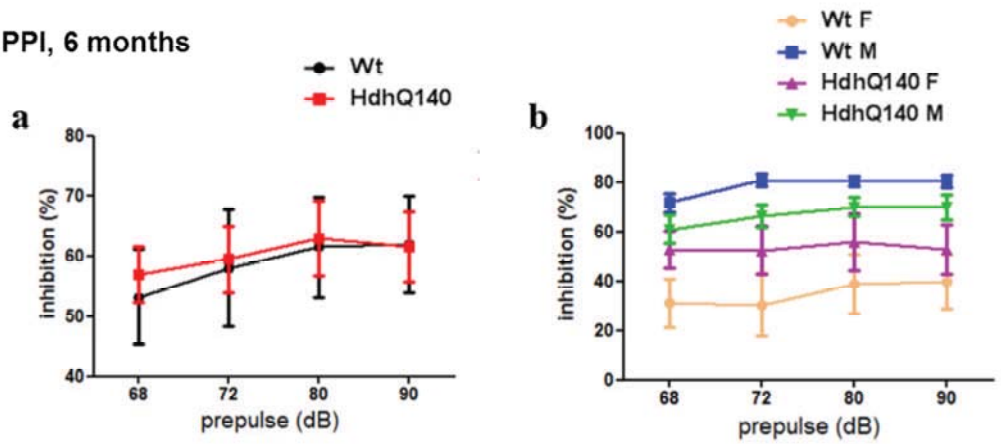

D PPI, 9 months

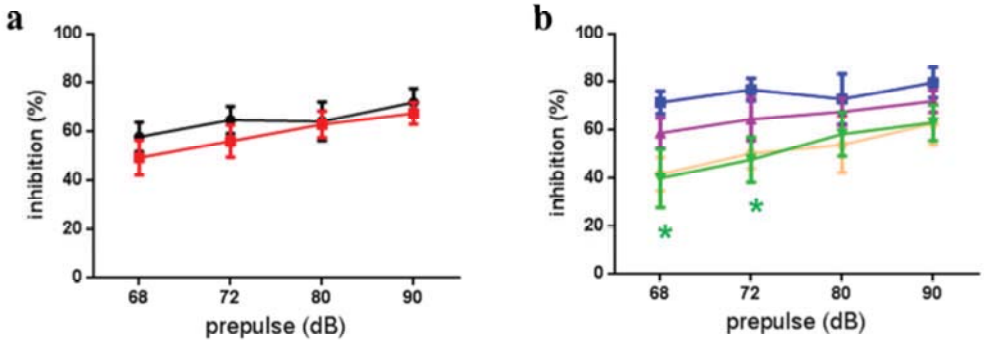

E PPI, 12 months

	Num. df	Den. df	F-value	p-value
weight (g)	1	20	25.66	< 0.001
gender	1	20	24.23	< 0.001
genotype	1	20	4.71	0.042
prepulse	3	63	25.06	< 0.001
gender:genotype	1	20	0.59	0.450
gender:prepulse	3	63	0.25	0.859
genotype:prepulse	3	63	3.85	0.014
gender:genotype:prepulse	3	63	0.29	0.832

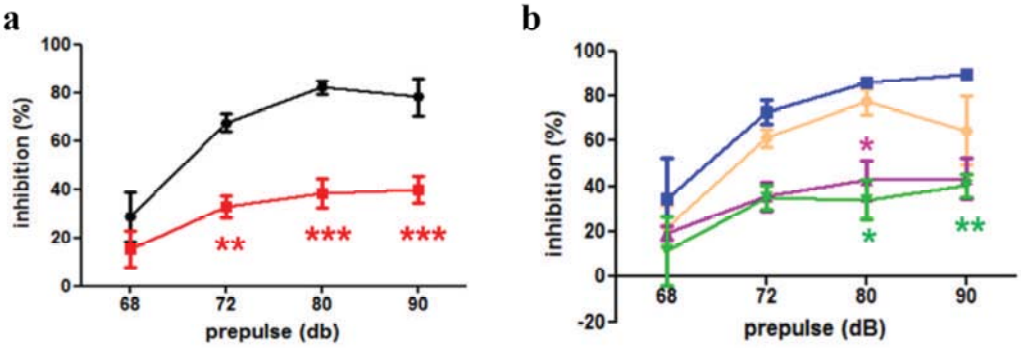

Fig. 32

Prepulse inhibition is altered in Hdh$^{Q140/Q140}$ mice at 12 months of age. *At 1 (A), 3 (B), 6 (C) and 9 (D) months of age, no significant impairment in PPI is found in HdhQ140 mice compared to controls (n = 12-14, mean±SEM, two-way repeated measures). (B-b, D-b) Significant lower % of PPI is found in HD males compared to WT males (n = 6-7, mean±SEM, 3-way ANOVA with Bonferroni post-hoc test, compared to wild-type,*, P<0.05). (E-a) at 12 months of age a significant genotype effect is found, with % of PPI significantly lower in the HD mice compared to the WT for all prepulses, together with a significant gender effect (E-b). The effect of gender/genotype/age interactions is reported in the table. Body weight was used as covariate in all statistical analyses.*

4.3.3 No impairment in learning and memory is detected in Hdh$^{Q140/Q140}$ mice with Spontaneous alternation and Novel object recognition tests

Among the cognitive tests which allow assessment of learning and memory, I chose the Spontaneous Alternation (SA) test and the Novel Object recognition (NOR) task to detect potential abnormalities in the HdhQ140 mice. These tests provide information about impairments in cognitive functions mainly controlled by hippocampus and perirhinal cortex (Wan et al., 1999, Lalonde, 2002).

Results from SA task revealed that all mice alternated arms higher than chance and that no genotype nor gender effects were found in the percentage of alternation (Fig. 33 a-b), suggesting no deficits in spatial working memory (Deacon and Rawlins, 2006) in the KI mice. However, not surprisingly, the measured number of arm entries of the HdhQ140 was significantly lower than the one of WT mice from 3 months of age (Fig. 33 c). These observations suggest reduced locomotor activity and motivation in these mice which are in agreement with data from the open-field test and overnight running wheel.

Spontaneous alternation

	Num. df	Den. df	F-value	p-value
gender	1	22	5.91	0.024
genotype	1	22	3.54	0.073
age (months)	4	85	1.18	0.324
gender:genotype	1	22	0.62	0.440
gender:age (months)	4	85	0.31	0.870
genotype:age (months)	4	85	1.36	0.256
gender:genotype:age (months)	4	85	1.04	0.393

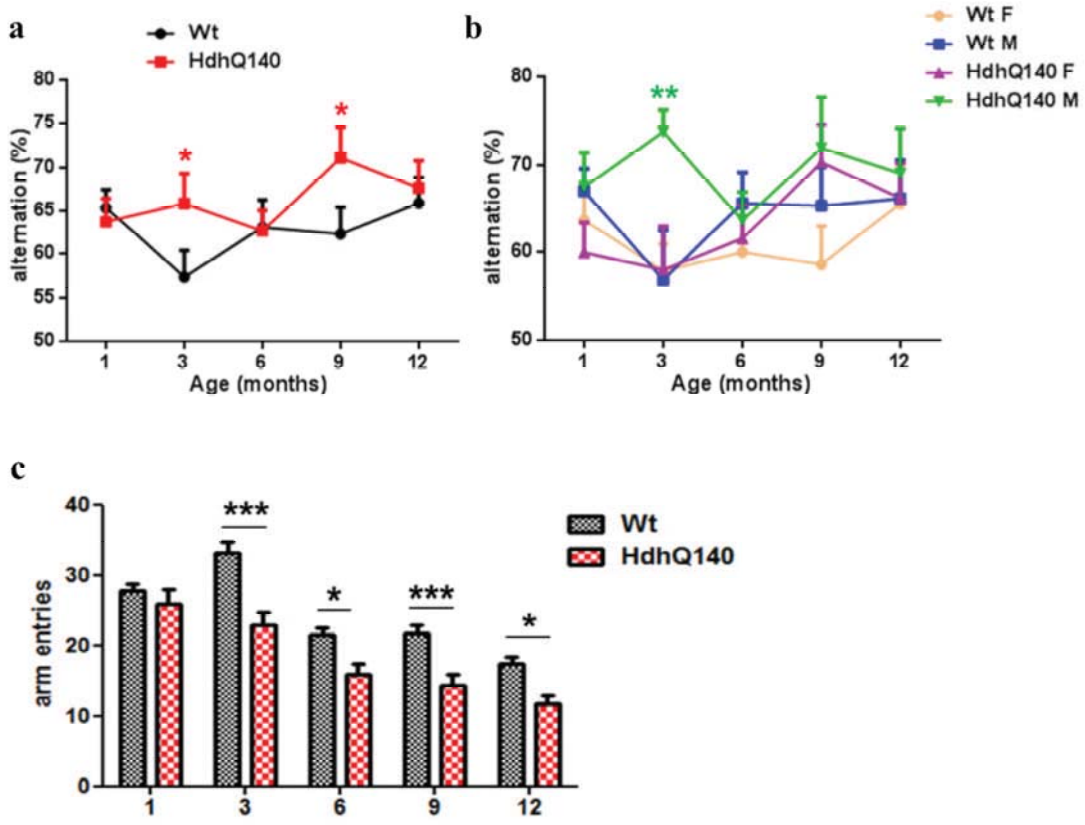

Fig. 33

Spontaneous alternation in Y-maze shows no impairments in Hdh$^{Q140/Q140}$ mice. *Mice were allowed to freely explore the maze over a period of 5 min and the number of arm entries and the percentage of alternation were measured. The spontaneous alternation rate was calculated as the ratio of alternations performed, out of the maximum number of alternations possible, by the total number of arm entries minus one. The effect of gender/genotype/age interactions is reported in the table. (a) Alternation performance is not impaired in HdhQ140 mice which do even better than WT mice at 3 and 9 months of age (n = 12-14, mean±SEM, two-way ANOVA followed by Bonferroni post-hoc test, compared to wild-type, *, P<0.05). (b) KI males overall alternate significantly more than WT males with a highly significant difference at 3 months (n = 6-7, mean±SEM, 3-way ANOVA with Bonferroni post-hoc test, compared to wild-type, **, P<0.01). (c) The number of arm entries is significantly lower in HdhQ140 mice from 3 months onwards (n = 12-14, mean±SEM, two-way ANOVA, *, P<0.05, ***, P<0.001).*

Data from NOR task also showed that mice performed higher than chance and that neither spatial memory (Fig. 34 A) nor recognition memory (Fig. 34 B) were impaired in HdhQ140 mice compared to WT controls at any time-point. No gender effect was also detected in both trials (tables).

A **Location**

	Num. df	Den. df	F-value	p-value
gender	1	22	0.03	0.863
genotype	1	22	2.18	0.154
age (months)	4	85	1.39	0.243
gender:genotype	1	22	0.19	0.664
gender:age (months)	4	85	0.41	0.802
genotype:age (months)	4	85	1.23	0.304
gender:genotype:age (months)	4	85	2.76	0.033

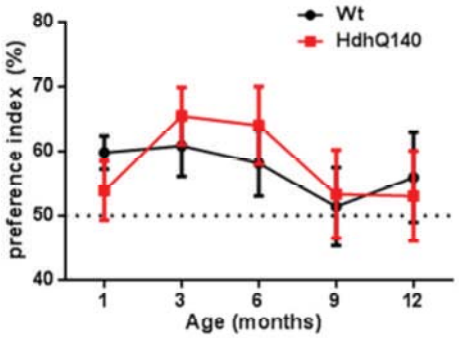

B **Discrimination**

	Num. df	Den. df	F-value	p-value
gender	1	22	0.02	0.894
genotype	1	22	0.07	0.793
age (months)	4	85	0.53	0.714
gender:genotype	1	22	1.97	0.174
gender:age (months)	4	85	0.95	0.439
genotype:age (months)	4	85	0.42	0.794
gender:genotype:age (months)	4	85	0.18	0.950

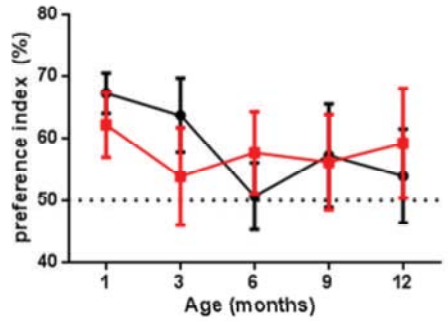

Fig. 34

Novel object recognition task reveals no alterations in spatial or recognition memory in Hdh$^{Q140/Q140}$ mice. *Mice were tested in Location and Discrimination tasks where one of the two objects in the arena was switched location and switched with a different object, respectively. The effect of gender/genotype/age interactions is reported in the tables. The preference index (preference in exploring the novel object) showed no significant difference at all time-points between the two genotypes (A, B) (n = 12-14, mean±SEM, 3-way ANOVA followed by Bonferroni post-hoc test, compared to wild-type).*

4.3.4 Hdh$^{Q140/Q140}$ mice show no anxiety-related behaviour in Open-field and Elevated plus maze tests

In order to assess behavioural symptoms in our HdhQ140 model, I tested mice in Open-field and Elevated Plus Maze (EPM) assays. EPM is a well-established paradigm successfully used to assess anxiety in mice (Holmes et al., 2003, Bailey et

al., 2007, Pellow and File, 1986) and also open-field test, in addition to general locomotor activity, can provide information regarding anxiety in rodents (Prut and Belzung, 2003).

Open field data revealed no overall significant difference in the distance run and in the time spent in the centre of the arena by the KI mice compared to the controls, suggesting a non-anxious behavior in HD mice (Fig. 35 A-a, B-a). No overall genotype or gender effects were found although multiple comparison analysis showed that at 9 months the distance and time in the centre were significantly lower for HdhQ140 mice with KI males performing worse than WT males (Fig. 35 A-b, B-b). However, this difference was not confirmed at 12 months of age.

A Distance moved in centre (%)

	Num. df	Den. df	F-value	p-value
gender	1	22	0.30	0.590
genotype	1	22	0.89	0.357
age (months)	4	85	40.83	< 0.001
gender:genotype	1	22	7.71	0.011
gender:age (months)	4	85	0.67	0.615
genotype:age (months)	4	85	4.92	0.001
gender:genotype:age (months)	4	85	0.65	0.629

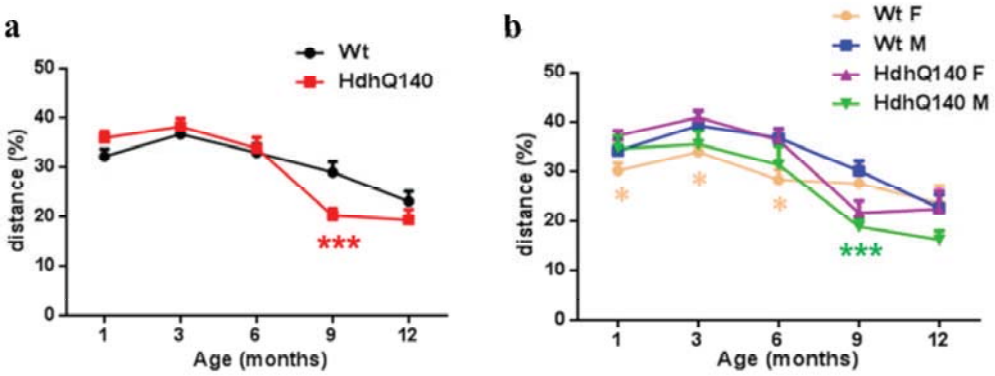

B Time spent in the centre (%)

	Num. df	Den. df	F-value	p-value
gender	1	22	0.80	0.382
genotype	1	22	0.03	0.857
age (months)	4	85	31.41	< 0.001
gender:genotype	1	22	5.96	0.023
gender:age (months)	4	85	1.04	0.394
genotype:age (months)	4	85	2.89	0.027
gender:genotype:age (months)	4	85	0.94	0.445

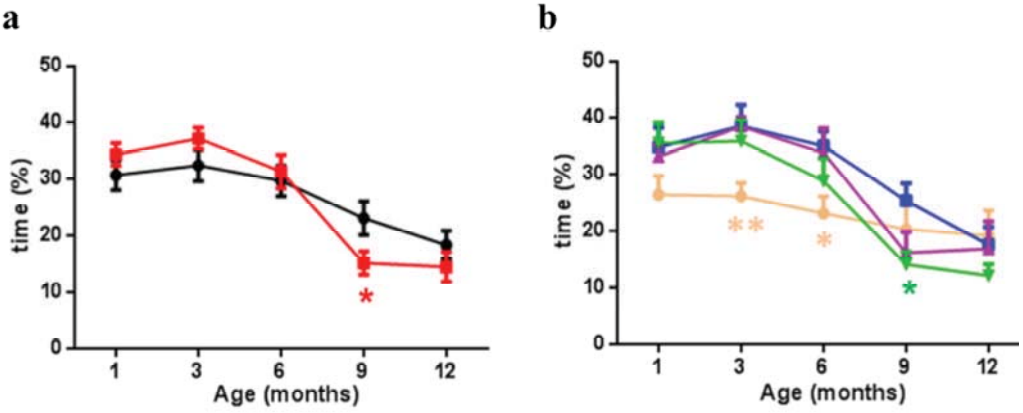

Fig. 35

Open-field test reveals no anxiety-like behavior in Hdh$^{Q140/Q140}$ mice. *The distance moved (A-a) and time spent (B-a) by the KI mice in the centre of the open-field arena is not significantly lower than that spent by the WT controls if not at 9 months (n = 12-14, mean±SEM, two-way ANOVA followed by*

*Bonferroni post-hoc test, compared to wild-type, ***, P<0.001) when the KI males do significantly worse than male WT for both parameters (A-b, B-b) (n = 6-7, mean±SEM, 3-way ANOVA with Bonferroni post-hoc test, compared to wild-type, *, P<0.05, ***, P<0.001). The effect of gender/genotype/age interactions is reported in the tables. Overall genotype and gender effects are not detected in this test, suggesting a non-anxious behaviour of the HD mice.*

Results from EPM test showed that the time spent in the open unprotected maze arms and the frequency of entry in those arms are progressively reduced in both genotypes. At 1 month of age, the time/frequency of HdhQ140 mice was s significantly lower than that spent of WT controls, suggesting an anxious behavior of KI mice at this time-point. Overall significant effects of genotype and gender were found. At all other time-points though, no significant difference between the two genotypes was appreciated (Fig. 36 C-D). General exploratory behavior, measured by the total distance moved, and the frequency of entries in all maze arms, were significantly reduced in the HD mice compared to the WT (Fig. 36 A-B), in agreement with the above mentioned results from locomotory tests (fig. 28 and 30). These observations taken together suggest a lack of motivation in initiating an action in the HdhQ140 mice.

A Total distance moved

	Num. df	Den. df	F-value	p-value
gender	1	22	2.85	0.105
genotype	1	22	5.44	0.029
age (months)	4	85	20.30	< 0.001
gender:genotype	1	22	0.60	0.448
gender:age (months)	4	85	0.82	0.519
genotype:age (months)	4	85	2.80	0.031
gender:genotype:age (months)	4	85	1.07	0.375

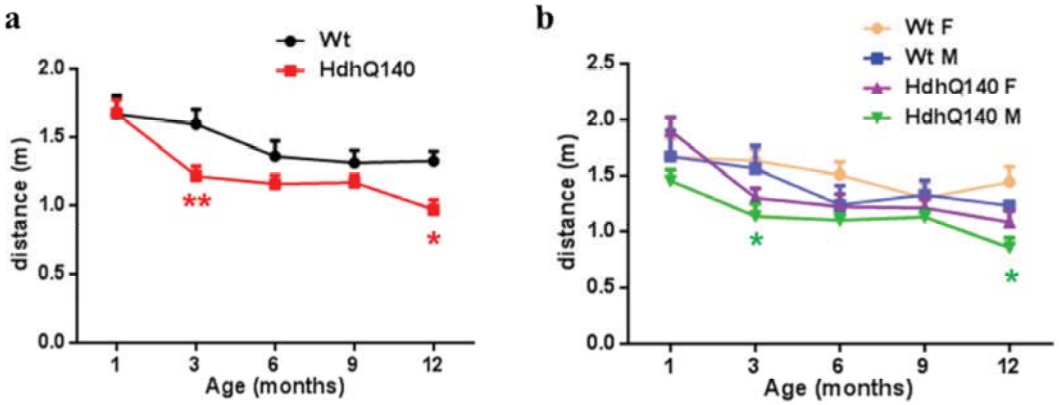

B Frequency of entry in all arms

	Num. df	Den. df	F-value	p-value
gender	1	22	0.65	0.430
genotype	1	22	7.55	0.012
age (months)	4	85	14.40	< 0.001
gender:genotype	1	22	0.70	0.411
gender:age (months)	4	85	0.49	0.743
genotype:age (months)	4	85	2.36	0.060
gender:genotype:age (months)	4	85	1.27	0.287

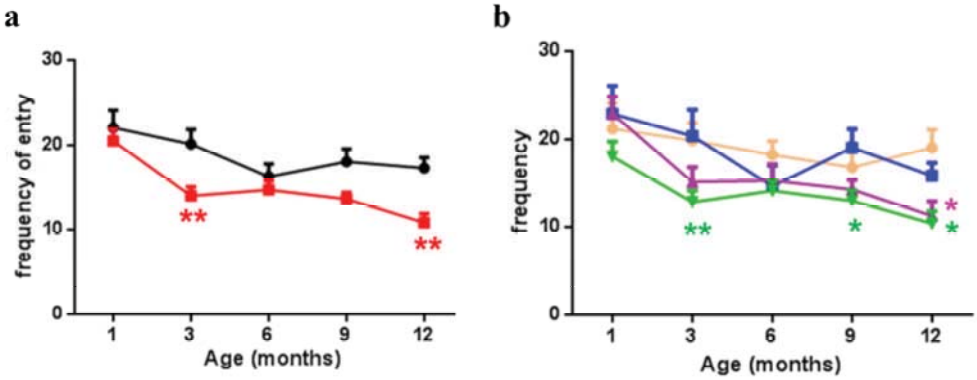

C Time spent in open arms

	Num. df	Den. df	F-value	p-value
gender	1	22	0.80	0.382
genotype	1	22	16.51	< 0.001
age (months)	4	85	35.96	< 0.001
gender:genotype	1	22	8.66	0.008
gender:age (months)	4	85	1.93	0.113
genotype:age (months)	4	85	6.50	< 0.001
gender:genotype:age (months)	4	85	2.40	0.057

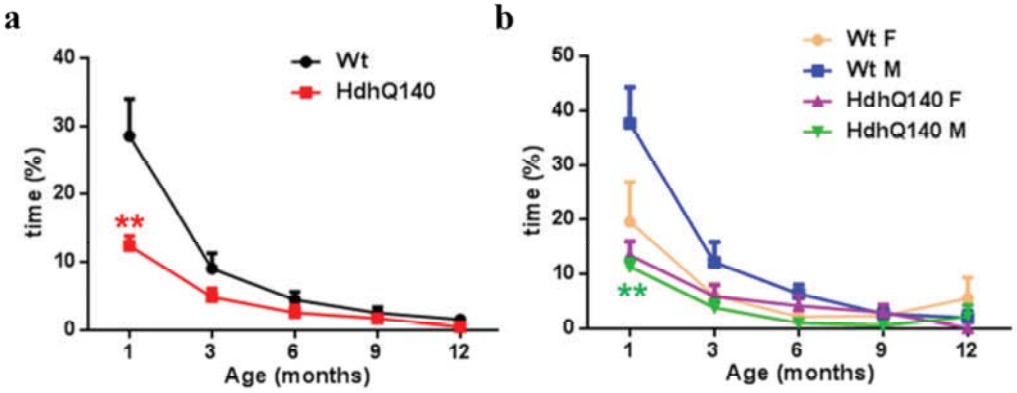

D Frequency of entry in open arms

	Num. df	Den. df	F-value	p-value
gender	1	22	0.10	0.752
genotype	1	22	4.40	0.048
age (months)	4	85	24.46	< 0.001
gender:genotype	1	22	2.62	0.120
gender:age (months)	4	85	0.97	0.426
genotype:age (months)	4	85	1.44	0.226
gender:genotype:age (months)	4	85	1.02	0.399

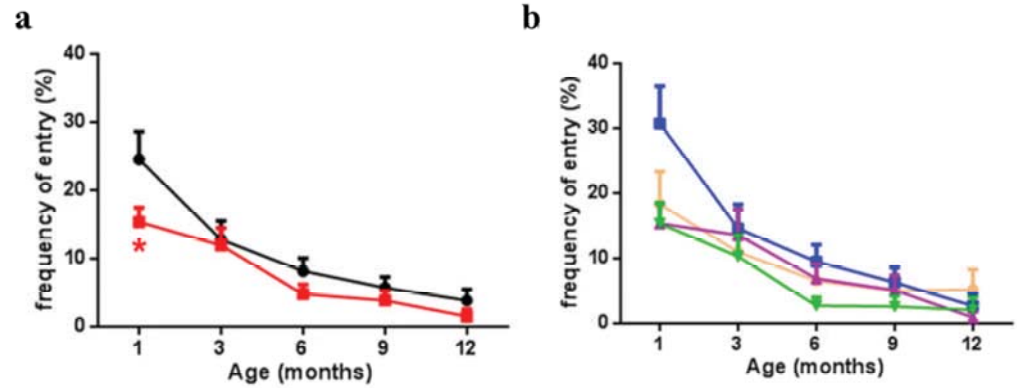

Fig. 36

Elevated Plus Maze test shows anxiety-related behaviour in Hdh$^{Q140/Q140}$ mice at 1 month of age. *Mice were allowed to freely explore the maze over a time of 5 min. The distance moved and the exploratory*

*behaviour were recorded. The effect of gender/genotype/age interactions is reported in the tables. The total distance moved in all arms of the maze is significantly reduced in the KI mice compared to the WT by 3 months of age (A-a) (n = 12-14, mean±SEM, two-way ANOVA followed by Bonferroni post-hoc test, compared to wild-type, **, P<0.01) with a significant decrease in HdhQ140 males compared to WT males (A-b) (n = 6-7, 3-way ANOVA with Bonferroni post-hoc test, compared to wild-type, *, P<0.05). Same result is found for the frequency of entry in all arms (B-a) with significant decrease observed also in HdhQ140 females versus WT females at 12 months (B-b), overall suggesting a reduction in locomotor activity in the HD mice. Time spent and frequency of entry in the open arms is significantly lower in the KI mice only at 1 month of age suggesting and anxious behaviour in these mice, while at all other time-points no difference between the genotypes is appreciated (C-a, D-a). Analysis as a function of sex shows significant lower time spent in the open arms by the HdhQ140 males compared to WT males (C-b) while no differences is found between the females (C-b) as well as no difference in the frequency of entry in open arms (D-b).*

Discussion

In this part of the study I investigated the behavioural phenotype of HdhQ140 homozygous mice. Arguably, analysis of both neuropathological and behavioural changes is important to fully characterise pathology in mice and to provide a platform for preclinical assessment of potential therapeutic strategies.

Overall, my results indicate an altered sensorimotor function in HdhQ140 mice, no abnormalities in cognition with the tests chosen for this study; and an obvious reduction in general locomotor activity. This seems to be explained by increased apathy and lack of motivation in starting action more than to motor impairment. Indeed, coordination and balance, assessed by rotarod test, were unaltered, in agreement with a previous study reporting no alteration in rotarod performance using the accelerated paradigm (Hickey et al., 2008). These results are in line with findings in human HD patients were apathy and lack of motivation are extensively described (Paulsen et al., 2001, Rosas et al., 2008). Possibly, the reduced latency to fall detected in these mice at 1 month of age only could be explained by the well documented hyperactivity of these mice at early age (Menalled et al., 2003). Despite hyperactivity was not confirmed by the open field tests at this time-point, I noticed a tendency of HdhQ140 mice to quickly jump off the rod.

Reduced exploratory behaviour found in these mice with the open-field and elevated plus maze tests seem also be explained by increased apathy more than by increased

anxiety. An increase in activity in the open arms of the elevated plus maze (duration and/or entries) or in the central part of the open field arena (distance run and/or time spent), reflects a non-anxious behavior. Both HdhQ140 and control mice showed no significant differences in these parameters, suggesting a normal behaviour of KI mice. This result was unexpected in light of the high number of axonal swellings detected in HdhQ140 mice at 6 months of age in *stria terminalis*, a brain area involved in fear and anxiety. However, we cannot exclude that other specific tests might detect alterations; and indeed, in the CAG140 mouse model, a previous study reported evidence of anxiety using light-dark choice (LDC) and fear-conditioning tests (Hickey et al., 2008).

Sensorimotor abnormalities were also detected in HdhQ140 mice by PPI test, one of the few paradigms in which humans and rodents are assessed in similar fashion. This test models pathology in HD patients who also show reduced PPI (Swerdlow et al., 1995), and in mouse models (Carter et al., 1999) although little or no alterations were previously described in knock-in HD models (Brooks et al., 2012a, Brooks et al., 2012b, Menalled et al., 2009). Altered PPI was found at the last time-point of this longitudinal study, 12 months, together with alterations in peak startle response and peak latency which were significantly decreased and increased, respectively. These findings parallel the increase in axonal swellings in corticostriatal projection neurons described in chapter 3, and may suggest a contributory role of axon degeneration in these neurons to symptom onset. In support of this, dysfunctions in the corticostriatal circuitry and limbic system are addressed as possible cause of PPI abnormalities in HD (Swerdlow et al., 1995).

Finally, cognitive function tests used in this study did not detect impairments in spatial learning and recognition in HdhQ140 mice at any time-point. This suggests no functional alterations at the level of hippocampus and perirhinal cortex in these mice at the time-points considered.

Behavioural abnormalities detected in HdhQ140 homozygous mice in this study were subtle and occurring late, in agreement with previous studies (Menalled and Chesselet, 2002). Indeed, knock-in models show a slower, more progressive impairment of behavioral phenotype (Menalled, 2005), in contrast to transgenic mice, particularly those transgenic mice which overexpress N-terminal fragments of mHTT such as the

R6/2 line, which show robust motor and cognitive symptoms and rapid disease progression (Carter et al., 1999, Lione et al., 1999, Stack et al., 2005). In this respect KI mice often represent a more suitable model to study behavioural symptoms which in patients progress over a long period of time. In R6/2 mice, possibly due to the high toxicity of mHTT fragments compared with the full-length protein (Goldberg et al., 1996, Cooper et al., 1998), death occurs prematurely around 12-15 months. This makes detailed analysis of behavioural phenotype, as well as that of pathology progression, more difficult. I have previously shown that little or no morphological abnormalities in corticostriatal projection neurons or other YFP+ neurons were detected in R6/2 mice at 3 months of age, final stage of the disease in these mice. This does not reflect the human condition where axon degeneration is well documented, together with the minimal loss of striatal neurons which is not representative of the robust loss observed in patients. The absence of axonal pathology (Fig. 17) and the little or no neuronal loss reported here (Fig. 16) and in other studies (Mangiarini et al., 1996, Davies et al., 1997), together with the acute behavioral phenotype of the R6/2 mice, seem to suggest that this is not a faithful model of HD and question the extensive use of this mice in preclinical testing which often fail in the clinical phase.

$Hdh^{Q140/Q140}$ mice instead showed progressive axon degeneration and the present behavioral analysis, together with reported studies (Rising et al., 2011, Hickey et al., 2008), suggests a more progressive onset and course of pathology, which can be of help in understanding the relationships between neurodegenerative changes in particular brain areas and symptom onset and progression.

In conclusion, these data suggest sensorimotor defects occur in HdhQ140 homozygous mice before cognitive and behavioural abnormalities. They also reveal that major impairments occur at late time-point, at 12 months of age, time when also axon pathology is most striking in these mice. At this time-point, high number of axonal swellings in corticostriatal projection neurons could contribute to apathy (Grillner et al., 2008) and abnormalities in PPI (Larrauri and Schmajuk, 2006) as dysfunctions in frontal-subcortical circuits seem to play a role in both processes (Bonelli and Cummings, 2007). At 6 months of age, swellings in *stria terminalis* could not be related to anxiety-like behaviour which was not detected in the KI mice with EPM and open-field tests. However, other tests such as PPI suggested possible

alterations in the limbic system in HD mice and leaves open the possibility that other tests could detect it.

CHAPTER 5

Axon pathology and NAD biosynthetic pathway

5.1 Introduction

5.1.1 NAD biosynthetic pathway and role in neuroprotection

Nicotinamide adenine dinucleotide (NAD) has been known for its important role in energy metabolism as a co-enzyme for oxidation/reduction reactions for over a century (Berger et al., 2004). NAD and its phosphorylated (NADP) and reduced (NADH, NADPH) forms are hydride-accepting and hydride-donating coenzymes and numerous hydride transfer enzymes or oxidoreductases interconvert either NAD and NADH or NADP and NADPH to reduce or oxidize small-molecule metabolites (Berger et al., 2004) (Fig. 37).

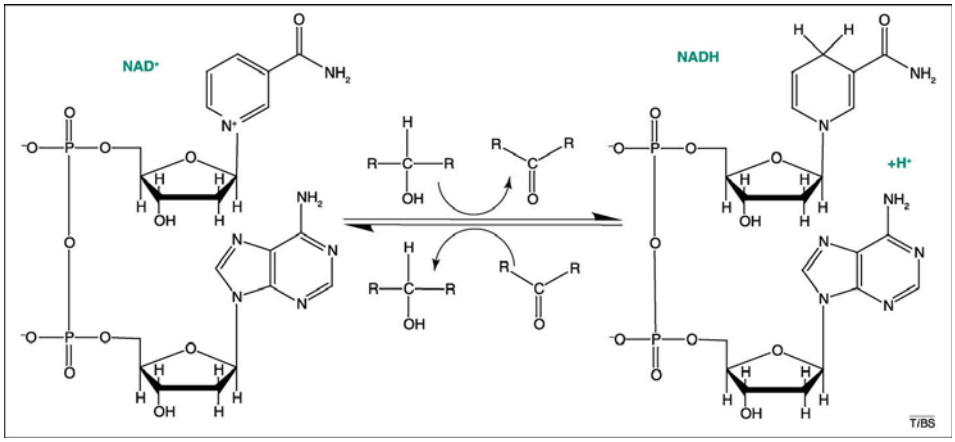

Fig. 37

NAD as a coenzyme for reversible hydride transfer. From (Belenky et al., 2007). *In a typical NAD-dependent oxidation, an alcohol is converted to the corresponding aldehyde with the production of NADH plus a proton. In the NADH-dependent direction, an aldehyde is reduced to an alcohol, which regenerates NAD.*

However, more recent studies have revealed that NAD has also a key role as signalling molecule in a variety of non-redox reactions. Other than being a cofactor for oxidoreductases, NAD is also substrate for protein post-translational modifications such as deacetylation and mono- and poly(ADP-ribosyl)ation and participates in Ca^{2+} signalling through its derivative nicotinic acid adenine dinucleotide phosphate (NAADP) and its degradation products ADP-ribose (ADPR) and cyclic ADP-ribose (cADPR) (Belenky et al., 2007, Berger et al., 2004) (Fig. 38). These reactions regulate

fundamental cellular processes such as gene expression, cell differentiation, apoptosis, aging, circadian rhythm, inflammation and neurodegeneration, thus a strong interest in the enzymes involved in NAD biosynthesis and the signalling mechanisms downstream NAD synthesis has been growing in the past few years.

NAD synthesising enzymes and role in neuroprotection

NAD synthesis takes place through the "de novo pathway", which produces NAD from quinolinic acid (QA), and through the "salvage pathways" which produce the dinucleotide starting either from nicotinic acid (NA), nicotinamide (NAM) or nicotinamide riboside (NR) (Fig. 38).

Alterations in the de novo pathway are reported in HD. In post-mortem HD human brains, the levels of the kynurenic acid, precursor of QA, are found decreased (Beal et al., 1990, Beal et al., 1992) while the levels of 3-hydroxykynurenine (3-HK) and QA increased (Pearson and Reynolds, 1992, Guidetti et al., 2004). QA is an excitotoxic NMDAR agonist and *in vivo* injections cause selective degeneration of MSSNs that can partially model HD (Beal et al., 1991, Beal et al., 1986). In R6/2 mice, also elevated 3-HK and increased activity of the biosynthetic enzyme of 3-HK, Kynurenine 3-monooxygenase (KMO) are detected (Guidetti et al., 2006, Sathyasaikumar et al., 2010). Altered levels of these metabolites seem to play a role in neurodegeneration in HD; For example, pharmacological or genetic inhibition of the KMO increases levels of the neuroprotective metabolite kynurenic acid relative to the neurotoxic metabolite 3-HK and ameliorates neurodegeneration in a *Drosophila* (Campesan et al., 2011) and a mouse model (Giorgini et al., 2013). However, the consequences of blocking KMO on NAD metabolism have not been investigated.

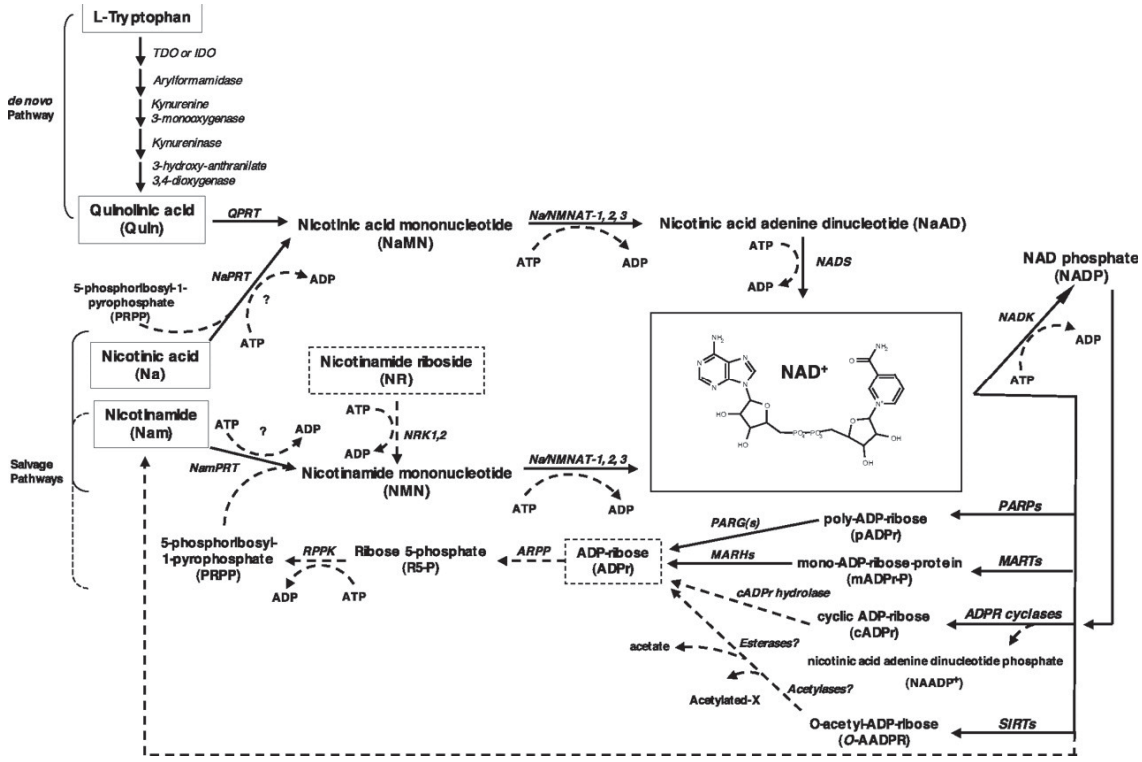

Fig. 38

Mammalian NAD metabolic pathways. ***From (Hassa et al., 2006).***

For most cells in mammals the salvage pathway from NAM is the most relevant (Di Stefano and Conforti, 2013). The enzyme nicotinamide phosphoribosyltransferase (NAMPT), which catalyses a rate-limiting step in this pathway (Revollo et al., 2004), is involved in several physiological functions (Imai and Kiess, 2009, Yang et al., 2006). NAMPT is found in both nucleus and cytoplasm where NAMPT-mediated NAD biosynthesis plays a critical role in the regulation of the NAD consuming enzymes Sirtuin1 (SIRT1) and mitochondrial Sirtuin3 (SIRT3) and Sirtuin4 (SIRT4) (Imai, 2009, Donmez and Outeiro, 2013). In a model of stroke NAMPT was shown to protect against neuronal death through activation of SIRT1-dependent adenosine monophosphate-activated kinase pathway (AMPK), suggesting NAMPT as a new therapeutic target for stroke. NAMPT levels decline with age (Liu et al., 2012) and this could lead to neurodegeneration.

All salvage pathways share the common final step catalysed by the enzyme NMNAT. In humans, three different NMNAT isoforms (NMNAT1, 2 and 3), differing in their oligomeric state, subcellular localization and catalytic properties, have been identified

and characterized (Berger et al., 2005). NMNAT1 is mainly localised in the nucleus while NMNAT2 and 3 are associated with Golgi apparatus and mitochondria, respectively.

NMNAT1 and Wld^S

Studies on *Wld*^{S} mouse, a spontaneous mutant mouse with delayed axonal degeneration of transected nerves (see chapters 1.7 and 1.8) have elucidated some of the mechanisms responsible for its protective phenotype. The WLD^s protein contains the amino (N)-terminal 70 amino acids (N70) fragment of the ubiquitination factor E4B (UBE4B), the complete sequence of the enzyme nicotinamide adenylyltransferase 1 (NMNAT1); and a linking portion of 18 AA originally belonging to the 5' untranslated region of the Nmnat1 gene (Fig. 7). Studies of structure-activity relationship have demonstrated that the enzymatic activity of NMNAT1 is required for axon survival (Conforti et al., 2009). Moreover, they showed that this activity needs to be present in axons to confer protection as shown that nuclear NMNAT1 does not affect axon degeneration even when over-expressed (Conforti et al., 2007b, Conforti et al., 2011, Cohen et al., 2012). Following redistribution of WLD^s to the axon, through the binding of VCP protein to the N16 region of the protein, the nuclear NMNAT1 can function in the axon and confer the protective phenotype (Conforti et al., 2009, Avery et al., 2009). How NMNAT activity exerts its protection is still not fully clarified. While initially an increase in NAD levels was believed to be responsible for neuroprotection (Araki et al., 2004, Wang et al., 2005), more recent studies have demonstrated its independence from NAD production, suggesting an alternative role for NMNAT enzymatic activity in the axon (Conforti et al., 2007b, Sasaki et al., 2009b). Moreover, neuroprotective effects could be mediated by different mechanisms of action not related to enzyme activity. In a *Drosophila* model of spinocerebellar ataxia 1 (SCA1), Zhai and collaborators showed that NMNAT functions as a chaperone in protecting neuronal degeneration independently from its NAD-synthesis activity (Zhai et al., 2008, Zhai et al., 2006); and in a *Drosophila* model of frontotemporal dementia with parkinsonism linked to chromosome 17 (FTDP-17), overexpression of NMNAT significantly ameliorated behavioural deficits and morphological neurodegenerative changes associated with tauopathy. In this fly model, NMNAT reduces the level of hyperphosphorylated tau and promotes ubiquitylation and clearance of the toxic tau oligomeric species (Ali et

al., 2012). In a mouse model, overexpression of NMNAT1 and NMNAT2 promotes clearance of hyperphosphorylated tau and reduces neurodegeneration (Ljungberg et al., 2012).

NMNAT2

The role of WLD^S in the axon is emerged from a recent study in which downregulation of NMNAT2, the endogenous isoform of NMNAT in the axon, caused spontaneous degeneration of not injured-axons, indicating that NMNAT2 acts as an endogenous survival factor (Gilley and Coleman, 2010). NMNAT2 is synthesised in the cell bodies and constantly delivered to the axon and axon terminal by fast axonal transport. However, it has a short half-life and when axons are injured or axonal transport is impeded, its axonal levels quickly decrease triggering degeneration and neither NMNAT1 nor NMNAT3 can compensate for the loss of NMNAT2 (Milde et al., 2013c, Gilley and Coleman, 2010, Gilley et al., 2013). In addition, NMNAT2 is required for normal axon growth in embryos (Gilley et al., 2013, Hicks et al., 2012). NMNAT2 is also neuroprotective in models of neurodegeneration; in mouse models of human tauopathies, NMNAT2 gene transcription is decreased while its over-expression ameliorates the pathology (Ljungberg et al., 2012). In *Wld*^{S} mice, the NMNAT1enzymatic activity of the WLD^S protein, when relocated to the axon, may compensate for loss of NMNAT2 maintaining axonal integrity (Conforti et al., 2009, Beirowski et al., 2009, Babetto et al., 2010, Gilley and Coleman, 2010, Gilley et al., 2013, Conforti et al., 2014). NMNAT1 is a more stable isoform and its action could explain the protective phenotype in these mice.

The role of NMNAT1 and 2 in neurodegeneration/protection in HD is not clear. HTT and the WLD^S protein, which contains the entire NMNAT1 sequence (see above), share a common binding partner, the abundant cellular protein VCP/p97 (Hirabayashi et al., 2001); and WLD^S preferentially distributes to nuclear foci resembling the localisation of mHTT aggregates. Moreover, VCP/p97 has been shown to be involved in clearance of polyubiquitylated aggregates and to reduce aggregate toxicity (Kobayashi et al., 2007). In addition, both HTT and NMNAT2 are palmitoylated. Palmitoylation of NMNAT2 at cysteine 164 and 165 is responsible for its association to Golgi vesicles, which is required for its axonal transport. In the absent of the

cysteine residues, NMNAT2 adopts a more diffuse cytosolic localisation (Milde et al., 2013c). HTT is palmitoylated at cystein 214 by HIP14 (see chapter 1.4) and this is essential for its trafficking and function (Yanai et al., 2006). Thus, the possibility raises that HTT and NMNAT2 are transported with the same vesicles and that mHTT could alter this normal process.

NAD consuming enzymes

In non-redox reactions, breakdown of NAD molecule is carried out by three classes of enzymes which cleave NAD to produce NAM and an ADP-ribosyl product (Fig. 38 and 39): ADP-ribosyl cyclases, that use NAD as a substrate to generate ADP-ribose and cyclic ADP-ribose (cADPR) (Lee, 2001); mono(ADP-ribose) transferases (ARTs) and poly(ADP-ribose) polymerases (PARPs) that use NAD to add one or more ADP-ribosyl groups to target proteins (Lautier et al., 1993); and Sirtuins (SIRTs) that have both mono-ribosyl transferase and deacetylase activity consuming one NAD for every ADP-ribosyl group they transfer to or every acetyl group they remove from a protein substrate (Tanner et al., 2000).

cADPR produced by the cyclases acts as a second messenger and participates in cytosolic Ca^{2+} regulation by binding to specific receptors on the surface of the endoplasmic reticulum. This results in Ca^{2+}release from intracellular stores (Galione, 1993). The activity of these enzymes is regulated by nitric oxide or glutamate activation and hyperactivation of these enzymes in diseases such as neurodegenerative disorders leads to rapid depletion of NAD (Balan et al., 2010) and increase in Ca^{2+} release that activates axonal proteases leading to axon degeneration *in vitro* (Stirling and Stys, 2010).

PARPs are key enzymes involved in DNA repair in response to DNA breakage and oxidative stress. Among the 17 PARP members, PARP1 is the first and best characterised. It has been related to caspase-independent cell death as its hyper-activation causes significant depletion of NAD and associated cell death (Hassa et al., 2006, Chiarugi, 2002). Hyper-activation occurs in many pathophysiological situations such as excitotoxicity, ischemia, and oxidative stress, when DNA damage is extensive. Thus PARP1 inhibition or genetic inactivation has proved to be beneficial in mouse models of ischemia (Chiarugi, 2002, Virag and Szabo, 2002) and neurodegenerative disorders (Liberatore et al., 1999).

In mammals, the NAD-dependent histone deacetylases (HDAC) Sirtuins are a group of 7 enzymes (SIRT1–7) involved in major cellular processes, including transcriptional silencing, DNA repair, DNA recombination and lifespan regulation (Imai and Guarente, 2010). These enzymes have protective effects against age-related diseases such as cancer, diabetes, cardiovascular and neurodegenerative diseases and therefore promising targets for therapeutic interventions (Donmez and Outeiro, 2013). In a *C. elegans* model of HD, up-regulation of the nuclear SIRT1 or treatment with resveratrol, a natural SIRT1 activator (Tadolini et al., 2000, Belguendouz et al., 1997), were found to rescue neurons from mHTT-induced toxicity and beneficial effects of resveratrol were also found in a KI mouse model, the HdhQ111 (Parker et al., 2005). In a study on N171‑82Q mice, overexpression of SIRT1 improved motor function, decreased brain atrophy, and attenuated the metabolic abnormalities and decline in BDNF concentration induced by mHTT (Jiang et al., 2012). In the same study mHTT was found to interact with SIRT1 and to inhibit its deacetylase activity, which prevents its pro-survival function. In the R6/2 mouse model, brain-specific knock-out of SIRT1 resulted in exacerbation of pathology whereas its overexpression improved survival (Jeong et al., 2012). SIRT2 has also been implicated in neurodegeneration and recent data have shown that its suppression ameliorates neurotoxicity in a variety of neuronal disease models such as HD (Pallos et al., 2008) and PD (Outeiro et al., 2007). SIRT2 is present mainly in the cytoplasm where it colocalises with microtubules and deacetylates the major component of microtubules α-tubulin (North et al., 2003) and plays a role in microtubule stability. The role of SIRT2 has also been investigated in HD and, in contrast to SIRT1, its inhibition is found to be beneficial. Indeed, inhibition of HDAC is neuroprotective. In an *in vitro* study, inhibition of the microtubule deacetylase 6 (HDCA6), enhanced MT-dependent transport through the recruitment of the molecular motors dynein and kinesin-1 to microtubules and rescued axonal transport defects in HD neurons (Dompierre et al., 2007). In a study on cerebellar granule cells from Wld^S mice, microtubule acetylation was found increased together with decreased cytoplasmic levels of NAD and SIRT2; and SIRT2 overexpression abolished the protection from axon degeneration induced by colchicine, suggesting that SIRT2-mediated tubulin deacetylation is involved in both microtubule hyperacetylation and resistance to axonal degeneration in Wld^S granule cells (Suzuki and Koike, 2007). However, in this study the link between Wld^S and the

decrease of NAD and SIRT2 remains unclear and would need further investigation. In a fly model of HD, decreased levels of SIRT2 promoted the viability of photoreceptor neurons (Pallos et al., 2008) and in cellular and invertebrate models its pharmacological inhibition resulted in neuroprotection through a negative regulation of sterol biosynthesis (Luthi-Carter et al., 2010).

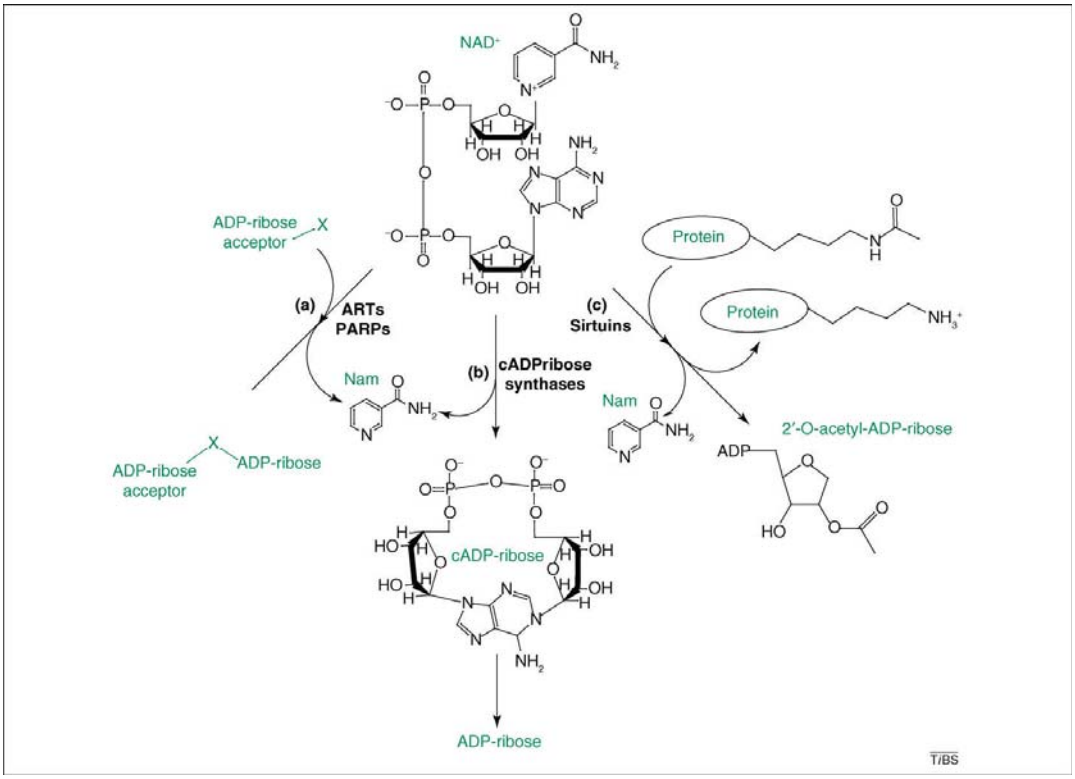

Fig. 39

NAD consuming enzymes. From (Belenky et al., 2007). *NAD as a substrate for ADP-ribose transfer, cADP-ribose synthesis and protein lysine deacetylation. (a) ARTs and PARPs transfer ADP-ribose from NAD as a protein modification with production of Nam. In the case of PARPs, the ADP-ribose acceptor, X, can also be ADP-ribose, forming poly(ADP-ribose). (b) cADP-ribose synthases cyclize the ADP-ribose moiety of NAD with production of Nam. These enzymes also hydrolyze cADP-ribose. (c) Sirtuins use the ADP-ribose moiety of NAD to accept the acetyl modification of a protein lysine, forming deacetylated protein plus Nam and, after acetyl-group rearrangement, a mixture of 20 and 30 O-acetylated ADP-ribose. Each NAD-consuming enzyme is inhibited by the Nam product.*

All this evidence reveals the importance of NAD biosynthetic pathway in physiological and pathological conditions and in particular its contribution to

neuroprotection. Thus, therapeutic strategies targeting the key enzymes in this pathway could have useful effects in several neurodegenerative disorders.

5.2 Hypothesis and aim of the chapter

In this chapter, the involvement of NAD biosynthetic pathway and its correlation to HD pathology is assessed in $Hdh^{Q140/Q140}$ mice. Alterations in NAD biosynthesis have been recently linked to axon survival and axon and synapses degeneration in many neurodegenerative disorders. In HD patients, altered levels of NAD precursors in the *de novo* synthetic pathway are reported (Beal et al., 1990, Guidetti et al., 2004). Moreover, HTT and NAD synthesizing enzymes share common binding partners. Based on this evidence, I hypothesized dysregulations in NAD metabolism in my HD mouse model as a consequence of the presence of mHTT which could aberrantly interact with the NAD synthesizing enzymes and interfere with their normal function.

5.3 Results

5.3.1 Striatal levels of NMN significantly increase with age

To assess alterations in NAD biosynthesis in $Hdh^{Q140/Q140}$ mice, which showed axon pathology by 6 months of age, I first analysed the levels of NAD and its precursor nucleotide NMN in cortex and striatum of 6 and 12 month old animals (Fig. 40). These levels were measured in brain homogenates by fluorimetric HPLC. Results showed no difference in the levels of NMN between the two genotypes but, interestingly, a significant increase was found in the striatum at 12 months, compared to 6 months of age, in both KI mice and control littermates (Fig. 40 A). In the cortex instead, a trend to decrease in NMN levels was detected in WT mice with time (Fig. 40A). In parallel, NAD decreased in both genotypes although this trend did not reach significant difference with the *n* number available (Fig. 40 B). Consequently, the calculated NAD/NMN ratio fell, reaching a significantly decreased value in HdhQ140 mice at 12 months of age (fig. 40 C).

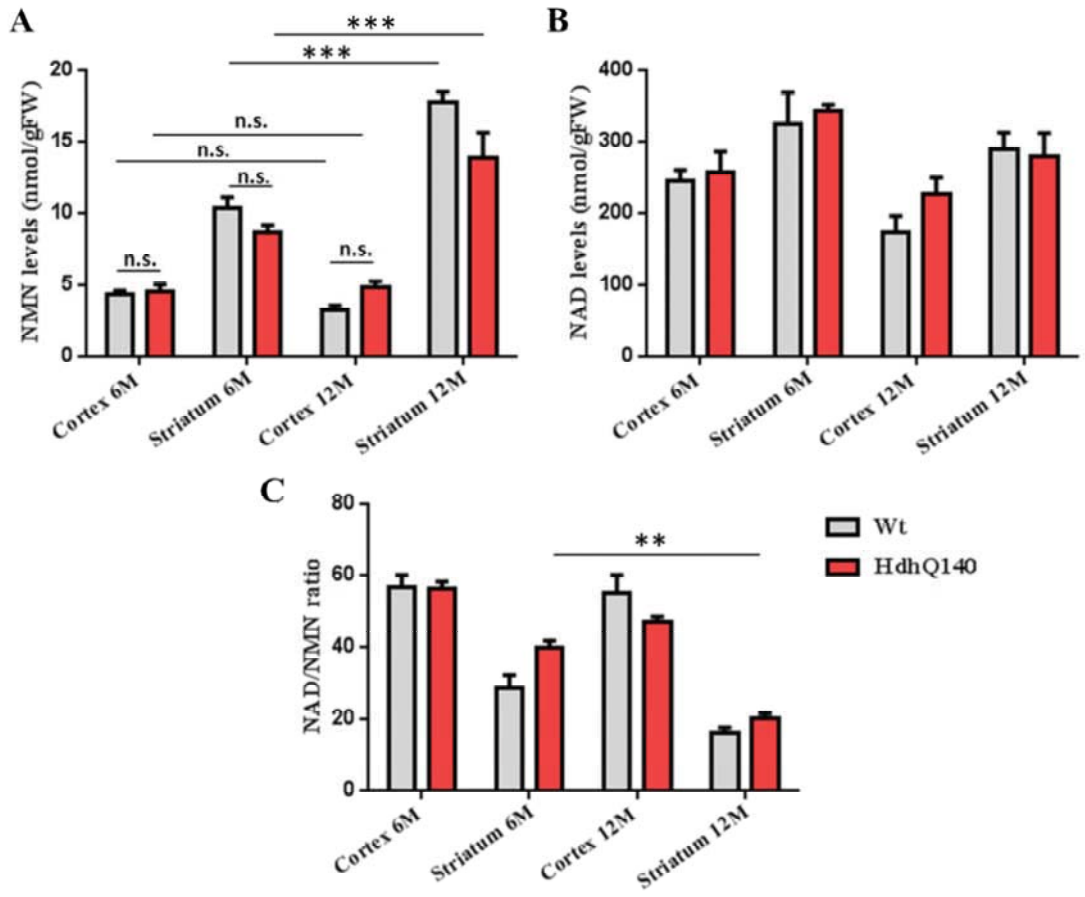

Fig. 40

NMN significantly increases in the striatum with age. *The levels of NMN and NAD were measured in cortical and striatal brain homogenates of 6 and 12 month old HdhQ140 and relative control mice. (A) Significant increase is found in striatal NMN levels at 12 months of age in both genotype and (B) NAD levels show a trend to decrease with age in both genotypes. (C) NAD/NMN ratio is significantly reduced in HdhQ140 mice with age (n=5-8, mean±SEM, one-way ANOVA followed by Bonferroni post hoc test, **, P<0.01, ***, P<0.001).*

Next, I measured the enzymatic activity of NMNATs enzymes to assess whether increased levels of NMN and reduced levels of NAD were due to reduced NMNAT enzymatic activity with age and also if there were differences between HdhQ140 and control mice. The low number of samples (n = 2) available for this analysis did not allow statistical analysis however, a trend to decrease was observed in the cortex of HdhQ140 mice at 12 months compared to 6 months of age. No gross difference between KI and WT mice was instead appreciated (Fig. 41).

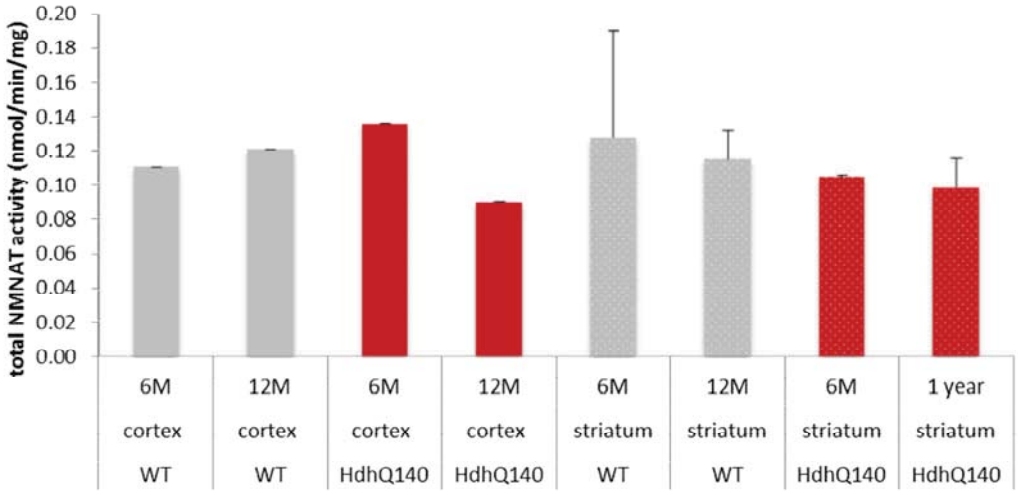

Fig. 41

NMNAT enzymatic activity is unaltered in Hdh$^{Q140/Q140}$ mice. *The total enzymatic activity of NMNATs was measured in cortical and striatal brain homogenates of 6 and 12 month old HdhQ140 mice and control littermates. No significant difference is found between the genotypes although a trend to decrease is appreciated in the cortex of HdhQ140 mice at 12 months compared to 6 months of age. (n = 2, mean±SD).*

I also measured the levels of nicotinamide phosphoribosyltransferase (NAMPT), the enzyme immediately upstream of NMNAT in the NAD salvage pathway, in cortex and striatum of 6 and 12 months HdhQ140 mice and relative controls by Western blot (Fig. 42). Despite NAMPT levels remained stable between genotypes, a trend to decrease was observed with age in both cortex (Fig. 42 A) and striatum (Fig. 42 B) and in the cortex of WT mice. In these mice, NAMPT decrease, consistent with published observations (Liu et al., 2012), could explain the trend to a reduction in cortical NMN levels observed with HPLC.

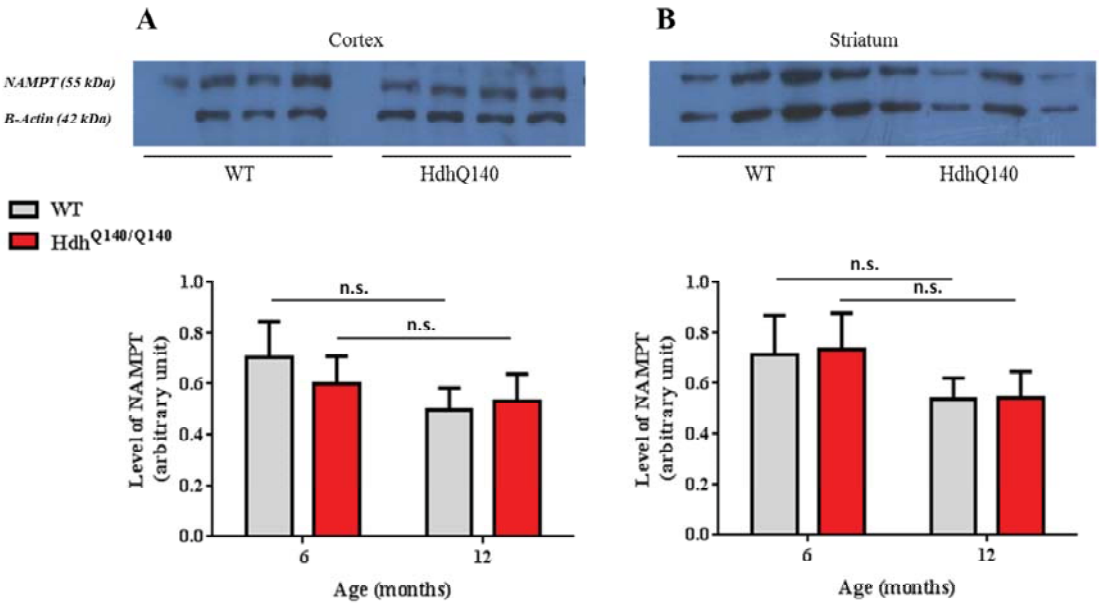

Fig. 42

NAMPT levels are unaltered in Hdh$^{Q140/Q140}$ mice. *Western Blots of mouse brain homogenates probed with antibodies against the NAD synthesizing enzyme NAMPT (kDa 55). β-Actin was used as a loading control in all blots (kDa 42). Quantitative analysis of blots from (A) cortical and (B) striatal brain homogenates of 6 and 12 month old HdhQ140 mice and control littermates show no significant difference of NAMPT levels in HdhQ140 mice compared to WT mice. Also the decrease in NAMPT levels with age does not reach statistical significance with age (n = 4, mean±SEM, one-way ANOVA followed by Bonferroni post hoc test).*

5.3.2 mHTT and NAD biosynthetic enzymes: possible interaction and altered axonal transport

In parallel to the study on HD mouse brains, I used cellular models of HD to investigate whether HTT/mHTT interacts with the NAD synthesizing enzymes. Despite the little differences found between HdhQ140 and control mice in the level of nucleotides and enzymes involved in this pathway, interaction between these enzymes and mHTT could contribute to axon degeneration. In addition, WLD^s retains the sequence of NMNAT1 and NAD biosynthetic activity.

mHTT colocalises with WLD^s but not with NMNAT1 in the nucleus of PC12 cells

First, I looked at possible colocalisation between mHTT and WLD^s protein in the nucleus of Tet-ON PC12 cells. As mentioned in the introduction to the chapter, both HTT and WLD^s bind to VCP/p97 and WLD^s preferentially distributes to nuclear foci

resembling the localisation of mHTT aggregates, thus opening the possibility of an interaction between the two proteins.

Tet-ON PC12 Q72 cells were transfected with *Wld*^{S} and, on the same day, treated with doxycycline to induce mHTT expression and aggregate formation and imaged 3 days after transfection. Confocal images confirmed a colocalisation between WLD^{s} and the nuclear mHTT aggregates (Fig. 43).

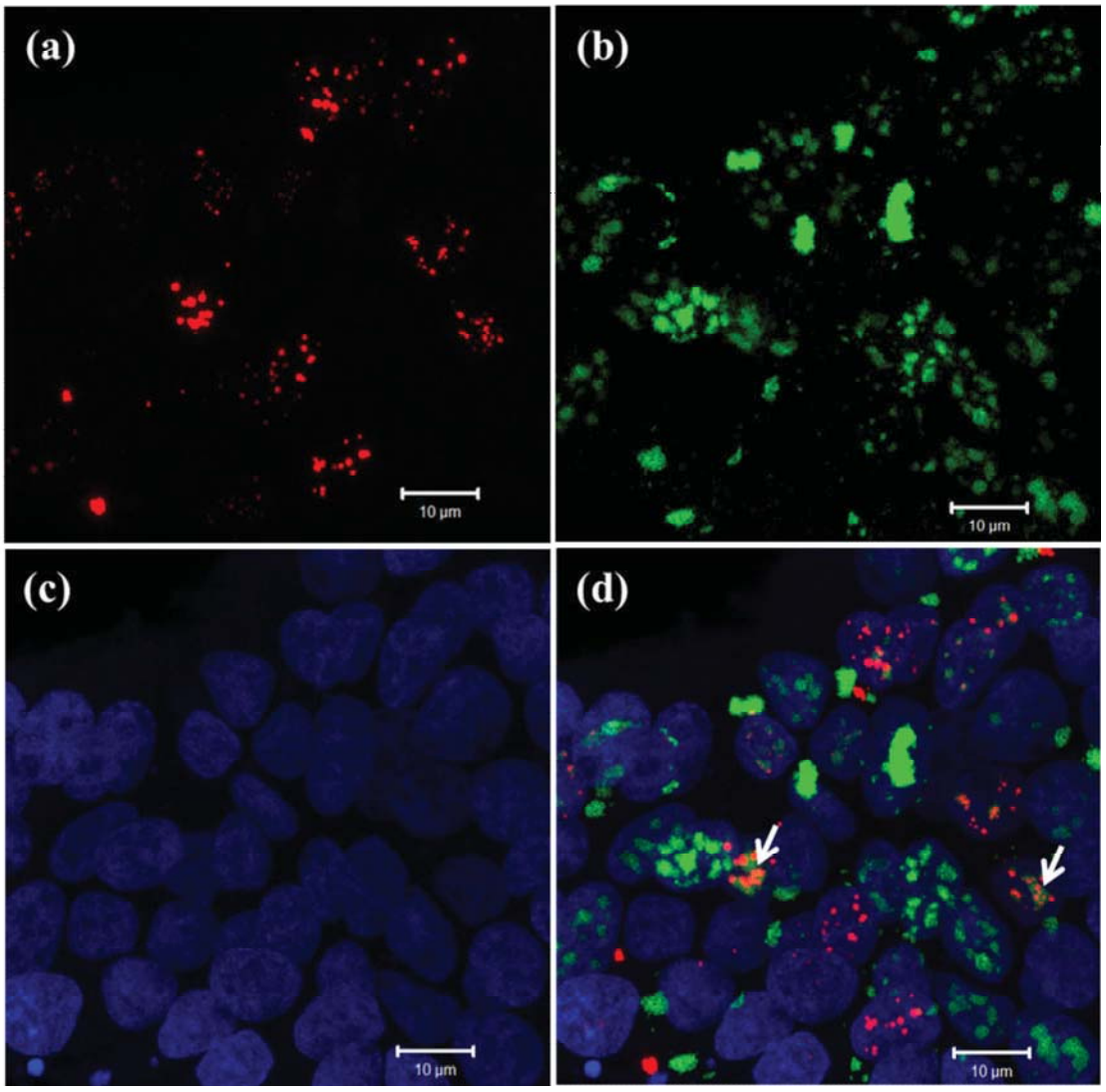

Fig. 43

WLD^{s} colocalises with nuclear mHTT aggregates. *Confocal images (63X) of PC12 Q72 cells transfected with Wld^{S} in DsRed vector and treated with doxycycline to induce mHtt aggregates formation. Some cells show colocalisation between mHtt aggregates and WLD^{s} in the nucleus (arrows). (a) red: WLD^{s}, (b) green: mHTT, (c) blue: Hoechst, (d) merged channels. Scale bar, 10µm.*

Then I checked whether colocalisation extended also to the NMNAT1 component of WLD^S underlying possible interaction. In the nuclei of Tet-ON PC12 Q72 cells, an NMNAT1-DsRed vector fusion protein showed a discrete distribution in nuclear foci. This could reflect an association of NMNAT1 with specific sub-nuclear domains, although we cannot exclude mis-localisation due to the overexpression of the DsRed fusion protein (Laser et al., 2006, Wilbrey et al., 2008). NMNAT1-DsRed did not colocalise with mHTT aggregates (Fig. 44) which remained in different pools, possibly suggesting that the full WLD^S sequence is needed for the interaction and further studies should address this.

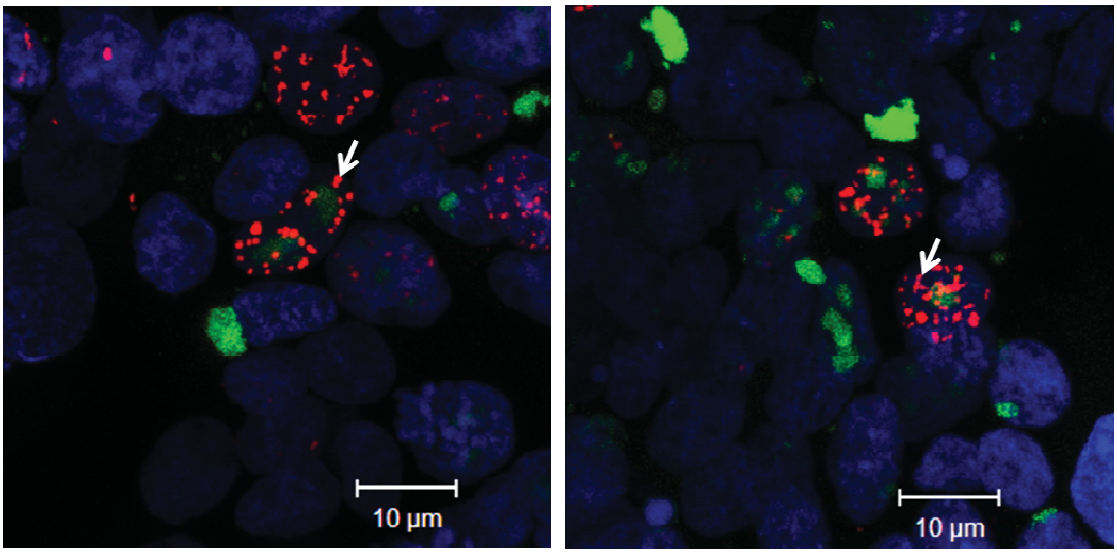

Fig. 44

NMNAT1 does not colocalise with nuclear mHTT aggregates. *Confocal images (63X) of Tet-ON PC12 Q72 cells transfected with Nmnat1 in DsRed vector (arrows) show no colocalisation with mHTT aggregates. Red: NMNAT1, green: mHTT, blue: Hoechst. Scale bar, 10µm.*

WLD^S overexpression does not increase percentage of projections and healthy nuclei in mHTT expressing cells

Previous studies have shown the toxic effect of mHTT aggregates on an inducible model of PC12 cells (Wyttenbach et al., 2000, Wyttenbach et al., 2001). This has been recently confirmed in a study from our laboratory which showed that mHTT aggregates significantly reduce the number of neuritic projections and unhealthy

nuclei (Othman, Pardon and Conforti, unpublished). An interaction between WLD^S and mHTT aggregates could play a role in aggregate formation and toxicity and provide insights into the feasibility to investigate a potential protective effect of the WLD^S protein in HD.

I explored the possibility that expression of WLD^S could rescue the toxic effect of mHTT aggregates on Tet-ON PC12 cells and restore normal neuritic formation. To this aim, Tet-ON PC12 with an expanded CAG repeat (PC12 Q72) treated with doxycycline to express mHTT, were transfected with constructs encoding for a WLD^S-DsRed fusion protein and, 3 days after transfection, the number of projections (Fig. 45 A) and the number of Hoechst-stained healthy nuclei (Fig. 45 B), were counted over the total number of transfected cells. Cells transfected with DsRed vector, for expression of the red fluorescence protein only, were used as control. Unexpectedly, overexpression of WLD^S in PC12 cells revealed a toxic effect and caused a decrease in cell viability (Fig 45 B). WLD^S expression did not result in a higher percentage of projections and healthy nuclei compared to the controls without WLD^S.

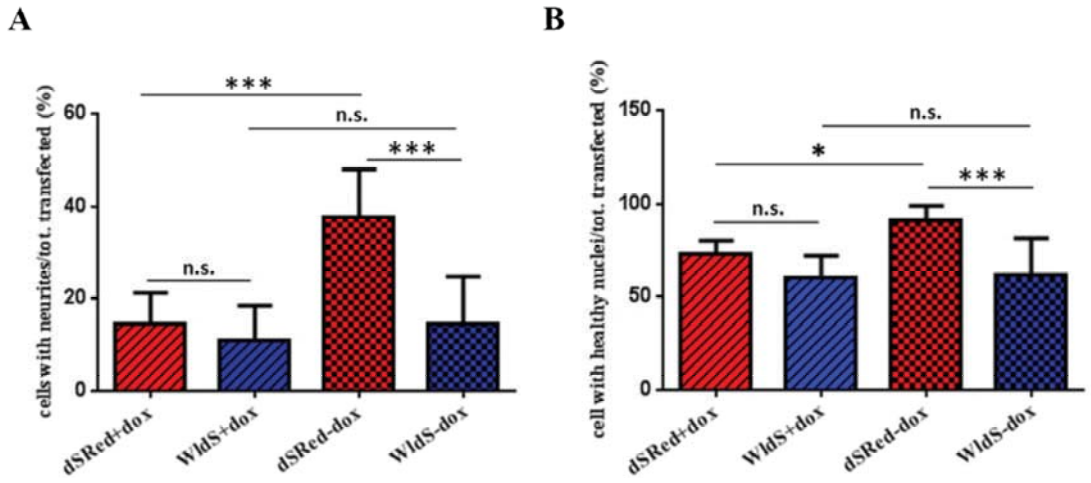

Fig. 45

WLD^S overexpression is toxic in PC12 cells. *Tet-ON PC12 Q72 cells were transfected with Wld^S in DsRed vector and after 3 days the number of cells with neurites was counted over the total of transfected cells as well as the number of healthy DAPI-stained nuclei over the total transfected. Cells transfected with DsRed only were used as control. WLD^S does not increase the number of neuritic projections neither the percentage of healthy nuclei in cells expressing mHTT. However, WLD^S overexpression reduces viability in Tet-ON PC12 cells Q72 (n = 3, mean±SEM, one-way ANOVA followed by Bonferroni post hoc test,*, P<0.05, ***, P< 0.001).*

mHTT colocalises with NMNAT2

To study possible colocalisation between mHTT and NMNAT2, the endogenous NMNAT isoform present in axons, I first looked at a possible colocalisation between the two proteins in HEK293 cells, using the synthetic plasmid (pARIS-htt) expressing full-length human HTT with either normal or expanded CAG repeat (Fig. 46) (Pardo et al., 2010). Given the large size of the full-length HTT construct, we used HEK cells where a high efficiency of transfection can be obtained. Cells were cotransfected with plasmids encoding NMNAT2-EGFP and pARIS-htt(Q20/Q100)-mCherry and imaged 2 days after transfection. Confocal images suggested that both wild-type and mutant HTT were enriched at a perinuclear location consistent with that of the Golgi apparatus, where they colocalised with NMNAT2 (Fig. 46). Indeed, as reported in (Pardo et al., 2010) pARIS-htt constructs conserve the region of HTT necessary for Golgi association.

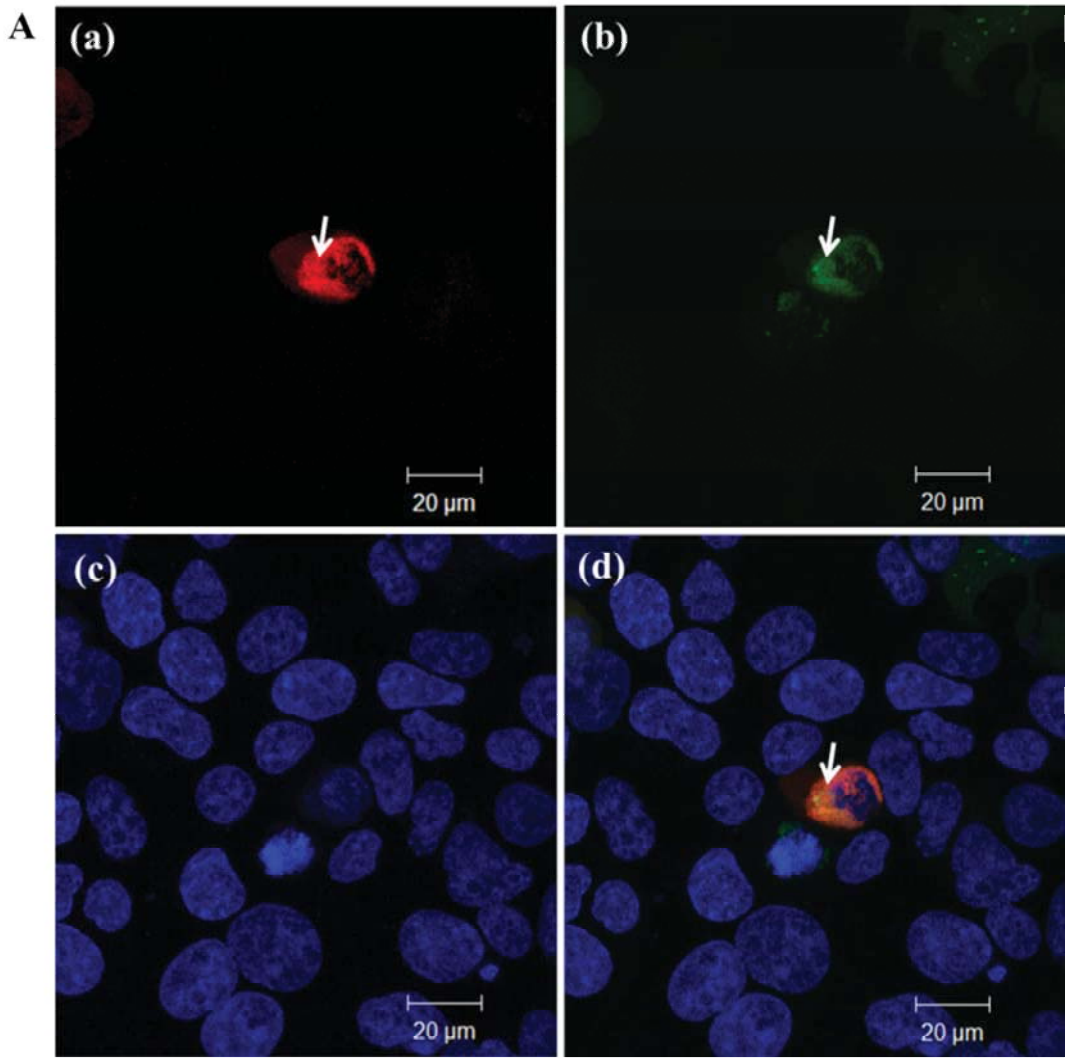

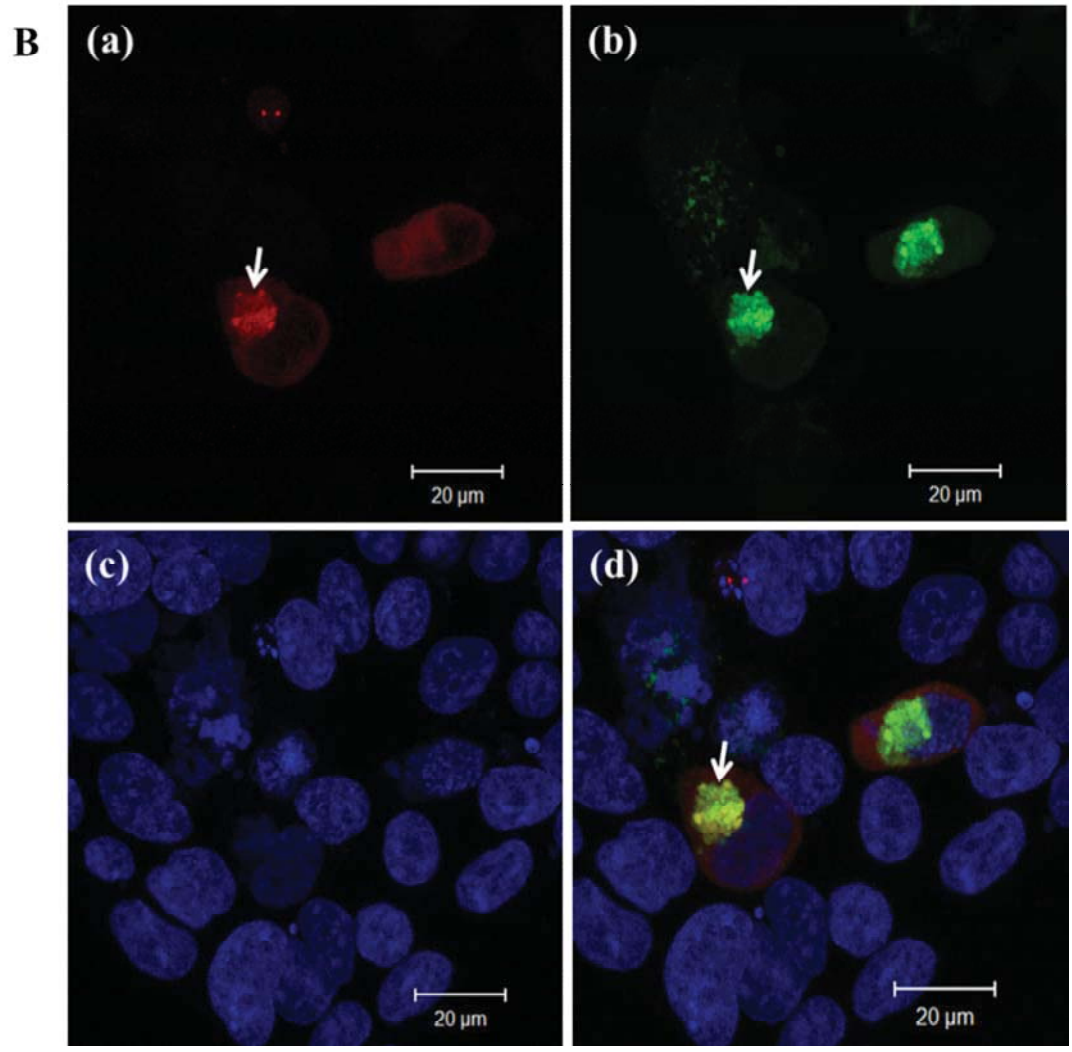

Fig. 46

NMNAT2 colocalises with both wild-type and mHTT in HEK293 cells. *Confocal images (63X) of HEK293 cells, cotrasfected with NMNAT2-EGFP and (A) full-length pARIS-httQ23-mCherry and (B) full-length pARIS-httQ100-mCherry, reveal proteins colocalise in a perinuclear formation, suggestive of Golgi structure (arrows), independently from the CAG repeat length. (a) Red: pARIS, (b) green: NMNAT2, (c) blue: Hoechst, (d) merged channels. Scale bar, 20µm.*

Next, I microinjected the same plasmids in dissociated SCGs to study colocalisation in the axon. Dissociated SCGs have the advantage to extend long projections allowing the study of axonal transport of fluorescent molecules. Red fluorescence was absent in neurites and weak in cell bodies, possibly due to the lower efficiency of transfection and expression of the large HTT expressing constructs in these cells. I then microinjected SCGs with shorter versions of pARIS expressing only the N-terminal

part of human HTT with normal or expanded CAG number (pARIS htt 1-586-Q23/Q100). These fragment constructs still retained the palmitoylation site important for vesicle association which is likely to contribute to the colocalisation with NMNAT2 at the Golgi. Confocal images acquired on the day following the microinjection, showed expression of the fragment HTT in both cell body and axons (Fig. 47 and 48 A) and confirmed colocalisation with NMNAT2 in the cell body (Fig. 47).

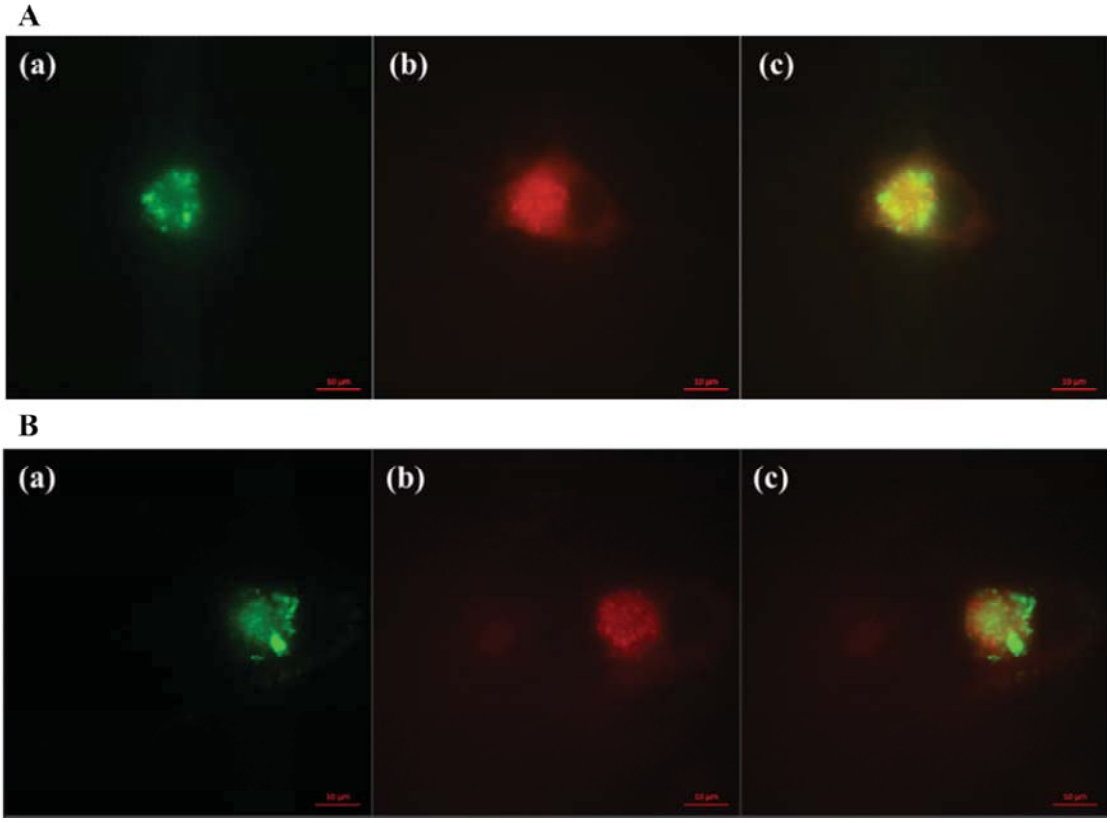

Fig. 47

NMNAT2 colocalises with both wild-type and mHTT in the cell body of SCGs. *Fluorescent images (100X) of dissociated SCGs co-injected with NMNAT2-EGFP and (A) pARIS htt 1-586-Q23-mCherry or (B) pARIS htt 1-586-Q23-mCherry reveal colocalisation between the two proteins (arrows), independently from the CAG repeat length. (A) Red: pARIS, (B) green: NMNAT2, (C) merged channels. Scale bar, 10 µm.*

HTT is important for axonal transport and mHTT disrupts this process, therefore I tested whether overexpression of HTT and mHTT could affect axonal transport of NMNAT2, which is essential for axon maintenance.

I studied the movement of NMNAT2 fluorescent molecules along the axons of dissociated SCGs microinjected with N-terminal-httQ20/Q100 pARIS-mCherry and NMNAT2-EGFP, to determine any potential change in NMNAT2 transport due to the expression of these proteins. Time-lapse imaging and video analysis were carried out as described in section 2.5.7. No significant difference neither in NMNAT2 particle speed nor in the particle count and % of moving particles/frame, in the presence of mHTT compared to wild-type HTT, was found upon analysis using Difference tracker ImageJ plugin (Andrews et al., 2010) (Fig. 48 and suppl. video 2). However, a trend to increase of all parameters was found in the presence of mHTT, possibly suggesting abnormal axonal transport. Analysis of a larger number of axons is needed to confirm these observations.

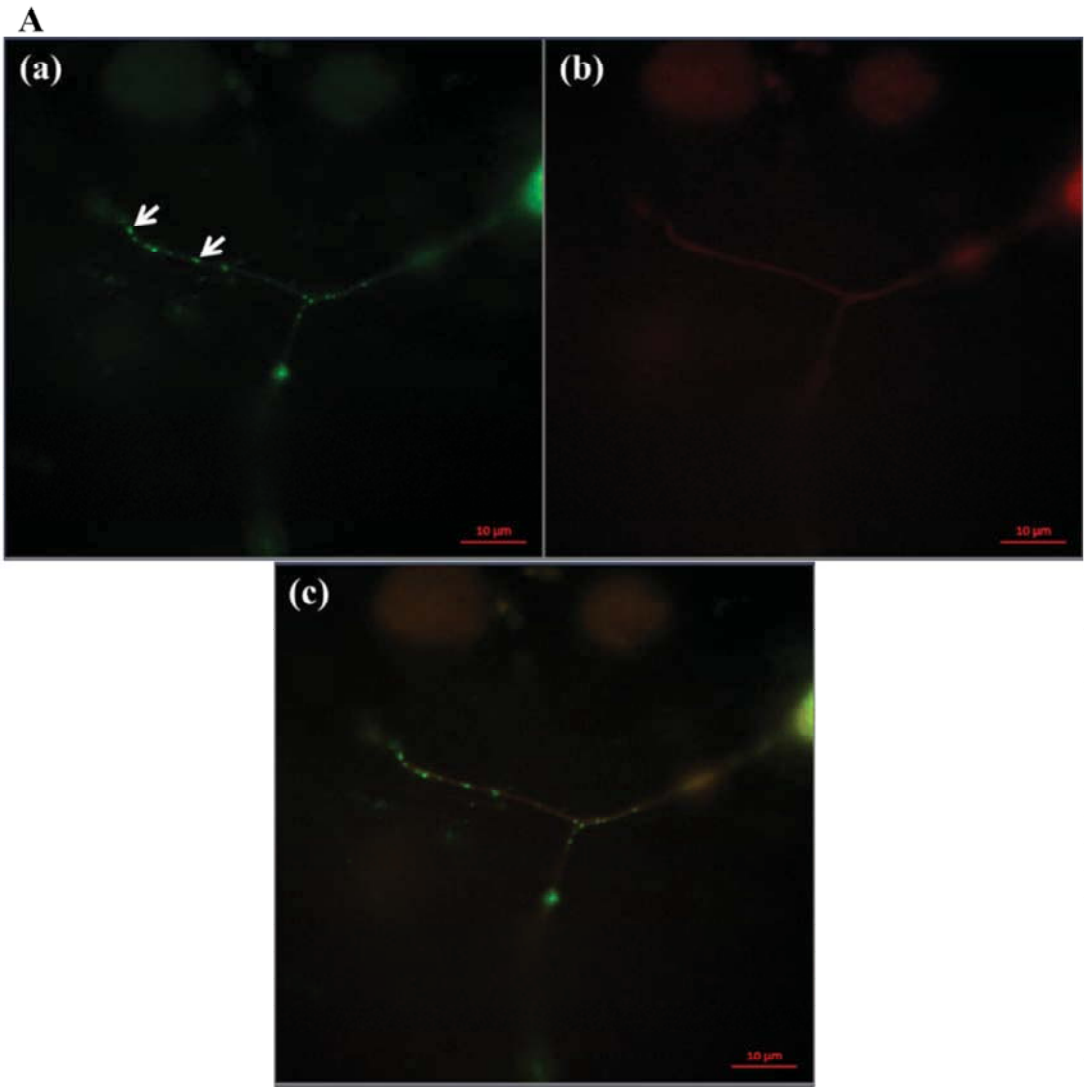
A
(a)
(b)
(c)
10 µm
10 µm
10 µm
B
n.s.
average speed/track (µm/sec)
2.5
2.0
1.5
1.0
0.5
0.0
HTTQ23-NMNAT2
HTTQ100-NMNAT2
C
n.s.
average counts per frame
6
4
2
0
HTTQ23-NMNAT2
HTTQ100-NMNAT2
D
n.s.
% counts moving
50
40
30
20
10
0
HTTQ23-NMNAT2
HTTQ100-NMNAT2

Fig. 48

Axonal transport of NMNAT2 is not significantly altered in the presence of mHTT. *(A) Fluorescent image (100X) of dissociated SCGs co-injected with NMNAT2-EGFP and pARIS-htt 1-586-Q100-mCherry. (a) green: NMNAT2-EGFP, (b) red: pARIS htt 1-586-NQ100-mCherry, (c) merged channels. Scale bar, 10 µm. Analysis of time-lapse videos shows no significant changes neither in NMNAT2 particle speed (B) nor in number of particle and % of moving particles/frame (C, D), in the presence of HTTQ100 compared to HTTQ23, however a trend to increase is found in the presence of mHTT (n = 4, mean±SEM, unpaired Student's t-test).*

5.4 Discussion

Results from this part of the study revealed altered NAD metabolism in mice. Genotype differences were not detected in brain samples but in HD cellular models potential interaction of mHTT with NAD synthesizing enzymes, which could alter normal enzyme trafficking and function, might contribute to axon pathology.

NAD role in axon protection has been questioned by several studies and unpublished data from our lab suggest that an increase in NMN, rather than an increase in NAD, underlines the protective effect of NMNAT and WLD^s (Di Stefano et al., unpublished). Interestingly, NMN as well as quinolinic acid, both NAD precursors, exert a toxic role. In this context, increased NMN levels detected in HD and control mouse brain striata at 12 months of age could contribute to the pathological changes observed in axons. Indeed, in many age-related neurodegenerative diseases or during normal ageing, widespread axonal swellings are visible (Adalbert and Coleman, 2012). In analogy to injured axons, where loss of NMNAT2 initiates a pro-axon death pathway, a decline in axonal transport during aging which could be exacerbated in disease, could also lead to reduced delivery of NMNAT2 and consequent rise in NMN levels in axons. Indeed a decrease in axonal transport of mitochondria and synaptic vesicles during aging and in disease is described (Kimura et al., 2012, Gilley et al., 2012, Adalbert and Coleman, 2012). NAD decrease between 6 and 12 months of age in both genotypes, despite this does not reach statistical significance with this group size, consistent with the idea that NMNAT2 may be in limited supply in older animals.

Importantly, these results also reveal a regional alteration in nucleotide levels as the increase in NMN was found significant only in the striatum and not in the cortex.

Previous studies described a regional reduction in NAD synthesis in aged animals (Mouchiroud et al., 2013, Massudi et al., 2012), confirming the importance of analysing single brain areas to spot local deficiencies which could be missed in the whole-brain due to the heterogeneity of cell types and structures. The alteration of NAD metabolism in striatum could contribute to the increased susceptibility of this brain area to degeneration in HD.

HD mutation seems not to contribute to alterations in the NAD biosynthetic pathway at the age of analysis. However, as KI mice have a normal lifespan and slow onset and progression of pathology, we cannot exclude that nucleotide levels at later stage of the disease could be altered in these mice with respect to the controls.

The increase in NMN and decrease in NAD was accompanied by little reduction in NMNAT total enzymatic activity with age but this analysis was carried out only in few samples; thus, further investigation with larger number might detect a significant reduction. Moreover, our analysis considered only the total NMNAT enzymatic activity, while alterations in one specific isoform are difficult to detect and cannot be excluded. Alternatively, we have to consider that the enzymatic activity *in vitro* might not be the same as *in vivo* where a much higher reduction in NMNAT activity could be observed.

qRT-PCR analysis of expression levels of NMNAT1, 2 and 3 and NAMPT, carried out by other members of the laboratory (Othman et al., unpublished), found no differences between HdhQ140 and control mice suggesting no transcriptional dysregulation of this enzymatic pathway in HD, however post-translational regulation, which is not taken into consideration by this technique, could be altered and affect enzyme turnover or functionality.

I also detected a trend to a decrease in NAMPT in both genotypes and in both brain areas, consistent with published observations (Imai, 2010). In WT mice, decrease in NAMPT levels could explain the reduction in NMN in the cortex.

Interesting results also come from studies on cell models. In a Tet-ON PC12 cell model of HD, mHTT aggregates colocalise with the UBE4B/NMNAT1 fusion protein WLD^S but not with NMNAT1, suggesting that the full-length sequence of WLD^S is required for the interaction. More experiments are required to assess if actual

interaction is occurring between the two proteins and whether this is direct or indirect via a common binding partner. Possibly, the N16 binding site for VCP/p97, protein which also binds to expanded polyQ-containing proteins (Hirabayashi et al., 2001), is necessary for the interaction. In Tet-ON PC12 cells, WLD^S expression is toxic for the cells at the concentration used for transfection. This is surprising in view of the several reports of a beneficial effect of WLD^S in axons and cell bodies in *in vivo* and *in vitro* models of disease (Coleman and Freeman, 2010). Further studies are needed to elucidate the mechanism of this toxicity.

Colocalisation between mHTT and NMNAT2 was instead studied in HEK293 cells and disassociated SCGs. Since NMNAT2 is a cytoplasmic protein transported by fast axonal transport, dissociated SCGs, which can extend long neurites, represented a good preliminary model to study colocalisation in the axon and possible alterations in its transport due to mutant HTT. Colocalisation was found in the cell body while in the axon, a diffuse distribution of mHTT which possibly requires a longer time after transfection to form aggregates, made it impossible to establish whether this was present at the level of the well visible NMNAT2 vesicles. Despite these results, a co-transport of mHTT and NMNAT2 on the same vesicles is likely to occur as both proteins contain palmitoylation sites crucial for association to Golgi membranes (Yanai et al., 2006). Moreover, it has been recently reported that the glycolytic enzyme glyceraldehyde-3-phosphate dehydrogenase (GADPH) located on fast moving vesicles provides local energy critical for fast axonal transport and that HTT is important to scaffold GADPH on vesicles (Zala et al., 2013). NMNAT2 in these vesicles could provide local NAD pool for the action of GADPH enzymes. In the presence of mHTT, altered scaffolding function could play a detrimental role on FAT axonal transport of NMNAT2, although further investigations are needed to assess whether NMNAT2 is present in GADPH-containing vesicles.

Analysis of NMNAT2 axonal transport in these cells did not detect significant difference in speed, particle count or percentage of moving particle, in the presence of mHTT compared to wild-type HTT. However, a trend to increase was found in the presence of the mutant protein. A reduced detachment of NMNAT2 from vesicles in the presence of overexpressed mHTT; and a consequent alteration of NMNAT2 de-palmitoylation and detachment could be hypothesised. Non-vesicular, cytosolic NMNAT2 is more stable and more protective than the vesicle-associated form, thus its

reduction could play a role in axon degeneration (Milde et al., 2013b, Milde et al., 2013a). Further studies are needed to confirm this result and explore the mechanisms of mHTT toxicity.

CHAPTER 6

Conclusive remarks and future directions

In this thesis I have explored several aspects of the HD pathology with a particular focus on axon pathology during disease progression in relation to behavioural abnormalities, using a variety of cell biology, biochemistry and immunohistochemistry methodologies and behavioral analysis. I have demonstrated that age-dependent axonal swellings are an early feature of HdhQ140 homozygous mice crossed to YFP-H; that behavioural abnormalities also worsen with age and I have given insights into the possible mechanisms underlying these neurodegenerative changes. These findings initiate many avenues for further investigation, some of which have been discussed in the previous chapters.

The data illustrated in chapter 3 strongly suggest that axonal pathology in $Hdh^{Q140/Q140}$ mice precedes dysfunction of other neuronal compartments and occurs in the form of axonal swellings in otherwise continuous axons and healthy looking soma, supporting the idea of still metabolically active cell bodies and continued axonal transport. This raises the prospect of a therapeutic window for functional rescue of individual neurons after formation of swellings and before cell body death, as suggested also for other neurodegenerative disease models (Adalbert et al., 2009). Moreover, as early axonal swellings in still continuous axons are shared by different models, therapeutic intervention could be useful for the treatment of several neurodegenerative diseases. Indeed ample evidence suggests that WLD^{s} protects from axon degeneration in many disease models (Conforti et al., 2014). Therefore, it would be of great interest to cross $Hdh^{Q140/Q140}$/YFP-H mice with *Wld*^{S} mice to determine if the protective phenotype is reproduced in these mice. A delayed onset of axonal swellings and behavioural abnormalities would be hypothesized.

Data from this chapter also suggest that it would be interesting to cross the HdhQ140 mice to other lines of Tg mice expressing fluorescent markers in order to study additional subsets of neurons and determine which ones are affected first and at what age. Indeed, one of the main questions arising from our YFP-H model is that only restricted subsets of neurons are fluorescently labelled and the D2 MSSNs, the most affected in HD, are not among these. In this regard, crossing to Drd2-EGFP Tg mice, which express YFP+ D2 striatal neurons, could be relevant to assess axon degeneration in this neuronal population. As an alternative, *in vivo* Diffusion Tensor Imaging (DTI) (Wu et al., 2013) could be used, as succesfully done in patients (Rosas et al., 2006, Weaver et al., 2009), to identify axon degeneration and loss in HdhQ140

mouse brain, although a limitation of this model is that little changes in specific subsets of neurons could be difficult to detect.

Another part of the study worth further investigations is the behavioural phenotype of HdhQ140 homozygous mice. This, similarly to the morphological changes in axons, showed a progressive deterioration indicating that both morphological and behavioural aspects of the disease, model well disease progression in humans. Thus, behavioural assessment, together with *in vitro* analysis, could be an important readout to evaluate future therapeutic strategies targeting protection of the axon.

As these mice have mild phenotype and normal life-span, it would be interesting to test them also at later time-point, to see whether dysfunctions, other than the ones detected at 12 months of age, are observed and if these parallel the progression of axonal abnormalities. Additional tests of fear and anxiety-related behaviour such as contextual fear conditioning or light/dark exploration tests would also be useful to better determine the early contribution of axonal swellings found in *stria terminalis*.

Furthermore, additional cognitive tasks more specific for striatal dysfunction such as delayed alternation or Serial Implicit Learning Task (SILT), together with histological analysis of fluorescent neurons in HdhQ140/Drd2-EGFP mice, could reveal early impairment of striatal neuron function.

Also, the data reported in chapter 5, contribute to the investigation of the mechanisms of axon degeneration in $Hdh^{Q140/Q140}$ mice. Interesting preliminary analysis links mHTT to NMNAT2, a NAD synthesizing enzyme and important axon survival factor, in a cellular model of HD. Despite tissue-specific measurements of nucleotide and enzyme levels did not show abnormal NAD metabolism in KI mice compared to the control, defective processes local to individual neuronal compartments not detected with these techniques could still contribute to degeneration in these mice. In support of this, the increased number of axonal swellings which preceded cell body degeneration, together with increased behavioural symptoms, suggests dysfunctions are local to axons in these mice and contribute to pathology. Likely, impaired axonal transport of vesicles containing important axon survival factors contributes to this pathology as axonal transport defects are extensively described in HD patients and mouse models. Despite the immunofluorescently labeled mHTT aggregates in mouse brain were not found in YFP+ axons, a non-aggregated, soluble and possibly more

toxic fraction of mHTT could play a role. Further experiments are needed to elucidate if this is the case. However, the observation in SCG cellular model that HTT/mHTT colocalises with NMNAT2; and the alterations found in NMNAT2 vesicular transport, opens the possibility that mHTT interacts with NMNAT2 and interferes with its transport and crucial activity in axons. An open question remains whether colocalisation underlies interaction. Further experiments including pull-down and immunoprecipitation, would be needed to assess binding. Attempts of pull-down experiments were made using the full length human HTT (pARIS-htt) transiently expressed in HEK cells, but proved unsuccessful due to the difficulties of expression of this large protein which could not be detected in immunoblots. Future experiments should be carried out using first the human HTT fragment (pARIS-htt 1-586) which still retains the palmitoylation site responsible for association to vesicles and which showed much higher transfection efficiency in SCGs.

Future additional experiments, in particular to increase the group size, are also needed to confirm the changes observed in the measurement of the NMNAT enzyme activity in mouse brain tissue and to establish whether alterations occur with age and in HD compared to control mice. In addition, a discrimination assay, measuring the activity of the individual NMNAT isoforms could be useful to understand the contribution of the single enzymes and in particular of NMNAT2 in parallel to the *in vitro* results. Moreover, if specific antibodies against NMNAT2 became available, future experiments of Western blot could measure the levels of protein in brain homogenates. A larger group size could also better clarify whether a significant NAD decrease accompanies NMN increase in the striatum.

In conclusion, this work brings contribution to the understanding of the mechanisms of axon degeneration in HD mouse models and of the role of axon pathology in the development of disease. We have identified many questions that remain open and addressing these questions should help us finding a therapeutic strategy to cure or at least delay symptom onset and progression in HD and other neurodegenerative disorders.

References

ADALBERT, R. & COLEMAN, M. P. 2012. Axon pathology in age-related neurodegenerative disorders. *Neuropathol Appl Neurobiol,* 39**,** 90-108.

ADALBERT, R., GILLINGWATER, T. H., HALEY, J. E., BRIDGE, K., BEIROWSKI, B., BEREK, L., WAGNER, D., GRUMME, D., THOMSON, D., CELIK, A., ADDICKS, K., RIBCHESTER, R. R. & COLEMAN, M. P. 2005. A rat model of slow Wallerian degeneration (WldS) with improved preservation of neuromuscular synapses. *Eur J Neurosci,* 21**,** 271-7.

ADALBERT, R., NOGRADI, A., BABETTO, E., JANECKOVA, L., WALKER, S. A., KERSCHENSTEINER, M., MISGELD, T. & COLEMAN, M. P. 2009. Severely dystrophic axons at amyloid plaques remain continuous and connected to viable cell bodies. *Brain,* 132**,** 402-16.

AGGARWAL, M., DUAN, W., HOU, Z., RAKESH, N., PENG, Q., ROSS, C. A., MILLER, M. I., MORI, S. & ZHANG, J. 2012. Spatiotemporal mapping of brain atrophy in mouse models of Huntington's disease using longitudinal in vivo magnetic resonance imaging. *Neuroimage,* 60**,** 2086-95.

ALBIN, R. L., REINER, A., ANDERSON, K. D., DURE, L. S. T., HANDELIN, B., BALFOUR, R., WHETSELL, W. O., JR., PENNEY, J. B. & YOUNG, A. B. 1992. Preferential loss of striato-external pallidal projection neurons in presymptomatic Huntington's disease. *Ann Neurol,* 31**,** 425-30.

ALBIN, R. L., REINER, A., ANDERSON, K. D., PENNEY, J. B. & YOUNG, A. B. 1990a. Striatal and nigral neuron subpopulations in rigid Huntington's disease: implications for the functional anatomy of chorea and rigidity-akinesia. *Ann Neurol,* 27**,** 357-65.

ALBIN, R. L., YOUNG, A. B., PENNEY, J. B., HANDELIN, B., BALFOUR, R., ANDERSON, K. D., MARKEL, D. S., TOURTELLOTTE, W. W. & REINER, A. 1990b. Abnormalities of striatal projection neurons and N-methyl-D-aspartate receptors in presymptomatic Huntington's disease. *N Engl J Med,* 322**,** 1293-8.

ALEXANDER, G. E., CRUTCHER, M. D. & DELONG, M. R. 1990. Basal ganglia-thalamocortical circuits: parallel substrates for motor, oculomotor, "prefrontal" and "limbic" functions. *Prog Brain Res,* 85**,** 119-46.

ALEXANDER, G. E., DELONG, M. R. & STRICK, P. L. 1986. Parallel organization of functionally segregated circuits linking basal ganglia and cortex. *Annu Rev Neurosci,* 9**,** 357-81.

ALI, Y. O., RUAN, K. & ZHAI, R. G. 2012. NMNAT suppresses tau-induced neurodegeneration by promoting clearance of hyperphosphorylated tau oligomers in a Drosophila model of tauopathy. *Hum Mol Genet,* 21**,** 237-50.

ALMQVIST, E. W., BLOCH, M., BRINKMAN, R., CRAUFURD, D. & HAYDEN, M. R. 1999. A worldwide assessment of the frequency of suicide, suicide attempts, or psychiatric hospitalization after predictive testing for Huntington disease. *Am J Hum Genet,* 64**,** 1293-304.

ALMQVIST, E. W., BRINKMAN, R. R., WIGGINS, S., HAYDEN, M. R. & CANADIAN COLLABORATIVE STUDY OF PREDICTIVE, T. 2003. Psychological consequences and predictors of adverse events in the first 5 years after predictive testing for Huntington's disease. *Clin Genet,* 64**,** 300-9.

ANDERSON, K. E. & MARDER, K. S. 2001. An overview of psychiatric symptoms in Huntington's disease. *Curr Psychiatry Rep,* 3**,** 379-88.

ANDRADE, M. A. & BORK, P. 1995. HEAT repeats in the Huntington's disease protein. *Nat Genet,* 11**,** 115-6.

ANDRE, V. M., CEPEDA, C., VENEGAS, A., GOMEZ, Y. & LEVINE, M. S. 2006. Altered cortical glutamate receptor function in the R6/2 model of Huntington's disease. *J Neurophysiol,* 95**,** 2108-19.

ANDREWS, S., GILLEY, J. & COLEMAN, M. P. 2010. Difference Tracker: ImageJ plugins for fully automated analysis of multiple axonal transport parameters. *J Neurosci Methods,* 193**,** 281-7.

ANNE, S. L., SAUDOU, F. & HUMBERT, S. 2007. Phosphorylation of huntingtin by cyclin-dependent kinase 5 is induced by DNA damage and regulates wild-type and mutant huntingtin toxicity in neurons. *J Neurosci,* 27**,** 7318-28.

ARAKI, T., SASAKI, Y. & MILBRANDT, J. 2004. Increased nuclear NAD biosynthesis and SIRT1 activation prevent axonal degeneration. *Science,* 305**,** 1010-3.

ARRASATE, M., MITRA, S., SCHWEITZER, E. S., SEGAL, M. R. & FINKBEINER, S. 2004. Inclusion body formation reduces levels of mutant huntingtin and the risk of neuronal death. *Nature,* 431**,** 805-10.

AUBRY, L., BUGI, A., LEFORT, N., ROUSSEAU, F., PESCHANSKI, M. & PERRIER, A. L. 2008. Striatal progenitors derived from human ES cells mature into DARPP32 neurons in vitro and in quinolinic acid-lesioned rats. *Proc Natl Acad Sci U S A,* 105**,** 16707-12.

AVANZINI, G., GIROTTI, F., CARACENI, T. & SPREAFICO, R. 1979. Oculomotor disorders in Huntington's chorea. *J Neurol Neurosurg Psychiatry,* 42**,** 581-9.

AVERY, M. A., SHEEHAN, A. E., KERR, K. S., WANG, J. & FREEMAN, M. R. 2009. Wld S requires Nmnat1 enzymatic activity and N16-VCP interactions to suppress Wallerian degeneration. *J Cell Biol,* 184**,** 501-13.

BABETTO, E., BEIROWSKI, B., JANECKOVA, L., BROWN, R., GILLEY, J., THOMSON, D., RIBCHESTER, R. R. & COLEMAN, M. P. 2010. Targeting NMNAT1 to axons and synapses transforms its neuroprotective potency in vivo. *J Neurosci,* 30**,** 13291-304.

BACHOUD-LEVI, A. C., GAURA, V., BRUGIERES, P., LEFAUCHEUR, J. P., BOISSE, M. F., MAISON, P., BAUDIC, S., RIBEIRO, M. J., BOURDET, C., REMY, P., CESARO, P., HANTRAYE, P. & PESCHANSKI, M. 2006. Effect of fetal neural transplants in patients with Huntington's disease 6 years after surgery: a long-term follow-up study. *Lancet Neurol,* 5**,** 303-9.

BACHOUD-LEVI, A. C., REMY, P., NGUYEN, J. P., BRUGIERES, P., LEFAUCHEUR, J. P., BOURDET, C., BAUDIC, S., GAURA, V., MAISON, P., HADDAD, B., BOISSE, M. F., GRANDMOUGIN, T., JENY, R., BARTOLOMEO, P., DALLA BARBA, G., DEGOS, J. D., LISOVOSKI, F., ERGIS, A. M., PAILHOUS, E., CESARO, P., HANTRAYE, P. & PESCHANSKI, M. 2000. Motor and cognitive improvements in patients with Huntington's disease after neural transplantation. *Lancet,* 356**,** 1975-9.

BAE, B. I., XU, H., IGARASHI, S., FUJIMURO, M., AGRAWAL, N., TAYA, Y., HAYWARD, S. D., MORAN, T. H., MONTELL, C., ROSS, C. A., SNYDER, S. H. & SAWA, A. 2005. p53 mediates cellular dysfunction and behavioral abnormalities in Huntington's disease. *Neuron,* 47**,** 29-41.

BAILEY, K. R., PAVLOVA, M. N., ROHDE, A. D., HOHMANN, J. G. & CRAWLEY, J. N. 2007. Galanin receptor subtype 2 (GalR2) null mutant mice display an anxiogenic-like phenotype specific to the elevated plus-maze. *Pharmacol Biochem Behav,* 86**,** 8-20.

BALAN, I. S., FISKUM, G. & KRISTIAN, T. 2010. Visualization and quantification of NAD(H) in brain sections by a novel histo-enzymatic nitrotetrazolium blue staining technique. *Brain Res,* 1316**,** 112-9.

BALDUCCI, E., EMANUELLI, M., RAFFAELLI, N., RUGGIERI, S., AMICI, A., MAGNI, G., ORSOMANDO, G., POLZONETTI, V. & NATALINI, P. 1995. Assay methods for nicotinamide mononucleotide adenylyltransferase of wide applicability. *Anal Biochem,* 228**,** 64-8.

BATES, E. A., VICTOR, M., JONES, A. K., SHI, Y. & HART, A. C. 2006. Differential contributions of Caenorhabditis elegans histone deacetylases to huntingtin polyglutamine toxicity. *J Neurosci,* 26**,** 2830-8.

BATES, G. P. 2001. Huntington's disease. Exploiting expression. *Nature,* 413**,** 691, 693-4.

BAXENDALE, S., ABDULLA, S., ELGAR, G., BUCK, D., BERKS, M., MICKLEM, G., DURBIN, R., BATES, G., BRENNER, S. & BECK, S. 1995. Comparative sequence analysis of the human and pufferfish Huntington's disease genes. *Nat Genet,* 10**,** 67-76.

BEAL, M. F., FERRANTE, R. J., SWARTZ, K. J. & KOWALL, N. W. 1991. Chronic quinolinic acid lesions in rats closely resemble Huntington's disease. *J Neurosci,* 11**,** 1649-59.

BEAL, M. F., KOWALL, N. W., ELLISON, D. W., MAZUREK, M. F., SWARTZ, K. J. & MARTIN, J. B. 1986. Replication of the neurochemical characteristics of Huntington's disease by quinolinic acid. *Nature,* 321**,** 168-71.

BEAL, M. F., MATSON, W. R., STOREY, E., MILBURY, P., RYAN, E. A., OGAWA, T. & BIRD, E. D. 1992. Kynurenic acid concentrations are reduced in Huntington's disease cerebral cortex. *J Neurol Sci,* 108**,** 80-7.

BEAL, M. F., MATSON, W. R., SWARTZ, K. J., GAMACHE, P. H. & BIRD, E. D. 1990. Kynurenine pathway measurements in Huntington's disease striatum: evidence for reduced formation of kynurenic acid. *J Neurochem,* 55**,** 1327-39.

BEGLINGER, L. J., NOPOULOS, P. C., JORGE, R. E., LANGBEHN, D. R., MIKOS, A. E., MOSER, D. J., DUFF, K., ROBINSON, R. G. & PAULSEN, J. S. 2005. White matter volume and cognitive dysfunction in early Huntington's disease. *Cogn Behav Neurol,* 18**,** 102-7.

BEIROWSKI, B., BABETTO, E., COLEMAN, M. P. & MARTIN, K. R. 2008. The WldS gene delays axonal but not somatic degeneration in a rat glaucoma model. *Eur J Neurosci,* 28**,** 1166-79.

BEIROWSKI, B., BABETTO, E., GILLEY, J., MAZZOLA, F., CONFORTI, L., JANECKOVA, L., MAGNI, G., RIBCHESTER, R. R. & COLEMAN, M. P. 2009. Non-nuclear Wld(S) determines its neuroprotective efficacy for axons and synapses in vivo. *J Neurosci,* 29**,** 653-68.

BEIROWSKI, B., BEREK, L., ADALBERT, R., WAGNER, D., GRUMME, D. S., ADDICKS, K., RIBCHESTER, R. R. & COLEMAN, M. P. 2004. Quantitative and qualitative analysis of Wallerian degeneration using restricted axonal labelling in YFP-H mice. *J Neurosci Methods,* 134**,** 23-35.

BELENKY, P., BOGAN, K. L. & BRENNER, C. 2007. NAD+ metabolism in health and disease. *Trends Biochem Sci,* 32**,** 12-9.

BELGUENDOUZ, L., FREMONT, L. & LINARD, A. 1997. Resveratrol inhibits metal ion-dependent and independent peroxidation of porcine low-density lipoproteins. *Biochem Pharmacol,* 53**,** 1347-55.

BERGER, F., LAU, C., DAHLMANN, M. & ZIEGLER, M. 2005. Subcellular compartmentation and differential catalytic properties of the three human nicotinamide mononucleotide adenylyltransferase isoforms. *J Biol Chem,* 280**,** 36334-41.

BERGER, F., RAMIREZ-HERNANDEZ, M. H. & ZIEGLER, M. 2004. The new life of a centenarian: signalling functions of NAD(P). *Trends Biochem Sci,* 29**,** 111-8.

BILNEY, B., MORRIS, M. E. & PERRY, A. 2003. Effectiveness of physiotherapy, occupational therapy, and speech pathology for people with Huntington's disease: a systematic review. *Neurorehabil Neural Repair,* 17**,** 12-24.

BITTNER, T., FUHRMANN, M., BURGOLD, S., OCHS, S. M., HOFFMANN, N., MITTEREGGER, G., KRETZSCHMAR, H., LAFERLA, F. M. & HERMS, J. 2010. Multiple events lead to dendritic spine loss in triple transgenic Alzheimer's disease mice. *PLoS One,* 5**,** e15477.

BLOCK-GALARZA, J., CHASE, K. O., SAPP, E., VAUGHN, K. T., VALLEE, R. B., DIFIGLIA, M. & ARONIN, N. 1997. Fast transport and retrograde movement of huntingtin and HAP 1 in axons. *Neuroreport,* 8**,** 2247-51.

BONELLI, R. M. & CUMMINGS, J. L. 2007. Frontal-subcortical circuitry and behavior. *Dialogues Clin Neurosci,* 9**,** 141-51.

BONELLI, R. M., HEUBERGER, C. & REISECKER, F. 2003. Minocycline for Huntington's disease: an open label study. *Neurology,* 60**,** 883-4.

BOUDREAU, R. L., MCBRIDE, J. L., MARTINS, I., SHEN, S., XING, Y., CARTER, B. J. & DAVIDSON, B. L. 2009. Nonallele-specific silencing of mutant and wild-type huntingtin demonstrates therapeutic efficacy in Huntington's disease mice. *Mol Ther,* 17**,** 1053-63.

BRENDZA, R. P., O'BRIEN, C., SIMMONS, K., MCKEEL, D. W., BALES, K. R., PAUL, S. M., OLNEY, J. W., SANES, J. R. & HOLTZMAN, D. M. 2003. PDAPP; YFP double transgenic mice: a tool to study amyloid-beta associated changes in axonal, dendritic, and synaptic structures. *J Comp Neurol,* 456**,** 375-83.

BRETT, A. C., ROSENSTOCK, T. R. & REGO, A. C. 2014. Current therapeutic advances in patients and experimental models of Huntington's disease. *Curr Drug Targets,* 15**,** 313-34.

BRIDGE, K. E., BERG, N., ADALBERT, R., BABETTO, E., DIAS, T., SPILLANTINI, M. G., RIBCHESTER, R. R. & COLEMAN, M. P. 2009. Late onset distal axonal swelling in YFP-H transgenic mice. *Neurobiol Aging,* 30**,** 309-21.

BRINKMAN, R. R., MEZEI, M. M., THEILMANN, J., ALMQVIST, E. & HAYDEN, M. R. 1997. The likelihood of being affected with Huntington disease by a particular age, for a specific CAG size. *Am J Hum Genet,* 60**,** 1202-10.

BRODY, S. A., CONQUET, F. & GEYER, M. A. 2004. Effect of antipsychotic treatment on the prepulse inhibition deficit of mGluR5 knockout mice. *Psychopharmacology (Berl),* 172**,** 187-95.

BROOKS, S., HIGGS, G., JONES, L. & DUNNETT, S. B. 2012a. Longitudinal analysis of the behavioural phenotype in Hdh(CAG)150 Huntington's disease knock-in mice. *Brain Res Bull,* 88**,** 182-8.

BROOKS, S., HIGGS, G., JONES, L. & DUNNETT, S. B. 2012b. Longitudinal analysis of the behavioural phenotype in HdhQ92 Huntington's disease knock-in mice. *Brain Res Bull,* 88**,** 148-55.

BROOKS, S. P. & DUNNETT, S. B. 2009. Tests to assess motor phenotype in mice: a user's guide. *Nat Rev Neurosci,* 10**,** 519-29.

BROOKS, S. P. & DUNNETT, S. B. 2013. Cognitive deficits in animal models of basal ganglia disorders. *Brain Res Bull,* 92**,** 29-40.

BROUILLET, E., CONDE, F., BEAL, M. F. & HANTRAYE, P. 1999. Replicating Huntington's disease phenotype in experimental animals. *Prog Neurobiol,* 59**,** 427-68.

BUCKLEY, N. J., JOHNSON, R., ZUCCATO, C., BITHELL, A. & CATTANEO, E. 2010. The role of REST in transcriptional and epigenetic dysregulation in Huntington's disease. *Neurobiol Dis,* 39**,** 28-39.

BUCKMASTER, E. A., PERRY, V. H. & BROWN, M. C. 1995. The rate of Wallerian degeneration in cultured neurons from wild type and C57BL/WldS mice depends on time in culture and may be extended in the presence of elevated K+ levels. *Eur J Neurosci,* 7**,** 1596-602.

CAINE, E. D. & SHOULSON, I. 1983. Psychiatric syndromes in Huntington's disease. *Am J Psychiatry,* 140**,** 728-33.

CAMPESAN, S., GREEN, E. W., BREDA, C., SATHYASAIKUMAR, K. V., MUCHOWSKI, P. J., SCHWARCZ, R., KYRIACOU, C. P. & GIORGINI, F. 2011. The kynurenine pathway modulates neurodegeneration in a Drosophila model of Huntington's disease. *Curr Biol,* 21**,** 961-6.

CANALS, J. M., PINEDA, J. R., TORRES-PERAZA, J. F., BOSCH, M., MARTIN-IBANEZ, R., MUNOZ, M. T., MENGOD, G., ERNFORS, P. & ALBERCH, J. 2004. Brain-derived neurotrophic factor regulates the onset and severity of motor dysfunction associated with enkephalinergic neuronal degeneration in Huntington's disease. *J Neurosci,* 24**,** 7727-39.

CARONI, P. 1997. Overexpression of growth-associated proteins in the neurons of adult transgenic mice. *J Neurosci Methods,* 71**,** 3-9.

CARTER, R. J., LIONE, L. A., HUMBY, T., MANGIARINI, L., MAHAL, A., BATES, G. P., DUNNETT, S. B. & MORTON, A. J. 1999. Characterization of progressive motor deficits in mice transgenic for the human Huntington's disease mutation. *J Neurosci,* 19**,** 3248-57.

CATTANEO, E., ZUCCATO, C. & TARTARI, M. 2005. Normal huntingtin function: an alternative approach to Huntington's disease. *Nat Rev Neurosci,* 6**,** 919-30.

CAVISTON, J. P., ROSS, J. L., ANTONY, S. M., TOKITO, M. & HOLZBAUR, E. L. 2007. Huntingtin facilitates dynein/dynactin-mediated vesicle transport. *Proc Natl Acad Sci U S A,* 104**,** 10045-50.

CEPEDA, C., HURST, R. S., CALVERT, C. R., HERNANDEZ-ECHEAGARAY, E., NGUYEN, O. K., JOCOY, E., CHRISTIAN, L. J., ARIANO, M. A. & LEVINE, M. S. 2003. Transient and progressive electrophysiological alterations in the corticostriatal pathway in a mouse model of Huntington's disease. *J Neurosci,* 23**,** 961-9.

CHA, J. H. 2000. Transcriptional dysregulation in Huntington's disease. *Trends Neurosci,* 23**,** 387-92.

CHA, J. H. 2007. Transcriptional signatures in Huntington's disease. *Prog Neurobiol,* 83**,** 228-48.

CHA, J. H., FREY, A. S., ALSDORF, S. A., KERNER, J. A., KOSINSKI, C. M., MANGIARINI, L., PENNEY, J. B., JR., DAVIES, S. W., BATES, G. P. & YOUNG, A. B. 1999. Altered neurotransmitter receptor expression in transgenic mouse models of Huntington's disease. *Philos Trans R Soc Lond B Biol Sci,* 354**,** 981-9.

CHAN, E. Y., LUTHI-CARTER, R., STRAND, A., SOLANO, S. M., HANSON, S. A., DEJOHN, M. M., KOOPERBERG, C., CHASE, K. O., DIFIGLIA, M., YOUNG, A. B., LEAVITT, B. R., CHA, J. H., ARONIN, N., HAYDEN, M. R. & OLSON, J. M. 2002. Increased huntingtin protein length reduces the number of polyglutamine-induced gene expression changes in mouse models of Huntington's disease. *Hum Mol Genet,* 11**,** 1939-51.

CHANG, D. T., RINTOUL, G. L., PANDIPATI, S. & REYNOLDS, I. J. 2006. Mutant huntingtin aggregates impair mitochondrial movement and trafficking in cortical neurons. *Neurobiol Dis,* 22**,** 388-400.

CHEN, M., ONA, V. O., LI, M., FERRANTE, R. J., FINK, K. B., ZHU, S., BIAN, J., GUO, L., FARRELL, L. A., HERSCH, S. M., HOBBS, W., VONSATTEL, J. P., CHA, J. H. & FRIEDLANDER, R. M. 2000. Minocycline inhibits caspase-1 and caspase-3 expression and delays mortality in a transgenic mouse model of Huntington disease. *Nat Med,* 6**,** 797-801.

CHIARUGI, A. 2002. Poly(ADP-ribose) polymerase: killer or conspirator? The 'suicide hypothesis' revisited. *Trends Pharmacol Sci,* 23**,** 122-9.

CHOPRA, V., FOX, J. H., LIEBERMAN, G., DORSEY, K., MATSON, W., WALDMEIER, P., HOUSMAN, D. E., KAZANTSEV, A., YOUNG, A. B. & HERSCH, S. 2007. A small-molecule therapeutic lead for Huntington's disease: preclinical pharmacology and efficacy of C2-8 in the R6/2 transgenic mouse. *Proc Natl Acad Sci U S A,* 104**,** 16685-9.

CHRISTMAS, A. J. & MAXWELL, D. R. 1970. A comparison of the effects of some benzodiazepines and other drugs on aggressive and exploratory behaviour in mice and rats. *Neuropharmacology,* 9**,** 17-29.

COHEN, M. S., GHOSH, A. K., KIM, H. J., JEON, N. L. & JAFFREY, S. R. 2012. Chemical genetic-mediated spatial regulation of protein expression in neurons reveals an axonal function for wld(s). *Chem Biol,* 19**,** 179-87.

COLBY, D. W., CHU, Y., CASSADY, J. P., DUENNWALD, M., ZAZULAK, H., WEBSTER, J. M., MESSER, A., LINDQUIST, S., INGRAM, V. M. & WITTRUP, K. D. 2004. Potent inhibition of huntingtin aggregation and cytotoxicity by a disulfide bond-free single-domain intracellular antibody. *Proc Natl Acad Sci U S A,* 101**,** 17616-21.

COLEMAN, M. P., CONFORTI, L., BUCKMASTER, E. A., TARLTON, A., EWING, R. M., BROWN, M. C., LYON, M. F. & PERRY, V. H. 1998. An 85-kb tandem triplication in the slow Wallerian degeneration (Wlds) mouse. *Proc Natl Acad Sci U S A,* 95**,** 9985-90.

COLEMAN, M. P. & FREEMAN, M. R. 2010. Wallerian Degeneration, WldS, and Nmnat. *Annual Review of Neuroscience,* 33**,** 245-267.

CONFORTI, L., ADALBERT, R. & COLEMAN, M. P. 2007a. Neuronal death: where does the end begin? *Trends Neurosci,* 30**,** 159-66.

CONFORTI, L., FANG, G., BEIROWSKI, B., WANG, M. S., SORCI, L., ASRESS, S., ADALBERT, R., SILVA, A., BRIDGE, K., HUANG, X. P., MAGNI, G., GLASS, J. D. & COLEMAN, M. P. 2007b. NAD(+) and axon degeneration revisited: Nmnat1 cannot substitute for Wld(S) to delay Wallerian degeneration. *Cell Death Differ,* 14**,** 116-27.

CONFORTI, L., GILLEY, J. & COLEMAN, M. P. 2014. Wallerian degeneration: an emerging axon death pathway linking injury and disease. *Nat Rev Neurosci,* 15**,** 394-409.

CONFORTI, L., JANECKOVA, L., WAGNER, D., MAZZOLA, F., CIALABRINI, L., DI STEFANO, M., ORSOMANDO, G., MAGNI, G., BENDOTTI, C., SMYTH, N. & COLEMAN, M. 2011. Reducing expression of NAD+ synthesizing enzyme NMNAT1 does not affect the rate of Wallerian degeneration. *FEBS J,* 278**,** 2666-79.

CONFORTI, L., TARLTON, A., MACK, T. G., MI, W., BUCKMASTER, E. A., WAGNER, D., PERRY, V. H. & COLEMAN, M. P. 2000. A Ufd2/D4Cole1e chimeric protein and overexpression of Rbp7 in the slow Wallerian degeneration (WldS) mouse. *Proc Natl Acad Sci U S A,* 97**,** 11377-82.

CONFORTI, L., WILBREY, A., MORREALE, G., JANECKOVA, L., BEIROWSKI, B., ADALBERT, R., MAZZOLA, F., DI STEFANO, M., HARTLEY, R., BABETTO, E., SMITH, T., GILLEY, J., BILLINGTON, R. A., GENAZZANI, A. A., RIBCHESTER, R. R., MAGNI, G. & COLEMAN, M. 2009. Wld S protein requires Nmnat activity and a short N-terminal sequence to protect axons in mice. *J Cell Biol,* 184**,** 491-500.

COOPER, J. K., SCHILLING, G., PETERS, M. F., HERRING, W. J., SHARP, A. H., KAMINSKY, Z., MASONE, J., KHAN, F. A., DELANOY, M., BORCHELT, D. R., DAWSON, V. L., DAWSON, T. M. & ROSS, C. A. 1998. Truncated N-terminal fragments of huntingtin with expanded glutamine repeats form nuclear and cytoplasmic aggregates in cell culture. *Hum Mol Genet,* 7**,** 783-90.

CORNETT, J., CAO, F., WANG, C. E., ROSS, C. A., BATES, G. P., LI, S. H. & LI, X. J. 2005. Polyglutamine expansion of huntingtin impairs its nuclear export. *Nat Genet,* 37**,** 198-204.

COSTA, V. & SCORRANO, L. 2012. Shaping the role of mitochondria in the pathogenesis of Huntington's disease. *EMBO J,* 31**,** 1853-64.

COYLE, J. T. & SCHWARCZ, R. 1976. Lesion of striatal neurones with kainic acid provides a model for Huntington's chorea. *Nature,* 263**,** 244-6.

CROOK, Z. R. & HOUSMAN, D. 2011. Huntington's disease: can mice lead the way to treatment? *Neuron,* 69**,** 423-35.

CROWE, S. E. & ELLIS-DAVIES, G. C. 2013. In vivo characterization of a bigenic fluorescent mouse model of Alzheimer's disease with neurodegeneration. *J Comp Neurol,* 521**,** Spc1.

CUI, L., JEONG, H., BOROVECKI, F., PARKHURST, C. N., TANESE, N. & KRAINC, D. 2006. Transcriptional repression of PGC-1alpha by mutant huntingtin leads to mitochondrial dysfunction and neurodegeneration. *Cell,* 127**,** 59-69.

CUMMINGS, D. M., MILNERWOOD, A. J., DALLERAC, G. M., VATSAVAYAI, S. C., HIRST, M. C. & MURPHY, K. P. 2007. Abnormal cortical synaptic plasticity in a mouse model of Huntington's disease. *Brain Res Bull,* 72**,** 103-7.

DAVIES, S. W., TURMAINE, M., COZENS, B. A., DIFIGLIA, M., SHARP, A. H., ROSS, C. A., SCHERZINGER, E., WANKER, E. E., MANGIARINI, L. & BATES, G. P. 1997. Formation of

neuronal intranuclear inclusions underlies the neurological dysfunction in mice transgenic for the HD mutation. *Cell,* 90**,** 537-48.

DAVIS, M. 1980. Neurochemical modulation of sensory-motor reactivity: acoustic and tactile startle reflexes. *Neurosci Biobehav Rev,* 4**,** 241-63.

DEACON, R. M. & RAWLINS, J. N. 2006. T-maze alternation in the rodent. *Nat Protoc,* 1**,** 7-12.

DECKWERTH, T. L. & JOHNSON, E. M., JR. 1994. Neurites can remain viable after destruction of the neuronal soma by programmed cell death (apoptosis). *Dev Biol,* 165**,** 63-72.

DEWHURST, K., OLIVER, J. E. & MCKNIGHT, A. L. 1970. Socio-psychiatric consequences of Huntington's disease. *Br J Psychiatry,* 116**,** 255-8.

DI STEFANO, M. & CONFORTI, L. 2013. Diversification of NAD biological role: the importance of location. *FEBS J,* 280**,** 4711-28.

DIFIGLIA, M. 1990. Excitotoxic injury of the neostriatum: a model for Huntington's disease. *Trends Neurosci,* 13**,** 286-9.

DIFIGLIA, M., SAPP, E., CHASE, K., SCHWARZ, C., MELONI, A., YOUNG, C., MARTIN, E., VONSATTEL, J. P., CARRAWAY, R., REEVES, S. A. & ET AL. 1995. Huntingtin is a cytoplasmic protein associated with vesicles in human and rat brain neurons. *Neuron,* 14**,** 1075-81.

DIFIGLIA, M., SAPP, E., CHASE, K. O., DAVIES, S. W., BATES, G. P., VONSATTEL, J. P. & ARONIN, N. 1997. Aggregation of huntingtin in neuronal intranuclear inclusions and dystrophic neurites in brain. *Science,* 277**,** 1990-3.

DIFIGLIA, M., SENA-ESTEVES, M., CHASE, K., SAPP, E., PFISTER, E., SASS, M., YODER, J., REEVES, P., PANDEY, R. K., RAJEEV, K. G., MANOHARAN, M., SAH, D. W., ZAMORE, P. D. & ARONIN, N. 2007. Therapeutic silencing of mutant huntingtin with siRNA attenuates striatal and cortical neuropathology and behavioral deficits. *Proc Natl Acad Sci U S A,* 104**,** 17204-9.

DIVAC, I., ROSVOLD, H. E. & SZWARCBART, M. K. 1967. Behavioral effects of selective ablation of the caudate nucleus. *J Comp Physiol Psychol,* 63**,** 184-90.

DOMPIERRE, J. P., GODIN, J. D., CHARRIN, B. C., CORDELIERES, F. P., KING, S. J., HUMBERT, S. & SAUDOU, F. 2007. Histone deacetylase 6 inhibition compensates for the transport deficit in Huntington's disease by increasing tubulin acetylation. *J Neurosci,* 27**,** 3571-83.

DONMEZ, G. & OUTEIRO, T. F. 2013. SIRT1 and SIRT2: emerging targets in neurodegeneration. *EMBO Mol Med,* 5**,** 344-52.

DRAGATSIS, I., LEVINE, M. S. & ZEITLIN, S. 2000. Inactivation of Hdh in the brain and testis results in progressive neurodegeneration and sterility in mice. *Nat Genet,* 26**,** 300-6.

DROUET, V., RUIZ, M., ZALA, D., FEYEUX, M., AUREGAN, G., CAMBON, K., TROQUIER, L., CARPENTIER, J., AUBERT, S., MERIENNE, N., BOURGOIS-ROCHA, F., HASSIG, R., REY, M., DUFOUR, N., SAUDOU, F., PERRIER, A. L., HANTRAYE, P. & DEGLON, N. 2014. Allele-specific silencing of mutant huntingtin in rodent brain and human stem cells. *PLoS One,* 9**,** e99341.

DUMAS, E. M., VAN DEN BOGAARD, S. J., RUBER, M. E., REILMAN, R. R., STOUT, J. C., CRAUFURD, D., HICKS, S. L., KENNARD, C., TABRIZI, S. J., VAN BUCHEM, M. A., VAN DER GROND, J. & ROOS, R. A. 2012. Early changes in white matter pathways of the sensorimotor cortex in premanifest Huntington's disease. *Hum Brain Mapp,* 33**,** 203-12.

DUNHAM, N. W. & MIYA, T. S. 1957. A note on a simple apparatus for detecting neurological deficit in rats and mice. *J Am Pharm Assoc Am Pharm Assoc (Baltim),* 46**,** 208-9.

DUNNETT, S. B. 1995. Functional repair of striatal systems by neural transplants: evidence for circuit reconstruction. *Behav Brain Res,* 66**,** 133-42.

DUNNETT, S. B., CARTER, R. J., WATTS, C., TORRES, E. M., MAHAL, A., MANGIARINI, L., BATES, G. & MORTON, A. J. 1998. Striatal transplantation in a transgenic mouse model of Huntington's disease. *Exp Neurol,* 154**,** 31-40.

DURE, L. S. T., YOUNG, A. B. & PENNEY, J. B. 1991. Excitatory amino acid binding sites in the caudate nucleus and frontal cortex of Huntington's disease. *Ann Neurol,* 30**,** 785-93.

DUYAO, M., AMBROSE, C., MYERS, R., NOVELLETTO, A., PERSICHETTI, F., FRONTALI, M., FOLSTEIN, S., ROSS, C., FRANZ, M., ABBOTT, M. & ET AL. 1993. Trinucleotide repeat length instability and age of onset in Huntington's disease. *Nat Genet,* 4**,** 387-92.

DUYAO, M. P., AUERBACH, A. B., RYAN, A., PERSICHETTI, F., BARNES, G. T., MCNEIL, S. M., GE, P., VONSATTEL, J. P., GUSELLA, J. F., JOYNER, A. L. & ET AL. 1995. Inactivation of the mouse Huntington's disease gene homolog Hdh. *Science,* 269**,** 407-10.

EHRNHOEFER, D. E., BIESCHKE, J., BOEDDRICH, A., HERBST, M., MASINO, L., LURZ, R., ENGEMANN, S., PASTORE, A. & WANKER, E. E. 2008. EGCG redirects amyloidogenic polypeptides into unstructured, off-pathway oligomers. *Nat Struct Mol Biol,* 15**,** 558-66.

ENGELENDER, S., SHARP, A. H., COLOMER, V., TOKITO, M. K., LANAHAN, A., WORLEY, P., HOLZBAUR, E. L. & ROSS, C. A. 1997. Huntingtin-associated protein 1 (HAP1) interacts with the p150Glued subunit of dynactin. *Hum Mol Genet,* 6**,** 2205-12.

ENRIGHT, L. E., ZHANG, S. & MURPHY, T. H. 2007. Fine mapping of the spatial relationship between acute ischemia and dendritic structure indicates selective vulnerability of layer V neuron dendritic tufts within single neurons in vivo. *J Cereb Blood Flow Metab,* 27**,** 1185-200.

FABER, P. W., ALTER, J. R., MACDONALD, M. E. & HART, A. C. 1999. Polyglutamine-mediated dysfunction and apoptotic death of a Caenorhabditis elegans sensory neuron. *Proc Natl Acad Sci U S A,* 96**,** 179-84.

FAN, M. M. & RAYMOND, L. A. 2007. N-methyl-D-aspartate (NMDA) receptor function and excitotoxicity in Huntington's disease. *Prog Neurobiol,* 81**,** 272-93.

FENG, G., MELLOR, R. H., BERNSTEIN, M., KELLER-PECK, C., NGUYEN, Q. T., WALLACE, M., NERBONNE, J. M., LICHTMAN, J. W. & SANES, J. R. 2000. Imaging neuronal subsets in transgenic mice expressing multiple spectral variants of GFP. *Neuron,* 28**,** 41-51.

FERGUSON, B., MATYSZAK, M. K., ESIRI, M. M. & PERRY, V. H. 1997. Axonal damage in acute multiple sclerosis lesions. *Brain,* 120 (Pt 3)**,** 393-9.

FERRANTE, R. J., ANDREASSEN, O. A., DEDEOGLU, A., FERRANTE, K. L., JENKINS, B. G., HERSCH, S. M. & BEAL, M. F. 2002. Therapeutic effects of coenzyme Q10 and remacemide in transgenic mouse models of Huntington's disease. *J Neurosci,* 22**,** 1592-9.

FERRANTE, R. J., KOWALL, N. W., BEAL, M. F., MARTIN, J. B., BIRD, E. D. & RICHARDSON, E. P., JR. 1987. Morphologic and histochemical characteristics of a spared subset of striatal neurons in Huntington's disease. *J Neuropathol Exp Neurol,* 46**,** 12-27.

FERRANTE, R. J., KOWALL, N. W., BEAL, M. F., RICHARDSON, E. P., JR., BIRD, E. D. & MARTIN, J. B. 1985. Selective sparing of a class of striatal neurons in Huntington's disease. *Science,* 230**,** 561-3.

FERRANTE, R. J., KOWALL, N. W. & RICHARDSON, E. P., JR. 1991. Proliferative and degenerative changes in striatal spiny neurons in Huntington's disease: a combined study using the section-Golgi method and calbindin D28k immunocytochemistry. *J Neurosci,* 11**,** 3877-87.

FERRANTE, R. J., KOWALL, N. W., RICHARDSON, E. P., JR., BIRD, E. D. & MARTIN, J. B. 1986. Topography of enkephalin, substance P and acetylcholinesterase staining in Huntington's disease striatum. *Neurosci Lett,* 71**,** 283-8.

FERRI, A., SANES, J. R., COLEMAN, M. P., CUNNINGHAM, J. M. & KATO, A. C. 2003. Inhibiting axon degeneration and synapse loss attenuates apoptosis and disease progression in a mouse model of motoneuron disease. *Curr Biol,* 13**,** 669-73.

FISCHER, L. R., CULVER, D. G., DAVIS, A. A., TENNANT, P., WANG, M., COLEMAN, M., ASRESS, S., ADALBERT, R., ALEXANDER, G. M. & GLASS, J. D. 2005. The WldS gene modestly prolongs survival in the SOD1G93A fALS mouse. *Neurobiol Dis,* 19**,** 293-300.

FISCHER, L. R., CULVER, D. G., TENNANT, P., DAVIS, A. A., WANG, M., CASTELLANO-SANCHEZ, A., KHAN, J., POLAK, M. A. & GLASS, J. D. 2004. Amyotrophic lateral sclerosis is a distal axonopathy: evidence in mice and man. *Exp Neurol,* 185**,** 232-40.

FISHER, S. P., BLACK, S. W., SCHWARTZ, M. D., WILK, A. J., CHEN, T. M., LINCOLN, W. U., LIU, H. W., KILDUFF, T. S. & MORAIRTY, S. R. 2013. Longitudinal analysis of the electroencephalogram and sleep phenotype in the R6/2 mouse model of Huntington's disease. *Brain,* 136**,** 2159-72.

FORMENTINI, L., MORONI, F. & CHIARUGI, A. 2009. Detection and pharmacological modulation of nicotinamide mononucleotide (NMN) in vitro and in vivo. *Biochemical Pharmacology,* 77**,** 1612-20.

FUSCO, F. R., CHEN, Q., LAMOREAUX, W. J., FIGUEREDO-CARDENAS, G., JIAO, Y., COFFMAN, J. A., SURMEIER, D. J., HONIG, M. G., CARLOCK, L. R. & REINER, A. 1999. Cellular localization of huntingtin in striatal and cortical neurons in rats: lack of correlation with neuronal vulnerability in Huntington's disease. *J Neurosci,* 19**,** 1189-202.

GAFNI, J. & ELLERBY, L. M. 2002. Calpain activation in Huntington's disease. *J Neurosci,* 22**,** 4842-9.

GALIONE, A. 1993. Cyclic ADP-ribose: a new way to control calcium. *Science,* 259**,** 325-6.

GALVIN, J. E., URYU, K., LEE, V. M. & TROJANOWSKI, J. Q. 1999. Axon pathology in Parkinson's disease and Lewy body dementia hippocampus contains alpha-, beta-, and gamma-synuclein. *Proc Natl Acad Sci U S A,* 96**,** 13450-5.

GAO, X., DENG, P., XU, Z. C. & CHEN, J. 2011. Moderate traumatic brain injury causes acute dendritic and synaptic degeneration in the hippocampal dentate gyrus. *PLoS One,* 6**,** e24566.

GAUTHIER, L. R., CHARRIN, B. C., BORRELL-PAGES, M., DOMPIERRE, J. P., RANGONE, H., CORDELIERES, F. P., DE MEY, J., MACDONALD, M. E., LESSMANN, V., HUMBERT, S. & SAUDOU, F. 2004. Huntingtin controls neurotrophic support and survival of neurons by enhancing BDNF vesicular transport along microtubules. *Cell,* 118**,** 127-38.

GEORGE, E. B., GLASS, J. D. & GRIFFIN, J. W. 1995. Axotomy-induced axonal degeneration is mediated by calcium influx through ion-specific channels. *J Neurosci,* 15**,** 6445-52.

GERBER, H. P., SEIPEL, K., GEORGIEV, O., HOFFERER, M., HUG, M., RUSCONI, S. & SCHAFFNER, W. 1994. Transcriptional activation modulated by homopolymeric glutamine and proline stretches. *Science,* 263**,** 808-11.

GEYER, M. A., MCILWAIN, K. L. & PAYLOR, R. 2002. Mouse genetic models for prepulse inhibition: an early review. *Mol Psychiatry,* 7**,** 1039-53.

GIAMPA, C., MONTAGNA, E., DATO, C., MELONE, M. A., BERNARDI, G. & FUSCO, F. R. 2013. Systemic delivery of recombinant brain derived neurotrophic factor (BDNF) in the R6/2 mouse model of Huntington's disease. *PLoS One,* 8**,** e64037.

GILLEY, J., ADALBERT, R., YU, G. & COLEMAN, M. P. 2013. Rescue of peripheral and CNS axon defects in mice lacking NMNAT2. *J Neurosci,* 33**,** 13410-24.

GILLEY, J. & COLEMAN, M. P. 2010. Endogenous Nmnat2 is an essential survival factor for maintenance of healthy axons. *PLoS Biol,* 8**,** e1000300.

GILLEY, J., SEEREERAM, A., ANDO, K., MOSELY, S., ANDREWS, S., KERSCHENSTEINER, M., MISGELD, T., BRION, J. P., ANDERTON, B., HANGER, D. P. & COLEMAN, M. P. 2012. Age-dependent axonal transport and locomotor changes and tau

hypophosphorylation in a "P301L" tau knockin mouse. *Neurobiol Aging,* 33**,** 621 e1-621 e15.

GIORGINI, F., HUANG, S. Y., SATHYASAIKUMAR, K. V., NOTARANGELO, F. M., THOMAS, M. A., TARARINA, M., WU, H. Q., SCHWARCZ, R. & MUCHOWSKI, P. J. 2013. Targeted deletion of kynurenine 3-monooxygenase in mice: a new tool for studying kynurenine pathway metabolism in periphery and brain. *J Biol Chem,* 288**,** 36554-66.

GODEMENT, P., VANSELOW, J., THANOS, S. & BONHOEFFER, F. 1987. A study in developing visual systems with a new method of staining neurones and their processes in fixed tissue. *Development,* 101**,** 697-713.

GOLDBERG, Y. P., NICHOLSON, D. W., RASPER, D. M., KALCHMAN, M. A., KOIDE, H. B., GRAHAM, R. K., BROMM, M., KAZEMI-ESFARJANI, P., THORNBERRY, N. A., VAILLANCOURT, J. P. & HAYDEN, M. R. 1996. Cleavage of huntingtin by apopain, a proapoptotic cysteine protease, is modulated by the polyglutamine tract. *Nat Genet,* 13**,** 442-9.

GOSSEN, M., FREUNDLIEB, S., BENDER, G., MULLER, G., HILLEN, W. & BUJARD, H. 1995. Transcriptional activation by tetracyclines in mammalian cells. *Science,* 268**,** 1766-9.

GRAEFF, R. & LEE, H. C. 2002. A novel cycling assay for cellular cADP-ribose with nanomolar sensitivity. *Biochem J,* 361**,** 379-84.

GRAHAM, R. K., DENG, Y., SLOW, E. J., HAIGH, B., BISSADA, N., LU, G., PEARSON, J., SHEHADEH, J., BERTRAM, L., MURPHY, Z., WARBY, S. C., DOTY, C. N., ROY, S., WELLINGTON, C. L., LEAVITT, B. R., RAYMOND, L. A., NICHOLSON, D. W. & HAYDEN, M. R. 2006. Cleavage at the caspase-6 site is required for neuronal dysfunction and degeneration due to mutant huntingtin. *Cell,* 125**,** 1179-91.

GRAHN, J. A., PARKINSON, J. A. & OWEN, A. M. 2009. The role of the basal ganglia in learning and memory: neuropsychological studies. *Behav Brain Res,* 199**,** 53-60.

GRAVELAND, G. A., WILLIAMS, R. S. & DIFIGLIA, M. 1985. Evidence for degenerative and regenerative changes in neostriatal spiny neurons in Huntington's disease. *Science,* 227**,** 770-3.

GREENE, L. A. & TISCHLER, A. S. 1976. Establishment of a Noradrenergic Clonal Line of Rat Adrenal Pheochromocytoma Cells Which Respond to Nerve Growth-Factor. *Proceedings of the National Academy of Sciences of the United States of America,* 73**,** 2424-2428.

GRILLNER, S., WALLEN, P., SAITOH, K., KOZLOV, A. & ROBERTSON, B. 2008. Neural bases of goal-directed locomotion in vertebrates--an overview. *Brain Res Rev,* 57**,** 2-12.

GUIDETTI, P., BATES, G. P., GRAHAM, R. K., HAYDEN, M. R., LEAVITT, B. R., MACDONALD, M. E., SLOW, E. J., WHEELER, V. C., WOODMAN, B. & SCHWARCZ, R. 2006. Elevated brain 3-hydroxykynurenine and quinolinate levels in Huntington disease mice. *Neurobiol Dis,* 23**,** 190-7.

GUIDETTI, P., CHARLES, V., CHEN, E. Y., REDDY, P. H., KORDOWER, J. H., WHETSELL, W. O., JR., SCHWARCZ, R. & TAGLE, D. A. 2001. Early degenerative changes in transgenic mice expressing mutant huntingtin involve dendritic abnormalities but no impairment of mitochondrial energy production. *Exp Neurol,* 169**,** 340-50.

GUIDETTI, P., LUTHI-CARTER, R. E., AUGOOD, S. J. & SCHWARCZ, R. 2004. Neostriatal and cortical quinolinate levels are increased in early grade Huntington's disease. *Neurobiol Dis,* 17**,** 455-61.

GULTNER, S., LAUE, M., RIEMER, C., HEISE, I. & BAIER, M. 2009. Prion disease development in slow Wallerian degeneration (Wld(S)) mice. *Neurosci Lett,* 456**,** 93-8.

GUNAWARDENA, S., HER, L. S., BRUSCH, R. G., LAYMON, R. A., NIESMAN, I. R., GORDESKY-GOLD, B., SINTASATH, L., BONINI, N. M. & GOLDSTEIN, L. S. 2003. Disruption of axonal transport by loss of huntingtin or expression of pathogenic polyQ proteins in Drosophila. *Neuron,* 40**,** 25-40.

GUO, X., DISATNIK, M. H., MONBUREAU, M., SHAMLOO, M., MOCHLY-ROSEN, D. & QI, X. 2013. Inhibition of mitochondrial fragmentation diminishes Huntington's disease-associated neurodegeneration. *J Clin Invest,* 123**,** 5371-88.

GUSELLA, J. F., WEXLER, N. S., CONNEALLY, P. M., NAYLOR, S. L., ANDERSON, M. A., TANZI, R. E., WATKINS, P. C., OTTINA, K., WALLACE, M. R., SAKAGUCHI, A. Y. & ET AL. 1983. A polymorphic DNA marker genetically linked to Huntington's disease. *Nature,* 306**,** 234-8.

GUTEKUNST, C. A., LI, S. H., YI, H., MULROY, J. S., KUEMMERLE, S., JONES, R., RYE, D., FERRANTE, R. J., HERSCH, S. M. & LI, X. J. 1999. Nuclear and neuropil aggregates in Huntington's disease: relationship to neuropathology. *J Neurosci,* 19**,** 2522-34.

HACKAM, A. S., SINGARAJA, R., WELLINGTON, C. L., METZLER, M., MCCUTCHEON, K., ZHANG, T., KALCHMAN, M. & HAYDEN, M. R. 1998. The influence of huntingtin protein size on nuclear localization and cellular toxicity. *J Cell Biol,* 141**,** 1097-105.

HALLIDAY, G. M., MCRITCHIE, D. A., MACDONALD, V., DOUBLE, K. L., TRENT, R. J. & MCCUSKER, E. 1998. Regional specificity of brain atrophy in Huntington's disease. *Exp Neurol,* 154**,** 663-72.

HANLEY, J., RASTEGARLARI, G. & NATHWANI, A. C. 2010. An introduction to induced pluripotent stem cells. *Br J Haematol,* 151**,** 16-24.

HARDINGHAM, G. E. & BADING, H. 2010. Synaptic versus extrasynaptic NMDA receptor signalling: implications for neurodegenerative disorders. *Nat Rev Neurosci,* 11**,** 682-96.

HARJES, P. & WANKER, E. E. 2003. The hunt for huntingtin function: interaction partners tell many different stories. *Trends Biochem Sci,* 28**,** 425-33.

HASBANI, D. M. & O'MALLEY, K. L. 2006. Wld(S) mice are protected against the Parkinsonian mimetic MPTP. *Exp Neurol,* 202**,** 93-9.

HASSA, P. O., HAENNI, S. S., ELSER, M. & HOTTIGER, M. O. 2006. Nuclear ADP-ribosylation reactions in mammalian cells: where are we today and where are we going? *Microbiol Mol Biol Rev,* 70**,** 789-829.

HDCRG 1993. A novel gene containing a trinucleotide repeat that is expanded and unstable on Huntington's disease chromosomes. *Cell* 72**,** 971-983.

HDIPSCCONSORTIUM 2012. Induced pluripotent stem cells from patients with Huntington's disease show CAG-repeat-expansion-associated phenotypes. *Cell Stem Cell,* 11**,** 264-78.

HEINSEN, H., RUB, U., BAUER, M., ULMAR, G., BETHKE, B., SCHULER, M., BOCKER, F., EISENMENGER, W., GOTZ, M., KORR, H. & SCHMITZ, C. 1999. Nerve cell loss in the thalamic mediodorsal nucleus in Huntington's disease. *Acta Neuropathol,* 97**,** 613-22.

HENG, M. Y., DETLOFF, P. J. & ALBIN, R. L. 2008. Rodent genetic models of Huntington disease. *Neurobiol Dis,* 32**,** 1-9.

HENG, M. Y., TALLAKSEN-GREENE, S. J., DETLOFF, P. J. & ALBIN, R. L. 2007. Longitudinal evaluation of the Hdh(CAG)150 knock-in murine model of Huntington's disease. *J Neurosci,* 27**,** 8989-98.

HERMEL, E., GAFNI, J., PROPP, S. S., LEAVITT, B. R., WELLINGTON, C. L., YOUNG, J. E., HACKAM, A. S., LOGVINOVA, A. V., PEEL, A. L., CHEN, S. F., HOOK, V., SINGARAJA, R., KRAJEWSKI, S., GOLDSMITH, P. C., ELLERBY, H. M., HAYDEN, M. R., BREDESEN, D. E. & ELLERBY, L. M. 2004. Specific caspase interactions and amplification are involved in selective neuronal vulnerability in Huntington's disease. *Cell Death Differ,* 11**,** 424-38.

HICKEY, M. A. & CHESSELET, M. F. 2003. The use of transgenic and knock-in mice to study Huntington's disease. *Cytogenet Genome Res,* 100**,** 276-86.

HICKEY, M. A., GALLANT, K., GROSS, G. G., LEVINE, M. S. & CHESSELET, M. F. 2005. Early behavioral deficits in R6/2 mice suitable for use in preclinical drug testing. *Neurobiol Dis,* 20**,** 1-11.

HICKEY, M. A., KOSMALSKA, A., ENAYATI, J., COHEN, R., ZEITLIN, S., LEVINE, M. S. & CHESSELET, M. F. 2008. Extensive early motor and non-motor behavioral deficits are followed by striatal neuronal loss in knock-in Huntington's disease mice. *Neuroscience,* 157**,** 280-95.

HICKS, A. N., LORENZETTI, D., GILLEY, J., LU, B., ANDERSSON, K. E., MILIGAN, C., OVERBEEK, P. A., OPPENHEIM, R. & BISHOP, C. E. 2012. Nicotinamide mononucleotide adenylyltransferase 2 (Nmnat2) regulates axon integrity in the mouse embryo. *PLoS One,* 7**,** e47869.

HIRABAYASHI, M., INOUE, K., TANAKA, K., NAKADATE, K., OHSAWA, Y., KAMEI, Y., POPIEL, A. H., SINOHARA, A., IWAMATSU, A., KIMURA, Y., UCHIYAMA, Y., HORI, S. & KAKIZUKA, A. 2001. VCP/p97 in abnormal protein aggregates, cytoplasmic vacuoles, and cell death, phenotypes relevant to neurodegeneration. *Cell Death Differ,* 8**,** 977-84.

HO, L. W., BROWN, R., MAXWELL, M., WYTTENBACH, A. & RUBINSZTEIN, D. C. 2001. Wild type Huntingtin reduces the cellular toxicity of mutant Huntingtin in mammalian cell models of Huntington's disease. *J Med Genet,* 38**,** 450-2.

HOCKLY, E., RICHON, V. M., WOODMAN, B., SMITH, D. L., ZHOU, X., ROSA, E., SATHASIVAM, K., GHAZI-NOORI, S., MAHAL, A., LOWDEN, P. A., STEFFAN, J. S., MARSH, J. L., THOMPSON, L. M., LEWIS, C. M., MARKS, P. A. & BATES, G. P. 2003. Suberoylanilide hydroxamic acid, a histone deacetylase inhibitor, ameliorates motor deficits in a mouse model of Huntington's disease. *Proc Natl Acad Sci U S A,* 100**,** 2041-6.

HODGSON, J. G., AGOPYAN, N., GUTEKUNST, C. A., LEAVITT, B. R., LEPIANE, F., SINGARAJA, R., SMITH, D. J., BISSADA, N., MCCUTCHEON, K., NASIR, J., JAMOT, L., LI, X. J., STEVENS, M. E., ROSEMOND, E., RODER, J. C., PHILLIPS, A. G., RUBIN, E. M., HERSCH, S. M. & HAYDEN, M. R. 1999. A YAC mouse model for Huntington's disease with full-length mutant huntingtin, cytoplasmic toxicity, and selective striatal neurodegeneration. *Neuron,* 23**,** 181-92.

HOLMES, A., KINNEY, J. W., WRENN, C. C., LI, Q., YANG, R. J., MA, L., VISHWANATH, J., SAAVEDRA, M. C., INNERFIELD, C. E., JACOBY, A. S., SHINE, J., IISMAA, T. P. & CRAWLEY, J. N. 2003. Galanin GAL-R1 receptor null mutant mice display increased anxiety-like behavior specific to the elevated plus-maze. *Neuropsychopharmacology,* 28**,** 1031-44.

HOLMQVIST, B. I., OSTHOLM, T. & EKSTROM, P. 1992. DiI tracing in combination with immunocytochemistry for analysis of connectivities and chemoarchitectonics of specific neural systems in a teleost, the Atlantic salmon. *J Neurosci Methods,* 42**,** 45-63.

HOOPFER, E. D., MCLAUGHLIN, T., WATTS, R. J., SCHULDINER, O., O'LEARY, D. D. & LUO, L. 2006. Wlds protection distinguishes axon degeneration following injury from naturally occurring developmental pruning. *Neuron,* 50**,** 883-95.

HUMBERT, S., BRYSON, E. A., CORDELIERES, F. P., CONNORS, N. C., DATTA, S. R., FINKBEINER, S., GREENBERG, M. E. & SAUDOU, F. 2002. The IGF-1/Akt pathway is neuroprotective in Huntington's disease and involves Huntingtin phosphorylation by Akt. *Dev Cell,* 2**,** 831-7.

HUNTINGTON STUDY, G. 2001. A randomized, placebo-controlled trial of coenzyme Q10 and remacemide in Huntington's disease. *Neurology,* 57**,** 397-404.

IMAI, S. 2009. Nicotinamide phosphoribosyltransferase (Nampt): a link between NAD biology, metabolism, and diseases. *Curr Pharm Des,* 15**,** 20-8.

IMAI, S. 2010. "Clocks" in the NAD World: NAD as a metabolic oscillator for the regulation of metabolism and aging. *Biochim Biophys Acta,* 1804**,** 1584-90.

IMAI, S. & GUARENTE, L. 2010. Ten years of NAD-dependent SIR2 family deacetylases: implications for metabolic diseases. *Trends Pharmacol Sci,* 31**,** 212-20.

IMAI, S. & KIESS, W. 2009. Therapeutic potential of SIRT1 and NAMPT-mediated NAD biosynthesis in type 2 diabetes. *Front Biosci (Landmark Ed),* 14**,** 2983-95.

JACKSON, G. R., SALECKER, I., DONG, X., YAO, X., ARNHEIM, N., FABER, P. W., MACDONALD, M. E. & ZIPURSKY, S. L. 1998. Polyglutamine-expanded human huntingtin transgenes induce degeneration of Drosophila photoreceptor neurons. *Neuron,* 21**,** 633-42.

JACOBSEN, J. C., BAWDEN, C. S., RUDIGER, S. R., MCLAUGHLAN, C. J., REID, S. J., WALDVOGEL, H. J., MACDONALD, M. E., GUSELLA, J. F., WALKER, S. K., KELLY, J. M., WEBB, G. C., FAULL, R. L., REES, M. I. & SNELL, R. G. 2010. An ovine transgenic Huntington's disease model. *Hum Mol Genet,* 19**,** 1873-82.

JEONG, H., COHEN, D. E., CUI, L., SUPINSKI, A., SAVAS, J. N., MAZZULLI, J. R., YATES, J. R., 3RD, BORDONE, L., GUARENTE, L. & KRAINC, D. 2012. Sirt1 mediates neuroprotection from mutant huntingtin by activation of the TORC1 and CREB transcriptional pathway. *Nat Med,* 18**,** 159-65.

JIANG, M., WANG, J., FU, J., DU, L., JEONG, H., WEST, T., XIANG, L., PENG, Q., HOU, Z., CAI, H., SEREDENINA, T., ARBEZ, N., ZHU, S., SOMMERS, K., QIAN, J., ZHANG, J., MORI, S., YANG, X. W., TAMASHIRO, K. L., AJA, S., MORAN, T. H., LUTHI-CARTER, R., MARTIN, B., MAUDSLEY, S., MATTSON, M. P., CICHEWICZ, R. H., ROSS, C. A., HOLTZMAN, D. M., KRAINC, D. & DUAN, W. 2012. Neuroprotective role of Sirt1 in mammalian models of Huntington's disease through activation of multiple Sirt1 targets. *Nat Med,* 18**,** 153-8.

KALCHMAN, M. A., GRAHAM, R. K., XIA, G., KOIDE, H. B., HODGSON, J. G., GRAHAM, K. C., GOLDBERG, Y. P., GIETZ, R. D., PICKART, C. M. & HAYDEN, M. R. 1996. Huntingtin is ubiquitinated and interacts with a specific ubiquitin-conjugating enzyme. *J Biol Chem,* 271**,** 19385-94.

KANTOR, S., SZABO, L., VARGA, J., CUESTA, M. & MORTON, A. J. 2013. Progressive sleep and electroencephalogram changes in mice carrying the Huntington's disease mutation. *Brain,* 136**,** 2147-58.

KARIYA, S., MAURICIO, R., DAI, Y. & MONANI, U. R. 2009. The neuroprotective factor Wld(s) fails to mitigate distal axonal and neuromuscular junction (NMJ) defects in mouse models of spinal muscular atrophy. *Neurosci Lett,* 449**,** 246-51.

KEGEL, K. B., MELONI, A. R., YI, Y., KIM, Y. J., DOYLE, E., CUIFFO, B. G., SAPP, E., WANG, Y., QIN, Z. H., CHEN, J. D., NEVINS, J. R., ARONIN, N. & DIFIGLIA, M. 2002. Huntingtin is present in the nucleus, interacts with the transcriptional corepressor C-terminal binding protein, and represses transcription. *J Biol Chem,* 277**,** 7466-76.

KHOSHNAN, A., KO, J. & PATTERSON, P. H. 2002. Effects of intracellular expression of anti-huntingtin antibodies of various specificities on mutant huntingtin aggregation and toxicity. *Proc Natl Acad Sci U S A,* 99**,** 1002-7.

KIM, Y. J., YI, Y., SAPP, E., WANG, Y., CUIFFO, B., KEGEL, K. B., QIN, Z. H., ARONIN, N. & DIFIGLIA, M. 2001. Caspase 3-cleaved N-terminal fragments of wild-type and mutant huntingtin are present in normal and Huntington's disease brains, associate with membranes, and undergo calpain-dependent proteolysis. *Proc Natl Acad Sci U S A,* 98**,** 12784-9.

KIMURA, N., OKABAYASHI, S. & ONO, F. 2012. Dynein dysfunction disrupts intracellular vesicle trafficking bidirectionally and perturbs synaptic vesicle docking via endocytic disturbances a potential mechanism underlying age-dependent impairment of cognitive function. *Am J Pathol,* 180**,** 550-61.

KIRKWOOD, S. C., SU, J. L., CONNEALLY, P. & FOROUD, T. 2001. Progression of symptoms in the early and middle stages of Huntington disease. *Arch Neurol,* 58**,** 273-8.

KLAPSTEIN, G. J., FISHER, R. S., ZANJANI, H., CEPEDA, C., JOKEL, E. S., CHESSELET, M. F. & LEVINE, M. S. 2001. Electrophysiological and morphological changes in striatal spiny neurons in R6/2 Huntington's disease transgenic mice. *J Neurophysiol,* 86**,** 2667-77.

KNOPMAN, D. & NISSEN, M. J. 1991. Procedural learning is impaired in Huntington's disease: evidence from the serial reaction time task. *Neuropsychologia,* 29**,** 245-54.

KOBAYASHI, T., MANNO, A. & KAKIZUKA, A. 2007. Involvement of valosin-containing protein (VCP)/p97 in the formation and clearance of abnormal protein aggregates. *Genes Cells,* 12**,** 889-901.

KOHR, G. 2006. NMDA receptor function: subunit composition versus spatial distribution. *Cell Tissue Res,* 326**,** 439-46.

KREMER, B., CLARK, C. M., ALMQVIST, E. W., RAYMOND, L. A., GRAF, P., JACOVA, C., MEZEI, M., HARDY, M. A., SNOW, B., MARTIN, W. & HAYDEN, M. R. 1999. Influence of lamotrigine on progression of early Huntington disease: a randomized clinical trial. *Neurology,* 53**,** 1000-11.

KREMER, B., SWAAB, D., BOTS, G., FISSER, B., RAVID, R. & ROOS, R. 1991. The hypothalamic lateral tuberal nucleus in Alzheimer's disease. *Ann Neurol,* 29**,** 279-84.

KRENCH, M. & LITTLETON, J. T. 2013. Modeling Huntington disease in Drosophila: Insights into axonal transport defects and modifiers of toxicity. *Fly (Austin),* 7.

KUDO, T., SCHROEDER, A., LOH, D. H., KULJIS, D., JORDAN, M. C., ROOS, K. P. & COLWELL, C. S. 2011. Dysfunctions in circadian behavior and physiology in mouse models of Huntington's disease. *Exp Neurol,* 228**,** 80-90.

KUEMMERLE, S., GUTEKUNST, C. A., KLEIN, A. M., LI, X. J., LI, S. H., BEAL, M. F., HERSCH, S. M. & FERRANTE, R. J. 1999. Huntington aggregates may not predict neuronal death in Huntington's disease. *Ann Neurol,* 46**,** 842-9.

KUMAR, A., VAISH, M. & RATAN, R. R. 2014. Transcriptional dysregulation in Huntington's disease: a failure of adaptive transcriptional homeostasis. *Drug Discov Today*.

KURY, P., STOLL, G. & MULLER, H. W. 2001. Molecular mechanisms of cellular interactions in peripheral nerve regeneration. *Curr Opin Neurol,* 14**,** 635-9.

LABBADIA, J. & MORIMOTO, R. I. 2013. Huntington's disease: underlying molecular mechanisms and emerging concepts. *Trends Biochem Sci,* 38**,** 378-85.

LACCONE, F., ENGEL, U., HOLINSKI-FEDER, E., WEIGELL-WEBER, M., MARCZINEK, K., NOLTE, D., MORRIS-ROSENDAHL, D. J., ZUHLKE, C., FUCHS, K., WEIRICH-SCHWAIGER, H., SCHLUTER, G., VON BEUST, G., VIEIRA-SAECKER, A. M., WEBER, B. H. & RIESS, O. 1999. DNA analysis of Huntington's disease: five years of experience in Germany, Austria, and Switzerland. *Neurology,* 53**,** 801-6.

LAFORET, G. A., SAPP, E., CHASE, K., MCINTYRE, C., BOYCE, F. M., CAMPBELL, M., CADIGAN, B. A., WARZECKI, L., TAGLE, D. A., REDDY, P. H., CEPEDA, C., CALVERT, C. R., JOKEL, E. S., KLAPSTEIN, G. J., ARIANO, M. A., LEVINE, M. S., DIFIGLIA, M. & ARONIN, N. 2001. Changes in cortical and striatal neurons predict behavioral and electrophysiological abnormalities in a transgenic murine model of Huntington's disease. *J Neurosci,* 21**,** 9112-23.

LAIGUILLON, M. C., HOUARD, X., BOUGAULT, C., GOSSET, M., NOURISSAT, G., SAUTET, A., JACQUES, C., BERENBAUM, F. & SELLAM, J. 2014. Expression and function of visfatin (Nampt), an adipokine-enzyme involved in inflammatory pathways of osteoarthritis. *Arthritis Res Ther,* 16**,** R38.

LALONDE, R. 2002. The neurobiological basis of spontaneous alternation. *Neurosci Biobehav Rev,* 26**,** 91-104.

LANDWEHRMEYER, G. B., DUBOIS, B., DE YEBENES, J. G., KREMER, B., GAUS, W., KRAUS, P. H., PRZUNTEK, H., DIB, M., DOBLE, A., FISCHER, W., LUDOLPH, A. C. & EUROPEAN HUNTINGTON'S DISEASE INITIATIVE STUDY, G. 2007. Riluzole in Huntington's disease: a 3-year, randomized controlled study. *Ann Neurol,* 62**,** 262-72.

LARRAURI, J. & SCHMAJUK, N. 2006. Prepulse inhibition mechanisms and cognitive processes: a review and model. *EXS,* 98**,** 245-78.

LASER, H., CONFORTI, L., MORREALE, G., MACK, T. G., HEYER, M., HALEY, J. E., WISHART, T. M., BEIROWSKI, B., WALKER, S. A., HAASE, G., CELIK, A., ADALBERT, R., WAGNER, D., GRUMME, D., RIBCHESTER, R. R., PLOMANN, M. & COLEMAN, M. P. 2006. The slow Wallerian degeneration protein, WldS, binds directly to VCP/p97 and partially redistributes it within the nucleus. *Mol Biol Cell,* 17**,** 1075-84.

LAUTIER, D., LAGUEUX, J., THIBODEAU, J., MENARD, L. & POIRIER, G. G. 1993. Molecular and biochemical features of poly (ADP-ribose) metabolism. *Mol Cell Biochem,* 122**,** 171-93.

LAWRENCE & AD 1998. Evidence for specific cognitive deficits in preclinical Huntington's disease.

LAWRENCE, A. D., HODGES, J. R., ROSSER, A. E., KERSHAW, A., FFRENCH-CONSTANT, C., RUBINSZTEIN, D. C., ROBBINS, T. W. & SAHAKIAN, B. J. 1998. Evidence for specific cognitive deficits in preclinical Huntington's disease. *Brain,* 121 (Pt 7)**,** 1329-41.

LAWRENCE, A. D., SAHAKIAN, B. J., HODGES, J. R., ROSSER, A. E., LANGE, K. W. & ROBBINS, T. W. 1996. Executive and mnemonic functions in early Huntington's disease. *Brain,* 119 (Pt 5)**,** 1633-45.

LEAVITT, B. R., GUTTMAN, J. A., HODGSON, J. G., KIMEL, G. H., SINGARAJA, R., VOGL, A. W. & HAYDEN, M. R. 2001. Wild-type huntingtin reduces the cellular toxicity of mutant huntingtin in vivo. *Am J Hum Genet,* 68**,** 313-24.

LEBLANC, A. C. & PODUSLO, J. F. 1990. Axonal modulation of myelin gene expression in the peripheral nerve. *J Neurosci Res,* 26**,** 317-26.

LEE, H. C. 2001. Physiological functions of cyclic ADP-ribose and NAADP as calcium messengers. *Annu Rev Pharmacol Toxicol,* 41**,** 317-45.

LERNER, R. P., TREJO MARTINEZ LDEL, C., ZHU, C., CHESSELET, M. F. & HICKEY, M. A. 2012. Striatal atrophy and dendritic alterations in a knock-in mouse model of Huntington's disease. *Brain Res Bull,* 87**,** 571-8.

LI, H., LI, S. H., CHENG, A. L., MANGIARINI, L., BATES, G. P. & LI, X. J. 1999a. Ultrastructural localization and progressive formation of neuropil aggregates in Huntington's disease transgenic mice. *Hum Mol Genet,* 8**,** 1227-36.

LI, H., LI, S. H., YU, Z. X., SHELBOURNE, P. & LI, X. J. 2001. Huntingtin aggregate-associated axonal degeneration is an early pathological event in Huntington's disease mice. *J Neurosci,* 21**,** 8473-81.

LI, H., WYMAN, T., YU, Z. X., LI, S. H. & LI, X. J. 2003. Abnormal association of mutant huntingtin with synaptic vesicles inhibits glutamate release. *Hum Mol Genet,* 12**,** 2021-30.

LI, J. & LE, W. 2013. Modeling neurodegenerative diseases in Caenorhabditis elegans. *Exp Neurol,* 250**,** 94-103.

LI, J. Y. & CONFORTI, L. 2013. Axonopathy in Huntington's disease. *Exp Neurol,* 246**,** 62-71.

LI, S. H., CHENG, A. L., LI, H. & LI, X. J. 1999b. Cellular defects and altered gene expression in PC12 cells stably expressing mutant huntingtin. *J Neurosci,* 19**,** 5159-72.

LI, S. H., GUTEKUNST, C. A., HERSCH, S. M. & LI, X. J. 1998. Interaction of huntingtin-associated protein with dynactin P150Glued. *J Neurosci,* 18**,** 1261-9.

LI, S. H. & LI, X. J. 2004. Huntingtin and its role in neuronal degeneration. *Neuroscientist,* 10**,** 467-75.

LIBERATORE, G. T., JACKSON-LEWIS, V., VUKOSAVIC, S., MANDIR, A. S., VILA, M., MCAULIFFE, W. G., DAWSON, V. L., DAWSON, T. M. & PRZEDBORSKI, S. 1999. Inducible nitric oxide synthase stimulates dopaminergic neurodegeneration in the MPTP model of Parkinson disease. *Nat Med,* 5**,** 1403-9.

LILLIE, R. D. 1965. Histopathologic Technic and Practical Histochemistry. *McGraw-Hill Book Co., New York,* 3rd ed.

LIN, C. H., TALLAKSEN-GREENE, S., CHIEN, W. M., CEARLEY, J. A., JACKSON, W. S., CROUSE, A. B., REN, S., LI, X. J., ALBIN, R. L. & DETLOFF, P. J. 2001. Neurological abnormalities in a knock-in mouse model of Huntington's disease. *Hum Mol Genet,* 10**,** 137-44.

LIONE, L. A., CARTER, R. J., HUNT, M. J., BATES, G. P., MORTON, A. J. & DUNNETT, S. B. 1999. Selective discrimination learning impairments in mice expressing the human Huntington's disease mutation. *J Neurosci,* 19**,** 10428-37.

LIU, L. Y., WANG, F., ZHANG, X. Y., HUANG, P., LU, Y. B., WEI, E. Q. & ZHANG, W. P. 2012. Nicotinamide phosphoribosyltransferase may be involved in age-related brain diseases. *PLoS One,* 7**,** e44933.

LJUNGBERG, M. C., ALI, Y. O., ZHU, J., WU, C. S., OKA, K., ZHAI, R. G. & LU, H. C. 2012. CREB-activity and nmnat2 transcription are down-regulated prior to neurodegeneration, while NMNAT2 over-expression is neuroprotective, in a mouse model of human tauopathy. *Hum Mol Genet,* 21**,** 251-67.

LONDON, E. D., YAMAMURA, H. I., BIRD, E. D. & COYLE, J. T. 1981. Decreased receptor-binding sites for kainic acid in brains of patients with Huntington's disease. *Biol Psychiatry,* 16**,** 155-62.

LUBINSKA, L. 1977. Early course of Wallerian degeneration in myelinated fibres of the rat phrenic nerve. *Brain Res,* 130**,** 47-63.

LUBINSKA, L. 1982. Patterns of Wallerian degeneration of myelinated fibres in short and long peripheral stumps and in isolated segments of rat phrenic nerve. Interpretation of the role of axoplasmic flow of the trophic factor. *Brain Res,* 233**,** 227-40.

LUESSE, H. G., SCHIEFER, J., SPRUENKEN, A., PULS, C., BLOCK, F. & KOSINSKI, C. M. 2001. Evaluation of R6/2 HD transgenic mice for therapeutic studies in Huntington's disease: behavioral testing and impact of diabetes mellitus. *Behav Brain Res,* 126**,** 185-95.

LUNKES, A., LINDENBERG, K. S., BEN-HAIEM, L., WEBER, C., DEVYS, D., LANDWEHRMEYER, G. B., MANDEL, J. L. & TROTTIER, Y. 2002. Proteases acting on mutant huntingtin generate cleaved products that differentially build up cytoplasmic and nuclear inclusions. *Mol Cell,* 10**,** 259-69.

LUNN, E. R., PERRY, V. H., BROWN, M. C., ROSEN, H. & GORDON, S. 1989. Absence of Wallerian Degeneration does not Hinder Regeneration in Peripheral Nerve. *Eur J Neurosci,* 1**,** 27-33.

LUO, S., VACHER, C., DAVIES, J. E. & RUBINSZTEIN, D. C. 2005. Cdk5 phosphorylation of huntingtin reduces its cleavage by caspases: implications for mutant huntingtin toxicity. *J Cell Biol,* 169**,** 647-56.

LUTHI-CARTER, R., STRAND, A., PETERS, N. L., SOLANO, S. M., HOLLINGSWORTH, Z. R., MENON, A. S., FREY, A. S., SPEKTOR, B. S., PENNEY, E. B., SCHILLING, G., ROSS, C. A., BORCHELT, D. R., TAPSCOTT, S. J., YOUNG, A. B., CHA, J. H. & OLSON, J. M. 2000. Decreased expression of striatal signaling genes in a mouse model of Huntington's disease. *Hum Mol Genet,* 9**,** 1259-71.

LUTHI-CARTER, R., STRAND, A. D., HANSON, S. A., KOOPERBERG, C., SCHILLING, G., LA SPADA, A. R., MERRY, D. E., YOUNG, A. B., ROSS, C. A., BORCHELT, D. R. & OLSON, J. M. 2002. Polyglutamine and transcription: gene expression changes shared by DRPLA and Huntington's disease mouse models reveal context-independent effects. *Hum Mol Genet,* 11**,** 1927-37.

LUTHI-CARTER, R., TAYLOR, D. M., PALLOS, J., LAMBERT, E., AMORE, A., PARKER, A., MOFFITT, H., SMITH, D. L., RUNNE, H., GOKCE, O., KUHN, A., XIANG, Z., MAXWELL, M. M., REEVES, S. A., BATES, G. P., NERI, C., THOMPSON, L. M., MARSH, J. L. & KAZANTSEV, A. G. 2010. SIRT2 inhibition achieves neuroprotection by decreasing sterol biosynthesis. *Proc Natl Acad Sci U S A,* 107**,** 7927-32.

MACDONALD, J. M., BEACH, M. G., PORPIGLIA, E., SHEEHAN, A. E., WATTS, R. J. & FREEMAN, M. R. 2006. The Drosophila cell corpse engulfment receptor Draper mediates glial clearance of severed axons. *Neuron,* 50**,** 869-81.

MACDONALD, V., HALLIDAY, G. M., TRENT, R. J. & MCCUSKER, E. A. 1997. Significant loss of pyramidal neurons in the angular gyrus of patients with Huntington's disease. *Neuropathol Appl Neurobiol,* 23**,** 492-5.

MACK, T. G., REINER, M., BEIROWSKI, B., MI, W., EMANUELLI, M., WAGNER, D., THOMSON, D., GILLINGWATER, T., COURT, F., CONFORTI, L., FERNANDO, F. S., TARLTON, A., ANDRESSEN, C., ADDICKS, K., MAGNI, G., RIBCHESTER, R. R., PERRY, V. H. & COLEMAN, M. P. 2001. Wallerian degeneration of injured axons and synapses is delayed by a Ube4b/Nmnat chimeric gene. *Nat Neurosci,* 4**,** 1199-206.

MANGIARINI, L., SATHASIVAM, K., SELLER, M., COZENS, B., HARPER, A., HETHERINGTON, C., LAWTON, M., TROTTIER, Y., LEHRACH, H., DAVIES, S. W. & BATES, G. P. 1996. Exon 1 of the HD gene with an expanded CAG repeat is sufficient to cause a progressive neurological phenotype in transgenic mice. *Cell,* 87**,** 493-506.

MARSH, J. L. & THOMPSON, L. M. 2006. Drosophila in the study of neurodegenerative disease. *Neuron,* 52**,** 169-78.

MARTIN, L. J., PAN, Y., PRICE, A. C., STERLING, W., COPELAND, N. G., JENKINS, N. A., PRICE, D. L. & LEE, M. K. 2006. Parkinson's disease alpha-synuclein transgenic mice develop neuronal mitochondrial degeneration and cell death. *J Neurosci,* 26**,** 41-50.

MARTIN, S. M., O'BRIEN, G. S., PORTERA-CAILLIAU, C. & SAGASTI, A. 2010. Wallerian degeneration of zebrafish trigeminal axons in the skin is required for regeneration and developmental pruning. *Development,* 137**,** 3985-94.

MARTINDALE, D., HACKAM, A., WIECZOREK, A., ELLERBY, L., WELLINGTON, C., MCCUTCHEON, K., SINGARAJA, R., KAZEMI-ESFARJANI, P., DEVON, R., KIM, S. U., BREDESEN, D. E., TUFARO, F. & HAYDEN, M. R. 1998. Length of huntingtin and its polyglutamine tract influences localization and frequency of intracellular aggregates. *Nat Genet,* 18**,** 150-4.

MASSUDI, H., GRANT, R., BRAIDY, N., GUEST, J., FARNSWORTH, B. & GUILLEMIN, G. J. 2012. Age-associated changes in oxidative stress and NAD+ metabolism in human tissue. *PLoS One,* 7**,** e42357.

MATTHEWS, R. T., YANG, L., BROWNE, S., BAIK, M. & BEAL, M. F. 1998. Coenzyme Q10 administration increases brain mitochondrial concentrations and exerts neuroprotective effects. *Proc Natl Acad Sci U S A,* 95**,** 8892-7.

MCFADYEN, M. P., KUSEK, G., BOLIVAR, V. J. & FLAHERTY, L. 2003. Differences among eight inbred strains of mice in motor ability and motor learning on a rotorod. *Genes Brain Behav,* 2**,** 214-9.

MCGEER, E. G. & MCGEER, P. L. 1976. Duplication of biochemical changes of Huntington's chorea by intrastriatal injections of glutamic and kainic acids. *Nature,* 263**,** 517-9.

MCGUIRE, J. R., RONG, J., LI, S. H. & LI, X. J. 2006. Interaction of Huntingtin-associated protein-1 with kinesin light chain: implications in intracellular trafficking in neurons. *J Biol Chem,* 281**,** 3552-9.

MENALLED, L., EL-KHODOR, B. F., PATRY, M., SUAREZ-FARINAS, M., ORENSTEIN, S. J., ZAHASKY, B., LEAHY, C., WHEELER, V., YANG, X. W., MACDONALD, M., MORTON, A. J., BATES, G., LEEDS, J., PARK, L., HOWLAND, D., SIGNER, E., TOBIN, A. & BRUNNER, D. 2009. Systematic behavioral evaluation of Huntington's disease transgenic and knock-in mouse models. *Neurobiol Dis,* 35**,** 319-36.

MENALLED, L., ZANJANI, H., MACKENZIE, L., KOPPEL, A., CARPENTER, E., ZEITLIN, S. & CHESSELET, M. F. 2000. Decrease in striatal enkephalin mRNA in mouse models of Huntington's disease. *Exp Neurol,* 162**,** 328-42.

MENALLED, L. B. 2005. Knock-in mouse models of Huntington's disease. *NeuroRx,* 2**,** 465-70.

MENALLED, L. B. & CHESSELET, M. F. 2002. Mouse models of Huntington's disease. *Trends Pharmacol Sci,* 23**,** 32-9.

MENALLED, L. B., SISON, J. D., DRAGATSIS, I., ZEITLIN, S. & CHESSELET, M. F. 2003. Time course of early motor and neuropathological anomalies in a knock-in mouse model of Huntington's disease with 140 CAG repeats. *J Comp Neurol,* 465**,** 11-26.

MENALLED, L. B., SISON, J. D., WU, Y., OLIVIERI, M., LI, X. J., LI, H., ZEITLIN, S. & CHESSELET, M. F. 2002. Early motor dysfunction and striosomal distribution of huntingtin microaggregates in Huntington's disease knock-in mice. *J Neurosci,* 22**,** 8266-76.

METZLER, M., CHEN, N., HELGASON, C. D., GRAHAM, R. K., NICHOL, K., MCCUTCHEON, K., NASIR, J., HUMPHRIES, R. K., RAYMOND, L. A. & HAYDEN, M. R. 1999. Life without huntingtin: normal differentiation into functional neurons. *J Neurochem,* 72**,** 1009-18.

METZLER, M., GAN, L., WONG, T. P., LIU, L., HELM, J., LIU, L., GEORGIOU, J., WANG, Y., BISSADA, N., CHENG, K., RODER, J. C., WANG, Y. T. & HAYDEN, M. R. 2007. NMDA receptor function and NMDA receptor-dependent phosphorylation of huntingtin is altered by the endocytic protein HIP1. *J Neurosci,* 27**,** 2298-308.

METZLER, M., HELGASON, C. D., DRAGATSIS, I., ZHANG, T., GAN, L., PINEAULT, N., ZEITLIN, S. O., HUMPHRIES, R. K. & HAYDEN, M. R. 2000. Huntingtin is required for normal hematopoiesis. *Hum Mol Genet,* 9**,** 387-94.

MI, W., BEIROWSKI, B., GILLINGWATER, T. H., ADALBERT, R., WAGNER, D., GRUMME, D., OSAKA, H., CONFORTI, L., ARNHOLD, S., ADDICKS, K., WADA, K., RIBCHESTER, R. R. & COLEMAN, M. P. 2005. The slow Wallerian degeneration gene, WldS, inhibits axonal spheroid pathology in gracile axonal dystrophy mice. *Brain,* 128**,** 405-16.

MILATOVIC, D., MONTINE, T. J., ZAJA-MILATOVIC, S., MADISON, J. L., BOWMAN, A. B. & ASCHNER, M. 2010. Morphometric analysis in neurodegenerative disorders. *Curr Protoc Toxicol,* Chapter 12**,** Unit 12 16.

MILDE, S., FOX, A. N., FREEMAN, M. R. & COLEMAN, M. P. 2013a. Deletions within its subcellular targeting domain enhance the axon protective capacity of Nmnat2 in vivo. *Sci Rep,* 3**,** 2567.

MILDE, S., GILLEY, J. & COLEMAN, M. P. 2013b. Axonal trafficking of NMNAT2 and its roles in axon growth and survival in vivo. *Bioarchitecture,* 3**,** 133-40.

MILDE, S., GILLEY, J. & COLEMAN, M. P. 2013c. Subcellular localization determines the stability and axon protective capacity of axon survival factor Nmnat2. *PLoS Biol,* 11**,** e1001539.

MILNERWOOD, A. J., CUMMINGS, D. M., DALLERAC, G. M., BROWN, J. Y., VATSAVAYAI, S. C., HIRST, M. C., REZAIE, P. & MURPHY, K. P. 2006. Early development of aberrant synaptic plasticity in a mouse model of Huntington's disease. *Hum Mol Genet,* 15**,** 1690-703.

MILNERWOOD, A. J., GLADDING, C. M., POULADI, M. A., KAUFMAN, A. M., HINES, R. M., BOYD, J. D., KO, R. W., VASUTA, O. C., GRAHAM, R. K., HAYDEN, M. R., MURPHY, T. H. & RAYMOND, L. A. 2010. Early increase in extrasynaptic NMDA receptor signaling and expression contributes to phenotype onset in Huntington's disease mice. *Neuron,* 65**,** 178-90.

MOREIRA, P. I., ZHU, X., WANG, X., LEE, H. G., NUNOMURA, A., PETERSEN, R. B., PERRY, G. & SMITH, M. A. 2010. Mitochondria: a therapeutic target in neurodegeneration. *Biochim Biophys Acta,* 1802**,** 212-20.

MOUCHIROUD, L., HOUTKOOPER, R. H., MOULLAN, N., KATSYUBA, E., RYU, D., CANTO, C., MOTTIS, A., JO, Y. S., VISWANATHAN, M., SCHOONJANS, K., GUARENTE, L. & AUWERX, J. 2013. The NAD(+)/Sirtuin Pathway Modulates Longevity through Activation of Mitochondrial UPR and FOXO Signaling. *Cell,* 154**,** 430-41.

MOULDER, K. L., ONODERA, O., BURKE, J. R., STRITTMATTER, W. J. & JOHNSON, E. M., JR. 1999. Generation of neuronal intranuclear inclusions by polyglutamine-GFP: analysis of inclusion clearance and toxicity as a function of polyglutamine length. *J Neurosci,* 19**,** 705-15.

MURPHY, K. P., CARTER, R. J., LIONE, L. A., MANGIARINI, L., MAHAL, A., BATES, G. P., DUNNETT, S. B. & MORTON, A. J. 2000. Abnormal synaptic plasticity and impaired spatial cognition in mice transgenic for exon 1 of the human Huntington's disease mutation. *J Neurosci,* 20**,** 5115-23.

MYERS, R. H., VONSATTEL, J. P., STEVENS, T. J., CUPPLES, L. A., RICHARDSON, E. P., MARTIN, J. B. & BIRD, E. D. 1988. Clinical and neuropathologic assessment of severity in Huntington's disease. *Neurology,* 38**,** 341-7.

NAGAHARA, A. H. & TUSZYNSKI, M. H. 2011. Potential therapeutic uses of BDNF in neurological and psychiatric disorders. *Nat Rev Drug Discov,* 10**,** 209-19.

NARAYANAN, S., FU, L., PIORO, E., DE STEFANO, N., COLLINS, D. L., FRANCIS, G. S., ANTEL, J. P., MATTHEWS, P. M. & ARNOLD, D. L. 1997. Imaging of axonal damage in multiple sclerosis: spatial distribution of magnetic resonance imaging lesions. *Ann Neurol,* 41**,** 385-91.

NASIR, J., FLORESCO, S. B., O'KUSKY, J. R., DIEWERT, V. M., RICHMAN, J. M., ZEISLER, J., BOROWSKI, A., MARTH, J. D., PHILLIPS, A. G. & HAYDEN, M. R. 1995. Targeted disruption of the Huntington's disease gene results in embryonic lethality and behavioral and morphological changes in heterozygotes. *Cell,* 81**,** 811-23.

NEUKOMM, L. J. & FREEMAN, M. R. 2014. Diverse cellular and molecular modes of axon degeneration. *Trends Cell Biol,* doi: S0962-8924(14)00064-6**,** Epub ahead of print.

NIHEI, K. & KOWALL, N. W. 1992. Neurofilament and neural cell adhesion molecule immunocytochemistry of Huntington's disease striatum. *Ann Neurol,* 31**,** 59-63.

NITHIANANTHARAJAH, J. & HANNAN, A. J. 2013. Dysregulation of synaptic proteins, dendritic spine abnormalities and pathological plasticity of synapses as experience-dependent mediators of cognitive and psychiatric symptoms in Huntington's disease. *Neuroscience,* 251**,** 66-74.

NORTH, B. J., MARSHALL, B. L., BORRA, M. T., DENU, J. M. & VERDIN, E. 2003. The human Sir2 ortholog, SIRT2, is an NAD+-dependent tubulin deacetylase. *Mol Cell,* 11**,** 437-44.

NUCIFORA, F. C., JR., ELLERBY, L. M., WELLINGTON, C. L., WOOD, J. D., HERRING, W. J., SAWA, A., HAYDEN, M. R., DAWSON, V. L., DAWSON, T. M. & ROSS, C. A. 2003. Nuclear localization of a non-caspase truncation product of atrophin-1, with an expanded polyglutamine repeat, increases cellular toxicity. *J Biol Chem,* 278**,** 13047-55.

OKAMOTO, S., POULADI, M. A., TALANTOVA, M., YAO, D., XIA, P., EHRNHOEFER, D. E., ZAIDI, R., CLEMENTE, A., KAUL, M., GRAHAM, R. K., ZHANG, D., VINCENT CHEN, H. S., TONG, G., HAYDEN, M. R. & LIPTON, S. A. 2009. Balance between synaptic versus extrasynaptic NMDA receptor activity influences inclusions and neurotoxicity of mutant huntingtin. *Nat Med,* 15**,** 1407-13.

ONA, V. O., LI, M., VONSATTEL, J. P., ANDREWS, L. J., KHAN, S. Q., CHUNG, W. M., FREY, A. S., MENON, A. S., LI, X. J., STIEG, P. E., YUAN, J., PENNEY, J. B., YOUNG, A. B., CHA, J. H. & FRIEDLANDER, R. M. 1999. Inhibition of caspase-1 slows disease progression in a mouse model of Huntington's disease. *Nature,* 399**,** 263-7.

ONDO, W. G., MEJIA, N. I. & HUNTER, C. B. 2007. A pilot study of the clinical efficacy and safety of memantine for Huntington's disease. *Parkinsonism Relat Disord,* 13**,** 453-4.

ORR, A. L., LI, S., WANG, C. E., LI, H., WANG, J., RONG, J., XU, X., MASTROBERARDINO, P. G., GREENAMYRE, J. T. & LI, X. J. 2008. N-terminal mutant huntingtin associates with mitochondria and impairs mitochondrial trafficking. *J Neurosci,* 28**,** 2783-92.

ORVOEN, S., PLA, P., GARDIER, A. M., SAUDOU, F. & DAVID, D. J. 2012. Huntington's disease knock-in male mice show specific anxiety-like behaviour and altered neuronal maturation. *Neurosci Lett,* 507**,** 127-32.

OUTEIRO, T. F., KONTOPOULOS, E., ALTMANN, S. M., KUFAREVA, I., STRATHEARN, K. E., AMORE, A. M., VOLK, C. B., MAXWELL, M. M., ROCHET, J. C., MCLEAN, P. J., YOUNG, A. B., ABAGYAN, R., FEANY, M. B., HYMAN, B. T. & KAZANTSEV, A. G. 2007. Sirtuin 2 inhibitors rescue alpha-synuclein-mediated toxicity in models of Parkinson's disease. *Science,* 317**,** 516-9.

PALLOS, J., BODAI, L., LUKACSOVICH, T., PURCELL, J. M., STEFFAN, J. S., THOMPSON, L. M. & MARSH, J. L. 2008. Inhibition of specific HDACs and sirtuins suppresses pathogenesis in a Drosophila model of Huntington's disease. *Hum Mol Genet,* 17**,** 3767-75.

PANG, T. Y., DU, X., ZAJAC, M. S., HOWARD, M. L. & HANNAN, A. J. 2009. Altered serotonin receptor expression is associated with depression-related behavior in the R6/1 transgenic mouse model of Huntington's disease. *Hum Mol Genet,* 18**,** 753-66.

PANOV, A. V., GUTEKUNST, C. A., LEAVITT, B. R., HAYDEN, M. R., BURKE, J. R., STRITTMATTER, W. J. & GREENAMYRE, J. T. 2002. Early mitochondrial calcium defects in Huntington's disease are a direct effect of polyglutamines. *Nat Neurosci,* 5**,** 731-6.

PARDO, R., MOLINA-CALAVITA, M., POIZAT, G., KERYER, G., HUMBERT, S. & SAUDOU, F. 2010. pARIS-htt: an optimised expression platform to study huntingtin reveals functional domains required for vesicular trafficking. *Mol Brain,* 3**,** 17.

PARK, I. H., ARORA, N., HUO, H., MAHERALI, N., AHFELDT, T., SHIMAMURA, A., LENSCH, M. W., COWAN, C., HOCHEDLINGER, K. & DALEY, G. Q. 2008. Disease-specific induced pluripotent stem cells. *Cell,* 134**,** 877-86.

PARKER, J. A., ARANGO, M., ABDERRAHMANE, S., LAMBERT, E., TOURETTE, C., CATOIRE, H. & NERI, C. 2005. Resveratrol rescues mutant polyglutamine cytotoxicity in nematode and mammalian neurons. *Nat Genet,* 37**,** 349-50.

PARKER, J. A., CONNOLLY, J. B., WELLINGTON, C., HAYDEN, M., DAUSSET, J. & NERI, C. 2001. Expanded polyglutamines in Caenorhabditis elegans cause axonal abnormalities and severe dysfunction of PLM mechanosensory neurons without cell death. *Proc Natl Acad Sci U S A,* 98**,** 13318-23.

PAULSEN, J. S. 2011. Cognitive impairment in Huntington disease: diagnosis and treatment. *Curr Neurol Neurosci Rep,* 11**,** 474-83.

PAULSEN, J. S., READY, R. E., HAMILTON, J. M., MEGA, M. S. & CUMMINGS, J. L. 2001. Neuropsychiatric aspects of Huntington's disease. *J Neurol Neurosurg Psychiatry,* 71**,** 310-4.

PEARSON, C. E. 2003. Slipping while sleeping? Trinucleotide repeat expansions in germ cells. *Trends Mol Med,* 9**,** 490-5.

PEARSON, S. J. & REYNOLDS, G. P. 1992. Increased brain concentrations of a neurotoxin, 3-hydroxykynurenine, in Huntington's disease. *Neurosci Lett,* 144**,** 199-201.

PELLOW, S. & FILE, S. E. 1986. Anxiolytic and anxiogenic drug effects on exploratory activity in an elevated plus-maze: a novel test of anxiety in the rat. *Pharmacol Biochem Behav,* 24**,** 525-9.

PERLSON, E., MADAY, S., FU, M. M., MOUGHAMIAN, A. J. & HOLZBAUR, E. L. 2010. Retrograde axonal transport: pathways to cell death? *Trends Neurosci,* 33**,** 335-44.

PERRIN, V., REGULIER, E., ABBAS-TERKI, T., HASSIG, R., BROUILLET, E., AEBISCHER, P., LUTHI-CARTER, R. & DEGLON, N. 2007. Neuroprotection by Hsp104 and Hsp27 in lentiviral-based rat models of Huntington's disease. *Mol Ther,* 15**,** 903-11.

PERRY, V. H., LUNN, E. R., BROWN, M. C., CAHUSAC, S. & GORDON, S. 1990. Evidence that the Rate of Wallerian Degeneration is Controlled by a Single Autosomal Dominant Gene. *Eur J Neurosci,* 2**,** 408-13.

PETERSEN, A. & GABERY, S. 2012. Hypothalamic and limbic system changes in Huntington's disease. *Journal of Huntington's disease,* 1**,** 13-24.

PHAN, J., HICKEY, M. A., ZHANG, P., CHESSELET, M. F. & REUE, K. 2009. Adipose tissue dysfunction tracks disease progression in two Huntington's disease mouse models. *Hum Mol Genet,* 18**,** 1006-16.

POLITIS, M., PAVESE, N., TAI, Y. F., TABRIZI, S. J., BARKER, R. A. & PICCINI, P. 2008. Hypothalamic involvement in Huntington's disease: an in vivo PET study. *Brain,* 131**,** 2860-9.

PORRERO, C., RUBIO-GARRIDO, P., AVENDANO, C. & CLASCA, F. 2010. Mapping of fluorescent protein-expressing neurons and axon pathways in adult and developing Thy1-eYFP-H transgenic mice. *Brain Res,* 1345**,** 59-72.

POULADI, M. A., GRAHAM, R. K., KARASINSKA, J. M., XIE, Y., SANTOS, R. D., PETERSEN, A. & HAYDEN, M. R. 2009. Prevention of depressive behaviour in the YAC128 mouse model of Huntington disease by mutation at residue 586 of huntingtin. *Brain,* 132**,** 919-32.

POULADI, M. A., MORTON, A. J. & HAYDEN, M. R. 2013. Choosing an animal model for the study of Huntington's disease. *Nat Rev Neurosci,* 14**,** 708-21.

PRATLEY, R. E., SALBE, A. D., RAVUSSIN, E. & CAVINESS, J. N. 2000. Higher sedentary energy expenditure in patients with Huntington's disease. *Ann Neurol,* 47**,** 64-70.

PRUT, L. & BELZUNG, C. 2003. The open field as a paradigm to measure the effects of drugs on anxiety-like behaviors: a review. *Eur J Pharmacol,* 463**,** 3-33.

PUN, S., SANTOS, A. F., SAXENA, S., XU, L. & CARONI, P. 2006. Selective vulnerability and pruning of phasic motoneuron axons in motoneuron disease alleviated by CNTF. *Nat Neurosci,* 9**,** 408-19.

RAFF, M. C., WHITMORE, A. V. & FINN, J. T. 2002. Axonal self-destruction and neurodegeneration. *Science,* 296**,** 868-71.

RANEN, N. G., STINE, O. C., ABBOTT, M. H., SHERR, M., CODORI, A. M., FRANZ, M. L., CHAO, N. I., CHUNG, A. S., PLEASANT, N., CALLAHAN, C. & ET AL. 1995. Anticipation and instability of IT-15 (CAG)n repeats in parent-offspring pairs with Huntington disease. *Am J Hum Genet,* 57**,** 593-602.

RANGONE, H., POIZAT, G., TRONCOSO, J., ROSS, C. A., MACDONALD, M. E., SAUDOU, F. & HUMBERT, S. 2004. The serum- and glucocorticoid-induced kinase SGK inhibits mutant huntingtin-induced toxicity by phosphorylating serine 421 of huntingtin. *Eur J Neurosci,* 19**,** 273-9.

RAVIKUMAR, B., DUDEN, R. & RUBINSZTEIN, D. C. 2002. Aggregate-prone proteins with polyglutamine and polyalanine expansions are degraded by autophagy. *Hum Mol Genet,* 11**,** 1107-17.

RAVIKUMAR, B., VACHER, C., BERGER, Z., DAVIES, J. E., LUO, S., OROZ, L. G., SCARAVILLI, F., EASTON, D. F., DUDEN, R., O'KANE, C. J. & RUBINSZTEIN, D. C. 2004. Inhibition of mTOR induces autophagy and reduces toxicity of polyglutamine expansions in fly and mouse models of Huntington disease. *Nat Genet,* 36**,** 585-95.

READING, S. A., YASSA, M. A., BAKKER, A., DZIORNY, A. C., GOURLEY, L. M., YALLAPRAGADA, V., ROSENBLATT, A., MARGOLIS, R. L., AYLWARD, E. H., BRANDT, J., MORI, S., VAN ZIJL, P., BASSETT, S. S. & ROSS, C. A. 2005. Regional white matter change in pre-symptomatic Huntington's disease: a diffusion tensor imaging study. *Psychiatry Res,* 140**,** 55-62.

REDDY, P. H. & SHIRENDEB, U. P. 2012. Mutant huntingtin, abnormal mitochondrial dynamics, defective axonal transport of mitochondria, and selective synaptic degeneration in Huntington's disease. *Biochim Biophys Acta,* 1822**,** 101-10.

REDDY, P. H., WILLIAMS, M., CHARLES, V., GARRETT, L., PIKE-BUCHANAN, L., WHETSELL, W. O., MILLER, G. & TAGLE, D. A. 1998. Behavioural abnormalities and selective

neuronal loss in HD transgenic mice expressing mutated full-length HD cDNA. *Nature Genetics,* 20**,** 198-202.

REINER, A., ALBIN, R. L., ANDERSON, K. D., D'AMATO, C. J., PENNEY, J. B. & YOUNG, A. B. 1988. Differential loss of striatal projection neurons in Huntington disease. *Proc Natl Acad Sci U S A,* 85**,** 5733-7.

REINER, A., DRAGATSIS, I., ZEITLIN, S. & GOLDOWITZ, D. 2003. Wild-type huntingtin plays a role in brain development and neuronal survival. *Mol Neurobiol,* 28**,** 259-76.

REINER, A., HART, N. M., LEI, W. & DENG, Y. 2010. Corticostriatal projection neurons - dichotomous types and dichotomous functions. *Front Neuroanat,* 4**,** 142.

RENNA, M., JIMENEZ-SANCHEZ, M., SARKAR, S. & RUBINSZTEIN, D. C. 2010. Chemical inducers of autophagy that enhance the clearance of mutant proteins in neurodegenerative diseases. *J Biol Chem,* 285**,** 11061-7.

REVOLLO, J. R., GRIMM, A. A. & IMAI, S. 2004. The NAD biosynthesis pathway mediated by nicotinamide phosphoribosyltransferase regulates Sir2 activity in mammalian cells. *J Biol Chem,* 279**,** 50754-63.

RIGAMONTI, D., BAUER, J. H., DE-FRAJA, C., CONTI, L., SIPIONE, S., SCIORATI, C., CLEMENTI, E., HACKAM, A., HAYDEN, M. R., LI, Y., COOPER, J. K., ROSS, C. A., GOVONI, S., VINCENZ, C. & CATTANEO, E. 2000. Wild-type huntingtin protects from apoptosis upstream of caspase-3. *J Neurosci,* 20**,** 3705-13.

RIGAMONTI, D., SIPIONE, S., GOFFREDO, D., ZUCCATO, C., FOSSALE, E. & CATTANEO, E. 2001. Huntingtin's neuroprotective activity occurs via inhibition of procaspase-9 processing. *J Biol Chem,* 276**,** 14545-8.

RISING, A. C., XU, J., CARLSON, A., NAPOLI, V. V., DENOVAN-WRIGHT, E. M. & MANDEL, R. J. 2011. Longitudinal behavioral, cross-sectional transcriptional and histopathological characterization of a knock-in mouse model of Huntington's disease with 140 CAG repeats. *Exp Neurol,* 228**,** 173-82.

ROSAS, H. D., SALAT, D. H., LEE, S. Y., ZALETA, A. K., PAPPU, V., FISCHL, B., GREVE, D., HEVELONE, N. & HERSCH, S. M. 2008. Cerebral cortex and the clinical expression of Huntington's disease: complexity and heterogeneity. *Brain,* 131**,** 1057-68.

ROSAS, H. D., TUCH, D. S., HEVELONE, N. D., ZALETA, A. K., VANGEL, M., HERSCH, S. M. & SALAT, D. H. 2006. Diffusion tensor imaging in presymptomatic and early Huntington's disease: Selective white matter pathology and its relationship to clinical measures. *Mov Disord,* 21**,** 1317-25.

ROSENBLATT, A. 2007. Neuropsychiatry of Huntington's disease. *Dialogues Clin Neurosci,* 9**,** 191-7.

ROY, N. S., CLEREN, C., SINGH, S. K., YANG, L., BEAL, M. F. & GOLDMAN, S. A. 2006. Functional engraftment of human ES cell-derived dopaminergic neurons enriched by coculture with telomerase-immortalized midbrain astrocytes. *Nat Med,* 12**,** 1259-68.

SAJADI, A., SCHNEIDER, B. L. & AEBISCHER, P. 2004. Wlds-mediated protection of dopaminergic fibers in an animal model of Parkinson disease. *Curr Biol,* 14**,** 326-30.

SASAKI, Y., VOHRA, B. P., BALOH, R. H. & MILBRANDT, J. 2009a. Transgenic mice expressing the Nmnat1 protein manifest robust delay in axonal degeneration in vivo. *J Neurosci,* 29**,** 6526-34.

SASAKI, Y., VOHRA, B. P., LUND, F. E. & MILBRANDT, J. 2009b. Nicotinamide mononucleotide adenylyl transferase-mediated axonal protection requires enzymatic activity but not increased levels of neuronal nicotinamide adenine dinucleotide. *J Neurosci,* 29**,** 5525-35.

SATHYASAIKUMAR, K. V., STACHOWSKI, E. K., AMORI, L., GUIDETTI, P., MUCHOWSKI, P. J. & SCHWARCZ, R. 2010. Dysfunctional kynurenine pathway metabolism in the R6/2 mouse model of Huntington's disease. *J Neurochem,* 113**,** 1416-25.

SAUDOU, F., FINKBEINER, S., DEVYS, D. & GREENBERG, M. E. 1998. Huntingtin acts in the nucleus to induce apoptosis but death does not correlate with the formation of intranuclear inclusions. *Cell,* 95**,** 55-66.

SAWIAK, S. J., WOOD, N. I., WILLIAMS, G. B., MORTON, A. J. & CARPENTER, T. A. 2009. Use of magnetic resonance imaging for anatomical phenotyping of the R6/2 mouse model of Huntington's disease. *Neurobiol Dis,* 33**,** 12-9.

SCHIEFER, J., LANDWEHRMEYER, G. B., LUESSE, H. G., SPRUNKEN, A., PULS, C., MILKEREIT, A., MILKEREIT, E. & KOSINSKI, C. M. 2002. Riluzole prolongs survival time and alters nuclear inclusion formation in a transgenic mouse model of Huntington's disease. *Mov Disord,* 17**,** 748-57.

SCHILLING, G., BECHER, M. W., SHARP, A. H., JINNAH, H. A., DUAN, K., KOTZUK, J. A., SLUNT, H. H., RATOVITSKI, T., COOPER, J. K., JENKINS, N. A., COPELAND, N. G., PRICE, D. L., ROSS, C. A. & BORCHELT, D. R. 1999. Intranuclear inclusions and neuritic aggregates in transgenic mice expressing a mutant N-terminal fragment of huntingtin. *Hum Mol Genet,* 8**,** 397-407.

SCHILLING, G., COONFIELD, M. L., ROSS, C. A. & BORCHELT, D. R. 2001. Coenzyme Q10 and remacemide hydrochloride ameliorate motor deficits in a Huntington's disease transgenic mouse model. *Neurosci Lett,* 315**,** 149-53.

SCHLAEPFER, W. W. & BUNGE, R. P. 1973. Effects of calcium ion concentration on the degeneration of amputated axons in tissue culture. *J Cell Biol,* 59**,** 456-70.

SCHLAEPFER, W. W. & HASLER, M. B. 1979. Characterization of the calcium-induced disruption of neurofilaments in rat peripheral nerve. *Brain Res,* 168**,** 299-309.

SEO, H., KIM, W. & ISACSON, O. 2008. Compensatory changes in the ubiquitin-proteasome system, brain-derived neurotrophic factor and mitochondrial complex II/III in YAC72 and R6/2 transgenic mice partially model Huntington's disease patients. *Hum Mol Genet,* 17**,** 3144-53.

SHELBOURNE, P. F., KILLEEN, N., HEVNER, R. F., JOHNSTON, H. M., TECOTT, L., LEWANDOSKI, M., ENNIS, M., RAMIREZ, L., LI, Z., IANNICOLA, C., LITTMAN, D. R. & MYERS, R. M. 1999. A Huntington's disease CAG expansion at the murine Hdh locus is unstable and associated with behavioural abnormalities in mice. *Hum Mol Genet,* 8**,** 763-74.

SHERRIFF, F. E., BRIDGES, L. R. & SIVALOGANATHAN, S. 1994. Early detection of axonal injury after human head trauma using immunocytochemistry for beta-amyloid precursor protein. *Acta Neuropathol,* 87**,** 55-62.

SHIMOJO, M. 2008. Huntingtin regulates RE1-silencing transcription factor/neuron-restrictive silencer factor (REST/NRSF) nuclear trafficking indirectly through a complex with REST/NRSF-interacting LIM domain protein (RILP) and dynactin p150 Glued. *J Biol Chem,* 283**,** 34880-6.

SINADINOS, C., BURBIDGE-KING, T., SOH, D., THOMPSON, L. M., MARSH, J. L., WYTTENBACH, A. & MUDHER, A. K. 2009. Live axonal transport disruption by mutant huntingtin fragments in Drosophila motor neuron axons. *Neurobiol Dis,* 34**,** 389-95.

SINGARAJA, R. R., HADANO, S., METZLER, M., GIVAN, S., WELLINGTON, C. L., WARBY, S., YANAI, A., GUTEKUNST, C. A., LEAVITT, B. R., YI, H., FICHTER, K., GAN, L., MCCUTCHEON, K., CHOPRA, V., MICHEL, J., HERSCH, S. M., IKEDA, J. E. & HAYDEN, M. R. 2002. HIP14, a novel ankyrin domain-containing protein, links huntingtin to intracellular trafficking and endocytosis. *Hum Mol Genet,* 11**,** 2815-28.

SIPIONE, S., RIGAMONTI, D., VALENZA, M., ZUCCATO, C., CONTI, L., PRITCHARD, J., KOOPERBERG, C., OLSON, J. M. & CATTANEO, E. 2002. Early transcriptional profiles in huntingtin-inducible striatal cells by microarray analyses. *Hum Mol Genet,* 11**,** 1953-65.

SLOW, E. J., GRAHAM, R. K., OSMAND, A. P., DEVON, R. S., LU, G., DENG, Y., PEARSON, J., VAID, K., BISSADA, N., WETZEL, R., LEAVITT, B. R. & HAYDEN, M. R. 2005. Absence of

behavioral abnormalities and neurodegeneration in vivo despite widespread neuronal huntingtin inclusions. *Proc Natl Acad Sci U S A,* 102**,** 11402-7.

SLOW, E. J., VAN RAAMSDONK, J., ROGERS, D., COLEMAN, S. H., GRAHAM, R. K., DENG, Y., OH, R., BISSADA, N., HOSSAIN, S. M., YANG, Y. Z., LI, X. J., SIMPSON, E. M., GUTEKUNST, C. A., LEAVITT, B. R. & HAYDEN, M. R. 2003. Selective striatal neuronal loss in a YAC128 mouse model of Huntington disease. *Hum Mol Genet,* 12**,** 1555-67.

SMITH, R., BRUNDIN, P. & LI, J. Y. 2005. Synaptic dysfunction in Huntington's disease: a new perspective. *Cell Mol Life Sci,* 62**,** 1901-12.

SONG, C., ZHANG, Y., PARSONS, C. G. & LIU, Y. F. 2003. Expression of polyglutamine-expanded huntingtin induces tyrosine phosphorylation of N-methyl-D-aspartate receptors. *J Biol Chem,* 278**,** 33364-9.

SPARGO, E., EVERALL, I. P. & LANTOS, P. L. 1993. Neuronal loss in the hippocampus in Huntington's disease: a comparison with HIV infection. *J Neurol Neurosurg Psychiatry,* 56**,** 487-91.

SPIRES, T. L., MEYER-LUEHMANN, M., STERN, E. A., MCLEAN, P. J., SKOCH, J., NGUYEN, P. T., BACSKAI, B. J. & HYMAN, B. T. 2005. Dendritic spine abnormalities in amyloid precursor protein transgenic mice demonstrated by gene transfer and intravital multiphoton microscopy. *J Neurosci,* 25**,** 7278-87.

SQUITIERI, F., GELLERA, C., CANNELLA, M., MARIOTTI, C., CISLAGHI, G., RUBINSZTEIN, D. C., ALMQVIST, E. W., TURNER, D., BACHOUD-LEVI, A. C., SIMPSON, S. A., DELATYCKI, M., MAGLIONE, V., HAYDEN, M. R. & DONATO, S. D. 2003. Homozygosity for CAG mutation in Huntington disease is associated with a more severe clinical course. *Brain,* 126**,** 946-55.

STACK, E. C., KUBILUS, J. K., SMITH, K., CORMIER, K., DEL SIGNORE, S. J., GUELIN, E., RYU, H., HERSCH, S. M. & FERRANTE, R. J. 2005. Chronology of behavioral symptoms and neuropathological sequela in R6/2 Huntington's disease transgenic mice. *J Comp Neurol,* 490**,** 354-70.

STEFFAN, J. S., AGRAWAL, N., PALLOS, J., ROCKABRAND, E., TROTMAN, L. C., SLEPKO, N., ILLES, K., LUKACSOVICH, T., ZHU, Y. Z., CATTANEO, E., PANDOLFI, P. P., THOMPSON, L. M. & MARSH, J. L. 2004. SUMO modification of Huntingtin and Huntington's disease pathology. *Science,* 304**,** 100-4.

STEFFAN, J. S., BODAI, L., PALLOS, J., POELMAN, M., MCCAMPBELL, A., APOSTOL, B. L., KAZANTSEV, A., SCHMIDT, E., ZHU, Y. Z., GREENWALD, M., KUROKAWA, R., HOUSMAN, D. E., JACKSON, G. R., MARSH, J. L. & THOMPSON, L. M. 2001. Histone deacetylase inhibitors arrest polyglutamine-dependent neurodegeneration in Drosophila. *Nature,* 413**,** 739-43.

STIRLING, D. P. & STYS, P. K. 2010. Mechanisms of axonal injury: internodal nanocomplexes and calcium deregulation. *Trends Mol Med,* 16**,** 160-70.

STOLL, G., JANDER, S. & MYERS, R. R. 2002. Degeneration and regeneration of the peripheral nervous system: from Augustus Waller's observations to neuroinflammation. *J Peripher Nerv Syst,* 7**,** 13-27.

STOLL, G. & MULLER, H. W. 1999. Nerve injury, axonal degeneration and neural regeneration: basic insights. *Brain Pathol,* 9**,** 313-25.

STREHLOW, A. N., LI, J. Z. & MYERS, R. M. 2007. Wild-type huntingtin participates in protein trafficking between the Golgi and the extracellular space. *Hum Mol Genet,* 16**,** 391-409.

SUN, Y., SAVANENIN, A., REDDY, P. H. & LIU, Y. F. 2001. Polyglutamine-expanded huntingtin promotes sensitization of N-methyl-D-aspartate receptors via post-synaptic density 95. *J Biol Chem,* 276**,** 24713-8.

SUZUKI, K. & KOIKE, T. 2007. Mammalian Sir2-related protein (SIRT) 2-mediated modulation of resistance to axonal degeneration in slow Wallerian degeneration mice: a crucial role of tubulin deacetylation. *Neuroscience,* 147**,** 599-612.

SWERDLOW, N. R., GEYER, M. A. & BRAFF, D. L. 2001. Neural circuit regulation of prepulse inhibition of startle in the rat: current knowledge and future challenges. *Psychopharmacology (Berl),* 156**,** 194-215.

SWERDLOW, N. R., PAULSEN, J., BRAFF, D. L., BUTTERS, N., GEYER, M. A. & SWENSON, M. R. 1995. Impaired prepulse inhibition of acoustic and tactile startle response in patients with Huntington's disease. *J Neurol Neurosurg Psychiatry,* 58**,** 192-200.

TADOLINI, B., JULIANO, C., PIU, L., FRANCONI, F. & CABRINI, L. 2000. Resveratrol inhibition of lipid peroxidation. *Free Radic Res,* 33**,** 105-14.

TAKANO, H. & GUSELLA, J. F. 2002. The predominantly HEAT-like motif structure of huntingtin and its association and coincident nuclear entry with dorsal, an NF-kB/Rel/dorsal family transcription factor. *BMC Neurosci,* 3**,** 15.

TANG, T. S., TU, H., CHAN, E. Y., MAXIMOV, A., WANG, Z., WELLINGTON, C. L., HAYDEN, M. R. & BEZPROZVANNY, I. 2003. Huntingtin and huntingtin-associated protein 1 influence neuronal calcium signaling mediated by inositol-(1,4,5) triphosphate receptor type 1. *Neuron,* 39**,** 227-39.

TANNER, K. G., LANDRY, J., STERNGLANZ, R. & DENU, J. M. 2000. Silent information regulator 2 family of NAD- dependent histone/protein deacetylases generates a unique product, 1-O-acetyl-ADP-ribose. *Proc Natl Acad Sci U S A,* 97**,** 14178-82.

TARANTINO, L. M. & BUCAN, M. 2000. Dissection of behavior and psychiatric disorders using the mouse as a model. *Hum Mol Genet,* 9**,** 953-65.

TARTARI, M., GISSI, C., LO SARDO, V., ZUCCATO, C., PICARDI, E., PESOLE, G. & CATTANEO, E. 2008. Phylogenetic comparison of huntingtin homologues reveals the appearance of a primitive polyQ in sea urchin. *Mol Biol Evol,* 25**,** 330-8.

TEKIN, S. & CUMMINGS, J. L. 2002. Frontal-subcortical neuronal circuits and clinical neuropsychiatry: an update. *J Psychosom Res,* 53**,** 647-54.

THEVANDAVAKKAM, M. A., SCHWARCZ, R., MUCHOWSKI, P. J. & GIORGINI, F. 2010. Targeting kynurenine 3-monooxygenase (KMO): implications for therapy in Huntington's disease. *CNS Neurol Disord Drug Targets,* 9**,** 791-800.

THOMAS, M., ASHIZAWA, T. & JANKOVIC, J. 2004. Minocycline in Huntington's disease: a pilot study. *Mov Disord,* 19**,** 692-5.

THOMPSON, P. D., BERARDELLI, A., ROTHWELL, J. C., DAY, B. L., DICK, J. P., BENECKE, R. & MARSDEN, C. D. 1988. The coexistence of bradykinesia and chorea in Huntington's disease and its implications for theories of basal ganglia control of movement. *Brain,* 111 (Pt 2)**,** 223-44.

TORRES-PERAZA, J. F., GIRALT, A., GARCIA-MARTINEZ, J. M., PEDROSA, E., CANALS, J. M. & ALBERCH, J. 2008. Disruption of striatal glutamatergic transmission induced by mutant huntingtin involves remodeling of both postsynaptic density and NMDA receptor signaling. *Neurobiol Dis,* 29**,** 409-21.

TRUEMAN, R. C., BROOKS, S. P., JONES, L. & DUNNETT, S. B. 2009. Rule learning, visuospatial function and motor performance in the Hdh(Q92) knock-in mouse model of Huntington's disease. *Behav Brain Res,* 203**,** 215-22.

TRUSHINA, E., DYER, R. B., BADGER, J. D., 2ND, URE, D., EIDE, L., TRAN, D. D., VRIEZE, B. T., LEGENDRE-GUILLEMIN, V., MCPHERSON, P. S., MANDAVILLI, B. S., VAN HOUTEN, B., ZEITLIN, S., MCNIVEN, M., AEBERSOLD, R., HAYDEN, M., PARISI, J. E., SEEBERG, E., DRAGATSIS, I., DOYLE, K., BENDER, A., CHACKO, C. & MCMURRAY, C. T. 2004. Mutant huntingtin impairs axonal trafficking in mammalian neurons in vivo and in vitro. *Mol Cell Biol,* 24**,** 8195-209.

TSAI, J., GRUTZENDLER, J., DUFF, K. & GAN, W. B. 2004. Fibrillar amyloid deposition leads to local synaptic abnormalities and breakage of neuronal branches. *Nat Neurosci,* 7**,** 1181-3.

TURMAINE, M., RAZA, A., MAHAL, A., MANGIARINI, L., BATES, G. P. & DAVIES, S. W. 2000. Nonapoptotic neurodegeneration in a transgenic mouse model of Huntington's disease. *Proc Natl Acad Sci U S A,* 97**,** 8093-7.

VACHER, C., GARCIA-OROZ, L. & RUBINSZTEIN, D. C. 2005. Overexpression of yeast hsp104 reduces polyglutamine aggregation and prolongs survival of a transgenic mouse model of Huntington's disease. *Hum Mol Genet,* 14**,** 3425-33.

VAN DELLEN, A., DEACON, R., YORK, D., BLAKEMORE, C. & HANNAN, A. J. 2001. Anterior cingulate cortical transplantation in transgenic Huntington's disease mice. *Brain Res Bull,* 56**,** 313-8.

VAN DER BURG, J. M., BJORKQVIST, M. & BRUNDIN, P. 2009. Beyond the brain: widespread pathology in Huntington's disease. *Lancet Neurol,* 8**,** 765-74.

VAN RAAMSDONK, J. M., METZLER, M., SLOW, E., PEARSON, J., SCHWAB, C., CARROLL, J., GRAHAM, R. K., LEAVITT, B. R. & HAYDEN, M. R. 2007. Phenotypic abnormalities in the YAC128 mouse model of Huntington disease are penetrant on multiple genetic backgrounds and modulated by strain. *Neurobiol Dis,* 26**,** 189-200.

VAN RAAMSDONK, J. M., PEARSON, J., ROGERS, D. A., BISSADA, N., VOGL, A. W., HAYDEN, M. R. & LEAVITT, B. R. 2005a. Loss of wild-type huntingtin influences motor dysfunction and survival in the YAC128 mouse model of Huntington disease. *Hum Mol Genet,* 14**,** 1379-92.

VAN RAAMSDONK, J. M., PEARSON, J., SLOW, E. J., HOSSAIN, S. M., LEAVITT, B. R. & HAYDEN, M. R. 2005b. Cognitive dysfunction precedes neuropathology and motor abnormalities in the YAC128 mouse model of Huntington's disease. *J Neurosci,* 25**,** 4169-80.

VAN VUGT, J. P., VAN HILTEN, B. J. & ROOS, R. A. 1996. Hypokinesia in Huntington's disease. *Mov Disord,* 11**,** 384-8.

VAN WAESBERGHE, J. H. T. M., KAMPHORST, W., DE GROOT, C. J. A., VAN WALDERVEEN, M. A. A., CASTELIJNS, J. A., RAVID, R., NIJEHOLT, G. J. L. A., VAN DER VALK, P., POLMAN, C. H., THOMPSON, A. J. & BARKHOF, F. 1999. Axonal loss in multiple sclerosis lesions: Magnetic resonance imaging insights into substrates of disability. *Annals of Neurology,* 46**,** 747-754.

VANDE VELDE, C., GARCIA, M. L., YIN, X., TRAPP, B. D. & CLEVELAND, D. W. 2004. The neuroprotective factor Wlds does not attenuate mutant SOD1-mediated motor neuron disease. *Neuromolecular Med,* 5**,** 193-203.

VIDAL, M., MORRIS, R., GROSVELD, F. & SPANOPOULOU, E. 1990. Tissue-specific control elements of the Thy-1 gene. *EMBO J,* 9**,** 833-40.

VIRAG, L. & SZABO, C. 2002. The therapeutic potential of poly(ADP-ribose) polymerase inhibitors. *Pharmacol Rev,* 54**,** 375-429.

VONSATTEL, J. P. & DIFIGLIA, M. 1998. Huntington disease. *J Neuropathol Exp Neurol,* 57**,** 369-84.

VONSATTEL, J. P., MYERS, R. H., STEVENS, T. J., FERRANTE, R. J., BIRD, E. D. & RICHARDSON, E. P., JR. 1985. Neuropathological classification of Huntington's disease. *J Neuropathol Exp Neurol,* 44**,** 559-77.

WALLER, A. 1850. Experiments on the section of the glossopharyngeal and hypoglossal nerves of the frog, and observations on the alterations produced thereby in the structure of their primitive fibres. *Phil. Trans. R. Soc. Lond. B: Biol. Sci,* 140**,** 423-429.

WAN, H., AGGLETON, J. P. & BROWN, M. W. 1999. Different contributions of the hippocampus and perirhinal cortex to recognition memory. *J Neurosci,* 19**,** 1142-8.

WANG, J., ZHAI, Q., CHEN, Y., LIN, E., GU, W., MCBURNEY, M. W. & HE, Z. 2005. A local mechanism mediates NAD-dependent protection of axon degeneration. *J Cell Biol,* 170**,** 349-55.

WANG, J. T., MEDRESS, Z. A. & BARRES, B. A. 2012. Axon degeneration: molecular mechanisms of a self-destruction pathway. *J Cell Biol,* 196**,** 7-18.

WANG, N., GRAY, M., LU, X. H., CANTLE, J. P., HOLLEY, S. M., GREINER, E., GU, X., SHIRASAKI, D., CEPEDA, C., LI, Y., DONG, H., LEVINE, M. S. & YANG, X. W. 2014. Neuronal targets for reducing mutant huntingtin expression to ameliorate disease in a mouse model of Huntington's disease. *Nat Med,* 20**,** 536-41.

WANG, Y., LIN, F. & QIN, Z. H. 2010. The role of post-translational modifications of huntingtin in the pathogenesis of Huntington's disease. *Neurosci Bull,* 26**,** 153-62.

WEAVER, K. E., RICHARDS, T. L., LIANG, O., LAURINO, M. Y., SAMII, A. & AYLWARD, E. H. 2009. Longitudinal diffusion tensor imaging in Huntington's Disease. *Exp Neurol,* 216**,** 525-9.

WELLINGTON, C. L., ELLERBY, L. M., GUTEKUNST, C. A., ROGERS, D., WARBY, S., GRAHAM, R. K., LOUBSER, O., VAN RAAMSDONK, J., SINGARAJA, R., YANG, Y. Z., GAFNI, J., BREDESEN, D., HERSCH, S. M., LEAVITT, B. R., ROY, S., NICHOLSON, D. W. & HAYDEN, M. R. 2002. Caspase cleavage of mutant huntingtin precedes neurodegeneration in Huntington's disease. *J Neurosci,* 22**,** 7862-72.

WELLINGTON, C. L., SINGARAJA, R., ELLERBY, L., SAVILL, J., ROY, S., LEAVITT, B., CATTANEO, E., HACKAM, A., SHARP, A., THORNBERRY, N., NICHOLSON, D. W., BREDESEN, D. E. & HAYDEN, M. R. 2000. Inhibiting caspase cleavage of huntingtin reduces toxicity and aggregate formation in neuronal and nonneuronal cells. *J Biol Chem,* 275**,** 19831-8.

WEXLER, N. S., YOUNG, A. B., TANZI, R. E., TRAVERS, H., STAROSTA-RUBINSTEIN, S., PENNEY, J. B., SNODGRASS, S. R., SHOULSON, I., GOMEZ, F., RAMOS ARROYO, M. A. & ET AL. 1987. Homozygotes for Huntington's disease. *Nature,* 326**,** 194-7.

WHEELER, V. C., WHITE, J. K., GUTEKUNST, C. A., VRBANAC, V., WEAVER, M., LI, X. J., LI, S. H., YI, H., VONSATTEL, J. P., GUSELLA, J. F., HERSCH, S., AUERBACH, W., JOYNER, A. L. & MACDONALD, M. E. 2000. Long glutamine tracts cause nuclear localization of a novel form of huntingtin in medium spiny striatal neurons in HdhQ92 and HdhQ111 knock-in mice. *Hum Mol Genet,* 9**,** 503-13.

WHITE, J. K., AUERBACH, W., DUYAO, M. P., VONSATTEL, J. P., GUSELLA, J. F., JOYNER, A. L. & MACDONALD, M. E. 1997. Huntingtin is required for neurogenesis and is not impaired by the Huntington's disease CAG expansion. *Nature Genetics,* 17**,** 404-410.

WHITMORE, A. V., LINDSTEN, T., RAFF, M. C. & THOMPSON, C. B. 2003. The proapoptotic proteins Bax and Bak are not involved in Wallerian degeneration. *Cell Death Differ,* 10**,** 260-1.

WILBREY, A. L., HALEY, J. E., WISHART, T. M., CONFORTI, L., MORREALE, G., BEIROWSKI, B., BABETTO, E., ADALBERT, R., GILLINGWATER, T. H., SMITH, T., WYLLIE, D. J., RIBCHESTER, R. R. & COLEMAN, M. P. 2008. VCP binding influences intracellular distribution of the slow Wallerian degeneration protein, Wld(S). *Mol Cell Neurosci,* 38**,** 325-40.

WOLFGANG, W. J., MILLER, T. W., WEBSTER, J. M., HUSTON, J. S., THOMPSON, L. M., MARSH, J. L. & MESSER, A. 2005. Suppression of Huntington's disease pathology in Drosophila by human single-chain Fv antibodies. *Proc Natl Acad Sci U S A,* 102**,** 11563-8.

WONG, Y. C. & HOLZBAUR, E. L. 2014. The regulation of autophagosome dynamics by huntingtin and HAP1 is disrupted by expression of mutant huntingtin, leading to defective cargo degradation. *J Neurosci,* 34**,** 1293-305.

WU, D., XU, J., MCMAHON, M. T., VAN ZIJL, P. C., MORI, S., NORTHINGTON, F. J. & ZHANG, J. 2013. In vivo high-resolution diffusion tensor imaging of the mouse brain. *Neuroimage,* 83**,** 18-26.

WYTTENBACH, A., CARMICHAEL, J., SWARTZ, J., FURLONG, R. A., NARAIN, Y., RANKIN, J. & RUBINSZTEIN, D. C. 2000. Effects of heat shock, heat shock protein 40 (HDJ-2), and proteasome inhibition on protein aggregation in cellular models of Huntington's disease. *Proc Natl Acad Sci U S A,* 97**,** 2898-903.

WYTTENBACH, A., SWARTZ, J., KITA, H., THYKJAER, T., CARMICHAEL, J., BRADLEY, J., BROWN, R., MAXWELL, M., SCHAPIRA, A., ORNTOFT, T. F., KATO, K. & RUBINSZTEIN, D. C. 2001. Polyglutamine expansions cause decreased CRE-mediated transcription and early gene expression changes prior to cell death in an inducible cell model of Huntington's disease. *Hum Mol Genet,* 10**,** 1829-45.

XIA, J., LEE, D. H., TAYLOR, J., VANDELFT, M. & TRUANT, R. 2003. Huntingtin contains a highly conserved nuclear export signal. *Hum Mol Genet,* 12**,** 1393-403.

YAHATA, N., YUASA, S. & ARAKI, T. 2009. Nicotinamide mononucleotide adenylyltransferase expression in mitochondrial matrix delays Wallerian degeneration. *J Neurosci,* 29**,** 6276-84.

YAMAMOTO, A., LUCAS, J. J. & HEN, R. 2000. Reversal of neuropathology and motor dysfunction in a conditional model of Huntington's disease. *Cell,* 101**,** 57-66.

YANAI, A., HUANG, K., KANG, R., SINGARAJA, R. R., ARSTIKAITIS, P., GAN, L., ORBAN, P. C., MULLARD, A., COWAN, C. M., RAYMOND, L. A., DRISDEL, R. C., GREEN, W. N., RAVIKUMAR, B., RUBINSZTEIN, D. C., EL-HUSSEINI, A. & HAYDEN, M. R. 2006. Palmitoylation of huntingtin by HIP14 is essential for its trafficking and function. *Nat Neurosci,* 9**,** 824-31.

YANG, D., WANG, C. E., ZHAO, B., LI, W., OUYANG, Z., LIU, Z., YANG, H., FAN, P., O'NEILL, A., GU, W., YI, H., LI, S., LAI, L. & LI, X. J. 2010. Expression of Huntington's disease protein results in apoptotic neurons in the brains of cloned transgenic pigs. *Hum Mol Genet,* 19**,** 3983-94.

YANG, H., LAVU, S. & SINCLAIR, D. A. 2006. Nampt/PBEF/Visfatin: a regulator of mammalian health and longevity? *Exp Gerontol,* 41**,** 718-26.

YANG, S. H., CHENG, P. H., BANTA, H., PIOTROWSKA-NITSCHE, K., YANG, J. J., CHENG, E. C., SNYDER, B., LARKIN, K., LIU, J., ORKIN, J., FANG, Z. H., SMITH, Y., BACHEVALIER, J., ZOLA, S. M., LI, S. H., LI, X. J. & CHAN, A. W. 2008. Towards a transgenic model of Huntington's disease in a non-human primate. *Nature,* 453**,** 921-4.

YOUNG, A. B., GREENAMYRE, J. T., HOLLINGSWORTH, Z., ALBIN, R., D'AMATO, C., SHOULSON, I. & PENNEY, J. B. 1988. NMDA receptor losses in putamen from patients with Huntington's disease. *Science,* 241**,** 981-3.

ZALA, D., BENCHOUA, A., BROUILLET, E., PERRIN, V., GAILLARD, M. C., ZURN, A. D., AEBISCHER, P. & DEGLON, N. 2005. Progressive and selective striatal degeneration in primary neuronal cultures using lentiviral vector coding for a mutant huntingtin fragment. *Neurobiol Dis,* 20**,** 785-98.

ZALA, D., HINCKELMANN, M. V., YU, H., LYRA DA CUNHA, M. M., LIOT, G., CORDELIERES, F. P., MARCO, S. & SAUDOU, F. 2013. Vesicular glycolysis provides on-board energy for fast axonal transport. *Cell,* 152**,** 479-91.

ZEITLIN, S., LIU, J. P., CHAPMAN, D. L., PAPAIOANNOU, V. E. & EFSTRATIADIS, A. 1995. Increased apoptosis and early embryonic lethality in mice nullizygous for the Huntington's disease gene homologue. *Nat Genet,* 11**,** 155-63.

ZHAI, R. G., CAO, Y., HIESINGER, P. R., ZHOU, Y., MEHTA, S. Q., SCHULZE, K. L., VERSTREKEN, P. & BELLEN, H. J. 2006. Drosophila NMNAT maintains neural integrity independent of its NAD synthesis activity. *PLoS Biol,* 4**,** e416.

ZHAI, R. G., ZHANG, F., HIESINGER, P. R., CAO, Y., HAUETER, C. M. & BELLEN, H. J. 2008. NAD synthase NMNAT acts as a chaperone to protect against neurodegeneration. *Nature,* 452**,** 887-91.

ZHANG, N., AN, M. C., MONTORO, D. & ELLERBY, L. M. 2010. Characterization of Human Huntington's Disease Cell Model from Induced Pluripotent Stem Cells. *PLoS Curr,* 2**,** RRN1193.

ZHANG, S., BOYD, J., DELANEY, K. & MURPHY, T. H. 2005. Rapid reversible changes in dendritic spine structure in vivo gated by the degree of ischemia. *J Neurosci,* 25**,** 5333-8.

ZHOU, J., LIN, J., ZHOU, C., DENG, X. & XIA, B. 2011. Cytotoxicity of red fluorescent protein DsRed is associated with the suppression of Bcl-xL translation. *FEBS Lett,* 585**,** 821-7.

ZHOU, X., HOLLERN, D., LIAO, J., ANDRECHEK, E. & WANG, H. 2013. NMDA receptor-mediated excitotoxicity depends on the coactivation of synaptic and extrasynaptic receptors. *Cell Death Dis,* 4**,** e560.

ZUCCATO, C. & CATTANEO, E. 2007. Role of brain-derived neurotrophic factor in Huntington's disease. *Prog Neurobiol,* 81**,** 294-330.

ZUCCATO, C., CIAMMOLA, A., RIGAMONTI, D., LEAVITT, B. R., GOFFREDO, D., CONTI, L., MACDONALD, M. E., FRIEDLANDER, R. M., SILANI, V., HAYDEN, M. R., TIMMUSK, T., SIPIONE, S. & CATTANEO, E. 2001. Loss of huntingtin-mediated BDNF gene transcription in Huntington's disease. *Science,* 293**,** 493-8.

ZUCCATO, C., TARTARI, M., CROTTI, A., GOFFREDO, D., VALENZA, M., CONTI, L., CATAUDELLA, T., LEAVITT, B. R., HAYDEN, M. R., TIMMUSK, T., RIGAMONTI, D. & CATTANEO, E. 2003. Huntingtin interacts with REST/NRSF to modulate the transcription of NRSE-controlled neuronal genes. *Nat Genet,* 35**,** 76-83.

ZUCCATO, C., VALENZA, M. & CATTANEO, E. 2010. Molecular mechanisms and potential therapeutical targets in Huntington's disease. *Physiol Rev,* 90**,** 905-81.

Appendix

Movies on CD enclosed

Video 1A:

mHTT nuclear aggregates colocale with YFP+ cell bodies. 3D reconstruction of confocal z-stack images (63X) constituting the projection of Fig. 23 A. Colocalisation of the big NII aggregate with the cortical neuron nuclei indicated by the arrows is documented in the 3D rotation of the image. Green: YFP, red: mHTT, blue: DAPI.

Video 1B:

mHTT neuropil aggregates do not colocalise with YFP+ axons. 3D reconstruction of confocal z-stack images (63X) constituting the projection of Fig. 23 B. Lack of colocalisation between neuropil aggregates and YFP+ axons projecting to the striatum. Red neuropil aggregates are located in close proximity to green axons, but the 3D reconstruction shows they never colocalise. Green: YFP, red: mHTT.

Video 2:

Axonal transport of NMNAT2-EGFP in the presence of mHTT. Time-lapse imaging of axonal transport of NMNAT2 in dissociated SCGs. Cells were microinjected with plasmid for expression of NMNAT2-EGFP and pARIS-htt 1-586-Q100-mCherry fusion proteins and imaged (100X) with a TIRF microscope (Axio ObserverZ1, Zeiss) 24h after transfection. Green-fluorescent NMNAT2 moving vesicles are well visible while mHTT red-fluorescence is diffused. Green: NMNAT2-EGFP, red: pARIS-htt 1-586-Q100-mCherry.

Original manuscript on CD enclosed

Marangoni M, Adalbert R, Janeckova L, Patrick J, Kohli J, Coleman MP and Conforti L. 2014. Age-related axonal swellings precede other neuropathological hallmarks in a knock-in mouse model of Huntington's disease. Neurobiol Aging, 35, 2382-93.